

UNIVERSIDADE DE LISBOA
INSTITUTO SUPERIOR TÉCNICO

**¹¹¹In-labelled Peptides for Breast Cancer
Theranostics**

Filipe André Jardim dos Vultos

Supervisor: Doctor Maria de Lurdes Barreira Patrício Gano

Co-supervisor: Doctor Célia Maria da Cruz Fernandes

**Thesis approved in public session to obtain the PhD degree in
Chemistry**

Jury final classification: Pass with Distinction and Honour

UNIVERSIDADE DE LISBOA
INSTITUTO SUPERIOR TÉCNICO

**¹¹¹In-labelled Peptides for Breast Cancer
Theranostics**

Filipe André Jardim dos Vultos

Supervisor: Doctor Maria de Lurdes Barrela Patrício Gano

Co-supervisor: Doctor Célia Maria da Cruz Fernandes

**Thesis approved in public session to obtain the PhD degree in
Chemistry**

Jury final classification: Pass with Distinction and Honour

Jury

Chairperson: Doctor Maria Matilde Soares Duarte Marques, Instituto Superior Técnico, Universidade de Lisboa

Members of the Committee:

Doctor Paula Alexandra de Carvalho Gomes, Faculdade de Ciências, Universidade de Porto

Doctor João Domingos Galamba Correia, Instituto Superior Técnico, Universidade de Lisboa

Doctor Bruno Luís Jesus Pinto de Oliveira, Department of Chemistry, University of Cambridge

Doctor Maria de Lurdes Barrela Patrício Gano, Instituto Superior Técnico, Universidade de Lisboa

Funding Institution: Fundação para a Ciência e a Tecnologia

The work described in this Thesis was developed in the Radiopharmaceutical Sciences Group of C²TN, Center for Nuclear Sciences and Technologies, under the supervision of Dr. Lurdes Gano and Dr. Célia Fernandes. This work also involved the collaboration of Eindhoven University of Technology (Tu/e) and of Institut des Sciences Moléculaires de Marseille (ism2).

The work was financially supported by Fundação para a Ciência e Tecnologia through the PhD grant SFRH/BD/84509/2012 and projects EXCL/QEQ-MED/0233/2012 and UID/Multi/04349/2013.

Acknowledgements

I am deeply grateful to my supervisors Dr. Lurdes Gano and Dr. Célia Fernandes for their guidance and patience throughout every stage of my PhD. I am deeply indebted to them for all their contributions of ideas, directions and time. Their supervision was fundamental to keep me motivated and goal-oriented throughout the most challenging phases of my PhD, and for that I am deeply thankful to them. Additionally, I thank Dra. Lurdes Gano for her involvement in the animal and cell studies. To Dra. Célia Fernandes, I am thankful for all the fruitful discussions on the synthetic pathways and for her help in the development of HPLC methods and in the acquisition of ESI-MS spectra.

I would like to express my gratitude to Prof. Dr. Isabel Rego dos Santos for the opportunity to integrate the Radiopharmaceutical Sciences Group. I am grateful for her encouragement and innovative ideas that helped me grow scientifically.

I also thank Dr. António Paulo for the opportunity of developing my PhD work at the Radiopharmaceutical Sciences Group of C2TN.

To Dr. João Galamba Correia, my gratitude for all the productive discussions about peptide synthesis and for being always available to help me finding solutions for the challenges related to the world of peptides.

To Dr. Filipa Mendes, I am thankful for all her help with the *in vitro* studies with DNA. I am also thankful for all her contributions related to the biological characterization of the synthesized ligands and complexes.

To Dr. Cristina Oliveira, I am very grateful for all her help and guidance on the peptide radioiodination work.

I thank Dr. Joaquim Marçalo for his help in acquiring and interpreting ESI-MS and MS/MS spectra. He was always available to help and teach me, and for that I am deeply grateful.

To Dr. Marcel Sheepstra and to Prof. Dr. Luc Brunsveld (from the University of Eindhoven) I am thankful for his involvement in the fluorescence polarization binding assays and for making me feel welcomed in Eindhoven.

To Dr. Olga Iranzo (from *Institut des Sciences Moléculaires de Marseille*) I am thankful for all the stimulating scientific discussions and for the opportunity to work in her lab in Marseille.

To Dr. Isabel Correia, I am thankful for her help and involvement with the spectroscopic studies performed at IST.

To Elisabete Correia, I am deeply thankful for her kindness and for her help with the animal studies.

To Adelaide Cruz, I am thankful for her help in distilling solvents and for her advices and friendship.

To Joana Guerreiro, my office mate, I am thankful for her good humor, optimistic spirit and advices.

To Eser Ucar, I am thankful for the good humor, friendship (even at distance) and for the good memories from the time he spent in Portugal.

To Vera Ferreira, Letícia Quental and Maria Belo, I am thankful for the friendship and for the good times that we spent together. They made me smile and laugh even during the most difficult times and thanks to them this journey was more enjoyable. Mostly important, they made be a better person, and for that I am deeply grateful.

Ao Cristiano, agradeço todo o apoio, estímulo e paciência.

Por fim, um agradecimento muito especial aos meus pais e à minha avó.

Resumo

O objetivo do trabalho apresentado nesta tese consistiu no *design*, síntese e avaliação pré-clínica de complexos de In-111 contendo péptidos dirigidos ao receptor de estrogénio (ER). Com a seleção do radionuclido In-111 pretendeu-se explorar o potencial das novas sondas para teranóstica dos tumores mamários ER(+).

Para a concretização deste objectivo foram sintetizados pequenos péptidos contendo a sequência de aminoácidos LXXLL (**cER1**, **ER2** e **ER3**) ou contendo uma tirosina fosforilada (**pY**) que foram conjugados aos quelantes bifuncionais DOTA, DOTAGA e DTPA. Os conjugados foram marcados com In-111 com elevado rendimento e pureza radioquímica utilizando condições de elevada actividade específica.

Os complexos de In(III) com péptidos contendo a sequência LXXLL demonstraram afinidade de ligação ao ER. Adicionalmente, os complexos radioactivos [¹¹¹In]DOTA-ER3 e [¹¹¹In]DOTA-cER1 revelaram nos estudos *in vivo* rápida depuração sanguínea, fixação selectiva nos tecidos ricos em ER e estabilidade metabólica moderada. No entanto, os compostos [¹¹¹In]DTPA-pY e [¹¹¹In]DOTAGA-pY apresentaram rápida degradação proteolítica.

O péptido **ER3** foi também iodado e o derivado [**I**]-ER3 revelou elevada afinidade de ligação ao ER. O péptido radioiodado, [¹²⁵I]-ER3, demonstrou capacidade de internalização no núcleo de células tumorais ER(+), sugerindo potencial para terapia Auger.

Com vista à dupla vectorização de complexos de In-111, foram desenvolvidos ligandos proquelantes acíclicos e macrocíclicos susceptíveis de serem funcionalizados com duas moléculas dirigidas a diferentes alvos biológicos (ER e núcleo). Os complexos sintetizados através desta aproximação ([¹¹¹In]ER3AO, [¹¹¹In]E2NLS e [¹¹¹In]E2AO) revelaram elevada capacidade de internalização no núcleo de células tumorais ER(+). Para além disso, os complexos de In-111 contendo a unidade intercaladora **AO** demonstraram em ensaios *in vitro* capacidade de induzir danos na molécula de DNA.

No contexto do desenvolvimento de novas plataformas de radioteranóstica, foi ainda proposto um conjugado peptídico destinado a veicular o radionuclido In-111 para sequências específicas do DNA.

Abstract

The work described in this thesis was focused on the design, synthesis and pre-clinical evaluation of new ^{111}In -compounds for breast cancer theranostics.

To this end, small peptides comprising the LXXLL (L= leucine, X= any other amino acid) sequence (**cER1**, **ER2** and **ER3**) or a phosphorylated tyrosine (**pY**) were synthesized by solid phase synthesis and conjugated to the bifunctional chelators DOTA, DOTAGA or DTPA. The peptide-based ^{111}In -complexes were prepared with high radiochemical yield and purity, at high specific activities. The inactive In-complexes bearing the LXXLL peptides kept the binding affinity to the target receptor: the estrogen receptor (ER). Furthermore, the *in vivo* studies indicated fast blood clearance and selective uptake in the ER-rich tissues of [^{111}In]DOTA-ER3 and [^{111}In]DOTA-cER1, along with moderate resistance towards proteolytic degradation. Indeed, these biological results represent favourable properties for imaging purposes. However, the radioactive complexes bearing the **pY** peptide ([^{111}In]DTPA-pY and [^{111}In]DOTAGA-pY), which were aimed at targeting ER-mediated non-genomic mechanisms, revealed rapid degradation in blood, both *in vitro* and *in vivo*.

The **ER3** peptide was also iodinated at the histidine residue and the resulting [**I**]-ER3 revealed ability to bind to the ER with high affinity. The radioiodinated peptide, [^{125}I]-ER3, demonstrated a significant nuclear internalization in ER(+) breast cancer cells, thus showing potential for Auger therapy.

Convenient synthetic pathways were established for the synthesis of DTPA- and DOTA-based prochelators for the dual-vectorization of ^{111}In -labelled probes with different biological targeting vectors. This multifunctional approach yielded the bivalent radioactive complexes [^{111}In]ER3AO, [^{111}In]E2NLS and [^{111}In]E2AO, which revealed high nuclear internalization in ER(+) breast cancer cells. Moreover, acridine orange (**AO**) containing ^{111}In -complexes revealed ability to induce DNA damage.

Lastly, in the context of the development of new ^{111}In -based radiotheranostic platforms, a DNA-binding peptide based on the amino acid sequence of a transcription factor was proposed in this thesis.

Palavras-Chave

Radiofármacos

Índio-111

Receptor de Estrogénio

Péptidos

Teranóstica

Keywords

Radiopharmaceuticals

Indium-111

Estrogen Receptor

Peptides

Theranostics

General Index

	Page
Acknowledgments	iii
Resumo	v
Abstract	vii
Palavras-Chave	ix
Keywords	ix
General Index	xi
Figures	xvii
Schemes	xxi
Tables	xxiii
List of Symbols and Abbreviations	xxv
<i>Chapter 1: Introduction</i>	3
1.1. Breast Cancer	3
1.1.1. Overview of the Disease	3
1.1.2. Biological and Molecular Heterogeneity of Breast Cancer	5
1.1.3. Therapeutic Strategies	8
1.2. Estrogen Receptor	11
1.2.1. Estrogen Receptor Subtypes and Localization	11
1.2.2. Genomic ER-mediated Transcription Mechanism	13
1.2.3. Non-genomic Model of ER Action	14
1.2.4. Crosstalk between ER and Growth Factor Pathways	16
1.3. Molecular Imaging in Breast Cancer Management	17
1.3.1. Concept and Goals	17
1.3.2. Nuclear Medicine	18
1.3.3. Theranostics	23
1.4. Auger Therapy	24
1.5. Chemistry and Radiochemistry of Indium for Medical Applications	26
1.6. Radiolabelled Peptides	32
1.7. Solid Phase Peptide Synthesis	35

1.8. Thesis Aim and Outline	38
<i>Chaper 2: ¹¹¹In-labelled Peptides towards the Estrogen Receptor</i>	43
2.1. Radiolabelled LXXLL-based Peptides	43
2.1.1. LXXLL Peptides	43
2.1.2. Synthesis and Characterization of the Peptide Conjugates	47
2.1.3. Synthesis and Characterization of the In(III) Complexes	51
2.1.4. Evaluation of the Binding Affinity towards ER α	53
2.1.5. Radiolabelling of the Peptide Conjugates and <i>In Vitro</i> Evaluation of the ¹¹¹ In-labelled Peptides	59
2.1.6. Cellular Uptake Studies of the ¹¹¹ In-labelled Peptides	63
2.1.7. Biodistribution and <i>In Vivo</i> Stability of the Radiolabelled Peptides	66
2.2. Radiolabelled pY-derivatives	72
2.2.1. pY Peptide	72
2.2.2. Synthesis and Characterization of the pY Peptide	73
2.2.3. Synthesis and Characterization of the pY-derivatives	75
2.2.4. Synthesis and Characterization of the In(III) Complexes	79
2.2.5. Radiolabelling of the pY-based Conjugates	81
2.2.6. <i>In Vitro</i> Stability Studies	82
2.2.7. Biological Evaluation of the Radiolabelled Peptides	86
2.3. Conclusions	88
<i>Chapter 3: Radioiodinated ER-targeting Peptide</i>	93
3.1. Radioiodination of Biomolecules in Nuclear Medicine	93
3.2. Synthesis and Characterization of the (Radio)iodinated Peptide	98
3.2.1. Synthesis and Characterization of the ¹²⁷ I-iodinated Peptide	98
3.2.2. Peptide Radioiodination with I-125	100
3.3. Evaluation of the Binding Affinity towards ERα	101
3.4. <i>In Vitro</i> Evaluation of the Radioiodinated Peptide	102
3.5. Biological Evaluation of the ¹²⁵I-labelled Peptide	104
3.5.1. Cell Studies	104
3.5.1. Biodistribution and <i>In Vivo</i> Stability	106
3.6. Conclusions	109

Chapter 4: Dual-targeting ¹¹¹In-labelled probes	113
4.1. Dual-targeting Radiolabelled Probes	113
4.2. Synthesis and Characterization of Prochelators for Dual-vectorization of In(III) Complexes	115
4.2.1. Acyclic “DTPA-like” Prochelator	115
4.2.2. Macrocyclic “DOTA-like” Prochelators	119
4.3. Molecular Vectors for Nuclear Targeting	129
4.3.1. DNA Intercalating Unit: Acridine Orange	128
4.3.1.1. Synthesis and Characterization of Acridine Orange Derivatives	130
4.3.1.2. Synthesis and Characterization of Macrocyclic Prochelators with Acridinium Pendant Arms	132
4.3.1.2.1. Validation of DOTAGA-AO as a DNA-binding Unit	137
4.3.2. Nuclear Targeting Peptide: Nuclear Localization Sequence	144
4.4. Molecular Units for ER Binding	146
4.4.1. Synthesis and Characterization of the LXXLL-based Peptide	146
4.4.2. Synthesis and Characterization of Estradiol Derivatives	147
4.5. Dual-targeting Probes	151
4.5.1. Synthesis and Biological Evaluation of a LXXLL-based Dual-targeting Radioconjugate	151
4.5.2. Synthesis and Biological Evaluation of Estradiol-based Dual-targeting Radioconjugates	158
4.6. Conclusions	165
Chapter 5: DNA-binding Peptide for Radiotheranostics	169
5.1. DNA-binding Peptides	169
5.2. Synthesis of the DNA-binding Dimeric Peptide	171
5.2.1. Synthesis by Solid-Phase Fragment Condensation	172
5.2.2. Synthesis by Fragment Condensation in Solution	179
5.3. Conclusions	182
Chapter 6: Conclusions and Future Perspectives	185

Chapter 7: Experimental Section	195
7.1. Solvents and Reagents	195
7.2. Purification and Characterization Techniques	196
7.2.1. Thin Layer Chromatography	196
7.2.2. Column Chromatography	196
7.2.3. High Performance Liquid Chromatography	196
7.2.4. Instant Thin Layer Chromatography	203
7.2.5. Nuclear Magnetic Resonance Spectroscopy	203
7.2.6. Mass Spectrometry: Electrospray Ionization	204
7.2.7. Mass Spectrometry: Matrix-Assisted Laser Desorption/Ionization – Time of Flight	204
7.3. Synthesis and Characterization of Peptides and Peptide Conjugates	204
7.3.1. Synthesis of ER1, ER2, ER3 and pY	205
7.3.2. Synthesis of DOTA-ER1, DOTA-ER2 and DOTA-ER3	207
7.3.3. Synthesis of cER1 and DOTA-cER1	208
7.3.4. Synthesis of DTPA-pY and DOTAGA-pY	209
7.3.5. Synthesis of GGNLS and ER3 peptides with protected side chains	209
7.3.6. Synthesis of GCN4-based Peptides	211
7.3.6.1. Synthesis of Fragment A	211
7.3.6.2. Synthesis of Fragment B	212
7.3.6.3. Conjugation by Solid Phase Fragment Condensation	213
7.3.6.4. Synthesis of Fragment A2	214
7.3.6.5. Conjugation by Fragment Condensation in Solution	216
7.4. Synthesis of the Peptide-based In(III) Complexes	216
7.4.1. Synthesis of [In]DOTA-cER1, [In]DOTA-ER2 and [In]DOTA-ER3	216
7.4.2. Synthesis of [In]DTPA-pY	217
7.4.3. Synthesis of [In]DOTAGA-pY	217
7.5. Synthesis of the Iodinated ER3 Peptide	217
7.6. Synthetic Protocols and Characterization of Prochelators	219
7.7. Synthesis and Characterization of Acridine Orange Derivatives	233
7.8. Synthesis and Characterization of Macrocyclic Prochelators with Acridinium Pendant Arms	235
7.9. Synthesis and Characterization of DOTAGA-AO and [In]DOTAGA-AO	239

7.10. Synthesis and Characterization of DOTA	240
7.11. Synthesis and Characterization of Estradiol Derivatives	241
7.12. Synthesis and Characterization of the Dual-targeting Conjugates and In(III) Complexes	244
7.13. Evaluation of the <i>In Vitro</i> Stability of pY and DOTAGA-pY in Human Serum	249
7.14. Fluorescence Polarization Binding Assay	249
7.15. Spectroscopic Studies of the Interaction of [In]DOTAGA-AO with DNA	249
7.16. Study of the Interaction of [In]DOTAGA-AO with DNA by Electrophoretic Mobility Shift Assay	250
7.17. Radiolabelling Procedures	251
7.17.1. Radiolabelling with In-111	251
7.17.2. Radiolabelling of ER3 with I-125	252
7.18. <i>In Vitro</i> Stability Studies with the Radiolabelled Compounds	253
7.19. Lipophilicity Determination	253
7.20. Cellular Uptake Studies	254
7.21. Cellular Fractionation Studies	254
7.22. Nuclear Uptake	254
7.23. Evaluation of Radiation-induced Damage to Plasmid DNA	255
7.24. Animal Studies	256
7.24.1. Ethical Statement	256
7.24.2. Biodistribution and <i>In Vivo</i> Stability in Normal Mice	256
7.24.3. Biodistribution in Mice with MCF-7 Xenografts	257
 References	 261

Figures

	Page
Figure 1.1. <i>Chemical structures of tamoxifen, anastrozole and fulvestrant</i>	9
Figure 1.2. <i>Structural domains of ERα and ERβ</i>	12
Figure 1.3. <i>Classic genomic ER-mediated mechanism</i>	14
Figure 1.4. <i>Signalling network activation by steroids</i>	15
Figure 1.5. <i>Schematic overview of SPECT and PET</i>	18
Figure 1.6. <i>Chemical structures of [^{18}F]-FES and Z-^{123}I]MIVE</i>	22
Figure 1.7. <i>Chemical structure of [^{18}F]-FFNP</i>	22
Figure 1.8. <i>Scheme representing the three pillars of the theranostic approach</i>	23
Figure 1.9. <i>Schematic representations of electron capture and Auger emission</i>	24
Figure 1.10. <i>Representation of the densely localized ionizations produced by Auger electrons within DNA and deposited energy in DNA by I-125 at different distances from the DNA center</i>	25
Figure 1.11. <i>^{111}In decay scheme by electron capture</i>	27
Figure 1.12. <i>Representation of a targeted radiopharmaceutical and its key components</i>	29
Figure 1.13. <i>Chemical structures of selected BFCs suitable for In(III) complexation</i>	31
Figure 1.14. <i>Structure of DTPA-octreotide and whole-body gamma-camera OctreoScan images</i>	34
Figure 1.15. <i>Schematic overview of the SPPS methodology</i>	36
Figure 2.1. <i>Representative ribbon diagram of ERα LBD bound to agonist ligand and coactivator LXXLL peptide</i>	44
Figure 2.2. <i>Comparison between the experimental and the simulated ESI-MS spectra of [In]DOTA-ER3</i>	53
Figure 2.3. <i>Fluorescence polarization curves of FL-SRC1B2SRC with increasing concentrations of the LXXLL peptides</i>	56
Figure 2.4. <i>Fluorescence polarization curves of FL-SRC1B2SRC with increasing concentrations of the Indium complexes</i>	58
Figure 2.5. <i>Representative chromatograms of [^{111}In]DOTA-ER3 and [In]DOTA-ER3</i>	60
Figure 2.6. <i>Radiochemical purity of the ^{111}In-labelled LXXLL peptides after incubation for 48 h (37 °C) in different media: saline, in the presence of excess apotransferrin and in the presence of DTPA</i>	61
Figure 2.7. <i>Radiochemical purity over time of ^{111}In-labelled LXXLL peptides incubated in human blood (37 °C)</i>	62
Figure 2.8. <i>Cellular uptake of the ^{111}In-labelled LXXLL peptides in MCF-7 cells</i>	64
Figure 2.9. <i>Subcellular localization of [^{111}In]DOTA-ER3 in MCF-7 cells (1 h, 37 °C)</i>	65

Figure 2.10.	<i>Comparison of the cellular uptake of [¹¹¹In]DOTA-ER3 in MCF-7, MDA-MB-231 and A431 cells</i>	66
Figure 2.11.	<i>Biodistribution profiles of the ¹¹¹In-labelled LXXLL peptides in CD-1 female mice, 15 min and 60 min p.i.</i>	68
Figure 2.12.	<i>Target/non-target ratios of [¹¹¹In]DOTA-cER1 and [¹¹¹In]DOTA-ER3 60 min p.i. (CD-1 female mice)</i>	69
Figure 2.13.	<i>Radiochromatograms of the injected radiopeptides and of the mice blood and urine 1 h p.i. (CD-1 female mice)</i>	70
Figure 2.14.	<i>Biodistribution profile of [¹¹¹In]DOTA-ER3 in female BALB/c nu/nu mice bearing MCF-7 xenografts at 15, 60 and 180 min p.i.</i>	70
Figure 2.15.	<i>Tumor/background ratios of [¹¹¹In]DOTA-ER3 at 15, 60 and 180 min p.i. (female BALB/c nu/nu mice bearing MCF-7 xenografts)</i>	71
Figure 2.16.	<i>ESI-MS spectrum of the pY peptide and representation of its chemical structure</i>	74
Figure 2.17.	<i>MS/MS spectrum of the pY peptide</i>	75
Figure 2.18.	<i>Radiochemical purity of the ¹¹¹In-labelled pY conjugates after incubation for 24 h (37 °C) in different media: in PBS, in the presence of an excess of apotransferrin and in the presence of DTPA</i>	82
Figure 2.19.	<i>Radiochromatograms of aliquots of human serum after incubation with [¹¹¹In]DTPA-pY and [¹¹¹In]DOTAGA-pY for 1 and 3 hours</i>	84
Figure 2.20.	<i>HPLC chromatograms of the DOTAGA-pY conjugate incubated in human blood serum at different time points (0, 6 and 24 h) and the ESI-MS spectrum of the peak assigned with # in the chromatogram of the 24 hours time point</i>	85
Figure 2.21.	<i>Cellular uptake of [¹¹¹In]DTPA-pY in MCF-7 and MDA-MB-231 cells</i>	86
Figure 2.22.	<i>Biodistribution profile of [¹¹¹In]DTPA-pY and [¹¹¹In]DOTAGA-pY in CD-1 mice 1 h p.i.</i>	87
Figure 3.1.	<i>Chloramine-T (CAT) mechanism in promoting the iodination of tyrosine</i>	96
Figure 3.2.	<i>Chemical structures of the ¹²⁵I-labelled prosthetic groups SIB and SIPC</i>	97
Figure 3.3.	<i>ESI-MS spectrum and chemical structure of [I]-ER3</i>	99
Figure 3.4.	<i>Representative chromatograms of [¹²⁵I]-ER3 (gamma detection) and [I]-ER3 (UV detection)</i>	101
Figure 3.5.	<i>Fluorescence polarization curves of FL-SRC1B2SRC with increasing concentrations of [I]-ER3</i>	102
Figure 3.6.	<i>Radiochromatogram of an aliquot of human serum after incubation for 1 h (37 °C) with [¹²⁵I]-ER3</i>	103
Figure 3.7.	<i>Cellular uptake of [¹²⁵I]-ER3 in MCF-7 and MDA-MB-231 cells</i>	104
Figure 3.8.	<i>Nuclear internalization of [¹²⁵I]-ER3 in MCF-7 cells</i>	105

Figure 3.9.	<i>HPLC radiochromatograms of mice serum and mice urine 1 h after injection of [¹²⁵I]-ER3 in CD-1 mice</i>	107
Figure 3.10.	<i>Biodistribution profile of [¹²⁵I]-ER3 in MCF-7 xenografted BALB/c nude female mice at 15, 60, and 180 min p.i.</i>	108
Figure 3.11.	<i>Tumor/blood and tumor/muscle radioactivity ratios of [¹²⁵I]-ER3 at 15, 60 and 180 min p.i.</i>	108
Figure 4.1.	<i>Representative ¹³C-NMR spectrum (CDCl₃) of the bisalkylated product 4.6</i>	118
Figure 4.2.	<i>ESI-MS spectrum of the acyclic prochelator PC1</i>	119
Figure 4.3.	<i>Zoom of a representative ¹³C-NMR spectrum (CD₃OD) of PC2 in the region between 77.5 and 180 ppm</i>	123
Figure 4.4.	<i>Representative ¹³C-NMR spectrum (CDCl₃) of PC3 with a zoom of the region between 170 and 176 ppm</i>	125
Figure 4.5.	<i>ESI-MS spectrum of the crude product of PC5</i>	126
Figure 4.6.	<i>Representative ¹³C-NMR spectrum (CDCl₃) of PC6</i>	127
Figure 4.7.	<i>Schematic representation of DNA intercalation</i>	128
Figure 4.8.	<i>Chemical structures of acridine and acridine orange (AO)</i>	129
Figure 4.9.	<i>ESI-MS spectrum of the crude product of PC5-AO</i>	133
Figure 4.10.	<i>HPLC chromatograms of the reaction mixture of the methyl ester deprotection at 1 and 3 hours after the addition of LiOH</i>	134
Figure 4.11.	<i>Representative ¹H-NMR spectrum (CDCl₃) and zoom of the ESI-MS spectrum of PC7-AO</i>	135
Figure 4.12.	<i>Representative ¹³C-NMR spectrum (CDCl₃) of PC8-AO</i>	136
Figure 4.13.	<i>Representative ¹H-NMR spectrum (CD₃OD) of DOTAGA-AO</i>	137
Figure 4.14.	<i>ESI-MS spectrum of [In]DOTAGA-AO</i>	138
Figure 4.15.	<i>Agarose gel electrophoresis of plasmid DNA incubated with [In]DOTAGA-AO and AO for 24 h at 37 °C in phosphate buffer</i>	139
Figure 4.16.	<i>Spectroscopic evaluation of DNA interaction. a) UV-Vis absorption spectra measured for solutions of [In]DOTAGA-AO and increasing amounts of CT-DNA; b) Fluorescence emission spectra for solutions containing [In]DOTAGA-AO and increasing amounts of CT-DNA</i>	140
Figure 4.17.	<i>Representative gel of plasmid DNA incubated with [¹¹¹In]DOTAGA-AO and [¹¹¹In]DOTA in the absence and in the presence of DMSO</i>	142
Figure 4.18.	<i>Quantitative analysis of the proportion of each DNA isoform (OC, L and SC) after incubation of the plasmid DNA with 2 different activities of [¹¹¹In]DOTAGA-AO and [¹¹¹In]DOTA, in the absence and in the presence of DMSO</i>	143
Figure 4.19.	<i>ESI-MS spectrum and amino acid sequence of GGNSprot</i>	145

Figure 4.20.	<i>ESI-MS spectrum and chemical structure of ER3prot</i>	147
Figure 4.21.	<i>Chemical structure of 17β-estradiol (E2)</i>	148
Figure 4.22.	<i>Representative ¹H-NMR spectrum (CDCl₃) of E2-1</i>	150
Figure 4.23.	<i>Representative ESI-MS spectrum of [In]ER3AO with a zoom showing the isotopic pattern</i>	153
Figure 4.24.	<i>Cellular uptake of [¹¹¹In]ER3AO in MCF-7 and MBA-MB-231 cells</i>	154
Figure 4.25.	<i>Nuclear internalization of [¹¹¹In]ER3AO in MCF-7 cells</i>	155
Figure 4.26.	<i>Representative gel of plasmid DNA incubated with [¹¹¹In]ER3AO in the absence and in the presence of DMSO</i>	156
Figure 4.27.	<i>Quantitative analysis of the proportion of each DNA isoform (OC, L and SC) after incubation of the plasmid DNA with 2 different activities of [¹¹¹In]ER3AO, in the absence and in the presence of DMSO</i>	156
Figure 4.28.	<i>Biodistribution studies of [¹¹¹In]ER3AO in female BALB/c nu/nu mice bearing MCF-7 xenografts at 60 min p.i. a) Biodistribution profile; b) Target/non-target ratios</i>	157
Figure 4.29.	<i>HPLC radiochromatograms of mice serum and mice urine of [¹¹¹In]ER3AO in Balb/C nu/nu mice bearing MCF-7 xenografts 1 h p.i.</i>	158
Figure 4.30.	<i>Zoom of the ESI-MS spectrum of [In]E2AO</i>	162
Figure 4.31.	<i>Cellular uptake of [¹¹¹In]E2NLS and [¹¹¹In]E2AO in MCF-7 and MBA-MB-231 cells</i>	163
Figure 4.32.	<i>Nuclear internalization of [¹¹¹In]E2AO and [¹¹¹In]E2NLS in MCF-7 cells</i>	164
Figure 5.1.	<i>Representation of the full bZIP DNA-binding domain and of a truncated artificial peptide dimer</i>	170
Figure 5.2.	<i>Representation of the proposed final DNA-binding dimeric construct</i>	171
Figure 5.3.	<i>ESI-MS spectrum of the crude product obtained after cleavage and deprotection of the peptide-bound resin obtained by automated-synthesis of the sequence: Fmoc-GPPGKDP AALKRARNTAARRSRARKLQ</i>	174
Figure 5.4.	<i>HPLC chromatogram of the protected peptide (Fragment B) obtained after cleavage from Sieber amide resin</i>	176
Figure 5.5.	<i>HPLC chromatogram of the crude (deprotected) peptide after the coupling reaction by SPFC</i>	178
Figure 5.6.	<i>HPLC chromatogram of the crude (deprotected) peptide after the coupling reaction in solution</i>	182

Schemes

	Page
Scheme 2.1. <i>Schematic representation of the chemical approach employed to synthesize the DOTA-peptide conjugates and the corresponding In complexes</i>	50
Scheme 2.2. <i>Coupling of DTPA and DOTAGA to pY peptide on solid phase</i>	77
Scheme 2.3. <i>Synthesis of DOTAGA(tBu)₄</i>	78
Scheme 2.4. <i>Synthesis of the inactive In(III) complexes of DTPA-pY and DOTAGA-pY</i>	80
Scheme 4.1. <i>Synthesis of the bromide intermediate 4.2</i>	116
Scheme 4.2. <i>Synthesis of the orthogonally protected amino acid 4.5</i>	116
Scheme 4.3. <i>Synthesis of the acyclic prochelator PC1</i>	118
Scheme 4.4. <i>Monoalkylation of DO2AtBu</i>	120
Scheme 4.5. <i>Synthesis of the symmetric prochelator PC2</i>	122
Scheme 4.6. <i>Synthesis of the asymmetric derivatives 4.12, 4.13 and 4.1.4</i>	123
Scheme 4.7. <i>Deprotection of the benzyl ester to yield PC3, PC4 and PC5</i>	124
Scheme 4.8. <i>Synthesis of the prochelator PC6</i>	127
Scheme 4.9. <i>Synthesis of the AO derivatives AO1 and AO2</i>	131
Scheme 4.10. <i>Conjugation of AO2 to PC3, PC4, PC5 and DOTAGA(tBu)₄</i>	133
Scheme 4.11. <i>Deprotection of the methyl- (PC3-AO) or the ethyl- (PC4-AO) ester to yield PC7-AO</i>	134
Scheme 4.12. <i>Alkylation of 4.10 with the AO derivative AO2 to yield PC8-AO</i>	136
Scheme 4.13. <i>Synthesis of DOTAGA-AO</i>	137
Scheme 4.14. <i>Preparation of [In/¹¹¹In]DOTAGA-AO</i>	138
Scheme 4.15. <i>Synthesis of the E2 derivatives functionalized at the 16α position with a four-carbon chain</i>	149
Scheme 4.16. <i>Synthesis of ER3AO</i>	152
Scheme 4.17. <i>Preparation of [In/¹¹¹In]ER3AO</i>	152
Scheme 4.18. <i>Synthetic route towards E2NLS</i>	159
Scheme 4.19. <i>Synthetic route towards E2AO</i>	160
Scheme 5.1. <i>Synthesis of Fragment A</i>	173
Scheme 5.2. <i>Synthesis of Fragment B</i>	175
Scheme 5.3. <i>Synthesis of Fragment A2</i>	180

Tables

	Page
Table 1.1. <i>Mortality rates among women in the EU</i>	4
Table 1.2. <i>Distinctive features of molecular subtypes of breast cancer</i>	6
Table 1.3. <i>Clinically relevant radionuclides for PET and SPECT imaging</i>	19
Table 1.4. <i>Clinically relevant radionuclides for therapy</i>	20
Table 1.5. <i>Mean number of Auger electrons emitted per decay</i>	25
Table 1.6. <i>Stability constants of complex formation between In(III) and selected chelators</i>	28
Table 2.1. <i>Examples of LXXLL-based peptides with high binding affinity towards ERα</i>	45
Table 2.2. <i>Amino acid sequences of the selected LXXLL peptides</i>	47
Table 2.3. <i>Characterization of ER1, cER1, ER2 and ER3 by HPLC and ESI-MS</i>	49
Table 2.4. <i>Characterization of the DOTA-peptide conjugates by HPLC and ESI-MS</i>	51
Table 2.5. <i>Characterization of the In-complexes of the LXXLL derivatives by HPLC and ESI-MS</i>	52
Table 2.6. <i>Binding affinities (IC₅₀) towards the ERα LBD of the unconjugated peptides</i>	56
Table 2.7. <i>Binding affinities (IC₅₀) towards the ERα LBD of the DOTA-conjugates and In-complexes</i>	57
Table 2.8. <i>Characterization of the ¹¹¹In-labelled LXXLL peptides and radiochemical yields</i>	60
Table 2.9. <i>Biodistribution data of [¹¹¹In]DOTA-ER3 in female BALB/c nu/nu mice bearing MCF-7 xenografts at 15, 60 and 180 min p.i.</i>	71
Table 2.10. <i>Characterization of pY peptide conjugates by HPLC and ESI-MS</i>	79
Table 2.11. <i>Characterization of the Indium complexes of the pY-derivatives by HPLC and ESI-MS</i>	80
Table 2.12. <i>Characterization of the ¹¹¹In-labelled pY conjugates and radiochemical yields</i>	81
Table 3.1. <i>Selected iodine radioisotopes used in nuclear medicine</i>	94
Table 3.2. <i>Comparison between the binding affinities of ER3 and [I]-ER3 towards ERα</i>	102
Table 3.3. <i>Biodistribution data of [¹²⁵I]-ER3 in female CD-1 mice at 60 min p.i.</i>	106
Table 4.1. <i>Alkylating agents and monoalkylation yields for the synthesis of compounds 4.7-4.10</i>	121
Table 4.2. <i>Characterization of E2NLS and E2AO by HPLC and ESI-MS</i>	161
Table 4.3. <i>Characterization of [In/¹¹¹In]E2NLS and [In/¹¹¹In]E2AO</i>	162
Table 5.1. <i>Characterization of the final peptide fragments by HPLC and ESI-MS</i>	177
Table 7.1. <i>Characterization of ¹¹¹In-labelled conjugates</i>	252

List of Symbols and Abbreviations

A

AET- Auger Electron Therapy
AF1- Activation Function 1
AI- Aromatase Inhibitor
Ala or A- Alanine
AO- Acridine Orange
ApoTf- Apotransferrin
aq- Aqueous
AR- Androgen Receptor
Arg or R- Arginine
Asn or N- Asparagine
Asp or D- Aspartic Acid

B

BC- Breast Cancer
BFC- Bifunctional Chelator
Boc- tert-Butyloxycarbonyl
Bq- Becquerel
BR- Basic Region
br- Broad
BRCA1- Breast cancer 1 gene
BRCA2- Breast cancer 2 gene
bZIP- Basic Leucine Zipper

C

CAT- Chloramine-T
CD- Circular Dichroism
CN- Coordination Number
cpm- Counts per minute
CT- Computed Tomography
CT-DNA- Calf Thymus DNA
Cys or C- Cysteine

D

d- Doublet
DBD- DNA-binding Domain
dd- Doublet of doublets
DIPEA- N,N- Diisopropylethylamine
DIPEA- N,N-Diisopropylethylamine
DMF- Dimethylformamide
DMSO- Dimethyl sulfoxide
DNA- Deoxyribonucleic Acid
DO2AtBu- Di-tert-butyl-2,2'-(1,4,7,10-tetraazacyclododecane-1,4-diyl)diacetate
DO3AtBu- Tri-tert-butyl-1,4,7,10-tetraazacyclododecane-1,4,7-triacetate
DOTA- 1,4,7,10-Tetraazacyclododecane-1,4,7,10-tetraacetic acid
DOTAGA- 1,4,7,10-Tetraazacyclododecane-1-glutaric acid-4,7,10-triacetic acid

DSB- Double Strand Breaks
DTPA- Diethylenetriaminepentaacetic acid

E

E2- 17 β -estradiol
EC- Electron Capture
EDT- 1,2-ethanedithiol
EGF- Epidermal Growth Factor
EGFR- Epidermal Growth Factor Receptor
EMA- European Medicines Agency
equiv- Molar Equivalent
ER- Estrogen Receptor
ESI-MS- Electrospray Ionization -Mass Spectrometry
ET- Endocrine Therapy
EU- European Union

F

FA- Fluorescence Anisotropy
FDA- Food and Drug Administration
FES- 16 α -fluoro-17 β -estradiol
FL- Fluorescein
Fmoc- 9-fluorenylmethoxycarbonyl
FP- Fluorescence Polarization

G

GEP- Gene Expression Profiling
Gln or Q- Glutamine
Glu or E- Glutamic Acid
Gly or G- Glycine
GPER1- G-protein Coupled Estrogen Receptor 1

H

h- Hour
HATU- O-(7-azabenzotriazole-1-yl)-1,1,3,3,-tetramethyluronium hexafluorophosphate
HBTU- 2-(1H-Benzotriazol-1-yl)-1,1,3,3-tetramethyluronium hexafluorophosphate
HER2- Human Epidermal Growth Factor Receptor 2
HF- Hydrofluoric Acid
His or H- Histidine
HOBt- 1-hydroxy-1*H*-benzotriazole
HPLC- High Performance Liquid Chromatography

I

I.A./g- Injected Activity per gram of tissue
IC- Internal Conversion
IC₅₀- Ligand concentration responsible for a 50% reduction of the biological activity
IHC- Immunohistochemistry
Ile or I- Isoleucine

ITLC- Instant Thin Layer Chromatography

ivDDE- 1-(4,4-Dimethyl-2,6-dioxocyclohexylidene)-3-methylbutyl

J

J- Coupling Constant

K

keV- Kiloelectron-volt

L

L (DNA)- Linear

LBD- Ligand-binding Domain

LDA- Lithium Diisopropylamide

LET- Linear Energy Transfer

Leu or L- Leucine

log $P_{o/w}$ - Logarithm of octanol/water partition coefficient

Lys or K- Lysine

M

m- Multiplet

mAb- Monoclonal Antibody

MALDI-TOF- Matrix-Assisted Laser Desorption/Ionization – Time of Flight

MAPK- Mitogen-activated Protein Kinase

mDTPA- Diethylenetriamine-N,N,N'',N''-tetra-tert-butyl acetate-N'-acetic acid

min- Minute

MIVE- 17 α -iodovinyl-11 β -methoxyestradiol

MS- Mass Spectrometry

MS/MS- Tandem Mass Spectrometry

Mtt- 4-Methyltrityl

N

NaOAc- Sodium acetate

NODAGA- 1,4,7-Triazacyclononane-1-glutaric acid-4,7-diacetic acid

NIS- Na⁺/I⁺ Symporter

NIS- Nuclear Localization Sequence

NOTA- 1,4,7-triazacyclononane-1,4,7-triacetic acid

NR- Nuclear Receptor

NMP- N-Methyl-2-pyrrolidone

NMR- Nuclear Magnetic Resonance

NHS- N-Hydroxysuccinimide

O

O-2-PhiPr- 2-Phenylisopropyl ester

OBzl- Benzyl ester

OtBu- tert-Butyl ester

OC- Open Circular

P

p.i.- post-injection

PARP- Poly (ADP-ribose) Polymerase

Pbf- Pentamethyl-2,3-dihydrobenzofuran-5-sulfonyl

PBS- Phosphate-buffered Saline

PET- Positron Emission Tomography

PI3-K- Phosphatidylinositol 3-Kinase

PR- Progesterone Receptor

Pro or P- Proline

PyBOP- Benzotriazol-1-yloxytri(pyrrolidino)-phosphonium hexafluorophosphate

Q

q- Quartet

R

RBA- Relative Binding Affinity

RCY- Radiochemical Yield

RCP- Radiochemical Purity

RNA- Ribonucleic Acid

RT- Room Temperature

Rt- Retention Time

R_f- Retardation Factor

rpm- Rotation per minute

S

s- singlet

SA- Specific Activity

SC- Supercoiled

Ser or S- Serine

SERD- Selective Estrogen Receptor Downregulator

SERM- Selective Estrogen Receptor Modulator

SIB- N-succinimidy-3-iodobenzoate

SIPC- N-succinimidyl-5-iodo-3-pyridine carboxylate

SPECT- Single Photon Emission Computerized Tomography

SPFC- Solid Phase Peptide Condensation

SPPS- Solid Phase Peptide Synthesis

Src- Tyrosine-protein Kinase

SSB- Single Strand Breaks

T

t- triplet

t_{1/2}- Half-life

TBDMS-Cl- tert-Butyldimethylsilyl chloride

TBTA- *tert*-Butyl-trichloroacetimidate

tBu- tert-Butyl
TF- Transcription Factor
TFA- Trifluoroacetic Acid
THF- Tetrahydrofuran
Thr or T- Threonine
TIS- Triisopropylsilane
TLC- Thin Layer Chromatography
TNBC- Triple-Negative Breast Cancer
Trt – Trityl
Tyr or Y- Tyrosine

U

UV- Ultraviolet
UV-Vis- Ultraviolet Visible

γ - Gamma
 α - Alpha
 β - Beta
 β^+ -Positron
 δ - Chemical Shift
 ε - Molar Absorptivity
 λ - Wavelength

Chapter 1

Introduction

1. Introduction

1.1. Breast Cancer

1.1.1. Overview of the Disease

Cancer is a leading cause of morbidity and mortality worldwide and constitutes an enormous burden on society. In 2012, 14 million new cases were diagnosed and this number is expected to rise about 70% in the next two decades [1, 2]. The occurrence of cancer is increasing due to the growth and aging of the population particularly in less developed countries which currently account for about 65% of cancer deaths worldwide. The adoption of lifestyle behaviours that are known to increase cancer risk, such as tobacco use, poor diet, physical inactivity, and reproductive changes have further contributed for the growing cancer burden. The five most common incident sites of cancer in 2012 were the lung (13%), breast (11.9%), colorectum (9.7%), prostate (7.9%) and stomach (6.8%) [1]. Besides the societal cost associated to the losses of lives, cancer has an escalating economic impact. In 2009, across the European Union (EU) the health-care costs of cancer were equivalent to 102€ per citizen and in Portugal the cancer-related health-care costs totalled 564 million euros [3]. Prevention and early detection have been described by the World Health Organization (WHO) as the cornerstones of the global response to cancer [4].

Breast cancer (BC) is the most frequently diagnosed cancer among females worldwide accounting for approximately 30% of the new cancer cases [5]. In 2012, nearly 1.7 million women were diagnosed with BC across the world [1]. BC is also, by far, the most prevalent cancer with 6.3 million survivors diagnosed within the previous five years [5]. The economic burden of this disease is evident as in 2009 BC accounted for the highest health-care costs in Europe (6.73 billion euros, 13% of all cancer-related health-care costs) with drug spending being the major component (46%) [3].

Some risk factors for BC have not favourably changed over the last decade. Thus, in the developed countries, parity has decreased, the age of first birth has increased and breastfeeding has become less frequent. Potentially modifiable BC risk factors have also included weight gain after the age of 18, being overweight or obese (for postmenopausal BC), use of menopausal hormone therapy (combined estrogen and progestin), physical inactivity and alcohol

consumption. However, important factors known to increase the risk of BC are not modifiable such as the older age, early menarche, late menopause and family history. Inherited mutations in *BRCA1* and *BRCA2* genes account for 15%-20% of all familial BCs and the risk of developing BC is between 45% and 65% for the mutation carriers [4, 5].

In Europe, the predicted BC mortality rate in 2017 is 14.0/100 000 women, the second highest cancer-related death rate surpassed only by lung cancer (Table 1.1) [6]. However, for young (< 45 years old) and elderly (> 74 years old) women BC still is the leading cause of cancer death. Nevertheless, BC mortality has shown a steady fall over the last 25-30 years both in Europe and in USA. From its peak in the late 1980's BC mortality declined by over 20% across the EU and specifically in Portugal the rate fell approximately 16% between 1997 and 2007 [7].

Table 1.1. Mortality rates among women in the EU for the year 2017 and comparison figures for data from 2012. Adapted from [6].

Cancer	Observed ASR ^a 2012	Predicted ASR ^a 2017
Stomach	3.20	2.76
Colorectum	9.98	9.31
Pancreas	5.43	5.62
Lung	13.84	14.55
Breast	15.19	14.03
Uterus	4.98	4.71
Leukaemias	2.74	2.42
All cancers	87.65	84.51

^aASR: age-standardized mortality rates using the world standard population.

The major contribution to the favourable BC mortality trend has been the advancements in BC treatments, in particular the wider adoption of adjuvant antiestrogens therapy and chemotherapy [7]. Mammography screening, which became widespread in the 1990's, and BC earlier diagnosis have also contributed for the persistent fall of the mortality rate. In fact, it is well-known that BC detection at an early stage enables more treatment options. Furthermore, the survival rates are lower among women with a more advanced stage of the disease at diagnosis. Despite the value of mammography in BC early diagnosis, not all BCs can be detected by this screening tool. Moreover, mammography has sometimes led to false-positive results as well as to overtreatment cases [1, 8].

Following the appropriate screening examination, if cancer is suspected, microscopic analysis of breast tissue is required for a definitive diagnosis and to determine the extent of spread (*in situ* or invasive) and characterize the type of the disease. Most diagnosed BCs (approximately 80%) have broken through the walls of the glands or ducts where they originated and have grown into the surrounding breast tissue and therefore are known as invasive BCs. The prognosis of this type of BC is strongly influenced by the extent or spread of the cancer when it is first diagnosed. In fact, metastatic BC (spread to distant organs) have a 5-year relative survival rate of only 22% compared with almost 100% if the tumor has not spread to the lymph nodes or distant sites [4].

1.1.2. Biological and Molecular Heterogeneity of Breast Cancer

Although BC is generally referred as a single disease, it is important to highlight that it is a heterogeneous complex of diseases characterized by different biological features that lead to differences in response patterns to various treatment modalities and to distinct clinical outcomes. Traditionally BC cases have been classified according to immunohistochemistry (IHC) markers including the presence or absence of estrogen receptor (ER), progesterone receptor (PR) and excess levels of human epidermal growth factor receptor 2 (HER2). However, the receptors' status along with the classical clinicopathological variables (tumor size, tumor grade and nodal involvement) have limitations for patient-tailored treatment strategies. In fact, the traditional classification system does not reflect the underlying complex genetic alterations and the biological events involved in BC development and clinical progression [9, 10].

The advent of high-throughput platforms for gene expression analysis such as microarrays has led to an expanding spectrum on BC subtypes with distinct gene expression patterns and molecular portraits [11]. In the beginning of the century, Sørlie et al. conducted pioneering studies of gene expression profiling (GEP) by investigating the expression pattern of thousands of genes in breast tumors and their correlation to specific phenotypic features and clinical outcomes [12]. The GEP study resulted in the classification of the disease into five different intrinsic subtypes as displayed in Table 1.2: luminal A, luminal B, HER2-enriched, basal and normal-like tumors. Each subtype is associated with a defined IHC status with the exception of normal-like tumors which share a similar IHC profile with the luminal A subtype [11].

Table 1.2. Distinctive features of molecular subtypes of BC. Adapted from [11, 13].

Molecular Subtype	Frequency	ER/PR/HER2 Status	Genes of proliferation	Prognosis
Basal-like	10-20%	ER(-) PR(-) HER2(-)	High	Bad
HER2-enriched	15-20%	ER(-) PR(-) HER2(+)	High	Bad
Normal-like	5-10%	ER(+) PR(+) HER2(-)	Low	Intermediate
Luminal A	50-60%	ER(+) PR(+) HER2(-)	Low	Excellent
Luminal B	15-20%	ER(+) PR(+) HER2(-) ER(+) PR(+) HER2(+)	High	Intermediate Bad

Approximately 75% of breast cancers are positive for ER and/or PR and express genes that encode typical proteins of luminal epithelial cells, thus constituting the luminal group of breast tumors. The luminal-A is the most common subtype and is the one with the best prognosis and the lowest relapse rate. Despite having the same ER(+) and PR(+) status, the luminal B subtype presents an increased expression of proliferation-related genes thus having a more aggressive phenotype and a worst prognosis [9]. In clinical practice the level of the proliferation marker Ki67 has been used to differentiate between luminal-A and luminal-B tumors [14].

HER2-enriched cancer accounts for 15-20% of BC cases. These tumors are characterized by high expression of the HER2 gene and other genes associated with the HER2 signalling pathway. Tumors belonging to this subtype do not express hormone receptors or their expression is too low compared with the luminal group. On the other hand, the HER2 overexpression confers more aggressiveness to the tumor and can lead to a worse prognosis [9]. However, currently this subtype of BC is often successfully treated with targeted therapies aimed at the HER2 protein and consequently the overall survival of patients has significantly increased in the last 15 years [15].

The third type of BC tumors belong to the basal-like subgroup and express high levels of basal myoepithelial markers such as cytokeratins 5/14/17 and laminin. This subtype does not express ER, PR and HER2, hence being referred as triple-negative breast cancer (TNBC). However, the term triple-negative refers only to the IHC classification of breast tumors lacking ER, PR and HER2 expression, whereas the basal-like classification can only be defined via gene expression microarray analysis which is not currently available in most clinical settings [16]. In

fact, only 75% of TNBC cases can be classified as basal-like [9]. Women carrying the mutated BRCA-1 gene have a 50% chance of developing TNBC and this subtype is more frequent in women of African ancestry, particularly below the age of 50 years [17]. These tumors are of particular interest because they follow an aggressive clinical course with a high rate of metastasis to the brain and lung and a high recurrence rate within the first 3 years after the diagnosis. The lack of targeted systemic therapies contributes for the poor prognosis and higher mortality rate of this subtype of breast tumors [18].

Finally, breast tumors grouped in the last subtype, normal-like, are poorly characterized and express characteristics of adipose tissues, presenting an intermediate prognosis between luminal and basal-like cancers. These tumors have been sparsely studied and their clinical significance remains unclear [9].

This classification into different molecular intrinsic subtypes incorporate a powerful prognostic and predictive value and has been accepted by the international community as the basis for the therapeutic decisions. However, for practical reasons the subtypes are usually approximated using the four IHC markers (ER, PR, HER2 and Ki67) rather than gene expression profiles [19].

Nevertheless, in the last decade several multigene tests have become commercially available for predicting the outcome in patients with newly diagnosed BC. These tests primarily rely on quantification of ER and proliferation-related genes and combine these into multivariate prediction models. In fact, there is growing consensus that these assays provide prognostically relevant information in patients with ER(+) and HER2(-) early-stage BC in particular the assessment of the risk of recurrence within the first 5 years. Although relatively expensive to perform, use of some multigene signatures such as MammaPrint (Agilent, Amsterdam, Netherlands) and Oncotype DX (Genomic Health, Redwood City, CA, USA) has shown to be cost-effective as they reduce the use of adjuvant chemotherapy in patients that would not benefit from it. The development of extended multivariate prediction models has been an area of intense research [20, 21].

1.1.3. Therapeutic Strategies

The selection of the best therapeutic approach for each BC patient depends on both tumor- and patient-related factors. Tumor factors primarily include the presence or absence of targetable features such as hormone receptors and HER2, and the evaluation of the metastatic potential, as reflected in measures of proliferation and anatomic extent of the disease. On the other hand, patient factors include menopausal status, age and comorbidities [22].

The first step and most common form of treatment for non-metastatic BC is surgery. The primary goals of BC surgery are the complete resection of the primary tumor from the breast and the determination of the stage of the disease by removing and evaluating one or more regional lymph nodes [23, 24]. Surgery is usually followed by adjuvant therapy with the aim of eradicating any undetected tumor cells (micrometastases) that may remain after resection of the primary tumor. Adjuvant treatments for BC can involve locoregional radiotherapy and systemic therapies that include chemotherapy, endocrine therapy (ET) and targeted therapies [22, 24, 25]. These systemic therapies can also be applied as neoadjuvant (preoperative) treatments to reduce the tumor burden before surgery [23, 26]. Furthermore, systemic therapies are the first line of treatment for advanced (metastatic) BC [27].

In the historical perspective of BC pharmacological treatment, the development of endocrine and HER2-targeted therapies constituted major milestones by allowing a shift from the aggressive chemotherapy protocols to more targeted and better tolerated treatments. In fact, these therapies have contributed greatly for the improvement of both survival and quality of life of BC patients [15, 28]. The combination of different therapeutic approaches to best adjust to the molecular and clinical profile of each BC has been a frequent strategy to optimize treatment efficacy [29, 30].

Endocrine Therapy

ER-positive breast cancers rely strongly on estrogen signalling for proliferation, and hence the most effective strategy to inhibit the growth of these hormone-sensitive tumors has been to block estrogen action using endocrine therapy (ET). ET aims to modulate or to disrupt the function or presence of the ER or the endogenous production of estrogens [29].

First synthesized in 1960s, tamoxifen (Figure 1.1) is a selective ER modulator (SERM) that acts as an antagonist of the ER in BC cells. This SERM has until recently been the gold standard

for the adjuvant (post-operative) treatment of ER-positive BCs, showing effectiveness in reducing the recurrence rates by half when given for five years [29]. Tamoxifen has also been used for BC prevention in high-risk women, being effective in reducing the risk in 38% over ten years. Although several other SERMs have entered clinical development, including droloxifene, idoxifene, toremifene, miproxifene and raloxifene, none has shown to be of superior efficacy comparing to tamoxifen [28].

Aromatase inhibitors (AIs) represent another class of drugs that are used in ET. AIs act by competitively binding to the aromatase enzyme preventing the synthesis of estrogens in peripheral tissues, which are the main source of estrogens in postmenopausal women. The first and second generations of AIs were supplanted by the third generation which have demonstrated increased potency, greater specificity and reduced toxicity. Anastrozole (Figure 1.1) was the first third-generation AI to be approved for treatment of patients with advanced BC who had progressed following tamoxifen. However, further studies have been showing that anastrozole as well as exemestane and letrozole are superior to tamoxifen in post-menopausal women leading to their approval as first line treatment [28, 29, 31].

Fulvestrant (Figure 1.1), approved in 2002, is a selective estrogen receptor downregulator (SERD) and has a different mode of action comparing to the other ET drugs [29]. Unlike tamoxifen, which has a partial agonist activity in some tissues (bone, endometrium, vasculature), fulvestrant is a pure ER antagonist. The molecule is approved as treatment in post-menopausal women with advanced BC who have progressed or recurred after prior anti-estrogen therapy [28].

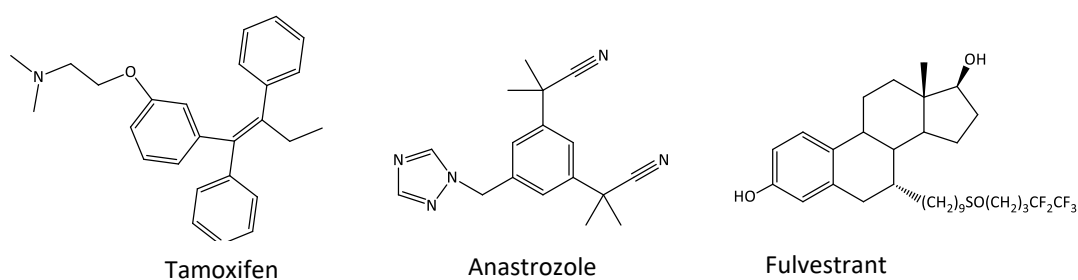


Figure 1.1. Chemical structures of tamoxifen (SERM), anastrozole (AI) and fulvestrant (SERD).

Despite the benefits of endocrine therapy in the treatment of ER(+) breast cancer, resistance to treatment eventually occurs in a large number of patients. Studies have shown that recurrence on adjuvant endocrine therapy occurs in approximately 10-15% of patients within 5

years and the recurrence rate can reach 30% by 15 years [32]. Moreover, the long-term effects of ET in metastatic disease are limited to an average of 15 months after which there is development of resistance in more than 80% of treated woman [33]. This unequivocally represents an unmet need for personalized therapy for hormone-positive breast tumors.

HER2-targeted Therapies

For the treatment of breast tumors that overproduce the growth-promoting protein HER2 there are targeted therapies available that have improved the prognosis for this subtype. The monoclonal antibody trastuzumab was the first commercially available HER2 targeting agent and has pharmacological action by binding to an extracellular domain of HER2 [34]. Trastuzumab, when used in combination with chemotherapy, extends the overall survival and slows disease progression. However, approximately 50% of the HER2 positive metastatic BCs have shown *de novo* or acquired resistance to trastuzumab [35]. Pertuzumab, another humanized anti-HER2 monoclonal antibody, binds to a different subdomain of the HER2, effectively blocking its dimerization. The theoretical advantage of dual targeting of the HER2 has been investigated by evaluating the potential benefit of combining trastuzumab and pertuzumab. The good clinical results led to the approval of pertuzumab by FDA and EMA in combination with docetaxel and trastuzumab as first line therapy for HER2 positive metastatic BCs [34, 36]. Lapatinib, a small-molecule inhibitor of the intracellular tyrosine kinase domain of HER2 has shown to block the growth factor downstream signaling pathways and hence has also been used to overcome resistance to trastuzumab [37].

Therapeutic Approaches for Triple-Negative Breast Cancers

Treatment of TNBC has been particularly challenging due to the absence of targeted therapies. Anthracycline and taxane-based chemotherapy has been the standard treatment for this subtype of BC. More recently, two new chemotherapeutic options, ixabepilone and eribulin, were introduced for taxane-refractory metastatic breast cancers [17]. BRAC-like TNBC tumors present high sensitivity to alkylating and platinum drugs due to the deficiencies in the DNA repair mechanisms in consequence of the BRCA mutations, and therefore the addition of carboplatin and cisplatin has been suggested for these patients. Poly (ADP-ribose) polymerase-1 (PARP) inhibitors, such as olaparib, can also take advantage of these repair deficiencies promoting DNA

lesions in mutation carriers [38]. Additional promising molecular targets for TNBC treatment include the androgen receptor (AR), the nonreceptor tyrosine kinase Src, the growth factor PI3K-Akt-mTor pathway, and cyclin-dependent kinases. The study of the effectiveness of the combination of novel targeted agents with standard chemotherapeutic regimens has been an area of intense research in the last years [17, 39, 40].

1.2. Estrogen Receptor

1.2.1. Estrogen Receptor Subtypes and Localization

Nuclear receptors (NRs) are DNA-binding and ligand-regulated transcriptional factors that play crucial roles in many aspects of human physiology and consist of an important family of drug targets. This superfamily is divided into two classes: I and II, according to specific features in the ligand binding domain (LBD) sequences of the receptors. Class I NR includes the steroid hormone receptors: ER α , ER β , PR A, PR B, glucocorticoid receptor, mineralocorticoid receptor, and the androgen receptor (AR). These receptors bind to response elements in DNA as homodimers. On the other hand, class II NR represents the retinoic acid receptor, retinoid X receptor, vitamin D receptor, peroxisome proliferator activated receptor and the thyroid receptor. Class II receptors exist in the nucleus as heterodimers with RXR receptors as partners [41-43].

In the early 1960s, it was demonstrated that a specific protein, now known as ER, was responsible for the concentration of physiological levels of estradiol and for a long time it was assumed that only one human ER (ER α) was present in cells. However, in the late 1990s a second receptor, the human ER β , was identified and characterized [44].

Like other nuclear receptors, the ERs have a multidomain structure consisting of six functional regions, from the N-terminal A/B domain to the C-terminal F domain (Figure 1.2) with various degrees of sequence homology.

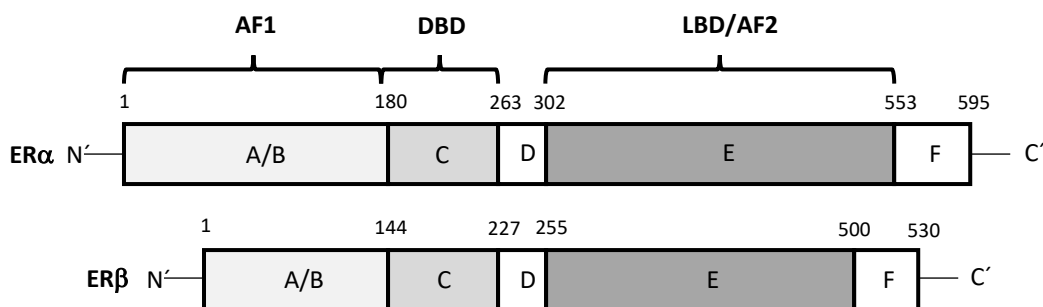


Figure 1.2. Structural domains of ER α (595 amino acids) and ER β (530 amino acids). Adapted from [45].

The poorly conserved A/B domain, also called activation function 1 (AF1), is responsible for protein-protein interactions and transactivation. The functions of AF1 are not dependent on ligand binding [44].

The subsequent C domain harbors the DNA-binding domain (DBD) and is highly homologous. This domain is characterized by two zinc-finger motifs which are responsible for DNA-binding and for the receptors dimerization [42, 44, 45].

On the other hand, the ligand-binding domain (LBD) is located in the E region (also called AF2), which is linked to the DBD by the D domain. The E-domain also presents an interaction site for coactivators and corepressors. The binding pocket binds a wide range of compounds including estrogens, polycyclic aromatic hydrocarbons, phthalates, pesticides and a class of estrogen-like substances termed xenoestrogens. The ligand binding cavity as well as the interaction site with regulatory peptides contains 11 α -helices (H1, H3-H12) organized in a three-layered sandwich structure with H4, H5, H6, H8 and H9 flanked on one side by H1 and H3, and on the other side by H7, H10 and H11 [42, 46]. The ligand pocket is closed after hormone binding on one side by an antiparallel β -sheet and on the other side by H12. The LBD has much less homology between ER α and ER β (53%) comparing to the DBD (96%) [47].

Despite the modest overall sequence identity (47%), tissue localization studies have revealed distinct expression patterns for each receptor. Whereas ER α is the predominant subtype expressed in breast, uterus, ovaries, and vagina, ER β is primarily detected in the prostate, testis, spleen, intestines and lung [48].

The intracellular distribution of ERs is a matter of controversy and is now thought to be a result of a complex dynamic influenced by factors such as protein-protein interactions, post-translational modifications and ligand binding. Repeated studies with both liganded and

unliganded ER have shown that the great majority of the receptor resides in the cell nucleus. However, this distribution pattern does not necessarily mean that ER is irreversibly confined in the nuclear compartment, since it has been demonstrated that nuclear hormone receptors undergo a dynamic shuttling between nuclear and cytoplasmic compartments resulting from a dynamic equilibrium between nuclear import and export [49].

Evidence has been presented that steroids can also bind to receptors belonging to the 7-transmembrane spanning family, known as G-protein coupled receptors. GPR30, which has now been renamed G-protein coupled estrogen receptor 1 (GPER1), was first described to have all the characteristics of a membrane ER, including high affinity and saturable estradiol binding. In addition, it was demonstrated that GPER1 transduce the signals of estrogenic compounds resulting in up-regulation of adenylyl cyclase activity [50]. The receptor was found to bind SERMs, *e.g.* tamoxifen, as well as antagonists, *e.g.* fulvestrant, creating in both cases an agonistic response, which has raised some questions about the role of GPER1 in the failure of ET in some BC cases [51].

1.2.2. Genomic ER-mediated Transcription Mechanism

In mammals, steroids influence cell proliferation, inflammatory response, cardiovascular health, immunity, bone integrity, cognition and behavior. These effects have so far been attributed to the genomic effects exerted by these hormones through the ERs [52]. According to this classic model, in response to hormone binding, ER undergoes a conformational change, called “activation”, which is accompanied by the dissociation of heat shock proteins (hsp70 and hsp90) forming ultimately a ER homodimer. The enhancement of transcriptional activity can then be mediated by two mechanisms. In the “direct binding” mechanism (Figure 1.3), the agonist-occupied ER binds directly to the DNA through a specific sequence called estrogen response element (ERE) and interacts with coactivator proteins and components of the RNA polymerase II transcription initiation complex. On the other hand, in the “tethering” mechanism, instead of binding directly to the DNA, the ER interacts with other DNA bound transcription factors stabilizing their binding to the DNA and/or recruiting coactivators to the complex [53]. The ERs transcriptional activity is therefore dependent on their ability to recruit coactivators which present intrinsic enzymatic activities (histone acetyltransferase, ubiquitin ligase, and arginine methyltransferase) [54]. The most widely studied group of ER coactivators is the p160 protein family that consists of three members, namely: SRC-1/NCoA-1, SRC-2/TIF-2/NCoA-2, and

SRC-3/p/CIP/AIB-1/TRAM-1/RAC-3/ACTR [55, 56]. These coactivators present multiple LXXLL (L-leucine; X - any amino acid) signature motifs called NR boxes that allow the interaction with the AF2 domain of ligand-bound receptors, forming an amphipathic α -helix which makes critical contacts with the residues of H3, H4, H5 and H12 that are part of the hydrophobic groove of the LBD [57]. SRC-1 contains four NR boxes, while SRC-2 and SRC-3 contains three NR boxes each [55]. It is now believed that there are LXXLL recognition sites in other domains other than the LBD. Recently a LXXLL-binding motif has been identified in the proximity of ER α DBD [58].

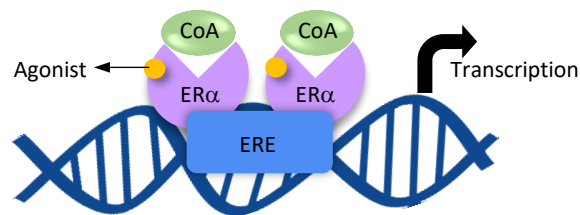


Figure 1.3. Classic genomic signalling in which ligand-activated ER α dimers attach to estrogen response elements (EREs) on DNA and activate transcription through the interaction with coactivators (CoAs). Adapted from [59].

Despite the overlapping properties, ER α and ER β have distinct roles *in vivo* regarding the transcriptional activity. Although ER α enhances the transcription of proliferative genes in BC cells, ER β has been shown to inhibit human BC cells proliferation by repressing the transcription of the *c-myc*, *cyclin D₁* and *cyclin A* genes and increasing the expression of the cyclin-dependent kinase inhibitors, p21 and p27, leading to cell cycle arrest in the G₂ phase. In that respect it is thought that ER β can sequester coactivators affecting the positive transcription of the ER α -regulated genes and/or can stimulate the expression of ER α -regulated repressive genes [56]. Therefore, it is believed that the ER α /ER β ratio is a key element in the regulation of the estrogen transcriptional activity in BC cells [60].

1.2.3. Non-genomic Model of ER Action

For more than 50 years it has been known that rapid effects of steroid hormones resulting from rapid signal transduction pathways can also occur [61]. Depending on the cell origin, activation of these pathways produces different effects, such as proliferation, survival, vasorelaxation, migration and differentiation. Various estrogen-induced signaling cascades have

been identified in the extra-nuclear compartment [62]. The non-genomic pathway involves activation of the tyrosine-protein kinase (Src), mitogen-activated protein kinases (MAPK), phosphatidylinositol 3-kinase (PI3-K), protein kinase C and heterotrimeric G-proteins in the cytoplasm or membrane of cells [60].

Castoria et al. showed that estradiol treatment of the human breast adenocarcinoma MCF-7 cells rapidly induces association of cytoplasmatic ER α with Src and with the regulatory/adaptor p85 subunit of PI3-K (Figure 1.4). One of the PI3-K targets that has received much attention is a serine-threonine kinase named AKT (also known as protein kinase B). Estradiol-activated PI3-K triggers AKT, which in turn upregulates cyclin D1 production, stimulating DNA synthesis and cell cycle progression [63]. PI3-K also plays an important role in non-proliferative hormonal effects, such as cytoskeletal changes through the activation of the GTPase Rac [64]. It has also been recently reported that estrogens activation of PI3-K/AKT pathway controls the nuclear export of the ER α in MCF-7 stimulating the cell cycle progression by increasing the cytoplasmatic pool of ER and therefore promoting the non-genomic proliferative action [65]. Estrogens also stimulate the Src/Shc/Ras/Erk signaling pathway [64]. The association of ER with Src has revealed to be crucial for the activation of the entire signaling network. This association is dependent on the phosphorylation of the tyrosine residue 537 of the ER α that is involved in the interaction with the Src SH2 domain [66].

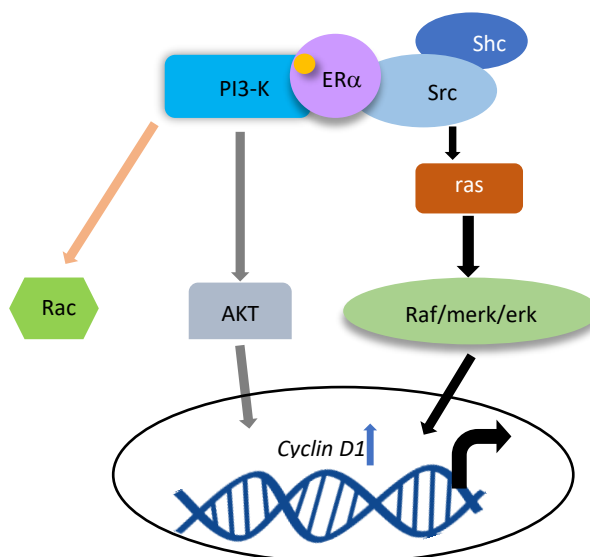


Fig.1.4. Signalling network activation by steroids. The two main signal transduction pathways (Src/Ras/Erk and PI3-K/AKT) that stimulate cell proliferation are represented. Adapted from [64].

Estrogens can also elicit rapid non-genomic effects through GPER1, promoting the rapid activation of MAPKs Erk-1 and -2 and stimulating the PI3-K pathway as studies in fibroblast-like COS7 cells transfected with the receptor demonstrated [67]. Calcium mobilization and an increase in the production of cyclic adenosine monophosphate are also effects mediated by GPER1 [68, 69].

The two mechanisms (genomic and non-genomic) do not represent all the complexity of ER action. In fact, there is evidence that the genomic and non-genomic actions of ER are integrated [62]. The non-genomic ER-mediated activation of Erk is thought to induce phosphorylation of the co-activator SRC-3 leading to its translocation to the nucleus where affects positively the ER-mediated transcription. These observations provide evidence for an early non-genomic action of ER that regulates the downstream genomic effects of steroids [70].

1.2.4. Crosstalk between ER and Growth Factor Pathways

There is growing evidence that BC growth is regulated by coordinated actions of ER and various growth factor receptor signaling pathways, especially the epidermal growth factor receptor (EGFR) family [71]. Actually, it is known that epidermal growth factor (EGF) activity converges on the ER in human mammary cancer cells eliciting cell proliferation and cytoskeleton rearrangement. Migliaccio et al. showed that EGF induces tyrosine phosphorylation of ER preassociated with AR triggering the assembly of the ER/AR/Src complex with EGFR. This observation led to the important conclusion that EGF induces, through EGFR, ligand-independent extranuclear ER activation [72]. Conversely, ERs mediate the transcription of the EGFR itself and of growth factor ligands (*e.g.* TGF α) and intracellular signaling intermediates of the growth factor cascades (*e.g.* IRS-1) [73]. GPER1 is also known to transactivate EGFR by promoting the release of heparin-bound EGF [68]. Evidence suggests that the crosstalk between ER and growth factor receptor pathways is an important mechanism in the development of endocrine-resistance [74].

1.3. Molecular Imaging in Breast Cancer Management

1.3.1. Concept and Goals

The evaluation of the hormone receptor status in BC is a powerful tool for guiding treatment and predicting clinical outcomes for each individual patient. As previously explained, therapeutic decisions are currently mostly based on the knowledge of the molecular profile of each BC [19]. In fact, the availability of targeted therapies reinforces the importance of this evaluation in order to select the patients that can benefit from ET and identify the ones that need other therapeutic approaches [25, 75].

The assessment of the receptor status of the breast tumor is usually performed in a tissue sample obtained by a biopsy. However, the analysed sample may not represent the tumor heterogeneity, particularly in the case of metastatic disease in which the receptor status can differ greatly between the primary tumor and the metastatic lesions and even between the different metastatic sites. Moreover, the location of the metastatic disease may not be amenable to biopsy (e.g., brain or bone) [76]. On the other hand, the emerging genomic and proteomic technologies have increasingly led to therapeutic approaches that are tailored for each patient. Therefore, there has been the need to develop standard methods to assess the heterogeneity of the tumors that could integrate molecular and physiological information specific of each patient. Molecular imaging can address these issues and is a key component of the new healthcare *paradigma* of personalized medicine [75, 77].

Molecular imaging is the noninvasive *in vivo* characterization and measurement of biological processes at the cellular and molecular levels. Besides allowing the localization of the tumor in the body, it also provides imaging of the expression/activity of specific molecules (such as receptors and protein kinases), as well as biological processes (such as angiogenesis and hypoxia) which influence tumor behaviour and response to treatment [78].

In BC management, molecular imaging agents have been developed to achieve the following goals: (i) the early detection of molecular or physiological alterations that indicate the presence of the tumor, (ii) the characterization of the disease in terms of intrinsic molecular subtype, (iii) the ability to evaluate and adjust the treatment protocols for each patient in real time, and (iv) the ability to streamline the drug development process [75].

1.3.2. Nuclear Medicine

Nuclear medicine is the branch of medical molecular imaging that uses drugs that incorporate a radionuclide in its constitution, named radiopharmaceuticals, for diagnostic and therapeutic purposes. In nuclear medicine imaging, radiopharmaceuticals are administered in a subnanomolar concentration range and therefore are not intended to have any pharmacological effect. Instead, the emission of photons associated to radionuclides' decay allows to generate an image that provides relevant information about specific biochemical and physiological processes in the tissues [79, 80].

Radionuclide selection for diagnostic imaging is mainly based on two imaging modalities: Single Photon Emission Computerized Tomography (SPECT) or Positron Emission Tomography (PET). The principles of the two modalities are represented in Figure 1.5.

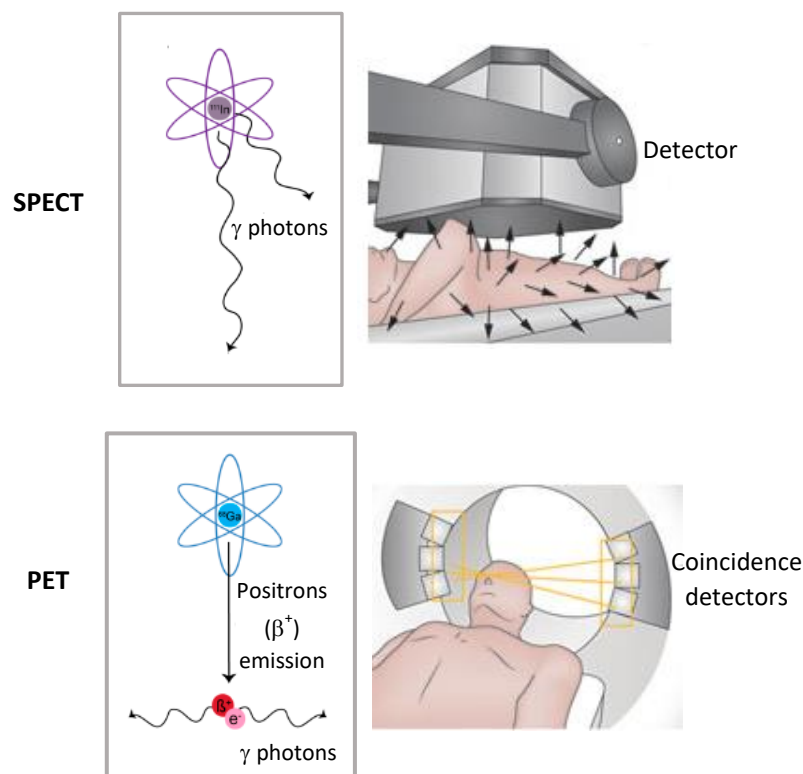


Figure 1.5. Schematic overview of the physics principles of SPECT and PET (on the left) and representation of SPECT and PET scanners (on the right). Adapted from [64, 81].

For SPECT imaging, gamma (γ) photons resulting from radionuclides, such as ^{111}In , are captured by detectors at multiple positions around the longitudinal axis of the patient. The

gamma ray energy should be high enough to minimize attenuation in the patient and low enough so that it can be efficiently stopped within the detector. Thus, the ideal gamma ray energy range for SPECT imaging is between 80 and 300 keV [82]. In this modality, the tomographic image is obtained through a gamma camera consisting of a NaI (TI) scintillation detector which rotates around the patient detecting the γ -radiation in the various anatomical planes. A signal is then generated and processed by computer for image reconstruction [83].

In PET imaging, positrons (β^+) emitted by radionuclides, such as ^{68}Ga , interact with electrons (annihilation reaction) resulting in the formation of two γ -rays (of 511 keV each) that are emitted in approximately opposite directions [84, 85]. These two photons are detected by two detectors in coincidence and data collected over many angles around the body axis of the patient are used to reconstruct the image of the activity distribution [83].

In Table 1.3 some of the most relevant radionuclides used for SPECT and PET imaging are presented.

Table 1.3. Clinically relevant radionuclides for PET and SPECT imaging and the respective half-lives ($t_{1/2}$). Adapted from [11, 13, 86].

SPECT		PET	
Radionuclide	$t_{1/2}$ (h)	Radionuclide	$t_{1/2}$ (h)
$^{99\text{m}}\text{Tc}$	6.02	^{18}F	1.83
^{111}In	67.9	^{68}Ga	1.13
^{67}Ga	78.3	^{64}Cu	12.7
^{123}I	13.2	^{86}Y	14.7

In addition to providing information about disease characterization and therapeutic response, nuclear tools can also have therapeutic value. By replacing the imaging isotope (i.e., gamma or positron emitters) with alpha (α), beta (β^-) or auger-electron emitters, or by integrating a cytotoxic drug in the imaging agent, a radiopharmaceutical can be turned into a therapeutic agent [87-89]. Table 1.4 presents selected radionuclides with relevant therapeutic properties.

Table 1.4. Clinically relevant radionuclides for therapy. Adapted from [86, 90, 91].

Radionuclide	$t_{1/2}$ (h)	Decay mode
^{177}Lu	161	β^- , γ
^{131}I	192	β^- , γ
^{67}Cu	61.9	β^- , γ
^{90}Y	64.1	β^-
^{111}In	67.9	EC ^a , γ , Auger e ⁻
^{211}At	7.2	α

^aEC: electron capture

Whether designed for diagnosis or therapy, specificity of radiopharmaceuticals is essential to minimize the unnecessary radiation exposure of the non-targeted tissues. Therefore, the radionuclide is frequently linked to a targeting biomolecule that determines the fate of the radiopharmaceutical when injected in the body [85]. The development of highly specific and selective radiopharmaceuticals capable of targeting disease-specific biomarkers and overcoming biological barriers has been a key issue facing the research community in nuclear medicine [92].

Radiopharmaceuticals for Breast Cancer Imaging

The critical importance of the ER status for the BC clinical management has made this receptor the most studied target in the development of radiopharmaceuticals for breast tumor imaging. In fact, in the past decades a greater emphasis has been placed on the synthesis of radioprobes intended for receptor-targeted nuclear imaging of BC using either SPECT or PET [76, 93-95]. However, the development of the “ideal” radiopharmaceutical for BC is still an unmet challenge due to issues such as specificity, sensitivity, feasible chemistry and cost-effectiveness [92].

The development of PET probes for BC management has received more attention due to the appearance of the promising ^{18}F -labelled estrogen derivative, 16α -[^{18}F]- 17β -estradiol ([^{18}F]-FES) (Figure 1.6). FES exhibited a relative binding affinity (RBA) towards ER α of 80% compared to estradiol (RBA = 100%) proving the high affinity towards the receptor. Studies have revealed that the radiofluorinated estradiol analogue can reliably detect ER-positive tumors and

that the low uptake of [^{18}F]-FES is a strong predictor of antihormonal therapy failure, in which case cytotoxic therapy should generate more benefit for the patient [35]. In the clinical setting, [^{18}F]-FES has generated clear PET images of primary and metastatic breast tumors [96]. The radiopharmaceutical has also shown to be useful in the evaluation of the early response to endocrine treatment and in the determination of the optimal dose of ER α antagonists [76, 97]. Computed tomography (CT) has been combined with PET (PET/CT) providing anatomic information useful for the accurate interpretation of the PET signal. However, fast metabolic degradation *in vivo* and high liver uptake are important drawbacks presented by [^{18}F]-FES. Furthermore, small volume BC lesions are often not identified by [^{18}F]-FES, which represents a limitation for perioperative detection [98]. Aiming to optimize the *in vivo* properties of this radiofluorinated radiopharmaceutical, several analogues functionalized with different substituents at positions 11, 17 and 6 of the estradiol ring have been described, although none has replaced [^{18}F]-FES in clinics [99-101].

Despite the high sensitivity, the need of an on-site cyclotron (due to the short half-life of ^{18}F and other PET radioisotopes) makes PET an expensive technology with only limited availability [75]. Therefore, efforts have been made to synthesize estradiol derivatives labelled with gamma emitters for SPECT imaging which remains the more practical approach for routine diagnostics in nuclear medicine due to the use of medium to long-lived radionuclides such as ^{123}I , $^{99\text{m}}\text{Tc}$ and ^{111}In . Many radioiodinated estradiol derivatives have been explored as potential SPECT agents with the most promising one being the ^{123}I -labelled *cis*-11 β -methoxy-17 α -iodovinylestradiol (Z-MIVE) (Figure 1.6), which besides demonstrating high ER affinity (RBA = 31%) and selectivity, has also demonstrated to be a useful tool to predict response or resistance to antiestrogen treatment *in vivo* [94, 102, 103].

Both steroidal and non-steroidal estrogen analogues have also been labelled with the widely available radionuclide $^{99\text{m}}\text{Tc}$ using pendant and integrated chelator approaches. Nayak et al. described a $^{99\text{m}}\text{Tc}$ -estradiol-pyridin-2-yl hydrazine derivative with an alkyne linkage that demonstrated receptor-mediated uptake in human breast adenocarcinoma MCF-7 tumors [104]. Estradiol analogues labelled with ^{111}In for hormone-receptor targeting have also been reported [88]. Despite the efforts, all of these radioprobes have failed to provide an alternative to [^{18}F]-FES (PET). In fact, the excessive lipophilicity of these agents and the high liver and intestine uptakes associated with the low tumor-to-background ratios have been important drawbacks for the development of ER-targeting probes for SPECT imaging. Moreover, the complex chemistry involved in the synthesis of these compounds and the low yields obtained have further hampered their development [88, 104, 105]. Therefore, there is a pressing need

for chemical strategies that can provide cost-effective imaging of breast tumor with clinical translation potential [106].

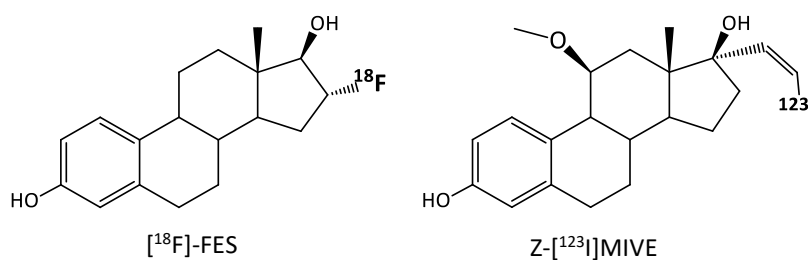


Figure 1.6. Chemical structures of 16 α -[^{18}F]-17 β -estradiol ([^{18}F]-FES) and of *cis*-11 β -methoxy-17 α -[^{123}I]iodovinylestradiol (Z-[^{123}I]MIVE).

Prognostic and predictive information can also be gained from knowledge of the PR status. In fact, PR expression is known to depend on the ER-signaling pathway and therefore can be used to measure the treatment-induced changes in the upstream signaling. The most promising agent for PR nuclear imaging has been 21- ^{18}F -fluoro-16 α ,17 α -[(*R*)-(1'- α -furylmethylidene)dioxy]-19-norpregn-4-ene-3,20-dione ([^{18}F]-FFNP) (Figure 1.7) that is currently being studied as early-response biomarker for response to endocrine therapy [76, 107].

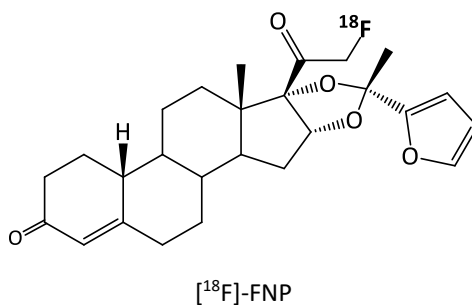


Figure 1.7. Chemical structure of 21- ^{18}F -fluoro-16 α ,17 α -[(*R*)-(1'- α -furylmethylidene)dioxy]-19-norpregn-4-ene-3,20-dione ([^{18}F]-FFNP)

The increasing evidence of the complementary role of growth factor activation and cell-cycle control pathways for the appearance of resistance to ET have led to the development of molecular imaging probes targeting not only HER2, but also unexplored targets such as the chemokine receptor CXCR4 and the σ_2 -receptor [87, 108, 109]. Aiming to achieve a better

assessment of the molecular complexity of the tumor in each patient, a multi-target imaging approach might be one interesting and fruitful option in the future [87].

1.3.3. Theranostics

The concept of theranostics, which refers to the combination of diagnostic imaging and therapeutic effect in a single agent, is rapidly gaining momentum in oncology. This approach involves the delivery of therapeutic cargo to cancer-specific targets that can be noninvasively imaged, thus sparing the normal tissue and optimizing the therapeutic/toxicity ratio in “real-time” (Figure 1.8). Theranostics provides the transition from the conventional “one size fits all” to the personalized medicine and represents an approach especially suited for complex and heterogeneous diseases such as BC [110, 111]. Integrating molecular imaging functionalities into therapy is expected to fulfil the promise of delivering “the right care to the right patient at the right time” [112].

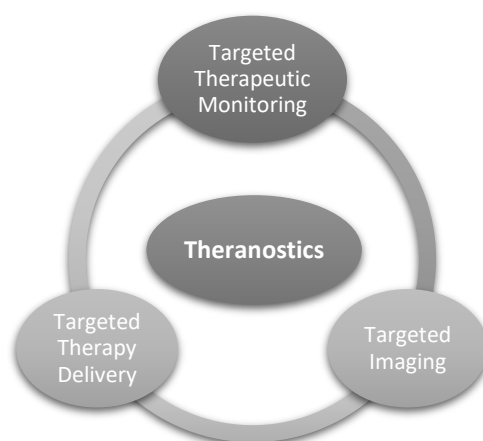


Figure 1.8. Scheme representing the three pillars of the theranostic approach. Adapted from [112].

For BC management, research for new theranostic nuclear tools has focused mainly in HER2-targeting antibodies or antibody fragments radiolabelled with the pair ^{68}Ga (β^+ , PET)/ ^{177}Lu (β^- , therapy), ^{123}I (γ , SPECT)/ ^{131}I (β^- , therapy), and with ^{111}In (SPECT and Auger therapy simultaneously) [113-116]. Peptides targeting the gastrin releasing peptide receptor (GRPR) radiolabelled with the pair $^{68}\text{Ga}/^{177}\text{Lu}$ have also been explored for BC theranostics [117]. Integrating a chemotherapeutic agent (*e.g.* doxorubicin) in targeted radioconjugates is also an approach that has been described for BC imaging and therapy [118].

1.4. Auger Therapy

More than 50% of all radionuclides commonly utilized for diagnostic imaging decay by electron capture (EC) or internal conversion (IC). In addition to diagnostically useful photons, these radionuclides emit numerous low-energy electrons through a complex series of atomic processes. Briefly, when radionuclides decay by EC or IC a vacancy is created in the inner atomic shell of the residual atom which consequently undergoes a series of transitions until the ground state is reached. These transitions can be radiative, which result in the emission of a characteristic X-ray, and nonradiative which are characterized by the ejection of an orbital electron [119]. The most common transitions of the latter type are the Auger transitions which were named in honor of the French physicist Pierre Auger that described the phenomenon for the first time in 1925. In an Auger transition an initial vacancy in a lower major shell is filled by an electron from a higher major shell and part of the released energy is transferred to another electron of an outer major shell that is ejected from the atom (Figure 1.9). As the innermost vacancy shell moves toward the valence shell, a cascade phenomenon develops with corresponding vacancy multiplication and emission of numerous electrons referred to as Auger electrons [119, 120].

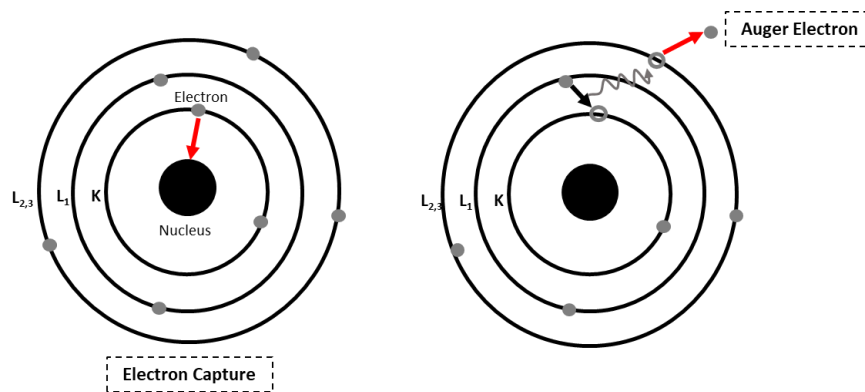


Figure 1.9. Schematic representation of electron capture (on the left) and Auger emission (on the right). Adapted from [121].

Auger electrons have very low energies (less than a few hundred eV), intermediate values of linear energy transfer (LET) (10-25 keV/μm), and extremely short ranges (several nm) in biological matter. After the cascade is completed, a very high local energy density is deposited within several cubic nanometers around the point of decay [119, 122]. The total Auger electron yield per decay for some clinically relevant radioisotopes is summarized in Table 1.5 [123].

Table 1.5. Mean number of Auger electrons emitted per decay for selected radionuclides. Adapted from [123].

Radionuclide	Auger yield
^{99m}Tc	4.0
^{67}Ga	4.7
^{111}In	14.7
^{123}I	14.9
^{125}I	24.9

The submicroscopic energy deposition of Auger electrons has been studied from the radiobiological point of view since DNA and the proteins that form the nucleoprotein complex have dimensions that are within the range of these electrons (Figure 1.10) [120]. The first studies in mammalian cells were performed using ^{125}I with the radioisotope directly incorporated into nuclear DNA. These studies demonstrated that the decay of DNA-incorporated ^{125}I was highly toxic to the cells leading to a monoexponential decrease in survival similar to the effect generated by the high-LET α particles [122, 124]. Furthermore, Monte Carlo calculations in which I-125 was positioned within or at very short distance (nm) from cylindrical double-stranded DNA predicted that the decay of this isotope can lead to the efficient production of double-strand breaks in DNA [120]. The same genotoxicity has been verified for other Auger emitters such as ^{99m}Tc and ^{111}In [113, 125, 126].

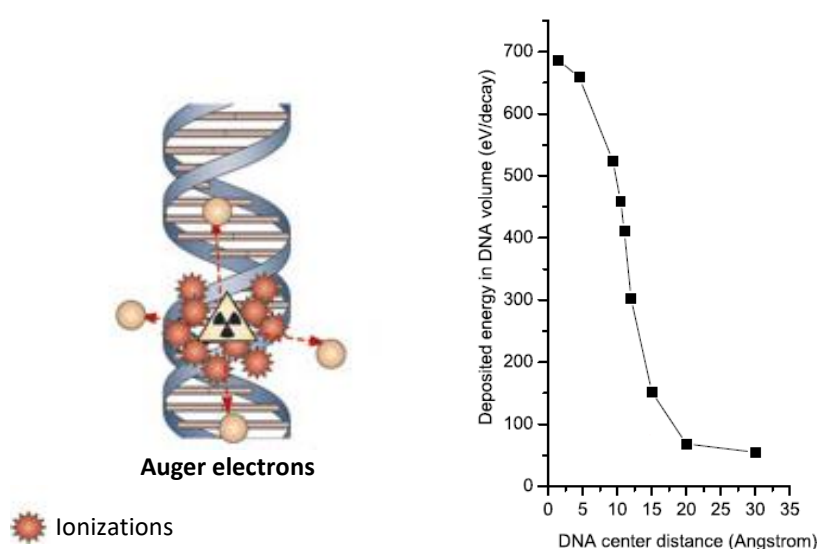


Figure 1.10. On the left: representation of the densely localized ionizations produced by Auger electrons within DNA (adapted from [127]). On the right: deposited energy in DNA by the Auger emitter I-125 at different distances from the DNA center (adapted from [125]).

An important prerequisite for Auger electrons to exert a cytotoxic effect is the localization in the cell nucleus in close proximity ($< 1 \mu\text{m}$) to DNA. In fact, it has been demonstrated that when produced in the cytoplasm, the effects of Auger electrons are not significantly lethal and the survival curves are typical of those caused by radiations of low LET [123].

The therapeutic effectiveness of Auger electron emitters for cancer treatment has been demonstrated in recent years with target-specific radioimmunoconjugates and radiopeptides labelled with ^{111}In demonstrating the ability to reduce tumor size or arrest tumor growth in animal models [128-130]. In this respect, Auger electron therapy (AET) has the important advantage of offering the possibility of targeted cytotoxicity with virtually minimal damage to the surrounding tissues due to the very short range of the emitted electrons. Furthermore, the emission of gamma photons by many of the Auger emitting radionuclides makes possible the combination of diagnostic imaging with therapeutic effect in a single theranostic agent [120].

1.5. Chemistry and Radiochemistry of Indium for Medical Applications

Indium (In) is an element of group IIIB of the periodic table with the electron configuration $[\text{Kr}]4d^{10}5s^25p^1$. Although it can assume lower oxidation states, Indium typically shows the +3 oxidation state in aqueous solution which is the most relevant state for radiopharmaceuticals. In acidic aqueous solution below pH 3.0, In(III) likely exists in the ionic form as the hexaaqua complex $[\text{In}(\text{H}_2\text{O})_6]^{3+}$, while at pH values higher than 3.4 the metal hydrolyzes and forms the insoluble hydroxide $\text{In}(\text{OH})_3$ which precipitates from solution. In fact, this propensity for hydrolysis represents a major challenge for the preparation of In(III) complexes for biomedical applications [131].

The most clinically relevant Indium radioisotope is In-111 (^{111}In) which has a half-life of 67.9 h (2.83 days). ^{111}In is cyclotron-produced by proton irradiation ((p,2n) reaction) of cadmium Cd-112 enriched target. The target is processed by ion exchange and solvent extraction techniques, evaporated to dryness from isopropyl ether and redissolved in sterile, pyrogen-free 0.05 M HCl. The relatively long half-life allows ^{111}In to be distributed over a wide geographical area from the production site.

The ^{111}In nucleus decays exclusively by electron capture (EC) to stable ^{111}Cd with associated gamma ray emissions at 171 keV and 245 keV with 90% or greater photon yields. The

produced gamma radiation has been extensively used for SPECT imaging in the clinical setting [132]. There is also some internal conversion (IC) generating Auger electron emissions in the range 19-23 keV which are suitable for therapeutic applications [133]. The ^{111}In decay scheme is shown in Figure 1.11.

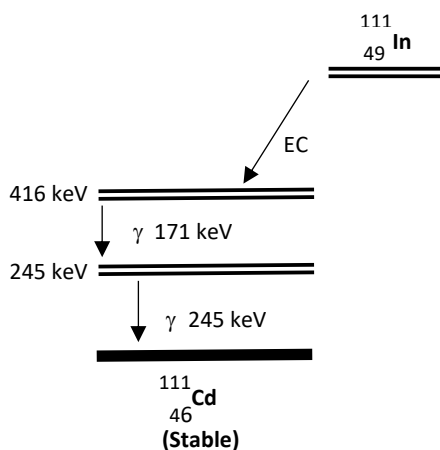


Figure 1.11. ^{111}In decay scheme by EC. Adapted from [131].

In(III) is considered a hard Lewis acid ($\text{pK}_a = 4.0$) and for this reason the formation of stable complexes usually requires the use of polydentate chelators presenting anionic oxygen donor groups and amines [85, 131]. The ionic radius of In^{3+} is 0.92 \AA and the coordination number (CN) can range from 4 to 8 with heptadentate and octadentate chelates offering the most stable complexes [134]. The formation of coordination complexes with this trivalent metal usually occurs by ligand exchange from weak complexes such as citrate and acetate, which are aimed to prevent hydrolysis at pH values around 5-6 while the higher stability complex is being formed with a stronger chelator. For *in vivo* applications, In(III) also needs to be in a highly stable complex to prevent transchelation to the serum iron transporter protein transferrin for which In^{3+} has high affinity due to its chemical similarities with Fe^{3+} [135]. The stability constants of In(III) complexes with selected chelators are shown in Table 1.6.

Table 1.6. Stability constants of complex formation between In(III) and selected chelators. Adapted from [131] and [136].

Chelator	log K_{ML}^a
DTPA	29.0
EDTA	21.7
DOTA	23.9
NOTA	26.2
Transferrin	18.7
Acetate	3.50

$$^a K_{ML} = [ML]/[M][L].$$

Bifunctional chelators for In(III) complexation

As previously stated, the development of target-specific radiopharmaceuticals is a challenging issue in nuclear medicine. The design of target-specific radiopharmaceuticals usually comprises four key components (Figure 1.12): a target-specific vector (peptide, small molecule or antibody), a bifunctional chelator, a linker, and the selected radiometal [137]. The bifunctional chelator (BFC) is an essential unit of a target-specific radiopharmaceutical and has the dual function of binding the radiometal and incorporating a chemically reactive functional group for covalent attachment to the biomolecule/targeting vector which is responsible for conferring biological specificity to the final radioconjugate. The attachment of the targeting moiety to the BFC is usually performed through a linker of variable length and nature that can be chemically modified in order to modulate the pharmacokinetics of the radioconjugate [79, 138]. The conjugation strategies usually involve functional groups such as carboxylic acids or activated esters for amide couplings, isothiocyanates for thiourea couplings, and maleimides for thiol couplings. In recent years click chemistry has also gained popularity for the conjugation of BFCs to targeting biomolecules [139].

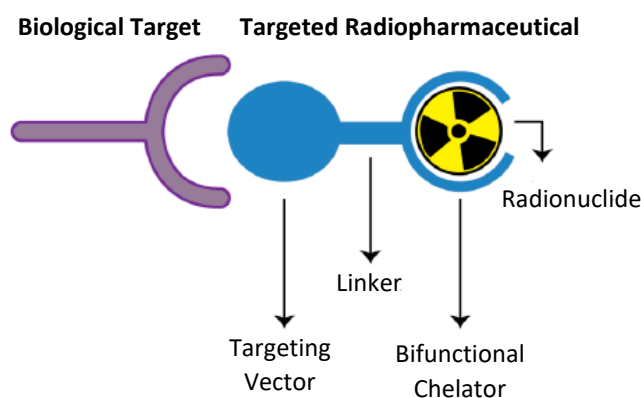


Figure 1.12. Representation of a targeted radiopharmaceutical and its key components. Adapted from [87].

Selection of an appropriate BFC is based on the best-fit of the radiometal governed by preferences in coordination chemistry and donor-ability of the chelator in order to form stable and inert metal-chelate complexes [140]. The most applied BFCs in the synthesis of target-specific In-based radiopharmaceuticals have been based on the acyclic diethylenetriaminepentaacetic acid (DTPA) and on the macrocycles 1,4,7,10-tetraazacyclododecane-1,4,7,10-tetraacetic acid (DOTA) and 1,4,7-triazacyclononane-1,4,7-triacetic acid (NOTA). However, it should be noted that acyclic chelator complexes are typically less kinetically inert *in vivo* than macrocyclic complexes despite exhibiting faster metal-binding kinetics [136]. Therefore, macrocycle chelators, especially DOTA-based, have been preferred for *in vivo* applications [141].

DTPA (Figure 1.13), the most used acyclic ligand, has been extensively used to coordinate In^{3+} . $[\text{In}]\text{-DTPA}$ complexes can feature both 7- as well as full 8-coordination by the chelator in distorted pentagonal bipyramidal and square antiprismatic geometries, respectively [136]. On the other hand, the attachment of a (bio)molecule to one of the carboxylic acids of DTPA leads to a heptadentate chelator in which the amide carbonyl oxygen remains uncoordinated [142]. For this conjugation reaction to take place, one of the five carboxylic acids of DTPA has to be activated. However, this strategy suffers from lack of selectivity [143]. Carboxylic activation can be also obtained by the transformation of DTPA in the corresponding cyclic bisanhydride (DTPA-bisanhydride) (Figure 1.12). A major drawback of this synthetic pathway is that after conjugation to the biomolecule through an amide bond two products are possible: DTPA-monoamide and DTPA-bisamide [141]. Therefore, to avoid the formation of dimers, the best option is to use tetra-protected DTPA derivatives with only one free carboxylic

acid available to react. A six-step process to perform the synthesis of these BFCs is reported, although it is not very straightforward and the yields are low [144]. However, tetra *tert*-butyl-protected DTPA is now commercially available.

Noteworthy, when one of the carboxylic acids is converted into a carboxamide, the stability constant of the metal complexes decreases [143]. Therefore, octadentate DTPA analogues substituted at the backbone with an isothiocyanate (*p*-SCN-Bn-DTPA) or an aminobenzyl (*p*-NH₂-Bn-DTPA) group for biomolecule coupling, have been in the last years a popular option for the construction of targeted radiopharmaceuticals [145, 146]. Furthermore, Williams and Rapoport and later Anneli et al. described an efficient and fast synthesis procedure of functionalized DTPA derivatives starting from inexpensive and readily available amino acids, such as glutamic acid, aspartic acid, lysine and phenylalanine, that are able to octacoordinate In(III) while linking the metal to a biomolecule [147-149].

The valuable macrocycle octadentate chelator DOTA (Figure 1.13) has also been shown to form a robust complex with In(III). Studies with monoamide armed (*p*-aminoanilide) derivatives have shown that in the solid state eight donor atoms (N₄O₄) are bonded to the In³⁺ center forming a complex with a twisted square antiprismatic geometry. However, in solution there is dissociation of the acetamide-oxygen from In³⁺ and the metal becomes heptacoordinated [150]. As in DTPA, in the construction of biologically targeted probes, the replacement of an anionic donor group (carboxylate) with a non-ionic functional group (amide) leads to a decrease in complex stability. Nevertheless, this decrease in thermodynamic stability has not compromised the utilization *in vivo* and most often the kinetic inertness is almost unchanged [143].

The synthesis of DOTA-like chelators has represented an intense field of research. In an approach similar to *p*-SCN-Bn-DTPA, the bifunctional chelator *p*-isothiocyanatobenzyl DOTA (*p*-SCN-Bn-DOTA) (Figure 1.13) has been widely used for attaching ¹¹¹In to peptides and antibodies of clinical interest [151]. Furthermore, the commercially available tris-protected DOTA (DOTA-tris(*tert*-butyl ester)) bearing a single free carboxylic acid has been a widespread option for the conjugation to peptides and small molecules [152]. DOTA-based BFCs with maleimide or thiol functionalities have also been described and used for the radiolabeling of peptides and antibodies [153, 154]. Mäcke and co-workers reported the synthesis of DOTAGA (Figure 1.13), a DOTA-like chelator comprising a glutamic acid sidearm, that after the conjugation to a biomolecule still presents four intact acetate arms giving the possibility of a CN of 8 for In(III) [143, 152, 155]. More recently, DOTA derivatives with alkyne, azide and cyclooctyne

functionalities intended for site-specific “click”-chemistry reactions with biomolecules have also been reported [156-158].

NOTA, although being the smallest member of the cyclic polyamino polycarboxylic ligand family and being more suitable for the complexation of Gallium (Ga), has also been used to coordinate In(III). Eisenwiener et al. described the synthesis of the derivative NODAGA (Figure 1.13), that apart from the three carboxylic acids of NOTA presents an extra pendant arm suitable for the coupling with targeting biomolecules [159]. NOTA derivatives with a isothiocyanate group in the backbone have also been used for the synthesis of In-based radiopharmaceuticals [160].

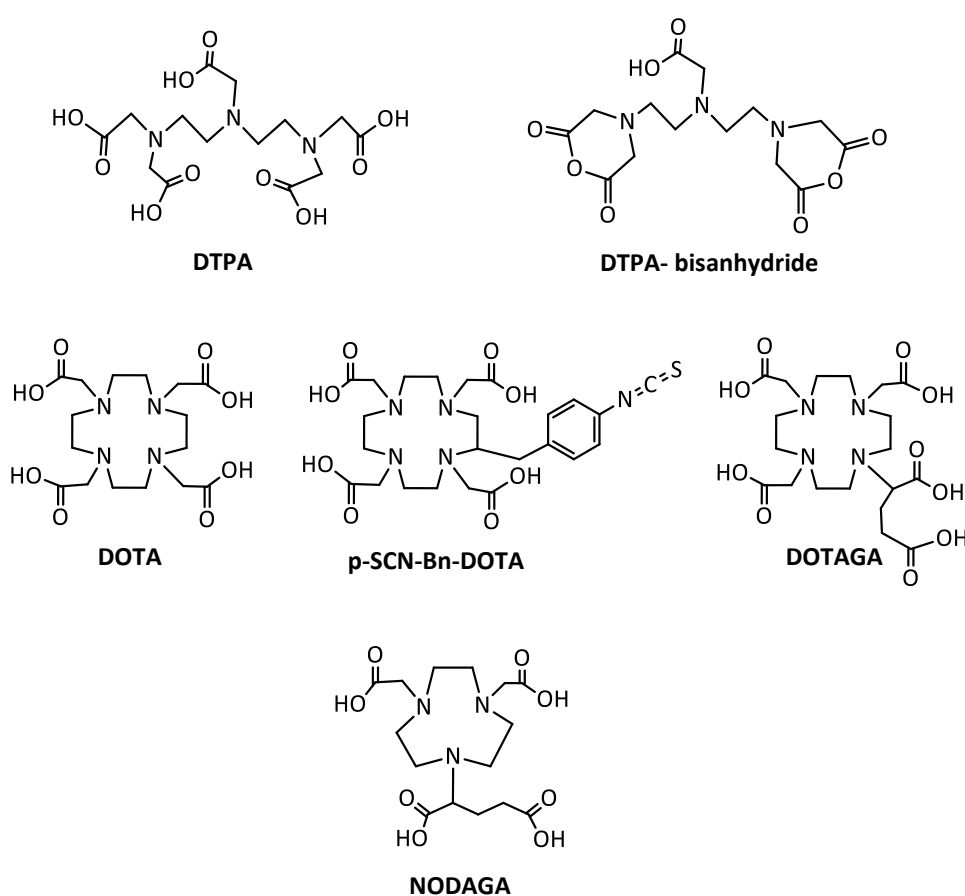


Fig.1.13. Chemical structures of selected BFCs suitable for In(III) complexation.

1.6. Radiolabelled Peptides

An ideal target-specific radiopharmaceutical should have high binding affinity and specificity for the targeted receptor. Furthermore, it should be rapidly cleared from non-target tissues in order to ensure an adequate target-to-background ratio. Therefore, the selection of the targeting vector is critical for the design of a successful targeted radiopharmaceutical. High stability and integrity under physiological conditions, low immunogenicity and cost-effective production are other important requirements that should be taken into account during the selection of the target specific-moiety [161, 162].

Monoclonal antibodies (mAbs) have long been considered potentially ideal targeting agents for the design of targeted radiopharmaceuticals. Several radiolabelled mAbs have been evaluated for both diagnosis and therapy in patients. Two radiopharmaceuticals based on mAbs have been approved by FDA ($^{111}\text{In}/^{90}\text{Y}$ -ibritumab tiuxetan, Zevalin[®] and ^{131}I -tositumomab, Bexxar[®]) for patients with non-Hodgkin lymphoma and introduced in clinics with high success rates. However, mAbs use has been limited by several disadvantages, which are mainly related to their high molecular weight. In fact, significant sequestration by reticuloendothelial cells and slow blood clearance and excretion rate are important pharmacokinetics-related drawbacks usually presented by antibodies. Although some improvements through protein engineering have been made in the last few years, the search for more effective targeting agents is still a demanding challenge facing the radiopharmaceutical chemistry community [79, 163].

Following the finding that a variety of disease-related cell receptors are able to bind small regulatory peptides with high affinity, the use of peptides has emerged as another approach for delivering radioactivity to specific targets. Indeed, analogues of regulatory peptides have been radiolabelled and studied for more than 20 years in the fields of oncology, neurology, cardiology, inflammation/infection, atherosclerosis and thrombosis [79, 163]. With the advent of phage display technology it has become possible to generate potential high-affinity peptides for any given target. In fact, this technique has contributed decisively for the expansion of the pool of targeting peptides available for the design of new targeted radiopharmaceuticals [79, 164].

Peptides as targeting moieties present unique advantages that make them especially suitable for imaging. Besides high binding affinity (in the nanomolar range) towards disease-related receptors, small peptides (up to 40 amino acids) usually present a rapid clearance from the blood due to high renal excretion and attain a high concentration in the target tissues.

Furthermore, peptides are not taken up by the reticuloendothelial system and therefore are expected to present minimal uptake in the bone marrow, liver or spleen.

In addition to the favorable pharmacokinetics, the clinical application of a peptide-based radiopharmaceutical relies greatly in the evaluation of its *in vivo* stability since naturally occurring peptides are usually highly susceptible to rapid degradation by various plasmatic peptidases [161, 165, 166]. Therefore, several chemical strategies have been reported to improve the enzymatic stability such as the introduction of D-amino acids, use of unusual amino acids or side-chains and amidation and/or acetylation of peptide C- and N-termini [79, 167, 168].

The developments on the field of solid phase peptide synthesis (SPPS) and the availability of automated peptide synthesizers have allowed the fast and easy large-scale synthesis of peptides as well as their facile chemical modification to link radionuclides and to modulate the pharmacokinetic profile [165, 166]. Therefore, these progresses have improved both the chemical feasibility and the cost-effectiveness of the synthesis of peptide-base radiopharmaceuticals.

Peptide-based Radiopharmaceuticals

To date, the vast majority of radiolabelled peptides have found application in oncology, where the same targeting peptide has been often exploited for both diagnostic imaging and targeted therapy by simply varying the radionuclide [169]. The first peptide used for tumor imaging in clinical practice was the somatostatin analogue octreotide. Octreotide, an octapeptide, binds to the somatostatin receptor subtype 2 (sst2) with high affinity and has a prolonged half-life *in vivo*. The peptide was conjugated at the N-terminus with the acyclic chelator DTPA (Figure 1.14) and radiolabelled with In-111 yielding [¹¹¹In]DTPA-octreotide (OctreoScan, Mallinckrodt Inc.) which was the first peptide-based radiopharmaceutical approved for commercialization in 1994. Since then, this ¹¹¹In-labelled analogue has been the gold standard for the detection, staging and follow-up of primary and metastatic neuroendocrine tumors by SPECT and by SPECT/CT [162, 170].

The amino acid sequence of octreotide has since been modified in order to improve the affinity for the different somatostatin receptor subtypes and to modulate the pharmacokinetics. Furthermore, the somatostatin analogues have been also conjugated with the versatile macrocyclic chelators DOTA and DOTAGA and have been radiolabelled with different radionuclides for both imaging and targeted therapy [171, 172]. Currently, besides [¹¹¹In]DTPA-

octreotide, the somatostatin analogues most widely used in the clinical setting for diagnostic purposes are [^{68}Ga]-DOTATOC/DOTATATE/DOTANOC for PET imaging. Additionally, [^{177}Lu]-DOTATATE and [^{90}Y]-DOTATOC have shown impressive therapeutic effects and have also been used in clinics [173].

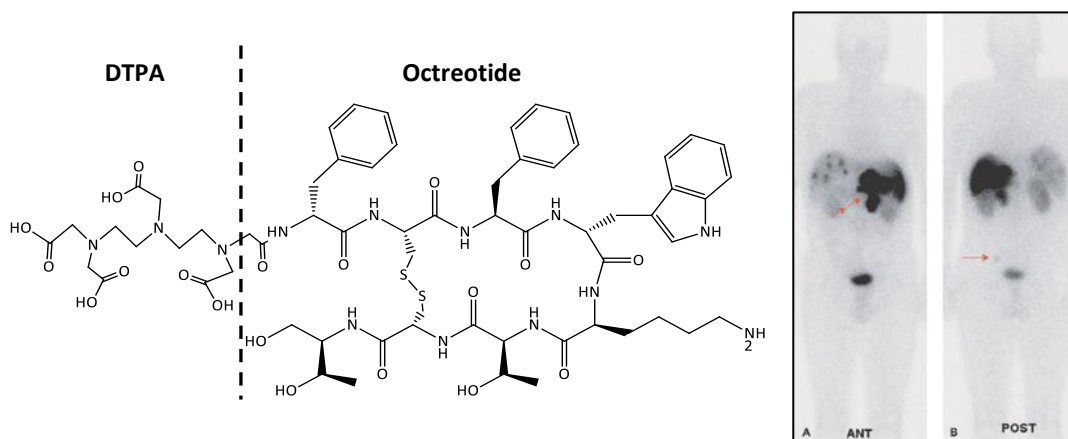


Figure 1.14. Structure of the somatostatin analogue DTPA-octreotide (on the left) that can be labelled with ^{111}In (OctreoScan), and whole-body gamma-camera OctreoScan images (on the right.) showing the detection of lesions (arrows). A: Anteroposterior; B: posteroanterior. Adapted from [174].

Many other naturally occurring peptide analogues such as bombesin, cholecystokinin/gastrin, glucagon-like peptide-1 (GLP-1)/exendin, arginine-glycine-aspartic acid (RGD), neurokinin type 1/substance P, and vasoactive intestinal peptide (VIP) have been explored during the last years and a number of radiolabelled probes with clinical potential have been derived from them. These peptide-based tracers have been labelled with medically relevant radionuclides including $^{99\text{m}}\text{Tc}$, trivalent radiometals (^{111}In , $^{86/90}\text{Y}$, ^{177}Lu , $^{67/68}\text{Ga}$), $^{64/67}\text{Cu}$, ^{18}F and $^{131/123/125}\text{I}$ [86, 158, 175-177]. In fact, the selection of both the radionuclide and the appropriate chelator is critical since it has been shown to strongly affect the receptor binding affinity and the pharmacokinetic pattern of the radiotracer [171, 178, 179].

1.7. Solid Phase Peptide Synthesis

Peptides have played a pivotal role in biological, medical and pharmaceutical research. Therefore, the synthesis of such polyamide structures has been a major focus of organic chemistry for over a century. In 1955, Vicent du Vigneaud was awarded the Nobel Prize for the first synthesis in solution of the neurohypophysial nonapeptide hormone oxytocin. However, for the assembly of longer peptides or small proteins, the repetitive procedures of coupling, deprotection of the N-terminal amino-protection group, isolation and purification of intermediates were found to be very laborious and time-consuming when carried out in solution [180].

In 1963 Merrifield achieved a breakthrough discovery of solid phase peptide synthesis (SPPS) when a functionalized solid support was used for the synthesis of peptide sequences. Since then, all aspects of the SPPS methodology have been further developed and refined, thus extending the reach of synthetic peptide chemistry tremendously.

The basic principles of SPPS are illustrated in Figure 1.15. The C-terminal amino acid (AA1) residue of the target peptide is first attached to an insoluble polymeric support (resin) via its carboxyl group. Any functional groups in amino acid side chains must be masked with semi-permanent protecting groups (Y) that are not affected by the reaction conditions employed during peptide chain assembly. On the other hand, a temporary protecting group (X) masking the α -amino group during the initial resin loading is removed. An excess of the second amino acid (AA2) is introduced with the carboxyl group of this amino acid being activated for amide bond formation by reaction with a coupling reagent (A). After coupling, excess reagents are removed by washing and the protecting group removed from the N-terminus of the dipeptide prior to the addition of the third amino acid residue. This process is repeated until the desired peptide sequence is assembled. In a final step, the peptide is released from the solid support and the side-chain protecting groups are removed [181, 182].

The two most widely used N α -protecting groups in SPPS are the tert-butoxycarbonyl (Boc), used by Merrifield, and the 9-fluorenylmethoxycarbonyl (Fmoc) introduced in 1970 by Carpino [183]. The Fmoc strategy has been preferred in recent years over the Boc strategy for routine synthesis, as the latter usually requires the use of corrosive and toxic hydrofluoric acid (HF) and the necessity for a HF-compatible specialized apparatus. On the other hand, the Fmoc group can be removed under basic mild conditions, usually by treatment with 20% piperidine in DMF, and is typically combined in the amino acid residues with acid-labile side-chain protecting

groups and resin-linkage agents that can be removed in acidic conditions with trifluoroacetic acid (TFA). Therefore, the Fmoc method involves an orthogonal protecting group strategy with the removal of the temporary and of the semi-permanent protection being performed by completely different chemical mechanisms [181].

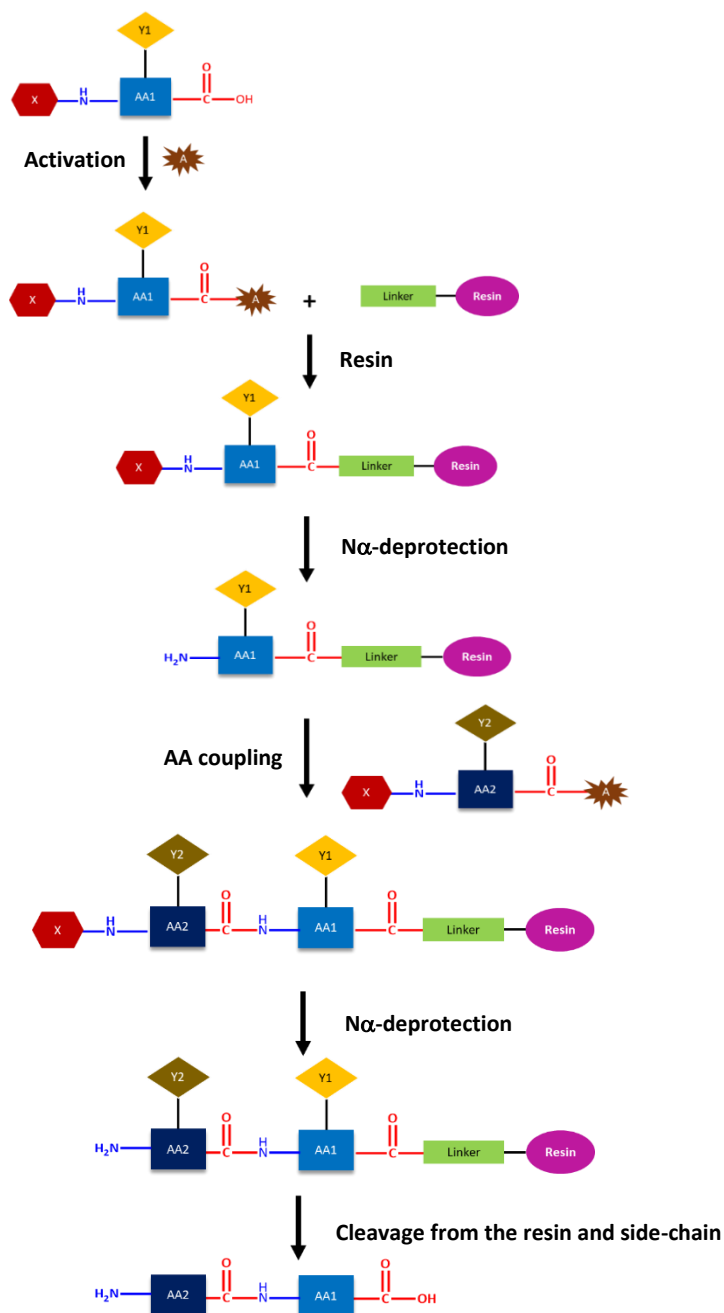


Figure 1.15. Schematic overview of the SPPS methodology. AA: amino acid; Y: side-chain protecting group (semi-permanent); X: N α -protecting group (temporary); A: coupling reagent.

The assembly of a peptide chain on an insoluble solid support has obvious benefits that lead to significant savings in time and labour compared to the corresponding operations in solution. Moreover, the development of commercially available automated peptide synthesizers has come a long way enabling a high degree of predictability and reproducibility. However, low purities and sometimes even failure in achieving the desired peptide sequences are still frequently occurring problems, especially for long peptides (> 30-50-mer peptides) [180, 184].

Heating has been found to be a useful strategy to improve the efficiency of peptide synthesis, in particular in the case of difficult sequences. In this regard, microwave instruments are especially advantageous since they can provide fast, precise, homogeneous and reproducible heating while being easily controllable. Microwave irradiation has in fact demonstrated to cause dramatic improvements both in terms of coupling/deprotection speed and in terms of product purity/yield. These enhancements are thought to derive from a purely kinetic effect due to the temperature increase of the reaction media. Bacsa et al. demonstrated that an increase of 60°C for both coupling and deprotection steps represented an estimated 50-fold increase in the reaction rate for both processes [184, 185]. The major concern when using heating during Fmoc deprotection is aspartimide formation, although this issue can be partially addressed by the substitution of piperidine with piperazine and the incorporation of acidic modifiers in the deprotection mixture [181]. Microwave-assisted peptide synthesizers are now widely available and have become the instruments of choice for the routine synthesis of peptides while also giving access to peptides of longer lengths (*e.g.* 80 residues) [186].

1.8. Thesis Aim and Outline

In the age of personalized therapy, the search for new tools for the characterization of the distinctive features of the disease in each patient is a pressing challenge. In this regard, nuclear medicine can provide relevant biochemical and physiological information through target-specific radiopharmaceuticals, as previously explained.

Breast cancer, which represents a major healthcare burden, is an example of a disease for which molecular imaging can provide essential information to support clinical decisions. However, despite the active research concerning the development of targeted-radiopharmaceuticals towards BC, a good-performing radiopharmaceutical for personalized treatment and follow-up of patients has not yet been achieved.

In this context, the general aim of the work presented in this thesis was the synthesis and pre-clinical evaluation of new peptide-based radiolabelled conjugates for BC management. The design of the radioconjugates was aimed to explore both the imaging ability and the Auger-therapy potential of the radioisotope In-111, thus offering the possibility of cancer theranostics.

As previously discussed, the design of radiopharmaceuticals with specific targeting abilities is a demanding task. In this work, the selection of the targeting moieties took into consideration the importance of the ER as a biomarker of BC. The peptide nature of the targeting vectors was expected to offer high specificity and a favourable pharmacokinetic profile *in vivo*.

In addition to the ER-targeting ability, the importance of delivering the radioisotope in close proximity to DNA in order to potentiate the Auger therapeutic effect was also an important point under consideration in the design of the targeted-radioconjugates.

The design, synthesis, radiolabelling and biological evaluation of the new targeted radioconjugates for BC theranostics is discussed in this thesis. For the sake of clarity, the work was subdivided in different chapters.

Chapter 2 is focused on the synthesis and *in vitro/in vivo* evaluation of ¹¹¹In-labelled small peptides targeting the ER-mediated genomic and non-genomic actions. These studies were performed to get insight on the stability and targeting properties of the radiolabelled peptides in order to evaluate their clinical potential for ER-positive BC theranostics.

Chapter 3 describes the radioiodination and the preliminary biological evaluation of a ER-targeting peptide selected from the studies described in chapter 2. The work was aimed to explore the radioiodination feasibility of the peptide sequence with ER-binding ability.

Furthermore, since certain iodine radioisotopes share the imaging and therapy potential of In-111, it was relevant to study clinically relevant properties of the radioiodinated peptide in the context of BC theranostics.

Chapter 4 is focused on the development of dual-targeting probes aimed at targeting the nucleus of BC cells to potentiate Auger therapy by the delivery of In-111 near DNA. The synthetic approaches to achieve doubly-vectorizable prochelators suitable for the construction of ^{111}In -based radiopharmaceuticals are described in this chapter. Furthermore, studies on the ability of nuclear-targeting molecules to enhance the nuclear uptake of bivalent radioconjugates and to interact with DNA are discussed. Overall these studies were aimed to identify the best chemical design strategy to achieve target-specific probes for imaging and therapy (Auger) of BC.

Chapter 5 describes the design and the synthesis of a DNA-binding peptide based on the sequence of a transcription factor of the basic leucine-zipper (bZIP) family. The peptide construct was intended to act as targeting moiety to deliver the radioisotope In-111 to the DNA. Therefore, the aim of the work described in this chapter was to identify a new DNA-targeting vector for the design of radiopharmaceuticals for Auger therapy.

Finally, main conclusions and future perspectives are presented in Chapter 6, followed by the detailed experimental procedures in Chapter 7.

Chapter 2

***¹¹¹In-labelled Peptides towards
the Estrogen Receptor***

2. ¹¹¹In-labelled Peptides towards the Estrogen Receptor

The search for the most suitable targeted radiopharmaceutical for BC management is still a demanding challenge, as already mentioned in the introductory chapter. Since ER is a very important biomarker of the disease, most of the research in this field has been focused on the development of nuclear imaging agents with targeting ability towards ER. As previously explained, the majority of the targeted radiopharmaceuticals developed for ER-targeting have integrated estradiol analogues as targeting moieties.

Looking for new targeting vectors suitable to the design of biospecific radiopharmaceuticals for BC management, two different approaches are exploited in this chapter. In the first approach, small peptides containing the LXXLL motif were studied as potential targeting vectors for the construction of ¹¹¹In-labelled conjugates targeting the coactivator binding site of ER. The second approach explored a different targeting vector for the design of targeted ¹¹¹In-based radioconjugates: a phosphorylated peptide (pY) known to bind with high affinity to a tyrosine kinase that interacts with ER. These two strategies were conceived aiming to target both the genomic and the non-genomic actions of the ER and their potential interest for the clinical management of ER-positive BC was evaluated.

2.1. Radiolabelled LXXLL-based Peptides

2.1.1. LXXLL Peptides

Ligand-dependent activation of gene transcription by ER relies on the recruitment of coactivators, including the p160 steroid receptor coactivators (SRC) family. Intriguingly, the p160 factors share a common motif containing a core consensus sequence LXXLL (L-Leucine, X- any amino acid), named NR-box, that is responsible for the interaction with the nuclear receptor. Crystal structures of the complex between the ER LBD and the NR-box have revealed that the LXXLL motifs adopt a α -helical conformation that binds to the AF2 surface (Figure 2.1). The crystallographic evidence suggests a model in which the glutamic acid of the AF2 H12 interacts through hydrogen bonds with the backbone amide of the first leucine of the motif and with the amino-terminal adjacent residue, while a critical lysine in H3 interacts through hydrogen bonding with the backbone carbonyls of leucines at position 4 and 5 of the LXXLL sequence. Therefore, according to this model the hydrophobic face of LXXLL is packed into a hydrophobic

pocket in which H12 and H3 define a charge clamp that allows the orientation and placement of the motif into the coactivator-binding site [187, 188]. H12 plays an important role since is highly mobile and in the absence of a ligand is not correctly positioned [57]. However, the binding of a receptor agonist stabilizes the helix and packs it against the LBD forming the appropriate coactivator binding surface. The XX residues of the core motif are exposed to the solvent which explains their variability [187].

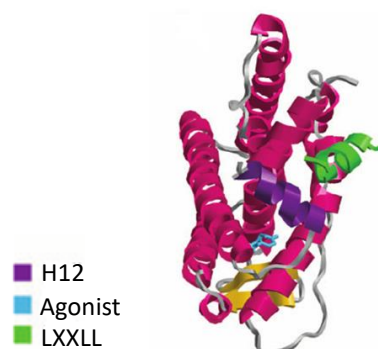


Figure 2.1. Representative ribbon diagram of ER α LBD bound to agonist ligand and coactivator LXXLL peptide. Adapted from [189].

Based on the knowledge provided by the crystallographic studies of complexes between ER LBD and the natural coactivators, synthetic small peptides have been prepared to evaluate the affinity and selectivity towards ER α and to demonstrate the feasibility of blocking the interaction between the receptor and coactivators, which could be of therapeutic value. In fact, previous studies have shown that the information within short LXXLL-containing peptides is sufficient to confer specific protein-protein interactions with nuclear receptors [187, 190].

As short linear peptides tend to adopt random or β -sheet structures and considering that the pentapeptide motif must assume a helical conformation to interact with ER, Leduc et al. synthesized short peptides with side-chain cyclization with the aim of inducing helicity. The authors used two different strategies to promote side chain to side chain cyclization: *i, i+4* amide formation between a lysine and a glutamic acid side-chain bond and a D-Cys, Cys *i, i+3* disulfide bridge. The disulfide-bridged analogue showed the greatest helical character by circular dichroism (CD) studies and was also the one with highest affinity towards ER α . Interestingly, replacement of the N-terminal lysine with arginine led to an increase of the helicity and of the ER α binding affinity, probably due to the stronger hydrogen bonding network of the guanidine moiety with the backbone carbonyl groups [191].

In another related work, Galande and co-workers prepared a series of linear unconstrained LXXLL peptides incorporating a single cysteine residue as counterparts of the disulfide-bridged peptides. Surprisingly, the class of monocysteine peptides demonstrated high affinities for the ER. It was believed that a disulfide bridge between the receptor and the peptidic ligand could be formed. The high affinity of linear peptides based on the LXXLL motif is not, however, restricted to monocysteine peptides. Replacing D-Cys and Cys in the cyclic peptides by i , $i+3$ D-Ser and Ser or by Ser and Ser or even by D-Ala and Ala originated peptides with nanomolar binding affinities towards ER α . These peptides also showed partial helical character in the CD studies, although the determined helicity did not correlate directly with the binding affinity [190]. These evidences led several authors to conclude that the receptor hydrophobic coactivator binding surface is capable of inducing helical character in linear peptides, which is required for their biological effects [54, 190, 192]. Table 2.1 shows selected examples of small LXXLL peptide sequences with binding affinity towards ER α .

Table 2.1. Examples of LXXLL-based peptides with high binding affinity (measured as K_i) towards ER α .

Sequence	K_i (nM)	Reference
H-Lys-cyclo(Glu-Ile-Leu-Arg-Lys)-Leu-Leu-Gln-NH ₂	220	[193]
H-Lys-cyclo(D-Cys-Ile-Leu-Cys)-Arg-Leu-Leu-Gln-NH ₂	25	[193]
H-Arg-cyclo(D-Cys-Ile-Leu-Cys)-Arg-Leu-Leu-Gln-NH ₂	11	[191]
H-Arg-Ile-Leu-Arg-Cys-Leu-Leu-Gln-NH ₂	13	[190]
H-Arg-D-Ser-Ile-Leu-Ser-Arg-Leu-Leu-Gln-NH ₂	60	[190]
H-Lys-Lys-Ile-Leu-His-Arg-Leu-Leu-Gln-NH ₂	170	[193]

The regions flanking the LXXLL motif are known to also have an impact on the receptor binding and in particular on the preferential targeting of ER α . Both the amino acid residues in some strategic positions and the overall charge of the C-terminus and N-terminus are reported to influence the selectivity of synthetic peptides. Nguyen et al. reported that peptides with an acidic C-terminus prefer ER β , while peptides with high C-terminus basicity have more selectivity for ER α [192]. Furthermore, Ko and co-workers demonstrated that serine at position -3 allows selective interactions for ER β versus ER α [194]. In contrast, arginine, lysine or isoleucine/leucine at the positions -2 and -1 were found to favor the selectivity towards ER in detriment of other nuclear receptors [187]. Conformational constraint was also reported as an important factor to improve selectivity since more flexible cyclic peptides have shown to be less selective [190].

These peptidomimetics represent a promising strategy to inhibit ER α -cofactor interactions and therefore to achieve clinical benefit in tumors that overexpress ER α . However, the fact that the cell membrane is generally impermeable to peptides could be a challenging obstacle to get cellular internalization and reach the ER. To overcome this problem, a cationic nona-arginine (R₉) tag that behaves as a cell penetrating-peptide has been linked to the C-terminus of a set of natural LXXLL-motif sequences with known affinity to ER α . Remarkably, the R₉ moiety has not shown to disturb the capacity of the peptides to bind to ER α . The hybrid peptides have demonstrated to be capable of inhibiting ER α gene-mediated transcription in human breast cancer MCF-7 cells by blocking the interaction between the receptor and co-activators [195]. In a different study, a peptide containing the LXXLL-motif of the human SRC-1 was linked to the cell-penetrating peptide transportan 10 (TP10) and the resulting conjugate induced dose-dependent cytotoxicity in BC cell lines [196]. These results highlight the therapeutic potential of the LXXLL-based peptides for ER-dependent health conditions.

Rationale for the study of LXXLL-based radioprobes

The high binding affinity towards ER α allied with the usually favorable pharmacokinetic profile presented by small peptides encouraged us to study the potential of LXXLL-based peptides as vectors for the synthesis of biospecific radiopharmaceuticals towards ER-positive breast tumors. This idea represents in fact a novel approach for targeted BC imaging since clinical research in this area has focused mainly in molecular probes of steroidal nature whose high lipophilicities lead to drawbacks in the biodistribution profiles (high liver and intestinal uptakes and slow blood clearance) [88, 104, 105]. Furthermore, the recognition site on the ER α LBD of the LXXLL motif is different from the binding site of steroid drugs and the radiopeptides can potentially provide specific functional information since their binding to the receptor is dependent on the activation of ER by agonists. To explore this new approach the radionuclide ¹¹¹In was selected since its clinical use for SPECT imaging using peptide-based radiopharmaceuticals is well-known and additionally due to its potential for Auger-electron therapy. The theranostic value of these LXXLL-based radioprobes could be particularly relevant for this application since the ER is localized mainly in the cell nucleus and therefore the targeted probes could deliver the Auger electrons in the proximity of DNA.

In the following sections, the chemical strategies used for the synthesis of the new LXXLL-based probes and the pre-clinical evaluation of the ^{111}In -labelled peptides is discussed in detail.

2.1.2. Synthesis and Characterization of the Peptide Conjugates

Synthesis and Characterization of the LXXLL Peptides

Three LXXLL based peptides with known affinity and selectivity towards ER α were synthesized and named **ER1**, **ER2** and **ER3** (Table 2.2). **ER1** is a nonapeptide with D-Cys and L-Cys residues located at i and i+3 positions intended for disulfide bond formation to yield a cyclic peptide (**cER1**) [193]. The use of D- and L- residues for the cyclization is reported to be important to lock the peptide into the helical conformation required for biological activity since the distance between the sulphhydryl groups in the case of L-Cys (i)/L-Cys (i+3) is not as optimal as in the case of D-Cys (i)/ L-Cys (i+3) to induce the structural constraint [197, 198]. **ER2** is a monocysteine peptide with the same amino acid residues as ER1 [190]. Lastly, **ER3** is a truncated peptide (residues 6 to 13) derived from box-2 of the ER coactivator SRC-1 with an extra Lys at the N-terminal [55, 193].

Table 2.2. Amino acid sequences of the selected LXXLL peptides.

Peptide	Sequence	Reference
ER1	H-Arg-DCys-Ile-Leu-Cys-Arg-Leu-Leu-Gln-NH ₂	[193]
ER2	H-Arg-Ile-Leu-Arg-Cys-Leu-Leu-Gln-NH ₂	[190]
ER3	H-Lys-Lys-Ile-Leu-His-Arg-Leu-Leu-Gln-NH ₂	[193]

The LXXLL based peptides were synthesized in solid phase in a microwave-assisted automated peptide synthesizer using the Fmoc-strategy. The resin of choice for the peptide synthesis was Rink Amide MBHA which is intended for the preparation of C-terminal amidated peptides. Keeping an amide in the C-terminal instead of a carboxylic acid removes the unnatural negative charge and better mimics the normal amide bond present in the natural coactivator peptides from which the small peptides are inspired, hence attempting to get a better biological activity. Furthermore, the C-terminal amidation improves the metabolic stability of the peptides

increasing the resistance towards exopeptidases [199]. 2-(1H-Benzotriazol-1-yl)-1,1,3,3-tetramethyluronium hexafluorophosphate (HBTU) was used for *in situ* activation of the Fmoc-protected amino acids. In fact, HBTU is the most cost-effective activator for peptide synthesis and is the most widely used for SPPS [200]. Double couplings were used for Arg to compensate the known potential for γ -lactam formation and to improve the amino acid coupling yield. In addition, lower temperatures (50°C) were used for the coupling of His and Cys to limit the amount of racemization [201]. In the end of the synthesis, the Fmoc group in the N-terminal of the peptide sequences was deprotected to afford free amine groups.

The cleavage from the resin and the side-groups deprotection were performed using the standard cleavage cocktail composed by the mixture trifluoroacetic acid (TFA)/ triisopropylsilane (TIS)/ water (95:2.5:2.5) for **ER3**, and the mixture TFA/1,2-ethanedithiol (EDT)/ TIS/ water (94:2.5:1:2.5) for the cysteine-containing peptides. The addition of EDT to the cleavage cocktail of peptides **ER1** and **ER2** is important since that is a more efficient scavenger for *tert*-butyl cations, thus preventing the S-alkylation of Cys during the deprotection step while also assisting in the removal of the trityl (Trt) protecting group [202]. The deprotected crude products were then purified by semi-preparative HPLC and the peptides were identified by ESI-MS and MS/MS.

ER1 and **ER2** were synthesized in high yield (>85%), while **ER3** was obtained from the automated synthesizer with a lower yield of approximately 56%. Indeed, the crude mixture of the **ER3** peptide showed two other major products besides the desired peptide that were identified by ESI-MS and MS/MS as being a truncated peptide lacking the final Lys residue ($m/z = 1119.61 [M+H]^+$), and a peptide sequence in which occurred a double addition of the His residue ($m/z = 1284.90 [M+H]^+$).

After cleavage and deprotection, **ER1** was oxidized to induce the formation of the disulfide bridge between the two Cys residues. Although on-resin cyclization is described in the literature, it would require different protecting groups for the Cys residues than the conventional Trt group which deprotection occurs simultaneously with the peptide cleavage from the resin [203]. Therefore, it was decided to induce the oxidation of the peptide in solution testing two different conditions: oxidation by air and oxidation by DMSO. In both cases, a pH 8.0 buffer was used because the slightly basic pH is known to favour the charged thiolate form (R-S⁻) in detriment of the protonated thiol form (R-SH) [204]. In the DMSO oxidation experiment, 50% (v/v) of DMSO was added to the buffer. DMSO is known to be a mild oxidizing agent effective for inducing disulfide bridge formation between thiol groups, producing water and dimethyl sulfide as byproducts [205]. The two methods were compared for a 12-hour reaction and the

yield of the cyclic peptide was 98.8% in the DMSO-induced oxidation compared to 62.4% for the oxidation by air. Therefore, air oxidation demonstrated to be a slower method than oxidation by DMSO. In fact, the presence of DMSO led to an almost quantitative conversion of the linear peptide to the cyclic analogue without any undesired byproducts in the reaction mixture, as analysed by HPLC. The disadvantage of this method relied on the necessity of DMSO removal in the end of the reaction, which was accomplished by semi-preparative HPLC.

The characterization of the peptides **ER1**, **cER1**, **ER2** and **ER3** is described in Table 2.3. The final peptides were obtained with a purity degree higher than 95% as determined by HPLC analysis.

Table 2.3. Characterization of ER1, cER1, ER2 and ER3 by HPLC and ESI-MS.

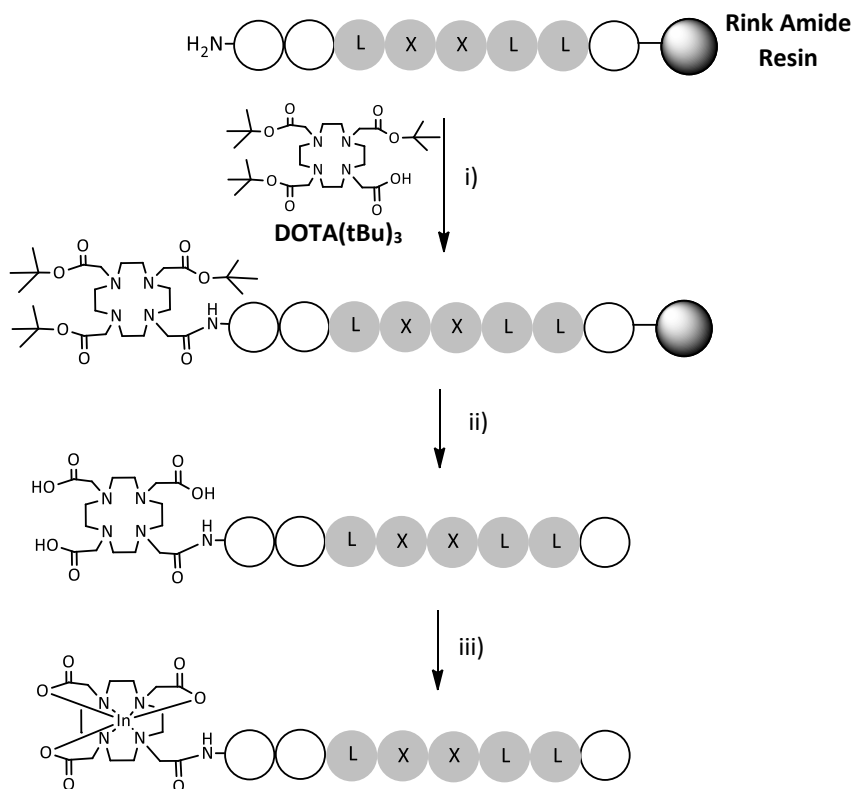
Peptide	HPLC	ESI-MS		Molecular Formula
	Rt (min)*	Calculated (m/z)	Found (m/z)	
ER1	17.10	1116.65 [M+H] ⁺ 558.8 [M+2H] ²⁺	1116.5 [M+H] ⁺ 559.1 [M+2H] ²⁺	C ₄₇ H ₈₉ N ₁₇ O ₁₀ S ₂
cER1	17.58	1114.63 [M+H] ⁺ 557.82 [M+2H] ²⁺	1114.9 [M+H] ⁺ 558.2 [M+2H] ²⁺	C ₄₇ H ₈₇ N ₁₇ O ₁₀ S ₂
ER2	14.61	1013.64 [M+H] ⁺ 507.32 [M+2H] ²⁺	1013.6 [M+H] ⁺ 507.7 [M+2H] ²⁺	C ₄₄ H ₈₄ N ₁₆ O ₉ S
ER3	12.43	1147.78 [M+H] ⁺ 574.39 [M+2H] ²⁺	1148.3 [M+H] ⁺ 574.8 [M+2H] ²⁺	C ₅₃ H ₉₈ N ₁₈ O ₁₀

*Method A (Eluents: A- 0.1% aq. TFA; B- 0.1% TFA/CH₃CN. Gradient (%): 90 A/100 B to 70 A/30 B in 10 min, 70 A/30 B to 55 A/45 B in 30 min).

Conjugation to the Bifunctional Chelator

Aiming the construction of targeted radioconjugates, a BFC able to coordinate the chosen radionuclide (¹¹¹In) and form complexes of high stability was conjugated to the peptides. Since peptides were synthesized by SPPS, the conjugation of the bifunctional chelator in solid phase was the most convenient choice. The commercially available DOTA-tris(*tert*-butyl ester) is a monoreactive macrocycle that besides being readily soluble in DMF has carboxylic acid protecting groups that are fully compatible with the standard SPPS methodology. Therefore, this

prochelator has been the most popular option for attaching a DOTA unit to a peptide in a solid support and it was used for the conjugation to the LXXLL based peptides (Scheme 2.1) [152].



Scheme 2.1. Schematic representation of the chemical approach employed to synthesize the DOTA-peptide conjugates and the corresponding In-complexes.

i) HATU, DIPEA, DMF, RT, 2 h (2x); **ii)** TFA:EDT:TIS:H₂O (DOTA-ER1 and DOTA-ER2) or TFA:TIS:H₂O (DOTA-ER3), RT, 6 h; **iii)** InCl₃, 0.1 M NaOAc pH 5.5, 95°C, 30 min.

DOTA-tris(*tert*-butyl ester), in DMF, was pre-incubated with the activating agent O-(7-azabenzotriazole-1-yl)-1,1,3,3,-tetramethyluronium hexafluorophosphate (HATU) and the organic base diisopropylethylamine (DIPEA) for 2 min in order to activate the carboxylate. HATU was selected to ensure a highly efficient and fast coupling [206]. The activated prochelator was added to the pre-swelled resin in a 2:1 proportion relatively to the peptide to perform the conjugation. The reaction was left for two hours, and after the appropriate resin washing, the coupling was repeated with fresh reagents for additional two hours. The Kaiser test performed with the resin beads was negative for the presence of free amines proving that the coupling was

successful. In fact, after the cleavage and deprotection of the DOTA-peptide conjugates, it was verified that for the three peptides the prochelator coupling yield was higher than 95%.

After purification, the **DOTA-ER1** conjugate was further exposed to mild oxidizing conditions using DMSO (as described above for the unconjugated peptide) to induce the formation of the disulfide bridge, yielding **DOTA-cER1** quantitatively after 12h. Table 2.4 summarizes the characterization of the three final DOTA-peptide conjugates (degree of purity higher than 95%).

Table 2.4. Characterization of the DOTA-peptide conjugates by HPLC and ESI-MS.

Conjugate	HPLC	ESI-MS		Molecular Formula
	Rt (min)*	Calculated (m/z)	Found (m/z)	
DOTA-cER1	17.49	1500.81 [M+H] ⁺ 750.91 [M+2H] ²⁺	1500.4 [M+H] ⁺ 751.3 [M+2H] ²⁺	C ₆₃ H ₁₁₃ N ₂₁ O ₁₇ S ₂
DOTA-ER2	15.48	1399.82 [M+H] ⁺ 700.41 [M+2H] ²⁺	1400.5 [M+H] ⁺ 700.7 [M+2H] ²⁺	C ₆₀ H ₁₁₀ N ₂₀ O ₁₆ S
DOTA-ER3	12.66	1533.96 [M+H] ⁺	1533.8 [M+H] ⁺	C ₆₉ H ₁₂₄ N ₂₂ O ₁₇

*Method A (Eluents: A- 0.1% aq. TFA; B- 0.1% TFA/CH₃CN. Gradient (%): 90 A/10 B to 70 A/30 B in 10 min, 70 A/30 B to 55 A/45 B in 30 min).

2.1.3. Synthesis and Characterization of the In(III) Complexes

The synthesis of the inactive (non-radioactive) In(III) complexes is a crucial task in the development of new ¹¹¹In-labelled radiopharmaceuticals. In fact, the chemical characterization of radiolabelled conjugates by the standard characterization techniques, such as NMR or ESI-MS, is not feasible due to the very low molar concentration of the radiometal in the final preparation. Therefore, the strategy applied for the chemical identification of the radioactive ¹¹¹In-complexes has been based on the characterization at the macroscopic level of the corresponding non-radioactive In-complexes. Given that the chemical structure of the inactive and of the radioactive complex is assumed to be the same, the chromatographic profiles of the two complexes are expected to be coincidence. Therefore, a coinjection of both In- and ¹¹¹In-complexes in the HPLC has been routinely used to corroborate the chemical identity of the

radiolabelled species [88, 207, 208]. Furthermore, the non-radioactive complexes are also used in this work for the determination of the binding affinity towards the target receptor (ER α), as will be explained later (section 2.1.4).

Preparation of the In(III) complexes (Scheme 2.1) was performed using anhydrous InCl₃ in a 1.2:1 proportion relatively to the DOTA-peptide conjugates. The reactions were performed at 95°C due to the slow complexation kinetics of DOTA [143]. The pH was kept at 5.5 using an acetate buffer solution for the reaction. The acetate ions are intended to act as mild chelating ions to reduce the propensity of In³⁺ to hydrolyse and form the insoluble In(OH)₃ [209]. After 30 minutes, the reaction mixtures were purified by HPLC. Despite the high temperature used, the peptide conjugates did not show signs of degradation demonstrating high thermostability. In fact, the yields of the complexation reactions were higher than 96% for the three peptide-based conjugates.

The Indium complexes were characterized by HPLC and ESI-MS (data presented in Table 2.5) with the isotopic pattern observed in the spectra being consistent with Indium complexation as shown in the representative spectrum of **[In]DOTA-ER3** in Figure 2.2.

Table 2.5. Characterization of the In-complexes of the LXXLL derivatives by HPLC and ESI-MS.

Conjugate	HPLC	ESI-MS		Molecular Formula
	Rt (min)*	Calculated (m/z)	Found (m/z)	
[In]DOTA-cER1	17.61	806.85 [M+2H] ²⁺	807.0 [M+2H] ²⁺	C ₆₃ H ₁₁₀ InN ₂₁ O ₁₇ S ₂
[In]DOTA-ER2	15.49	1511.70 [M+H] ⁺	1511.8 [M+H] ⁺	C ₆₀ H ₁₀₇ InN ₂₀ O ₁₆ S
[In]DOTA-ER3	12.78	1645.83 [M+H] ⁺	1645.7 [M+H] ⁺	C ₆₉ H ₁₂₁ InN ₂₂ O ₁₇
		823.42 [M+2H] ²⁺	823.7 [M+2H] ²⁺	

*Method A (Eluents: A- 0.1% aq. TFA; B- 0.1% TFA/CH₃CN. Gradient (%): 90 A/10 B to 70 A/30 B in 10 min, 70 A/30 B to 55 A/45 B in 30 min).

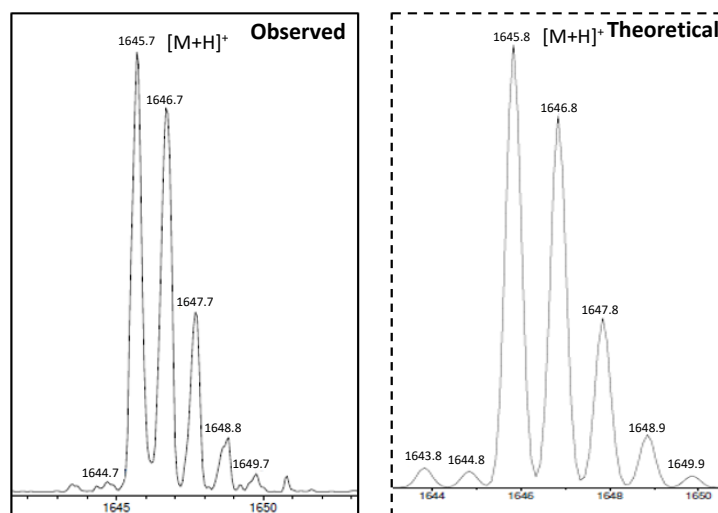


Figure 2.2. Comparison between the experimental (observed) and the simulated (theoretical) ESI-MS spectra of [In]DOTA-ER3 (m/z calcd for $C_{69}H_{122}InN_{22}O_{17}$ $[M+H]^+$: 1645.83, found: 1645.7 $[M+H]^+$).

2.1.4. Evaluation of the Binding Affinity towards ER α

The determination of the receptor binding affinity of the In(III) complexes is an essential task for evaluating the biological targeting ability of the ^{111}In -labelled peptides. This evaluation is particularly relevant since the chemical modifications introduced in the LXXLL peptides, specifically the DOTA conjugation and the In(III) complexation, can potentially modify their ability to bind to the ER α LBD.

Fluorescence Polarization Binding Assay: Theoretical Considerations

Fluorescence polarization/fluorescence anisotropy (FP/FA) is a solution-based technique that has been widely used to study molecular interactions, enzymatic activity and nucleic acid hybridization [210-213]. The principle of FP relies on the fact that the degree of polarization of a fluorophore is inversely related to its molecular rotation which is largely driven by Brownian motion. Quantitatively, FP/FA is defined as the difference of the emission light intensity parallel (I_{\parallel}) and perpendicular (I_{\perp}) to the excitation light plane normalized by the total fluorescence emission intensity (Equations 1 and 2).

$$FP = \frac{I_{\parallel} - I_{\perp}}{I_{\parallel} + I_{\perp}} \quad (\text{Equation 1})$$

or,

$$FA = \frac{I_{\parallel} - I_{\perp}}{I_{\parallel} + 2I_{\perp}} \quad (\text{Equation 2})$$

FP and FA are used interchangeably, although FA is preferable because it is more arithmetically convenient [210, 211]. The most important implication derived from equations 1 and 2 is that upon excitation, if the fluorescent entity becomes randomly re-oriented during its fluorophore's lifetime (τ), then FP (and FA) will become 0 (since $I_{\parallel} = I_{\perp}$). On the other hand, if there is no rotation of the molecule during τ , FP will reach the maximum value. The speed at which the fluorophore tumbles is determined by its rotational relaxation time (ρ) which is defined as the time taken for the molecule to rotate through 68.5° . For a spherical molecule, ρ is described by the Stoke's equation:

$$\rho = \frac{3\eta V}{RT} \quad (\text{Equation 3})$$

in which, V is the molecular volume, R is the universal gas constant, T is the absolute temperature and η is the solvent viscosity. From this equation is clear that the speed of tumbling is inversely related to the molecular volume provided that temperature and viscosity remain constant. Therefore, dissociation or binding events that affect the molecular size of the fluorescent entities directly cause changes in the degree of depolarization of plane polarized light. Therefore, FP provides a mean of measuring the association of fluorescent ligands with larger molecules such as proteins. Binding of a small fluorescent ligand to a larger protein increases FP with the measured total value (FP_m) being a sum that reflects the free and bound ligand according to the equation:

$$FP_m = F_f FP_f + F_b FP_b \quad (\text{Equation 4})$$

in which FP_f and FP_b are the polarization values for the free and bound ligand, respectively, and F_f and F_b are the fractions ($F_f + F_b = 1$) of each form of ligand (free or bound). This provides the basis for using FP to determine ligand binding to proteins such as G-protein-coupled receptors (GPCRs), nuclear receptors and enzymes. In fact, the FP assay has been very attractive for this application due to the fact that is inexpensive, non-destructive and has a straight-forward protocol with no need for separation and filtration steps [210, 211, 214].

Rodriguez et al. developed for the first time a FP-based assay to measure the binding of small ligands to the coactivator groove of the ER α by competition with a fluorophore-labelled coactivator peptide. As expected, the initial high FP (due to the immobilized receptor-bound fluorescent peptide) declined when small molecules capable of binding to the same site in the ER α LBD displaced the fluorescent coactivator peptide, providing data that allowed the determination of the binding affinities of different ligands [215]. Since then, the FP assay has become in the last decade the reference method to evaluate the binding affinity of small molecules or peptides to the coactivator binding groove of ER and other nuclear receptors [190, 193, 195, 212].

Determination of the Binding Affinities of the LXXLL-based Probes

A competitive FP assay was used to evaluate the binding affinity of the synthesized LXXLL-based peptides and, most importantly, of the corresponding DOTA conjugates and In-complexes. Fluorescein-labelled coactivator peptide SRC1 Box 2 (FL-SRC1B2) and the ER α LBD (302-553) protein were used in the experiments. Estradiol (E2) was also a key element in the reaction mixture since it has been shown that the binding of an agonist to the ER α is important for the adoption of a more favourable conformation of the protein for interaction with the LXXLL motifs [213].

The first step was the determination of the receptor concentration that should be used in the assay. To achieve that goal, a FP assay was performed by varying the concentration of ER α while keeping the concentrations of FL-SRC1B2 and E2 constants. The concentration of the receptor was chosen based on the amount that resulted in 75-90% of fluorescent tracer bound, yielding a high polarization value in the beginning of the plateau region of the curve relating FP with the ER α concentration. Accordingly, ligands to be tested were then serially diluted into a reaction buffer containing 500 nM of ER α , 100 nM of FL-SRC1B2 and 5 μ M of E2. To validate the conditions, the first peptide tested was the unlabelled coactivator peptide SRC1 Box 2. The

peptide was able to displace the fluorescent tracer and caused a decrease in the FP value that allowed the determination of a IC_{50} (defined as the peptide concentration responsible for a 50% reduction of the FP value) of 361 nM which is in accordance with the values found in the literature that range between 155 to 700 nM [190, 215]. Then, the three LXXLL-based unconjugated peptides **cER1**, **ER2**, and **ER3** were tested in the same experimental conditions. Although the binding affinities of these peptides towards $ER\alpha$ have been described in the literature, it was important to determine the binding affinities of the starting peptides with the experimental conditions established for the assays. In such way, a baseline to evaluate the impact of the chemical modifications on the ability to bind to the receptor could be obtained. The results of the FP assay and the determined IC_{50} values are displayed in Figure 2.3 and in Table 2.6.

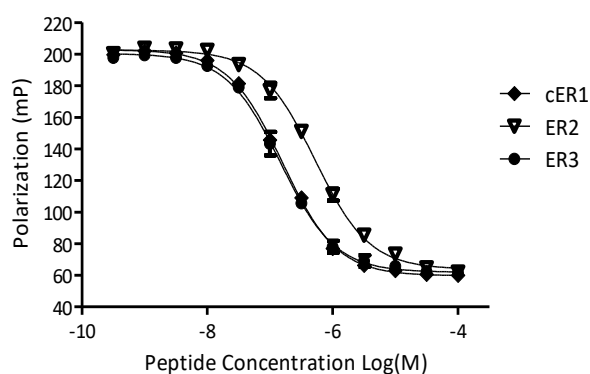


Table 2.6. Binding affinities (IC_{50}) towards the $ER\alpha$ LBD determined by the FP assay for the unconjugated peptides.

Peptide	IC_{50} (μM)
cER1	0.170 ± 0.049
ER2	0.560 ± 0.048
ER3	0.157 ± 0.008

Figure 2.3. FP curves of FL-SRC1B2SRC with increasing concentrations (Log(M)) of the LXXLL peptides.

The three peptides demonstrated nanomolar affinities towards the receptor, which is in accordance with the range found in literature for LXXLL peptides targeting the ER [190, 193]. In this experiment, **ER3** peptide showed the highest binding affinity while **ER2** displaced the fluorescent coactivator peptide with less efficiency thus yielding the highest IC_{50} . The **cER1** peptide although having a very similar sequence showed 3 times more potency compared to ER2. It should be pointed out that is difficult to compare the values obtained from this assay with the binding affinities reported in the literature (11 nM for **cER1**, 13 nM for **ER2** and 170 nM for **ER3**) which were based on different experimental conditions in which the receptor was immobilized on plates instead being in solution [55, 190]. Moreover, the binding potencies previously reported were based on a FP assay using the full-length $ER\alpha$. This fact also difficult

the comparison with the binding affinities obtained in this work using the ER α LBD since it is known that the full receptor and the LBD have different surface topologies when bound to E2 leading to significant differences on the binding ability of LXXLL peptides [195, 216]. Another point to have in consideration when comparing these values with the ones found in the literature for ligands targeting the coactivator site in the ER, is that the results shown derive always from two different events that have a causal relationship: the binding of E2 to the ER and the binding of the LXXLL peptides to the E2-bound ER [213]. Therefore, the concentration of E2 used is an important parameter that have a direct impact on the final results.

The attachment of a macrocycle chelator to a peptide sequence can hinder its biological targeting properties mainly due to steric hindrance. In the synthesized peptides, the bulky chelator is not directly attached to the LXXLL core, and this fact is expected to minimize the impact on the ability of the peptide sequence to bind to the coactivator groove in the ER [209]. On the other hand, Indium complexation of DOTA-peptide conjugates has demonstrated in some cases to increase the binding affinity compared to the non-complexed conjugates. This can be attributed to the fact that when the metal ion is coordinated, the chelator cavity becomes more compacted with less free rotations of the acetate groups [150, 207]. However, this is not always the case and the impact of the metal coordination on the charge and lipophilicity of the final complex can also lead to a weaker binding affinity, depending on the structure of the binding cavity of each receptor [217].

Table 2.7 summarizes the IC₅₀ values found for the DOTA-peptide conjugates and for the corresponding Indium complexes which binding curves obtained by the FP assay are represented in Figure 2.4.

Table 2.7. Binding affinities (IC₅₀) towards the ER α LBD determined by the FP assay for the DOTA-peptide conjugates and In-complexes.

Peptide Conjugate/Complex	IC ₅₀ (μ M)
DOTA-cER1	2.50 \pm 0.26
[In]DOTA-cER1	1.20 \pm 0.16
DOTA-ER2	1.78 \pm 0.24
[In]DOTA-ER2	1.49 \pm 0.05
DOTA-ER3	0.255 \pm 0.062
[In]DOTA-ER3	1.72 \pm 0.10

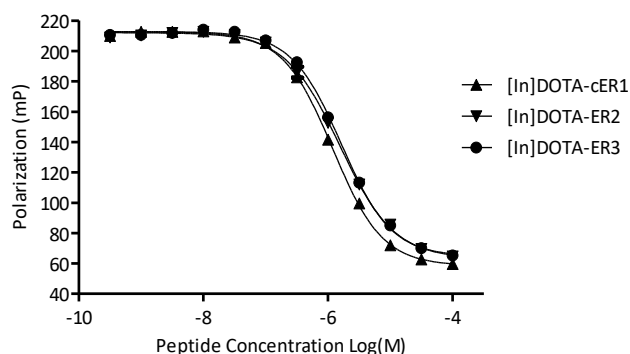


Figure 2.4. FP curves of FL-SRC1B2SRC with increasing concentrations (Log(M)) of the Indium complexes.

The peptide most negatively affected by the attachment of the chelator was **cER1**, which demonstrated a 15-fold increase in the IC_{50} value after DOTA conjugation. On the opposite side, the **ER3** peptide was the less impacted by the macrocycle attachment on the N-terminus demonstrating a 1.62-fold increase. Therefore, the binding of the three peptides showed different tolerances relatively to the addition of the bulky macrocycle, suggesting that the chelator interferes distinctly with critical amino acids in the three sequences and that the amino acid residues in the N-terminal between the DOTA chelator and LXXLL core possible play a more critical role in the cases of **cER1** and **ER2**, than in **ER3**. Interestingly, complexation with Indium led to a prominent reduction of the IC_{50} for the **DOTA-cER1** conjugation, and in a lesser extent also for **DOTA-ER2**. However, **[In]DOTA-ER3** demonstrated an opposite behaviour with the IC_{50} increasing 1.6 times relatively to **DOTA-ER3**, suggesting that in this case the higher rigidity of the coordinating sphere hindered the binding to the coactivator groove site in ER α LBD. Although a loss of potency was observed comparing to the free peptides, the three Indium complexes retained the binding affinity towards ER α . Carraz et al. modified truncated sequences of ER α coactivator peptides (16 to 19 amino acids) with PEG-Biotin and/or nona-arginine sequences and obtained final peptidic constructs with IC_{50} values between 2.5 to 9 μ M that demonstrated ability to compete with full-length coactivators in cells and to inhibit the ER α transcriptional activity [195]. Therefore, the binding affinities of the three Indium complexes (between 1.20 and 1.72 μ M) were found promising for the development of ER targeting probes.

2.1.5. Radiolabelling of the Peptide Conjugates and *In Vitro* Evaluation of the ^{111}In -labelled Peptides

Radiolabelling

Radiolabelling of the DOTA-peptide conjugates was achieved by adding $^{111}\text{InCl}_3$ (in 0.02 M HCl) to solutions of the conjugates in acetate buffer with pH 5.5, in a 1:20 to 1:8 proportion (in volume) depending on the desired final activity. The radiolabelling was performed at a peptide concentration of 1.0×10^{-5} M thus achieving high specific activity (SA). SA is an important parameter to maximize the radiotracer binding to the target receptor while avoiding saturation caused by the ligand binding [218]. Therefore, there was an attempt to lower the peptide concentration until 5.5×10^{-6} M. However the radiochemical yield (RCY) declined to values between 66% for [^{111}In]DOTA-cER1 and 78% for [^{111}In]DOTA-ER3 and thus peptide concentrations were kept at 1.0×10^{-5} M. The radiolabelling reactions were performed at 95°C for 25 minutes with longer reaction times failing to improve the RCY.

The quality control of the radioconjugates was performed by HPLC with gamma detection (Table 2.8). Radiochemical purity (RCP), which is defined by the fraction of the total activity associated with the desired radiochemical species, is a very important parameter for the quality of the final radiolabelled product. Indeed, the presence of radiolabelled impurities, such as uncoordinated ^{111}In or peptide degradation products, can affect considerably the biological behaviour of the ^{111}In -labelled peptides [80, 219]. Therefore, aiming to get radiolabelled peptides with a RCP higher than 98%, the radiolabelling mixtures were further purified by HPLC. Furthermore, the inactive Indium complexes described in the previous section were coinjected with the radiolabelled compounds to ascertain their chemical identity by comparing the UV-chromatograms with the gamma-chromatograms, as shown in Figure 2.5.

Table 2.8. Characterization of the ¹¹¹In-labelled LXXLL peptides by HPLC (gamma detection) and radiochemical yields (RCY) of the radiolabelling reactions (n=3). The retention times (UV detection) of the inactive Indium-complexes are indicated in brackets. Partition coefficients (log P) obtained by the “shake-flask” method are also displayed.

Radioconjugate	HPLC	RCY (%)	log <i>P</i> _{o/w}
	Rt (min)*		
[¹¹¹ In]DOTA-cER1	23.08 (22.96)	94.67 ± 0.89	- 2.41 ± 0.06
[¹¹¹ In]DOTA-ER2	21.02 (20.97)	95.07 ± 0.55	- 2.30 ± 0.05
[¹¹¹ In]DOTA-ER3	19.78 (19.33)	93.94 ± 1.69	- 3.09 ± 0.06

*Method B (Eluents: A- 0.1% aq. TFA; B- 0.1% TFA/CH₃CN. Gradient (%): 90 A/10 B to 50 A/50 B in 30 min, 50 A/50 B to 100 B in 10 min).

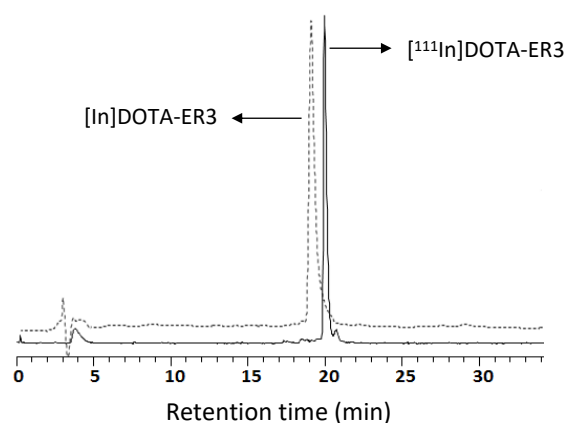


Figure 2.5. Representative chromatograms (Method B) of [¹¹¹In]DOTA-ER3 (full line, Rt = 19.78 min) obtained by gamma-detection and [In]DOTA-ER3 (dashed line, Rt = 19.33 min) obtained by UV-detection.

Lipophilicity of the ¹¹¹In-labelled Peptides

The lipophilicities of the radiolabelled peptides were evaluated by the shake-flask method using n-octanol and NaCl 0.9% to determine the partition coefficient log *P*_{o/w} (Table 2.8) [220]. The three ¹¹¹In-labelled peptides demonstrated to be highly hydrophilic with the radioconjugate [¹¹¹In]DOTA-ER3 being the most. The presence of hydrophilic and positively charged amino acids (at physiologic pH) such as Gln, Arg, Lys along with the hydrophilic chelating

moiety should have accounted for the hydrophilic character revealed by the radiopeptides. This character is expected to affect biological properties, in particular the cellular uptake and the clearance rate from non-target tissues *in vivo* [220].

***In Vitro* Stability Testing of the Radiolabelled Peptides**

The *in vitro* stability of the three radiopeptides was studied for 48 hours at 37°C in different media and the results are shown in Figure 2.6. The three peptides revealed high stability (> 95%) after 48 hours of incubation in saline. Challenging tests were performed by incubating the radiolabelled peptides with an excess of apotransferrin (ApoTf). Due to the similarities between In^{3+} and Fe^{3+} it is known that In^{3+} ions have high binding affinity towards the free iron-binding protein in bloodstream, ApoTf, which could compromise the desired kinetic inertness of the metal-chelator complex *in vivo* [221]. However, after 48 hours of incubation there was not any sign of transchelation of ^{111}In from DOTA-peptides to the ApoTf protein confirming the high stability constant of the complexes. Since DTPA is known to form Indium complexes with higher thermodynamic stability than DOTA, a competition assay was performed by incubating the radiopeptides with an excess of the acyclic chelator [140]. The kinetic inertness of the ^{111}In -labelled peptides was once again confirmed with the three peptides showing stability values higher than 90% after 48 hours of incubation at 37°C.

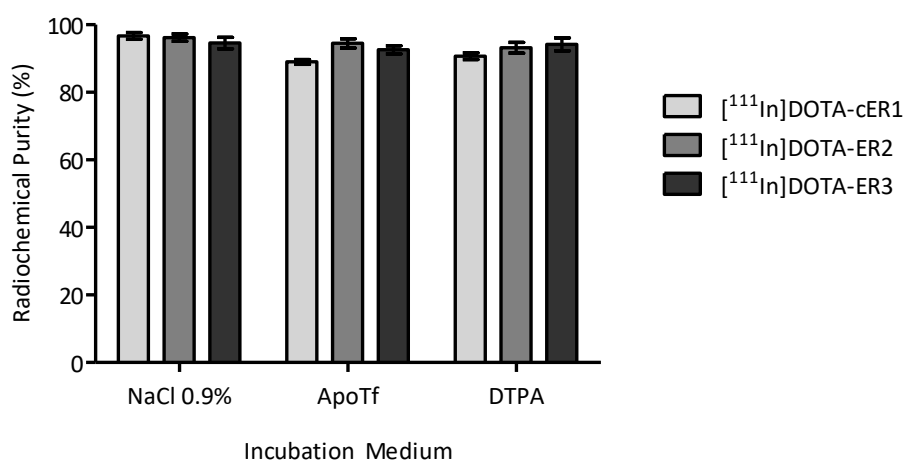


Figure 2.6. Radiochemical purity (determined by HPLC, $n=3$) of the ^{111}In -labelled LXXLL peptides after incubation for 48 h at 37°C in different media: in saline (NaCl 0.9%), in the presence of an excess of apotransferrin (ApoTf) and in the presence of DTPA.

Metabolic stability towards proteolytic degradation is a very important parameter to consider when designing novel peptidic probes for imaging and/or therapy. Good et al. demonstrated that besides having a key role in the accumulation of the radioconjugate in the biological target, peptide radiopharmaceuticals stability in blood plasma can also affect radiotoxicity [222]. The presence of the DOTA chelator in the N-terminus should improve the peptides stability towards aminopeptidases while the carboxamide in the C-terminus is known to improve the resistance to carboxypeptidases [223].

Serum stabilities were assessed by incubating the three ¹¹¹In-labelled LXXLL peptides in human blood serum at 37°C followed by HPLC analysis. For that purpose, aliquots were taken at different time points and treated with ethanol to precipitate the serum proteins before injection in the HPLC system. As it is show in Figure 2.7, the three peptides revealed different degrees of resistance towards proteolytic degradation in human serum which can be attributed to the differences in the amino acid sequences.

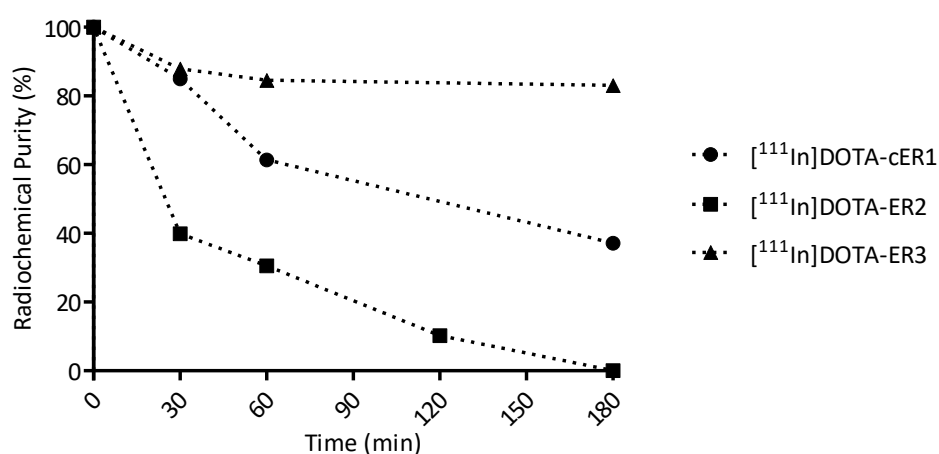


Figure 2.7. Radiochemical purity over time of the ¹¹¹In-labelled LXXLL peptides incubated in human serum at 37°C as determined by HPLC analysis (Method B).

[¹¹¹In]DOTA-ER3 showed the highest metabolic stability with more than 83% of intact radiopeptide present after three hours of incubation. In fact, this radioconjugate was the only one that could be detected in the serum after 24 hours of incubation although representing only 13% of the total radiochemical species at that time point. Despite the similarity between the primary sequences of the cysteine-containing peptides **cER1** and **ER2**, the two radiolabelled peptides demonstrated very different metabolic stabilities. [¹¹¹In]DOTA-ER2 revealed to be the least stable and it was completely degraded after 3 hours of incubation. In contrast to

[¹¹¹In]DOTA-ER3 where the gamma-chromatograms showed the appearance of more hydrophilic radiochemical species most probably due to the cleavage of the peptide sequence by endopeptidases, the gamma-chromatograms of **[¹¹¹In]DOTA-ER2** revealed the formation of both more hydrophilic and more lipophilic species with the latter being possibly attributed to reactions involving the nucleophilic sulfhydryl group of cysteine, in particular oxidation and other reactions with thiol-containing molecules [224]. On the contrary, **[¹¹¹In]DOTA-cER1** demonstrated higher serum stability with almost 40% of the intact radiopeptide still present after 3 hours of incubation. The presence of a disulfide bridge could make the peptide less susceptible to proteolytic cleavage. In fact, peptide cyclization has been an effective strategy to enhance the metabolic half-life of peptides [158, 225]. However, it should be noted that disulfide bridges can also be reduced by oxido-reductases leading to the loss of the secondary structure in serum. The introduction of a D-amino acid (D-Cys) into the sequence can also have contributed for the increased metabolic stability of **[¹¹¹In]DOTA-cER1** relatively to **[¹¹¹In]DOTA-ER2** [226].

2.1.6. Cellular Uptake Studies of the ¹¹¹In-labelled Peptides

The biological target of the LXXLL-based radioconjugates, the ER, is predominantly localized in the cell nucleus as explained in the introductory chapter. Therefore, the ER-targeting radiolabelled probes must have the ability to cross the plasma and nuclear membranes in order to reach and interact with the receptor. In this context, cellular uptake studies are essential to evaluate whether the ¹¹¹In-labelled peptides are effectively taken up by the ER-expressing cells.

The cellular uptake of the three ¹¹¹In-labelled peptides was studied in MCF-7 cells, a breast cancer cell line of human origin in which ER is expressed (ER+) and the results are represented in Figure 2.8. **[¹¹¹In]DOTA-ER3** showed the highest uptake with a maximum of 23% (of total activity) after one hour of incubation, followed by a slight decline suggesting some efflux of the radioconjugate from the cells. The same profile was verified for the two other radiopeptides although the uptake values were drastically lower with **[¹¹¹In]DOTA-cER1** and **[¹¹¹In]DOTA-ER2** reaching maximum values of 1.60% and 0.54%, respectively, after one hour of incubation with the ER(+) cells.

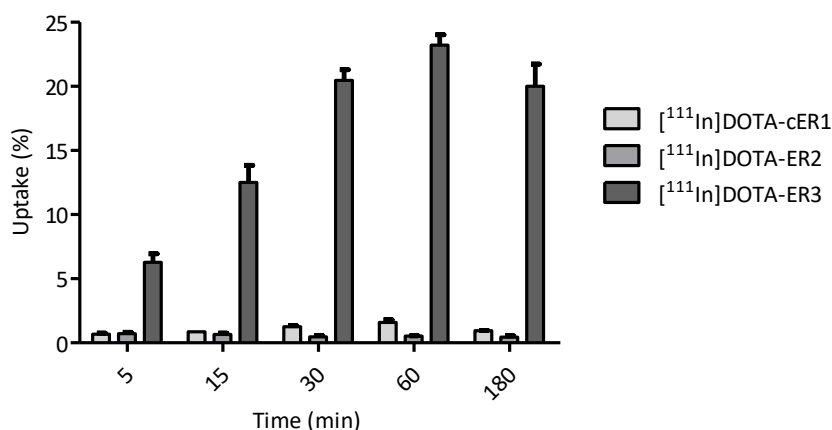


Figure 2.8. Cellular uptake (% of total applied activity \pm SD) of the ¹¹¹In-labelled LXXLL peptides in MCF-7 cells (n=3).

The highly hydrophilic character of the radiolabelled peptides is a factor that should represent an obstacle for the cellular uptake. However, the net charge is also known to influence the cellular uptake of the peptides, and in particular the interaction between the peptides and specific molecules of the cell membrane. The presence of basic aminoacids such as Lys and Arg that are protonated at pH 7, resulting in a net positive charge for the peptides, has been demonstrated to be an important feature for the interaction with negatively charged cell membrane components which include phosphatidylserine and glycoproteins [227]. In fact, membrane binding is regarded as a crucial initial step in the transport of cationic peptides into the cells. The presence of a cluster of 2 Lys residues in the ER3 peptide, besides the Arg within the LXXLL sequence, might provide an anchor for the adherence to the negatively charged cell surface by hydrogen-bonding and electrostatic interactions, which can explain, at least partially, the higher uptake verified for [¹¹¹In]DOTA-ER3 [228]. It should be mentioned also that the ¹¹¹In-labelled DOTA-ER3 peptide has the highest net positive charge (at pH 7) of the three peptides (+4 versus +3 for the radiolabelled DOTA-cER1 and DOTA-ER2) which reinforces the hypotheses of the stronger ionic interaction with the cells surface.

A more detailed study of the activity distribution in the different cell compartments was performed by doing a cell fractionation assay at the time of maximum uptake of [¹¹¹In]DOTA-ER3 by MCF-7 cells (1 hour). The results of the assay (Figure 2.9) revealed that the activity was mostly bound to the cell membrane (77% of total uptake), although approximately 16% of the

activity was found in the cytosol indicating that [^{111}In]DOTA-ER3 was successfully internalized into the cell. A small percentage (4.3%) was detected in the nuclear compartment. This is an important indication since ER α resides predominantly in the cell nucleus, and therefore nuclear uptake makes it possible for the radiopeptide to reach the receptor [229]. Furthermore, nuclear uptake is also an important requirement for Auger therapy making possible the delivery of In-111 near DNA.

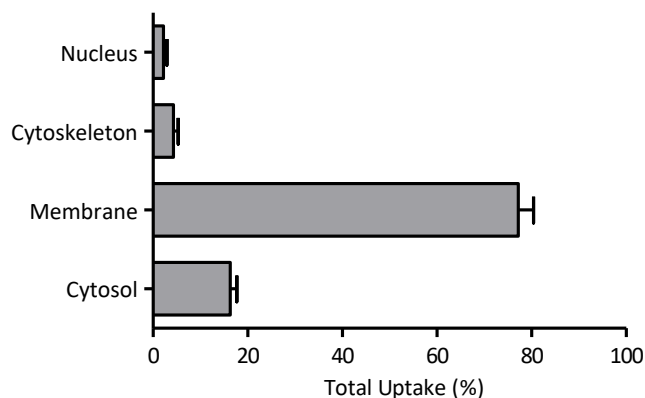


Figure 2.9. Subcellular localization of [^{111}In]DOTA-ER3 in MCF-7 cells after incubation for 1 hour at 37°C (n=3).

Cellular uptake of [^{111}In]DOTA-ER3 was further studied in other two cell lines of human origin: triple-negative (ER-, PR-, HER2-) breast cancer cells MDA-MB-231 and epidermoid carcinoma cells A431. The results of the study are shown in Figure 2.10. In ER(-) breast cancer cells a fast initial uptake of the radiopeptide was verified reaching a maximum of approximately 10% at 15 minutes followed by a steady decline until almost 3% at 3 hours of incubation. In the epidermoid carcinoma cells the uptake exhibited a slower rate but it also demonstrated a sharp decline after the maximum (9.7% at 30 min) reaching a 5% value at 3 hours. For both cell lines the verified [^{111}In]DOTA-ER3 uptake values were considerably lower comparing to the uptake in the MCF-7 cells. Furthermore, the retention of the activity in the cells were significantly weaker in the A431 and in the MDA-MB-231 comparing to the MCF-7 cells in which the uptake value after 3 hours was 4- to 6-fold higher. These results suggest specificity of [^{111}In]DOTA-ER3 for ER(+) cells which is promising for selective targeting of breast cancer cells.

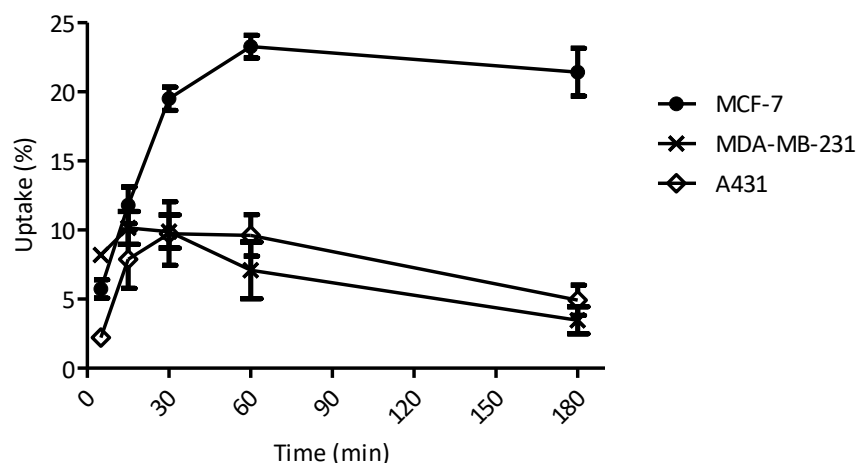


Figure 2.10. Comparison of the cellular uptake (% of total applied activity \pm SD) of [¹¹¹In]DOTA-ER3 in MCF-7, MDA-MB-231 and A431 cells (n=3).

2.1.1.7. Biodistribution and *In Vivo* Stability of the Radiolabelled Peptides

Biodistribution studies in animal models represent a crucial step in the pre-clinical evaluation of new radiopharmaceuticals. These *in vivo* studies provide important information about the biokinetics of the radiolabelled compounds, in particular the clearance rate from systemic blood circulation and the tissue/organ distribution of radioactivity over time. In this way, biodistribution studies can give a valuable insight about the selectivity of target-specific radioconjugates through the evaluation of the radioactivity uptake in the tissues/organs that (over)express the receptor target [88, 171, 230]. Furthermore, animal studies are also important to assess the *in vivo* stability of the radiolabelled compounds towards hydrolysis, proteolytic degradation and transchelation in physiological medium. In fact, the biodistribution profiles and hence the biological targeting properties are critically dependent on the *in vivo* integrity of the radiolabelled conjugates [231, 232].

In this work, the three ¹¹¹In-labelled LXXLL peptides were first studied in healthy female mice in order to: i) evaluate the clearance kinetics, ii) identify the main excretory pathways and iii) determine the radioactivity uptake in the ER-rich organs: ovaries and uterus. In the subsequent stage, the ability of a selected radiolabelled peptide to specifically target breast tumor tissue was studied in tumor-bearing mice. Given the susceptibility of peptide sequences

to metabolic degradation, the *in vivo* stability of the radiolabelled LXXLL peptides was also studied in the animal models.

Biodistribution in Healthy CD-1 Mice

The biodistribution profiles of the three radiolabelled peptides were studied in healthy CD-1 female mice at 15 and 60 minutes after intravenous (i.v.) injection of the ^{111}In -complexes. The results expressed as percentage of the injected activity per gram of tissue (% I.A./g) are represented in Figure 2.11. Overall the three radiopeptides showed a fast clearance from the blood primarily through renal excretion as shown by the high uptakes in this organ both at 15 min and at 60 min *p.i.* (*post injection*). In fact, for the three ^{111}In -labelled peptides more than 70% of the administered activity was excreted after one hour, corroborating the fast overall elimination rate. The low uptake in the liver and in the spleen suggest that there was no release of uncomplexed ^{111}In during circulation time in mice since the free radiometal would accumulate in these organs mainly via the formation of ^{111}In -transferrin complexes [233].

[^{111}In]DOTA-ER3 revealed the highest retention in the kidneys 1 hour after injection (23.1 ± 7.1 % I.A./g) as well as the most prominent clearance from the blood (a reduction of 53% between the two time points under study). The higher hydrophilicity and the stronger cationic character should have contributed for this behaviour. Retention of radiometabolites in the kidneys have been explained by the occurrence of tubular re-absorption into the renal cells after glomerular filtration. Several studies with ^{111}In -labelled peptides have revealed that in the renal cells the radiopeptides are transported to the lysosomal compartments where they are metabolized generating final radiometabolites that are responsible for the accumulation in the kidneys [232, 234]. **[^{111}In]DOTA-cER1** demonstrated slightly higher liver uptake (4.3 ± 7.1 % I.A./g, 1 h *p.i.*) comparing with the other two radioconjugates revealing some hepatobiliary excretion along with the main renal route.

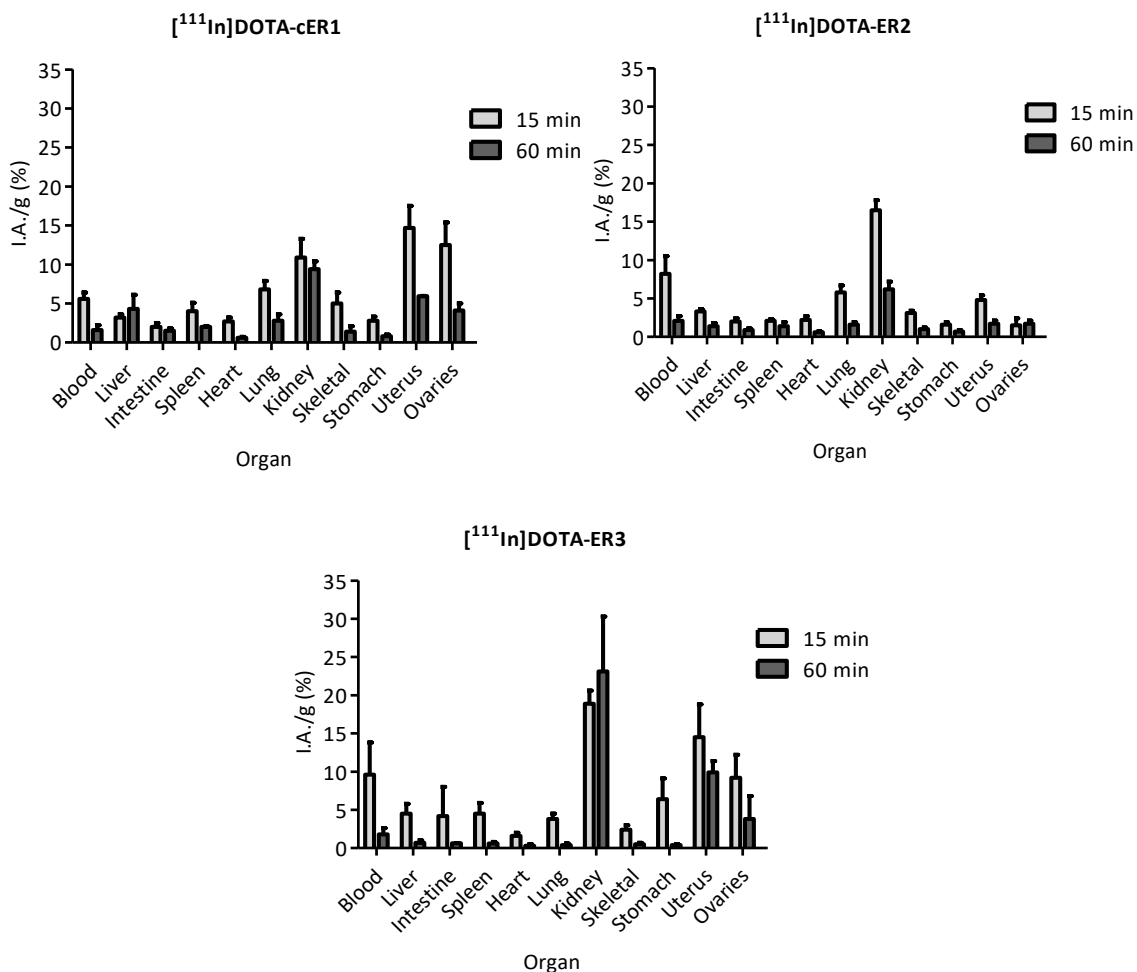


Figure 2.11. Biodistribution profiles (I.A./g (%) \pm SD) of the ¹¹¹In-labelled LXXLL peptides in CD-1 female mice, 15 min and 60 min *p.i.* (n=3).

Besides the uptake by the organs involved in the excretory pathways, [¹¹¹In]DOTA-cER1 and [¹¹¹In]DOTA-ER3 showed a high accumulation in the uterus and in the ovaries giving evidence of selective tissue uptake. Although some washout of the activity from these organs was verified between the two time points, at one hour *p.i.* [¹¹¹In]DOTA-cER1 and [¹¹¹In]DOTA-ER3 exhibited uptakes (expressed as % I.A./g), respectively, of 5.93 ± 0.04 and 9.90 ± 1.50 in the uterus, and 4.10 ± 0.90 and 3.80 ± 3.00 in the ovaries. Consequently, good radioactivity ratios between these ER-rich organs and the adjacent non-target tissues (muscle and blood) were found for the two radiolabelled peptides (1 h *p.i.*), as shown in Figure 2.12. In fact, the demonstrated target/non-target ratios were higher or comparable to the ones found in the literature for radiolabelled estradiol derivatives with good binding affinity towards ER α [104, 235-237], reinforcing the potential of these two radioconjugates for the imaging of ER(+) tissues.

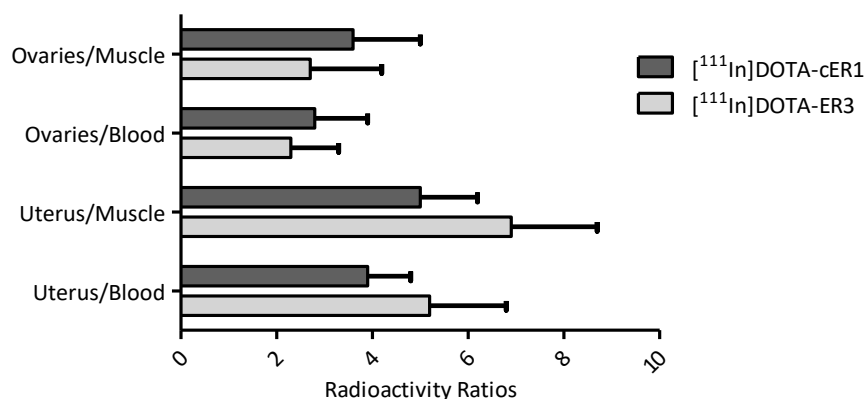


Figure 2.12. Target/non-target ratios (\pm SD) of [¹¹¹In]DOTA-cER1 and [¹¹¹In]DOTA-ER3 60 min *p.i.* (CD-1 mice).

Evaluation of the In Vivo Stability

The analysis of the mice urine by HPLC demonstrated that the three injected radiolabelled peptides suffered complete metabolization, most probably in the renal cells, leading to the formation of new radiochemical species with a different retention time compared with the initial ¹¹¹In-labelled complexes, as shown in the radiochromatograms in Figure 2.13. On the other hand, analysis of the mice serum revealed that [¹¹¹In]DOTA-ER2 was the only studied radiopeptide that was not present in its intact form in circulation 1 hour after injection, thus confirming *in vivo* the highest instability towards proteolytic cleavage demonstrated previously in the *in vitro* study with human serum. This metabolic degradation could have affected the biodistribution profile and could have impacted the ability to reach target organs. On the contrary, HPLC analysis of the mice serum after injection of [¹¹¹In]DOTA-cER1 and [¹¹¹In]DOTA-ER3 indicated that most of the injected radiolabelled peptides were present in the serum as a single radiochemical species with retention times similar to that of the injected complexes, as shown in Figure 2.13. Therefore, [¹¹¹In]DOTA-cER1 and [¹¹¹In]DOTA-ER3 were distributed to the different tissues mainly in their intact forms.

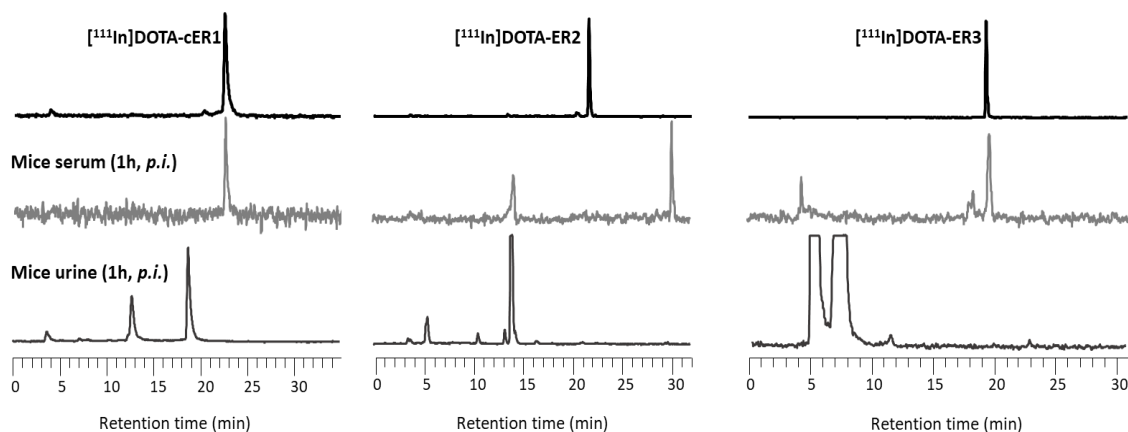


Figure 2.13. Radiochromatograms (Method B) of the injected radiopeptides (upper part of the figure) and of the mice blood (in the middle) and mice urine (lower part of the figure) 1 h after injection (CD-1 mice).

Biodistribution in Tumor-bearing BALB/c Mice

The tumor-targeting properties of [111In]DOTA-ER3 were studied in female BALB/c nu/nu mice bearing MCF-7 xenografts. The biodistribution profile (Figure 2.14 and Table 2.9) corroborated the fast blood clearance and the rapid whole-body radioactivity elimination by renal excretion found in the healthy animal model. In the three time points (15, 60 and 180 min), the kidneys were the organs that showed highest accumulation of activity (expressed as % I.A./g) although there was some washout between 1 and 3 hours *p.i.*.

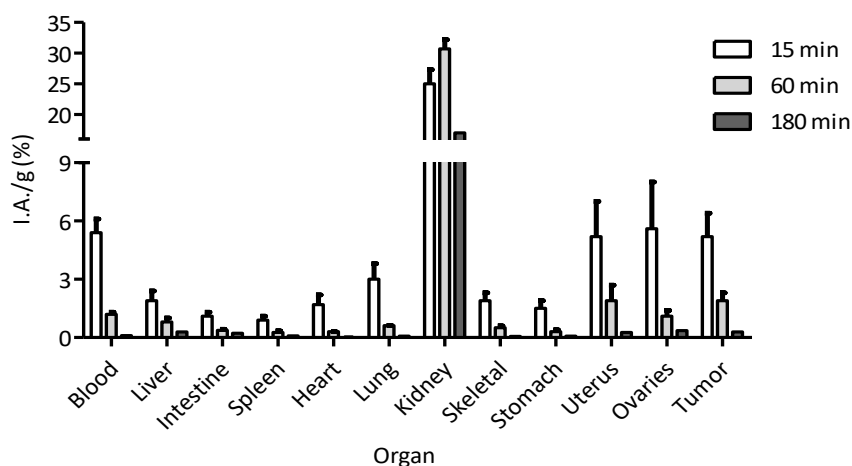


Figure 2.14. Biodistribution profile (I.A./g (%) \pm SD) of [111In]DOTA-ER3 in female BALB/c nu/nu mice bearing MCF-7 xenografts at 15, 60 and 180 min *p.i.* (n=3).

Table 2.9. Biodistribution data (I.A./g (%) \pm SD) of [^{111}In]DOTA-ER3 in female BALB/c nu/nu mice bearing MCF-7 xenografts at 15, 60 and 180 min *p.i.* (n=3).

Organ	% I.A./ g		
	15 min	1 h	3 h
Blood	5.4 \pm 0.7	1.2 \pm 0.1	0.10 \pm 0.02
Liver	1.9 \pm 0.5	0.8 \pm 0.2	0.29 \pm 0.06
Intestine	1.1 \pm 0.2	0.37 \pm 0.05	0.22 \pm 0.03
Spleen	0.9 \pm 0.2	0.27 \pm 0.07	0.09 \pm 0.01
Heart	1.7 \pm 0.5	0.30 \pm 0.01	0.04 \pm 0.01
Lung	3.0 \pm 0.8	0.62 \pm 0.01	0.08 \pm 0.02
Kidney	25.0 \pm 2.3	30.7 \pm 1.5	17.0 \pm 1.9
Muscle	1.6 \pm 0.2	0.3 \pm 0.0	0.03 \pm 0.00
Skeletal	1.9 \pm 0.4	0.5 \pm 0.1	0.06 \pm 0.01
Stomach	1.5 \pm 0.4	0.3 \pm 0.1	0.07 \pm 0.04
Ovaries	5.6 \pm 2.4	1.1 \pm 0.3	0.36 \pm 0.03
Uterus	5.2 \pm 1.8	1.9 \pm 0.8	0.26 \pm 0.07
Tumor	5.2 \pm 1.2	1.9 \pm 0.4	0.29 \pm 0.05

Following the excretory organs, most of the radioactivity was found in the ER-rich organs (ovaries and uterus) and in the xenotransplant tumor at 3h *p.i.*. The tumor to background ratios (Figure 2.15) increased over time up to 3 h (tumor/blood ratio: 3.0 ± 0.2 ; tumor/muscle ratio: 8.9 ± 1.7) suggesting some specific accumulation in the tumoral tissue. For the ER-rich organs, ovaries and uterus, the target/non-target ratios at 3 h *p.i.* were all higher than 2 (uterus/blood ratio: 2.7 ± 0.5 ; ovaries/blood ratio: 3.9 ± 1.0) providing also some evidence of ER-mediated uptake.

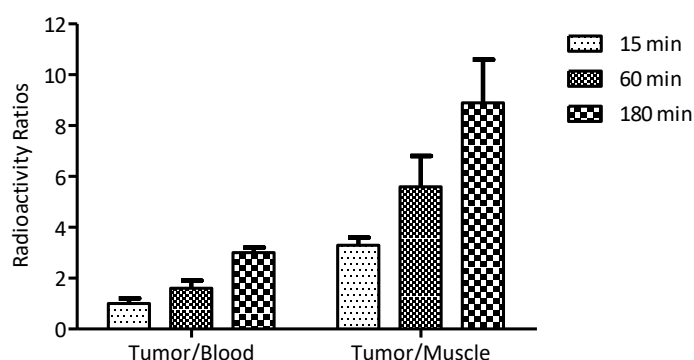


Figure 2.15. Tumor/Background ratios (\pm SD) of [^{111}In]DOTA-ER3 at 15, 60 and 180 min *p.i.* (n=3).

2.2. Radiolabelled pY-derivatives

2.2.1. pY Peptide

Identification of the rapid mitogenic actions of estradiol has suggested the development of molecules to interfere with the signaling pathway in ER-positive cancer cells [52, 168]. Based on the knowledge that the phosphotyrosine at position 537 in the ER α plays a critical role in the association to the tyrosine kinase Src, Varricchio et al. synthesized a six-residue peptide, the pY peptide (H-Leu-pTyr-Asp-Leu-Leu-Leu-NH₂), which is derived from residues 536-541 of ER α including the above-mentioned tyrosine 537. This small phosphorylated peptide demonstrated ability to bind to the Src SH2 domain with high affinity and to inhibit the DNA synthesis induced by estradiol, androgen or EGF in BC cells [66]. It was demonstrated that the phosphopeptide inhibited the ER α association with Src and consequently all the subsequent events including the Src/Erk pathway activation and the cyclin D1 expression. Experiments with the non-phosphorylated peptide revealed only a weak inhibitory effect proving that the phosphorylation of the tyrosine residue is important for the association to the Src [52, 168]. The effects of pY on *in vivo* MCF-7 cell growth were also investigated in female athymic nude mice and the peptide almost abolished the tumor growth for eight consecutive weeks [66]. In contrast with classic steroid antagonists, the peptide has not modified the ER-dependent transcriptional activity, and therefore has not targeted the hormonal effects mediated by the genomic pathway, leading to the conclusion that the pY peptide interferes exclusively in the ER non-genomic signaling network [168].

The potential interest of pY in the development of novel therapeutic approaches is highlighted by the fact that more than 70% of human breast tumors have shown a 2- to 50-fold increased activity of the Src tyrosine kinase compared to normal cells, which makes Src an attractive target [238]. Previous studies have shown that increased Src activity after long-term treatment with tamoxifen enhances cellular invasion and motility in BC cells thus contributing for the development of resistance to endocrine therapy and for the appearance of metastasis [239, 240]. Src inhibitors such as dasatinib and bosutinib have been developed to treat BC and have shown potential in the clinical setting in combination with aromatase inhibitors. However, the identification of the patients that would benefit from these combination therapies remains a challenge [239].

Hence, the goal of the work discussed in the following sections was the study of the pY peptide as a potential vector for the construction of radiolabelled imaging probes targeting Src. In fact, due to the heterogeneity of BC and the increasing need for personalized therapies, Src is an interesting imaging target whose overexpression is associated with more aggressive and metastatic types of BC. The synthesis of the pY-based probes, the preparation of the In-/¹¹¹In-complexes and the *in vitro* evaluation of the new radiolabelled conjugates is presented and discussed in the following sections.

2.2.2. Synthesis and Characterization of the pY Peptide

The development of synthetic strategies for phosphorylation of peptides has been a challenge, mainly because of the importance of phosphopeptides as tools for the study of protein expression and signal transduction. There are currently two general methods for the synthesis of phosphopeptides: global phosphorylation and the building block approach. Global phosphorylation involves post-synthetic phosphorylation of unprotected hydroxyl groups on the solid support by treatment with a dialkyl or diaryl phosphorochloridate or with a phosphoramidite followed by oxidation. On the other hand, the building block approach is the more straightforward strategy for preparing phosphopeptides since it involves only the incorporation of a suitable N α -protected phosphoamino acid into the appropriate point of the peptide chain. In this regard, methyl, benzyl, *tert*-butyl and alkylamide protected derivatives have been used for the incorporation of phosphotyrosine in Fmoc SPPS. However, these protecting groups often give rise to undesired by-products during deprotection steps [181, 241]. In 1994, Ottinger et al. demonstrated the utility of Fmoc-Tyr(PO₃H₂)-OH, with an unprotected phosphate group for the introduction of phosphotyrosine in the peptide chain. This method proved to be successful for the synthesis of small phosphopeptides (4 to 10 amino acids) in good yield and chemical purity [242]. The major limitation of the use of the tyrosine residue with the unprotected phosphate group is the tendency for the formation of intramolecular pyrophosphate linkages. However, this phenomenon was found to occur only when the phosphotyrosine residues are directly adjacent to one other and its severity is higher when longer coupling times are applied [243].

For the synthesis of the pY peptide (H-Leu-pTyr-Asp-Leu-Leu-Leu-NH₂), the use of the Fmoc-Tyr(PO₃H₂)-OH as building block was the selected strategy to introduce the phosphotyrosine residue. Besides being the most straightforward method, the short sequence

of the peptide (6 amino acids) and the lack of additional phosphotyrosine residues did not anticipate the occurrence of problematic side reactions. Therefore, the peptide was synthesized in a microwave-assisted automated peptide synthesizer using the HBTU/DIPEA chemistry with peptide elongation on a Rink Amide MBH resin to afford a final carboxyamided peptide. After cleavage with the standard TFA/TIS/water (95:2.5:2.5) cocktail, the crude product was analysed by HPLC and ESI-MS. Although the presence of the desired **pY** peptide was identified in the mixture (in 21% yield, determined by HPLC), the major product found in the crude (44% yield) corresponded to the peptide sequence lacking the final Lys residue (m/z 715.75 calcd. for $C_{31}H_{151}N_6O_{11}P$, found 715.8 $[M+H]^+$) which denotes difficulties regarding the attachment of the subsequent amino acid to the Tyr(PO_3H_2) residue. The undesired competitive phosphate activation on the unprotected phosphorylated residue could have contributed for the lower yield of the subsequent coupling [244]. After HPLC purification, the **pY** peptide was obtained with high purity (>95%) and was characterized by HPLC, ESI-MS and MS/MS. The ESI-MS spectrum obtained under the negative mode is shown in Figure 2.16. The presence of the phosphorylated amino acid was further confirmed by MS/MS by the observation of HPO_3 (-80 Da) and H_3PO_4 (-98 Da) losses from peptide fragments containing the Tyr residue, as shown in Figure 2.17.

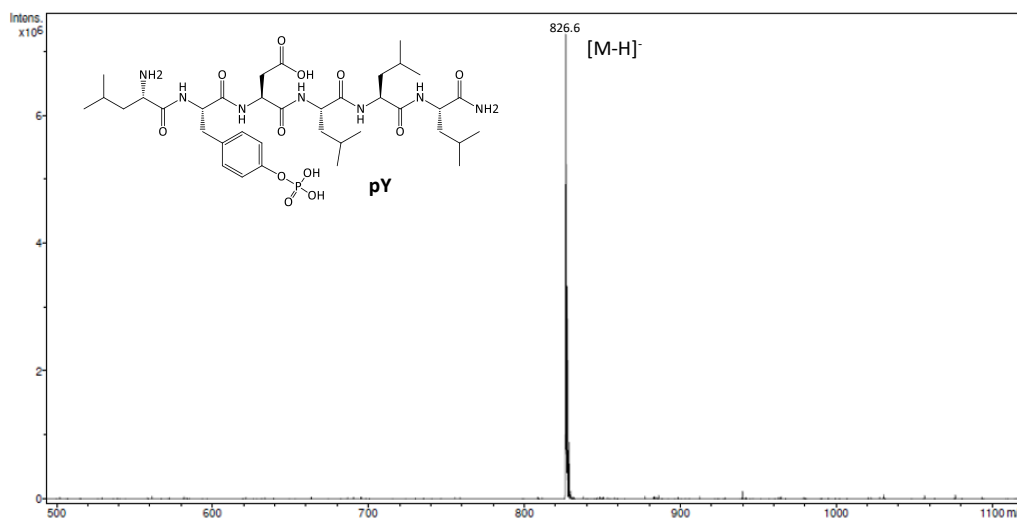


Figure 2.16. ESI-MS spectrum of the pY peptide in the negative ion mode (m/z calcd for $C_{37}H_{61}N_7O_{12}P$: 826.42 $[M-H]^-$, found: 826.6 $[M-H]^-$) and representation of its chemical structure.

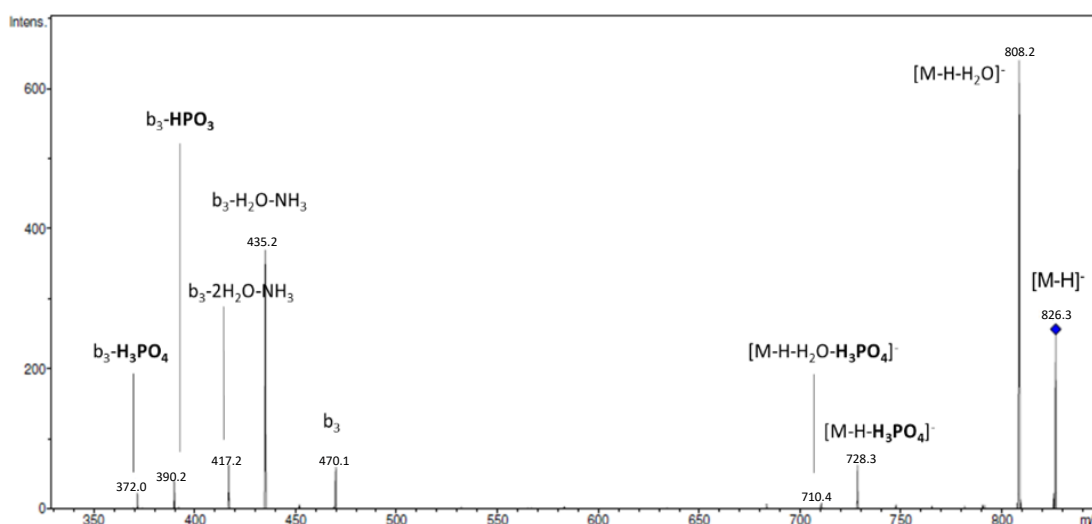


Figure 2.17. MS/MS spectrum of pY peptide under negative ion mode (isolation mass: 826.3, isolation width: 1.0 m/z, fragmentation amplitude: 0.35 V). The b_3 fragment corresponds to the sequence Leu-pTyr-Asp.

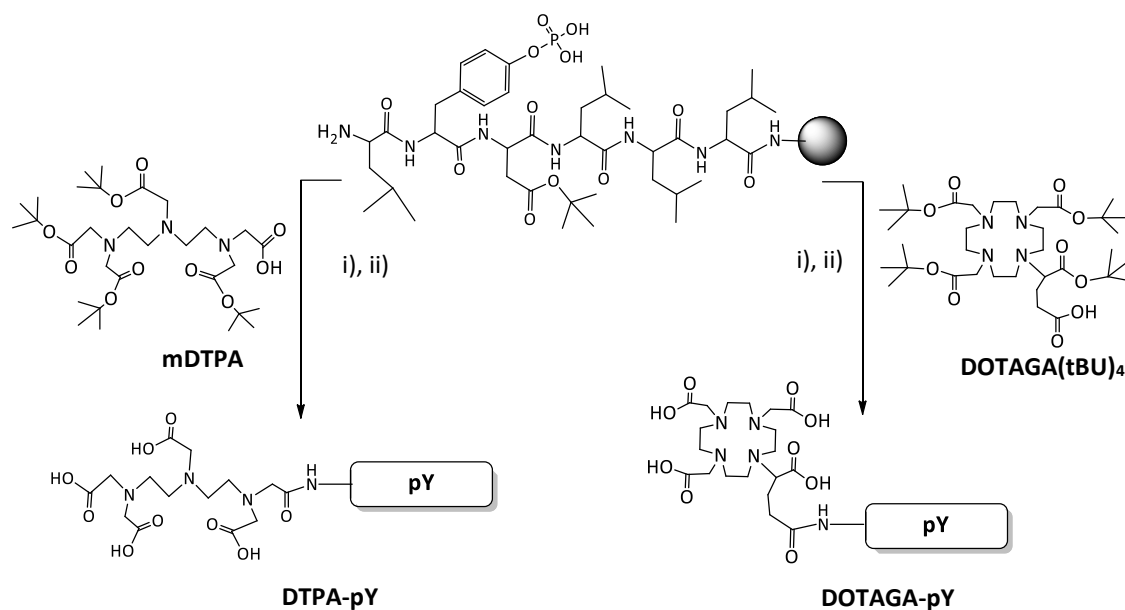
2.2.3. Synthesis and Characterization of the pY-derivatives

The presence of a phosphotyrosine in the sequence poses a specific challenge regarding the peptide's stability. Pennington et al. verified that the phosphate group from pTyr was more susceptible to hydrolysis in acidic pH (< 6) and concluded that this degradation process was time- and temperature- dependent [245]. Since the presence of the phosphorylated tyrosine is crucial for the peptide's biological activity, the issue of the stability had to be taken into consideration in the selection of the chelator moiety to be conjugated to the sequence.

The acyclic chelator DTPA is known to offer fast Indium complexation kinetics at room temperature which makes it a suitable chelator for the radiolabelling of thermolabile peptide sequences with In-111 [137]. For the preparation of DTPA-peptide conjugates, the most popular strategy until recent years was the conjugation to the peptide sequence of the cyclic diethylenetriaminepentaacetic dianhydride (cDTPA). However, this reagent led inevitably to the concomitant formation of the bisconjugated product and to intra- and intermolecular cross-linked products [141]. Therefore, a monoreactive DTPA (mDTPA) derivative with four carboxylates protected with acid-removable *tert*-butyl esters and bearing only one reactive carboxylic acid was developed and had been employed successfully for the synthesis of DTPA-peptide conjugates without the unfavourable by-product formation. The *tert*-butyl protection and its solubility in DMF makes it fully compatible with solid phase synthesis using the Fmoc-based chemistry. Although the synthetic procedure to obtain mDTPA is long and fastidious, the

fact that this monoreactive BFC is commercially available facilitates its use for the preparation of In-111 labelled peptides [246]. Therefore, in this work mDTPA (commercially acquired) was selected for the conjugation to the free N-terminus of the **pY** peptide on solid-phase. The first attempt for the conjugation was done using the powerful coupling reagent HATU (2.5 equiv) in two coupling cycles (2 hours each) [247]. However, these conditions failed to give the desired product yielding instead a by-product with an m/z of 958.8 (in the negative ion mode of ESI-MS) whose structure was not possible to propose. Therefore, another attempt was made by using the phosphonium-based coupling reagent PyBOP (benzotriazol-1-yloxytri(pyrrolidino)-phosphonium hexafluorophosphate) in combination with HOBt (1-hydroxybenzotriazole) which is typically used as an additive to ensure faster and more efficient couplings [200]. The coupling time was also extended to 3 hours, and 2 coupling cycles were performed. This approach was successful in the preparation of the **DTPA-pY** (Scheme 2.2) conjugate with high yield (approximately 88%) after cleavage from the resin and deprotection with the standard cocktail solution.

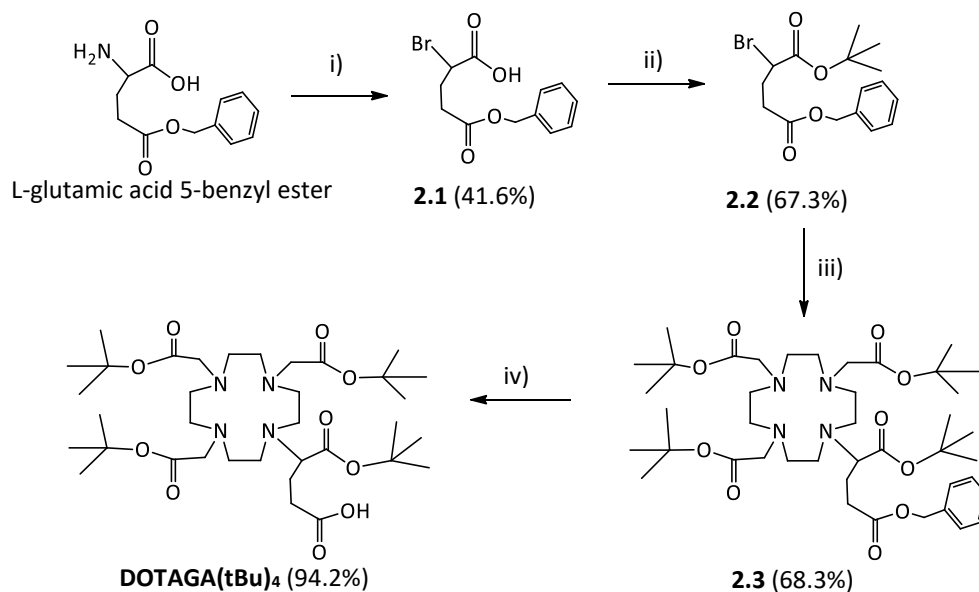
Several examples in the literature show that by using different chelating units it is possible to influence the stability, the targeting ability and the biodistribution profile of radiolabelled peptides [172, 178, 223, 248]. Therefore, aiming to compare with the **DTPA-pY** conjugate, the macrocyclic chelator DOTAGA was also conjugated to the pY peptide (Scheme 2.2). Due to the extra carboxylic acid available for metal coordination, DOTAGA is reported to offer faster complexation kinetics than the classic DOTA which can be advantageous for more sensitive peptides [222]. Furthermore, since it is a macrocycle chelator, DOTAGA is expected to provide higher kinetic stability for the In-complexes comparing with the acyclic DTPA [137].



Scheme 2.2. Coupling of the bifunctional chelators DTPA and DOTAGA to pY peptide on solid phase. The filled circle represents Rink Amide resin.

i) PyBOP, HOBT, DIPEA, DMF, RT, 6 h; ii) TFA, TIS, H₂O, RT, 3 h

The prochelator **DOTAGA(tBu)₄** was synthesized based on the procedure described by Eisenwiener et al. with some modifications (Scheme 2.3) [249]. The synthesis started with the α -bromination of the commercially available glutamic acid- γ -benzyl ester followed by the *tert*-butylation of the remaining carboxylic acid using *tert*-butyl-trichloroacetimidate (TBTA) as reagent, yielding α -bromoglutaric acid-1-*tert*-butylester-5-benzylester (**2.2**) with an overall yield of 28.0 %. The cyclen derivative DO3AtBu (tri-*tert*-butyl 1,4,7,10-tetraazacyclododecane-1,4,7-triacetate), commercially acquired, was then alkylated on the free nitrogen with the synthesized brominated arm (1.2 equiv) in a reaction that proceeded successfully at room temperature (18 h) with a yield of 68.3%. This strategy avoided the problematic step of cyclen monoalkylation of the original procedure. To obtain the final prochelator, a Pd/C-catalytic hydrogenation was performed to remove selectively the benzyl ester yielding **DOTAGA(tBu)₄** quantitatively.



Scheme 2.3. Synthesis of DOTAGA(tBu)₄.

i) NaNO₂, NaBr, 2 N HBr, 0°C, 3h; **ii)** TBTA, BF₃OEt₂, Cyclohexan, CHCl₃, DMA, RT, 96 h; **iii)** DO3AtBu, K₂CO₃, CH₃CN, RT, 18 h; **iv)** H₂, Pd/C, CH₃OH, RT, 8 h

For the solid phase coupling to the pY peptide, the same PyBOP/HOBt system previously tested for the mDTPA was applied, giving the desired **DOTAGA-pY** conjugate with 72.3% yield after cleavage and deprotection.

Characterization of **DTPA-pY** and **DOTAGA-pY** by HPLC and ESI-MS is summarized in Table 2.10. The presence in the sequence of the phosphorylated and Asp residues, which can easily lose protons, allowed the detection of both conjugates in the negative ion mode of the ESI-MS besides the usual positive mode.

Table 2.10. Characterization of the pY peptide conjugates by HPLC and ESI-MS.

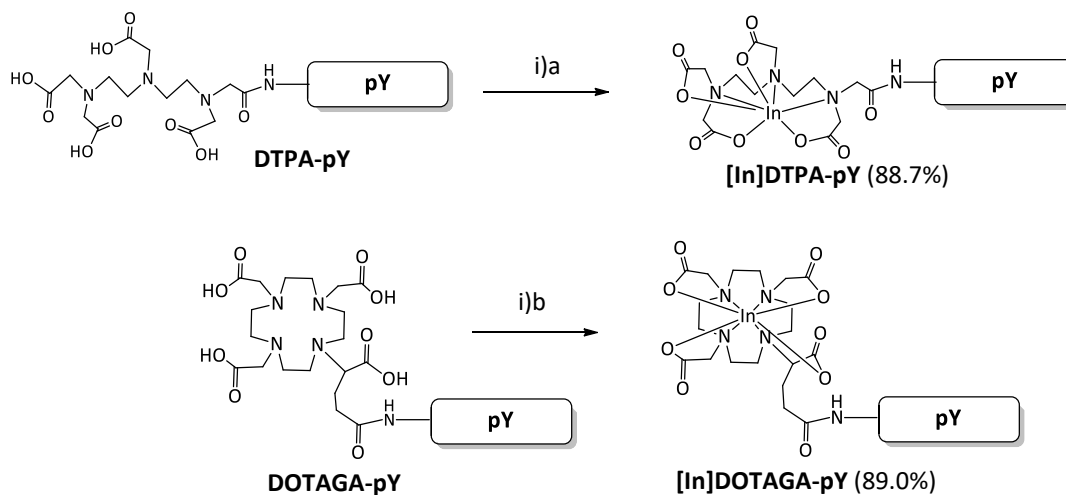
Conjugate	HPLC	ESI-MS		Molecular Formula
	Rt (min)*	Calculated (m/z)	Found (m/z)	
DTPA-pY	17.40	1203.55 [M+H] ⁺	1203.8 [M+H] ⁺	C ₅₁ H ₈₃ N ₁₀ O ₂₁ P
		602.28 [M+2H] ²⁺	602.5 [M+2H] ²⁺	
		-	-	
		1201.54 [M-H] ⁻	1201.9 [M-H] ⁻	
		600.27 [M-2H] ²⁻	600.5 [M-2H] ²⁻	
DOTAGA-pY	18.14	1286.63 [M+H] ⁺	1287.2 [M+H] ⁺	C ₅₆ H ₉₂ N ₁₁ O ₂₁ P
		-	-	
		1284.61 [M-H] ⁻	1284.3 [M-H] ⁻	
		641.80 [M-2H] ²⁻	642.1 [M-2H] ²⁻	
		-	-	

*Method A (Eluents: A- 0.1% aq. TFA; B- 0.1% TFA/CH₃CN. Gradient (%): 90 A/10 B to 70 A/30 B in 10 min, 70 A/30 B to 55 A/45 B in 30 min).

2.2.4. Synthesis and Characterization of the In(III) Complexes

Preparation of the inactive Indium complexes was done by incubating the conjugates with InCl₃ (1.2 equiv) in an acetate buffer pH 5.5 using different temperature conditions for the two chelator-peptide conjugates as depicted in Scheme 2.4. For the **DTPA-pY** conjugate the mixture was let to react at room temperature for 30 min while for the **DOTAGA-pY** the complexation reaction proceeded at 90°C for 15 min. After purification by HPLC the In-complexes were obtained in high yield (approximately 89%) for the two conjugates. The short period of time (15 min) used for heating the **DOTAGA-pY** conjugate did not lead to the hydrolysis of the phosphate group. The complexes were characterized by HPLC and ESI-MS (Table 2.11) with the isotopic distributions corroborating the In-complexation.

The metal in the [In]**DOTAGA-pY** complex is most likely octacoordinated (as suggested by the ESI-MS result) with the four carboxylates along with the four nitrogens of the macrocycle participating in the complexation. On the other hand, **DTPA-pY** is likely to be heptadentate with three nitrogens and four carboxylate-oxygen donors binding to the metal center after In-complexation [142].



Scheme 2.4. Synthesis of the inactive In(III) complexes of DTPA-pY and DOTAGA-pY.

i)a InCl_3 , 0.1 M NaOAc pH 5.5, RT, 30 min; **i)b** InCl_3 , 0.1 M NaOAc pH 5.5, 90°C, 15 min.

Table 2.11. Characterization of the Indium complexes of the pY-derivatives by HPLC and ESI-MS.

Complex	HPLC	ESI-MS		Molecular Formula
	Rt (min)*	Calculated (m/z)	Found (m/z)	
[In]DTPA-pY	17.56	1337.42 [M+H+Na] ⁺	1337.4 [M+H+Na] ⁺	[C ₅₁ H ₇₉ InN ₁₀ O ₂₁ P] ⁻
[In]DOTAGA-pY	18.80	699.76 [M+3H] ²⁺	700.0 [M+3H] ²⁺	[C ₅₆ H ₈₈ InN ₁₁ O ₂₁ P] ⁻
		1396.49 [M] ⁻	1396.4 [M] ⁻	

*Method A (Eluents: A- 0.1% aq. TFA; B- 0.1% TFA/CH₃CN. Gradient (%): 90 A/10 B to 70 A/30 B in 10 min, 70 A/30 B to 55 A/45 B in 30 min).

2.2.5. Radiolabelling of the pY-based Conjugates

Radiolabelling of the pY-derivatives with In-111 was performed in the same pH 5.5 acetate buffer as the inactive In-complexes. The **DTPA-pY** conjugate was radiolabelled at room temperature at a concentration of 5.5×10^{-6} M giving a radiochemical yield higher than 97% after just 10 minutes of reaction. For the **DOTAGA-pY** derivative, a temperature of 90°C was used for the radiolabelling reaction. The reaction time needed to achieve the maximum RCY was found to be between five to ten minutes. In this case, the lowest concentration of conjugate that was possible to radiolabel with a RCY higher than 80% was 1.0×10^{-5} M. Therefore, the specific activities achieved with the DOTAGA conjugate were lower than the ones obtained with the **DTPA-pY** which could be an advantageous property of [¹¹¹In]DTPA-pY in terms of *in vivo* biological targeting and background clearance.

Quality control of the radiolabelled conjugates was performed by HPLC with gamma detection. Characterization of the radioactive conjugates [¹¹¹In]DTPA-pY and [¹¹¹In]DOTAGA-pY is summarized in Table 2.12. A HPLC co-injection with the corresponding inactive In-complexes was used to ascertain the chemical identity of the radiolabelled peptides.

Table 2.12. Characterization of the ¹¹¹In-labelled pY conjugates by HPLC (gamma detection) and radiochemical yields (RCY) of the radiolabelling reactions (n=3). The retention times (UV detection) of the inactive Indium-complexes are indicated in brackets. Partition coefficients (log P) obtained by the “shake-flask” method are also displayed.

Radioconjugate	HPLC	RCY (%)	log P _{o/w}
	Rt (min)*		
[¹¹¹ In]DTPA-pY	13.58 (13.01)	98.36 ± 0.84	- 3.29 ± 0.02
[¹¹¹ In]DOTAGA-pY	14.43 (14.12)	97.55 ± 0.51	- 3.01 ± 0.03

*Method C (Eluents: A- 0.1% aq. TFA; B- 0.1% TFA/CH₃CN. Gradient (%): 95 A/5 B to 100 B in 18 min, 2 min 100 B).

Lipophilicity

The lipophilicity evaluation of the two radioconjugates by the “shake-flask” method demonstrated that both [¹¹¹In]DTPA-pY and [¹¹¹In]DOTAGA-pY are highly hydrophilic [220]. The

phosphate group, the aspartic acid and the chelating unit should be the major determinants of the demonstrated hydrophilicity. The DTPA conjugate presented a slightly higher hydrophilicity compared with the DOTAGA analogue which is in accordance with the shorter retention time of [¹¹¹In]DTPA-pY verified in the HPLC analysis. Since the peptide sequence is the same, this difference is attributed to differences in the coordination sphere.

2.2.6. *In Vitro* Stability Studies

In vitro stability of the radiolabelled conjugates was assessed at 37°C in PBS (pH 7.4) and in the presence of a large excess of ApoTf, in order to predict their kinetic inertness *in vivo*. Furthermore, [¹¹¹In]DOTAGA-pY was also challenged with an excess of DTPA to evaluate the strength of the In-111 complexation by the DOTAGA chelator. These results were compared to the stability of the radiopeptides in the radiolabelling solution (RS, pH 5.5) kept at room temperature. The results of these stability tests after 24 hours of incubation of the radiopeptides are displayed in Figure 2.18.

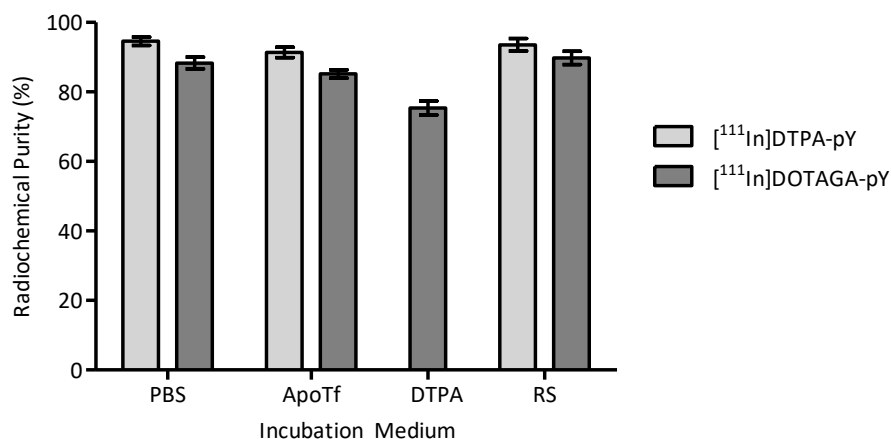


Figure 2.18. Radiochemical purity (determined by HPLC, Method C) of the ¹¹¹In-labelled pY conjugates after incubation for 24 h at 37°C in different media: in PBS, in the presence of an excess of apotransferrin (ApoTf) and in the presence of DTPA (only for the DOTAGA-pY conjugate). The stability in the radiolabelling medium (RS) at room temperature is also displayed for comparison.

Overall [¹¹¹In]DTPA-pY demonstrated higher stability (RCP > 90%) in the three media 24 hours after incubation, in comparison with the DOTAGA analogue. In the gamma-HPLC chromatograms of the radiolabelled DTPA conjugate, no free In-111 was detected regardless of the incubation medium suggesting a strong metal-chelator binding. However, a radiochemical

species with a slightly higher retention time appeared after 24 hours of incubation in all three media in percentages that ranged from 5.4 in PBS to 8.4 in the ApoTf media. No major differences were detected in the formation of this radiochemical impurity when comparing the radiolabelling mixture at room temperature and the other medium at 37°C, suggesting that neither the temperature nor the specific composition of the media played an important role in the observed degradation of the initial radiolabelled peptide during the 24h-incubation period. The same pattern was observed with the [¹¹¹In]DOTAGA-pY, with the formation of a new radioproduct with slightly higher retention time that appeared in the gamma-chromatograms of the samples collected from the four media in a percentage ranging between 2.4 to 8.6. However, for this conjugate it was also possible to detect the partial release of In-111 from the chelator during the incubation in the media. In fact, when challenged with an excess of DTPA for 24 hours, the peak in the solvent front of the [¹¹¹In]DOTAGA-pY radiochromatogram represented more than 20% of the total detected radioactivity. Since this value was more than double the ones found in the other incubation media (that were attributed solely to the free radiometal) and taken into account that the HPLC method used did not discriminate between free ¹¹¹In and [¹¹¹In]DTPA, it is reasonable to assume that there was some transchelation from the DOTAGA conjugated peptide to the unconjugated DTPA. Additionally, the new radioproduct with higher retention time observed for the two radiopeptides suggested that the peptide sequence suffered a degradation process with time that was independent of the conjugated chelator.

Stability in Human Serum

Stability of the radioconjugates was also studied along time by incubation at 37°C in human blood serum (Figure 2.19). The proteolytic activity of the human serum led to the rapid degradation of both [¹¹¹In]DTPA-pY and [¹¹¹In]DOTAGA-pY, confirming the formation of radiochemical impurities with the same retention time as the ones that were observed in the previous stability studies in the other media. After three hours of incubation, only 8.5% and 14.7% of the intact [¹¹¹In]DTPA-pY and [¹¹¹In]DOTAGA-pY, respectively, remained in the blood serum while the corresponding degradation products became the major radioactive species. These results reinforced the susceptibility of the pY peptide towards degradation which was clearly accelerated in the presence of serum peptidases.

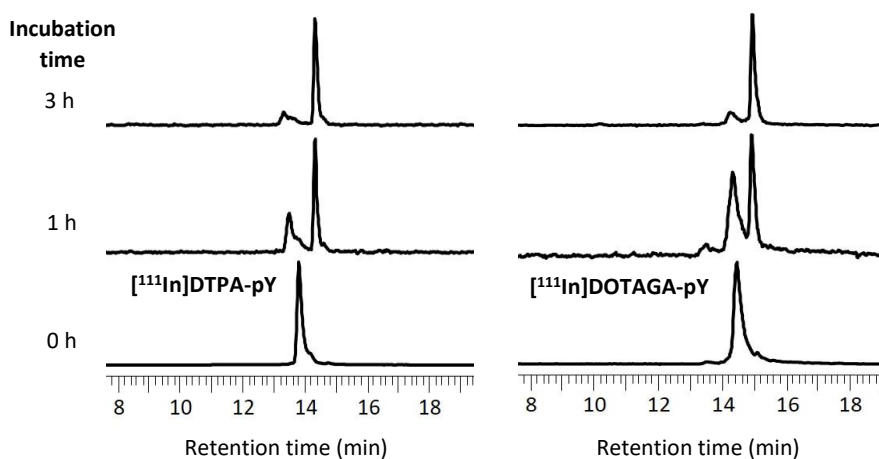
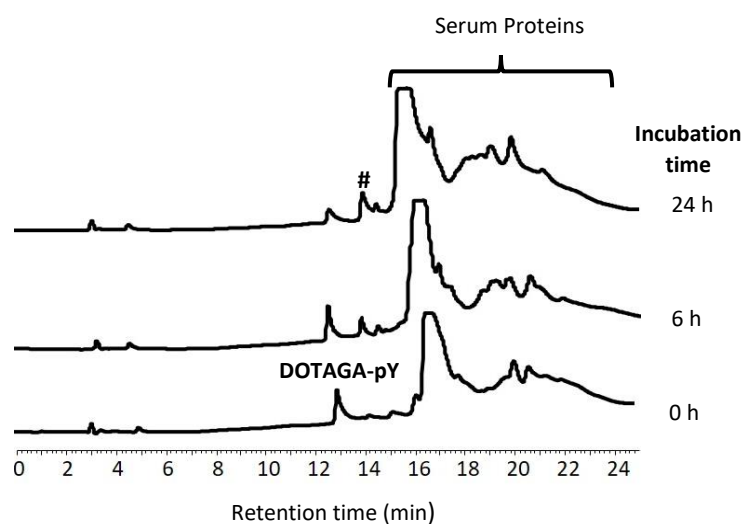


Figure 2.19. Radiochromatograms (HPLC, Method C) of aliquots of human serum after incubation with [¹¹¹In]DTPA-pY and [¹¹¹In]DOTAGA-pY for 1 and 3 hours. The radiochromatograms of the radiolabelled peptides before incubation are also shown (0 h) for comparison.

To study the possible degradation pathways involved in the observed instability, the **pY** peptide and the uncomplexed **pY-DOTAGA** conjugate were incubated in human blood serum at 37°C and aliquots of this medium were taken at specific time points and injected directly in the HPLC system. The aim of these stability assays was to identify, after HPLC purification, the degradation products formed with time. The HPLC method was adjusted to provide enough separation between the peptide and the serum proteins (albumin and globulins) in the chromatograms. Despite the fact that the degradation kinetics is not comparable to the one observed with the radiolabelled peptides, this study could provide an indication about the degradation products formed from [¹¹¹In]DTPA-pY and [¹¹¹In]DOTAGA-pY.

The stability study of the peptide in blood serum revealed the formation of a new chemical species with lower retention time which after 6 hours of incubation became the only product in the peptide region of the chromatogram while the initial **pY** peptide completely disappeared. The new species was purified and characterized by ESI-MS. The *m/z* of the peak with most intensity in the MS spectrum correlated well with the theoretical *m/z* of the pY peptide sequence without the last two amino acids (H-Asp-Leu-Leu-NH₂, *m/z* calcd for C₂₂H₄₂N₅O₆ [M+H]⁺: 472.31, *m/z* found: 472.5 [M+H]⁺). This finding suggests that the **pY** peptide with the free amine in the N-terminus is highly susceptible to the action of the aminopeptidases that are able to cleave the peptide bonds in the N-terminus releasing a dipeptide. However, since in the radiolabelled peptides the N-terminal amine is protected by the conjugation with the chelators, this is not the expected degradation pathway for [¹¹¹In]DTPA-pY and [¹¹¹In]DOTAGA-pY.

The incubation of the conjugate **pY-DOTAGA** in blood serum led to the formation of a new species with higher retention time as shown in Figure 2.20. The degradation of **pY-DOTAGA** was slower compared to the unconjugated peptide. In fact, after 24 hours of incubation there was still intact conjugate in the blood serum, although in less quantity than the degradation product.



ESI-MS spectrum of

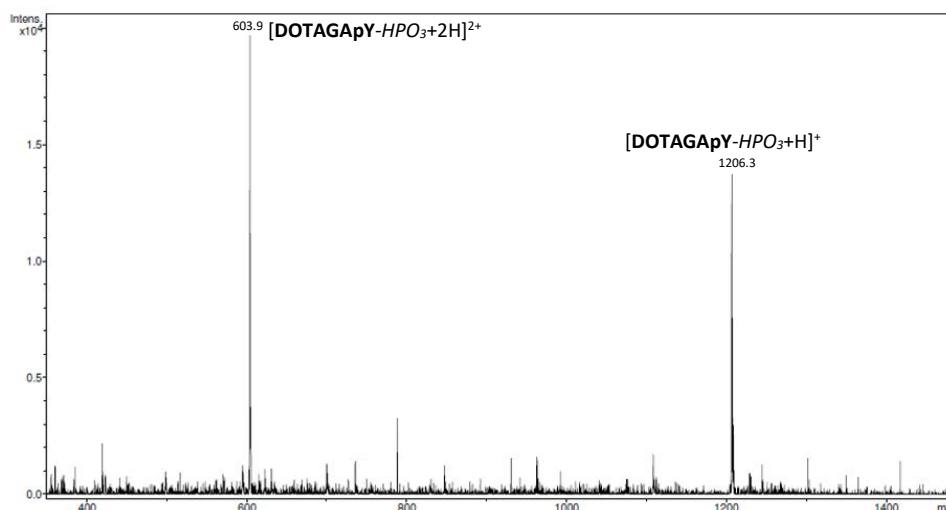


Figure 2.20. HPLC chromatograms (Method D) of the DOTAGA-pY conjugate incubated in human blood serum at different time points (0, 6 and 24 h) and the ESI-MS spectrum (positive mode) of the peak assigned with # in the HPLC chromatogram of the 24 hours time point (m/z calcd for $C_{57}H_{96}N_{11}O_{17}$ $[M+H]^+$, dephosphorylated DOTAGA-pY: 1206.69, m/z found 1206.3 $[M+H]^+$; 603.9 $[M+2H]^{2+}$).

The new species was purified and characterized by ESI-MS. The most intense peak in the spectrum (shown in Figure 2.20) presented an m/z that could be attributed to the loss of the

phosphate group (PO₃⁻) from the **pY-DOTAGA** conjugate. These results confirm the susceptibility of the peptide conjugates to enzymatic degradation, most probably through tyrosine dephosphorylation by serum phosphatases. Since this pathway leads to the formation of more lipophilic products (with slightly higher retention times in the HPLC chromatograms compared to the parent compounds), it is reasonable to presume that this is the same pathway responsible for the degradation of [¹¹¹In]DTPA-pY and [¹¹¹In]DOTAGA-pY.

2.2.7. Biological Evaluation of the Radiolabelled Peptides

Cellular Uptake

The cellular uptake of [¹¹¹In]DTPA-pY was studied in two human BC cell lines: ER(+) MCF-7 cells and ER(-) MDA-MB-231 cells. Despite the known interplay between Src and ER, it is known that the tyrosine kinase is also overexpressed in hormone negative breast cancers for which it has been considered a potential therapeutic target [250]. As shown in Figure 2.21, the uptake of [¹¹¹In]DTPA-pY in both cell lines was very low (about 1%) along the five hours of the assay. The expected negative charge of the radioactive complex and its highly hydrophilic character should hinder the ability of the radiopeptide to cross the cell membrane.

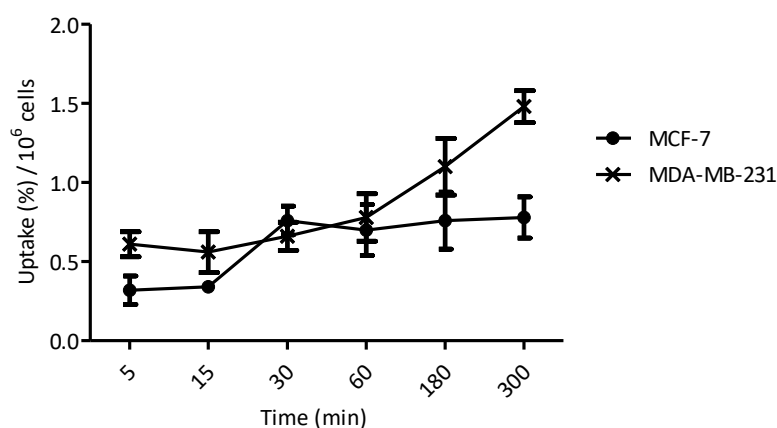


Figure 2.21. Cellular uptake (%/10⁶ cells ± SD) of [¹¹¹In]DTPA-pY in MCF-7 and MDA-MB-231 cells (n=3).

Preliminary Animal Studies

The *in vivo* behaviour of the two radiolabelled products was tested in healthy CD-1 mice to assess their stability and biodistribution profile. The mice serum and the mice urine 1h *p.i.* were analysed by HPLC (γ -detection). The HPLC analysis of blood serum revealed the presence of radiochemical impurities with similar profiles to those verified in the *in vitro* stability assays in human serum, showing at 1 hour the total conversion of the injected radiolabelled conjugates to single radiochemical species with slightly higher lipophilicity. On the other hand, hydrophilic metabolites were detected in mice urine.

In a preliminary biodistribution study (Figure 2.22), both radioconjugates demonstrated a high excretion rate at 1 h *p.i.* of around 80 % (expressed as % I.A.) which was expected due to their hydrophilic character and small size. Interestingly, for [^{111}In]DTPA-pY, the hepatobiliary route of excretion seemed to have played a more important role due to the high radioactivity uptake found in the intestines at 1 h *p.i.* ($6.7 \pm 0.5\%$ I.A./g) whereas for the analogue DOTAGA-conjugate most of the radioactivity was found in the kidneys ($8.5 \pm 1.0\%$ I.A./g). This difference reinforces the importance of the chelator choice for the tuning of the biodistribution profile of a radioactive probe.

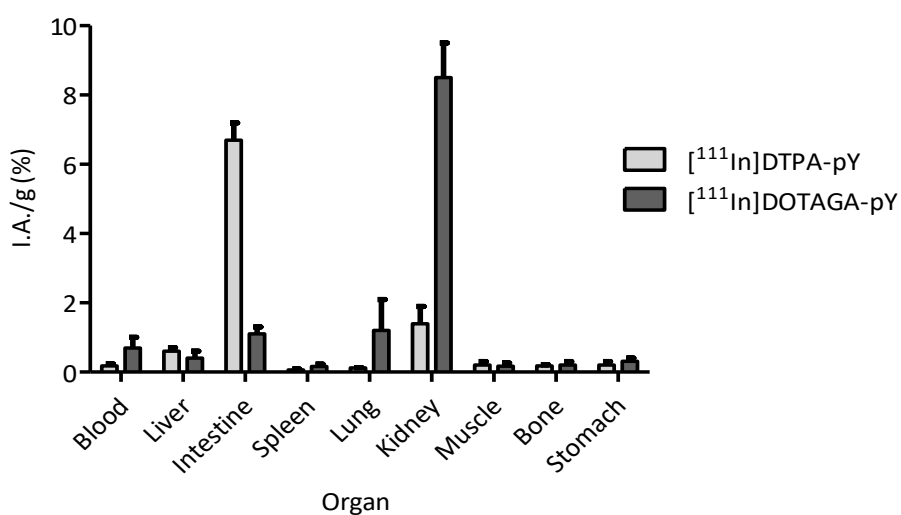


Figure 2.22. Biodistribution profile (I.A./g (%) \pm SD) of [^{111}In]DTPA-pY and [^{111}In]DOTAGA-pY in CD-1 mice 1 hour *p.i.* (n=3).

2.3. Conclusions

Four small peptides (6 to 9 amino acids) were successfully synthesized in a microwave-assisted automatic synthesizer and an adequate bifunctional chelator (DOTA, DTPA or DOTAGA) was coupled to the N-terminal amines, on solid-phase, yielding the peptide conjugates with high yields after appropriate cleavage and deprotection.

All the peptide conjugates demonstrated ability to form coordination complexes with In(III) and were successfully radiolabelled with In-111 at high specific activities, as it is desirable in the preparation of biospecific radioprobes for clinical applications. The In-111 complexes demonstrated high stability *in vitro* showing no considerable release of the radioisotope along time (up to 48 hours), even when challenged with an excess of apotransferrin. This finding corroborates the use of DTPA, DOTA and DOTAGA for the synthesis and radiolabelling with ¹¹¹In of peptide-based probes.

However, the major challenge regarding the stability of the radioconjugates was undoubtedly the susceptibility towards proteolytic degradation of the peptide sequences in blood serum. The radiolabelled conjugates of the LXXLL peptide **ER2** and of the **pY**-peptide demonstrated to be the least stable both *in vitro* and *in vivo*. In fact, the presence of a reactive cysteine residue in ER2 might have dictated its fast degradation in serum. In the case of the **pY**-peptide, the stability studies performed with the DOTAGA conjugate in human serum, demonstrated that the loss of the phosphate group might be the source of instability of the radiolabelled peptide. Interestingly, similar studies performed with the unconjugated peptide demonstrated a different degradation pathway involving the cleavage of the N-terminal amino acids, suggesting that the attachment of the bifunctional chelator protects the peptide from the action of N-terminal exopeptidases. The fast instability in serum strongly compromises the utility of these peptides as probes for clinical applications since it is expected to greatly affect the biodistribution and tumor-targeting ability.

The synthesis of ER-binding radioprobes was the aim of synthesizing LXXLL-bearing peptide conjugates for In-111 labelling. In this respect, the conducted FP ER α binding assays with the correspondent inactive In(III) complexes demonstrated that the three complexes were able to efficiently bind to the ER α LBD. However, comparing to the free peptides, the complexes showed a reduction of potency (4- to 10-fold) which reflects the impact of the chemical modifications on the binding of the peptides to ER α . Nevertheless, the fact that the binding

affinity was still kept encouraged us to pursue the evaluation on the clinical potential of the LXXLL-based probes.

From the biological evaluation point of view, [^{111}In]DOTA-ER3 showed the most favourable properties since it demonstrated high uptake in ER-positive BC cells, moderate metabolic stability *in vivo* and a biodistribution profile with fast blood clearance and high uptake in ER-rich organs. Furthermore, studies in tumor-bearing animals suggested selective accumulation of [^{111}In]-DOTAER3 in the tumor tissue which highlights the potential of this radioprobe for tumor imaging. However, it should be noted that [^{111}In]DOTA-cER1 although presenting low uptake in BC cells, also demonstrated promising *in vivo* properties regarding metabolic stability and ER-rich tissues targeting. Overall, this evaluation of the ^{111}In -labelled LXXLL peptides shows that this novel approach of ER-targeting should be further explored.

Regarding the pY-peptide, the highly unstable character of both [^{111}In]DTPA-pY and [^{111}In]DOTAGA-pY severely compromises their utility as radioprobes towards Src imaging in BC. Moreover, since the most probable degradation pathway corresponds to the loss of the phosphate group and taking into account that the phosphorylated amino acid is critical for the expected biological targeting ability, the results discussed in this chapter strongly suggest that the peptide would quickly lose the ability to bind to the tyrosine kinase target *in vivo*. In addition, the very low uptake in BC cells demonstrated by [^{111}In]DTPA-pY suggests that the peptide by itself is not able to cross the plasmatic membrane and reach the target, which also compromises its clinical potential. Taken together, these results show that [^{111}In]DTPA-pY and [^{111}In]DOTAGA-pY are not promising candidates for BC imaging.

Chapter 3

Radioiodinated ER-targeting

Peptide

3. Radioiodinated ER-targeting Peptide

Radioiodinated peptides have long been studied for medical applications. The gamma-emitting radioisotope I-125, although not having suitable imaging properties, is often used as a surrogate of other clinically relevant iodine radioisotopes ($^{123/124/131}\text{I}$) in the preliminary evaluation of new radioiodinated probes for diagnostic imaging [251-253]. In addition, ^{125}I is a very well-studied Auger emitter whose therapeutic applications have been thoroughly explored in the last decades. Therefore, I-125, in the same way as In-111, is a relevant radionuclide for the development of theranostic radiopharmaceuticals [103, 125, 254]. In this context, an LXXLL-based peptide targeting the ER was radioiodinated with I-125 and its clinical potential for BC management was evaluated. The peptide sequence to be radiolabelled with ^{125}I was selected from the studies performed in Chapter 2, taking into account the *in vitro/in vivo* stability and the biological selectivity/affinity demonstrated by the studied LXXLL peptides.

3.1. Radioiodination of Biomolecules in Nuclear Medicine

Radioiodination of biomolecules was established in 1948 when I-131 was the first iodine radioisotope to be used for the radiolabelling of antitumor antibodies. Since then, the radioiodination of proteins and peptides has gained popularity becoming central to a wide range of fundamental *in vitro* nuclear medicine and analytical biochemistry techniques [255]. In the clinical research setting, several targeted antibodies and peptides labelled with different iodine radioisotopes have been studied both for imaging and therapy [251-253].

A variety of iodine radioisotopes of interest for nuclear medicine exist from which ^{123}I , ^{125}I and ^{131}I are gamma emitters whereas ^{124}I is a positron emitter. For *in vivo* imaging, the most suitable nuclides are ^{124}I for PET and ^{123}I for SPECT. ^{125}I is not suitable for *in vivo* imaging due to its low energy of 35 keV, which is absorbed within a very short path length. However, this property along with the long half-life of 59.49 days makes ^{125}I very useful for *in vitro* biological and preliminary *in vivo* animal studies as a surrogate of ^{123}I which has a clinically useful half-life (13.22 h) and a photon energy of 159 keV suitable for diagnostic imaging [256]. Indeed, the main limitation for the widespread use of I-123 is the fact that this radioisotope is produced in a cyclotron which makes it more expensive compared with the reactor-produced I-125.

In addition to the gamma emission, ^{123}I and ^{125}I are also known Auger-emitting radionuclides and therefore have potential for targeted therapy. In fact, ^{125}I is the most studied Auger-emitting radionuclide and preclinical studies have already proved its ability to exert *in vivo* antitumoral effects when delivered inside the nucleus of cancer cells [103, 125, 254]. The radioisotope I-131, which has a half-life of 8.02 days, also presents theranostic value due to the simultaneous emission of gamma photons for SPECT imaging and β -particles for therapy. Table 3.1 summarizes the properties of the clinically relevant iodine radioisotopes.

Table 3.1. Selected iodine radioisotopes used in nuclear medicine. Adapted from [86, 90, 91, 257].

Radionuclide	$t_{1/2}$ (d)	Decay Mode	Main Emission (keV)
^{131}I	8.0	β^- γ	364 971
^{125}I	59.5	EC (γ , Auger)	35.5
^{124}I	4.2	β^+ , EC	603 (511)
^{123}I	0.6	EC (γ , Auger)	159

The thyroid gland has been an important target of iodinated radiopharmaceuticals due to the ability of thyrocytes to uptake iodide (I^-) through the Na^+/I^- symporter (NIS) and concentrate the ion by a factor of 20 to 40 in respect to the plasma compartment [258]. Taking advantage of this property, both ^{123}I - and ^{131}I -labelled sodium iodide ($\text{Na}^{123/131}\text{I}$) have been used in the clinical setting for the evaluation of the thyroid function and morphology by SPECT. In this context, these radiopharmaceuticals have been particularly useful for the diagnosis, staging and treatment follow-up of thyroid cancer. Furthermore, ^{131}I -labelled sodium iodide has been widely used in clinics for the treatment of thyroid-related diseases including hyperthyroidism and thyroid carcinomas [258, 259]. I-131 has also been an attractive choice for the design of targeted radioimmunotherapeutic agents in oncology. In fact, in the last two decades a number of ^{131}I -labelled antibodies were approved for the treatment of oncologic diseases such as hepatocellular carcinoma and non-Hodgkin's lymphoma [260, 261]. Antibodies and small peptides targeting cancer-related receptors (*e.g.* HER2) have also been labelled with the radioisotopes I-123 and I-125 in order to study the clinical potential of the radioiodinated agents for imaging and Auger-electron therapy [262-264].

Radioiodination Strategies

Numerous classic iodination methods are available for the preparation of radioiodinated radiopharmaceuticals. For the selection of the most suitable radioiodination method, several factors must be taken into account, specifically: (i) the labelling efficiency, (ii) the specific activity, (iii) the resistance to *in vivo* deiodination, and (iv) the preservation of the bioactivity of the ligand [103, 256].

The radioiodination strategies applied for the radiolabelling of peptides and proteins fall in two main categories: direct and indirect. The direct methods represent the most applied strategy for the radioiodination of proteins and involve the direct introduction of the iodine radioisotope into the amino acid sequence by an electrophilic aromatic substitution reaction. This iodination reaction requires the prior activation of iodide (I^-) by an oxidizing agent to form a reactive cationic species (I^+) which will allow a spontaneous electrophilic substitution on aromatic rings bearing a good leaving group [265]. Indeed, in peptides and proteins, the structures primarily iodinated are the tyrosyl residues and only to a lesser degree the histidyl or other aromatic ring structures. The chloramine-T (CAT) method (Figure 3.1), a procedure that uses sodium *N*-chloro-*p*-toluenesulfonamide (CAT) as oxidizing agent, is the most cited direct radioiodination method and have been used in the preparation of radioiodinated proteins with high SA. In reality, in this procedure the oxidation of iodide to I^+ is performed by the hypochlorous acid released from CAT in water [266, 267]. However, CAT is a strong oxidant and hence can cause denaturation and oxidative damage to proteins, which is an important drawback that can hamper the biological function of the iodinated protein. Therefore, a mild oxidizing agent named Iodogen (1,3,4,6-tetrachloro-3 α ,6 α -diphenylglycouril) was developed and has since been widely used for the radioiodination of peptides and antibodies. Polymer-bound CAT or vials coated with Iodogen have been popular choices for the radioiodination procedures by offering the advantage of easy separation of the reaction mixture from the immobilized oxidants [162]. The lactoperoxidase-catalysed iodination constitutes another method for the preparation of (radio)iodinated proteins and peptides in mild conditions. This method uses the enzyme lactoperoxidase to catalyse the oxidation of iodide using hydrogen peroxide as the enzyme substrate. However, this enzymatic method has the disadvantage of being very pH-dependent (the optimum pH for the reaction is between 6 and 7) and the lactoperoxidase-catalysed reactions are typically much slower compared to the reactions involving the chemical oxidants [268, 269].

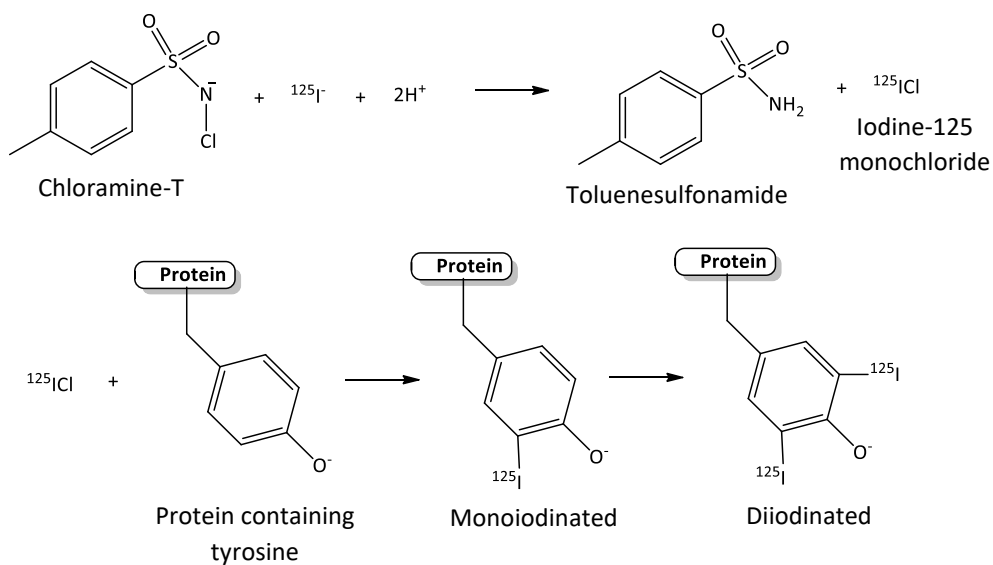


Figure 3.1. Chloramine-T (CAT) mechanism in promoting the iodination of tyrosine. Adapted from [266].

The straightforward direct radioiodination methods mentioned above, although having the advantage of causing a minimal structural change in proteins, are only feasible if accessible tyrosine or histidine residues are present in the amino acid sequence. Therefore, the indirect methods are often used as an alternative for the radioiodination of peptides or proteins. In this approach, the iodine radioisotope is incorporated by the application of a prosthetic group which contains two functional groups to enable both the radioiodination and the conjugation to the protein through an amino, aminoxy or thiol group. There are a variety of prosthetic groups used for the radioiodination, but the most frequently used are SIPC (N-succinimidy-5-[*I]iodo-3-pyridine carboxylate) and SIB (N-succinimidy-3-[*I]iodobenzoate) (Figure 3.2). The proper choice of a prosthetic group can allow an improvement of the *in vivo* stability against enzymatic deiodination of the radioiodinated protein compared with the direct labelling approach. This is due to the natural recognition of the iodinated tyrosine/histidine-containing proteins by the enzymes tyrosine/histidine deiodinases [270, 271].

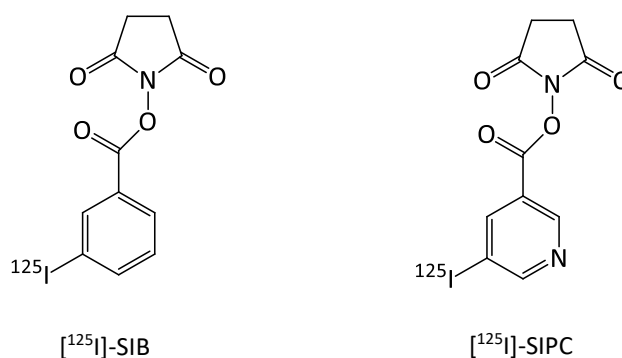


Figure 3.2. Chemical structures of the ^{125}I -labelled prosthetic groups SIB and SIPC.

Rationale for the Radioiodination of a LXXLL Peptide

Iodine-125 is a relevant radioisotope for the development of theranostic radiopharmaceuticals, as previously explained. In fact, besides being the most studied Auger-emitting radioisotope for therapeutic applications, ^{125}I is in fact a more potent Auger emitter than ^{111}In presenting a 1.7-fold higher Auger yield [123]. Furthermore, several radioiodination procedures are available that minimize the impact of the (radio)iodine introduction on the biological activity of the biomolecules. Therefore, these facts encouraged us to study the clinical potential of a radioiodinated ER-targeting peptide containing the LXXLL motif.

The selection of the peptide sequence for the radioiodination took into account the studies performed with the ^{111}In -labelled LXXLL-based peptides described in Chapter 2. Indeed, the ^{111}In -labelled conjugate of the selected peptide, the **ER3** peptide, showed high *in vivo* stability and good target/non-target radioactivity ratios in the animal studies previously performed. In addition, the amino acid sequence of **ER3** includes an histidyl residue that makes possible the direct radioiodination of the peptide. Indeed, this is an important advantage compared with the ^{111}In -labelled peptide, since the direct introduction of the radioisotope into the sequence, without the attachment of a bulky bifunctional chelator (such as DOTA or DTPA) or prosthetic group (such as SIB), can potentially lead to a better preservation of the ER α binding affinity of the unlabelled LXXLL peptide, which is a crucial factor for the development of more specific ER-targeting probes.

Hence, the main goal of the work described in this Chapter was the evaluation of the clinical potential of the radioiodinated **ER3** peptide as a ER-targeting radioprobe for BC

theranostics. The chemical strategy used for the (radio)iodination and the *in vitro/in vivo* studies performed with the ^{125}I -labelled **ER3** are discussed in detail in the following sections.

3.2. Synthesis and Characterization of the (Radio)iodinated Peptide

The synthesis of **ER3** peptide (H-Lys-Lys-Ile-Leu-His-Arg-Leu-Leu-Gln-NH₂) was performed in an automated peptide synthesizer as described in Chapter 2. The carboxyamidated peptide was obtained after cleavage from the resin and total deprotection of the side-chain protecting groups. After semi-preparative HPLC purification, **ER3** was obtained with high chemical purity (higher than 97%) and characterized by ESI-MS as reported in Section 2.1.2.

Aiming to (radio)iodinate the peptide at the histidyl residue, the straightforward CAT method was selected. Since the peptide does not contain any amino acid susceptible to oxidation, the harsh conditions provided by CAT could be used without major concern. Moreover, it is known that the rate of iodination at histidine can be 30 to 100 times slower than at tyrosine, which makes the use of a stronger chemical oxidant such as CAT desirable [272].

3.2.1. Synthesis and Characterization of the ^{127}I -iodinated Peptide

As explained before for the LXXLL-based In/ ^{111}In -complexes, the synthesis of the non-radioactive iodinated peptide is important not only for the characterization of the ^{125}I -radiolabelled peptide (by comparison of the HPLC chromatographic profiles), but also to assess its binding affinity towards ER α by the FP method.

The synthesis of the inactive iodinated peptide was performed by using the non-radioactive Na ^{127}I . Several parameters have been described to be crucial for the iodination reaction by CAT, specifically the pH and the peptide:NaI:CAT molar ratio.

The electrophilic substitution in the histidyl imidazole ring is pH-driven and therefore a buffer with an optimal pH is needed in the reaction medium. Although in the literature histidine iodination is reported to be favoured in the pH range between 8.0 and 8.5, the attempt to perform the iodination of the **ER3** peptide in a Tris-HCl buffer at pH 8.2 failed to give the desired iodinated product [273]. Therefore, phosphate buffer (0.1 M) at pH 7.4 was used for the ER3

iodination in the following attempts, proving to be a more suitable medium to achieve the peptide iodination.

Furthermore, it is known that the histidyl imidazole ring can be doubly iodinated, although 2,4-diiodohistidine is more likely to form at higher pH values (>8) [273]. Double iodination can significantly affect the biological properties of the peptide and therefore, in order to best preserve the biological activity, the monoiodinated peptide is preferred [265]. To produce the monoiodinated peptide the molar ratio between the peptide, sodium iodide, CAT and the reducing agent sodium metabisulfite should be 1:1:2:2 [272]. However, for the **ER3** peptide, this stoichiometry failed to give the desired iodinated ER3, **[I]-ER3**, in a reasonable yield. Hence, the reaction conditions were optimized and the molar ratio 1:1.5:2.5 (ER3:NaI:CAT) led to the successful formation of **[I]-ER3** in high yield (approximately 74%). The reaction was monitored by HPLC and was left stirring for 30 minutes, before the addition of 6 equivalents of sodium metabisulfite to reduce the reactive I^+ . The product was purified by HPLC and identified by ESI-MS, with the spectrum showing the presence of the singly-, doubly-, and triply-protonated **[I]-ER3** (Figure 3.3). The diiodinated peptide was also detected by ESI-MS in the reaction mixture although the verified yield was lower than 7%.

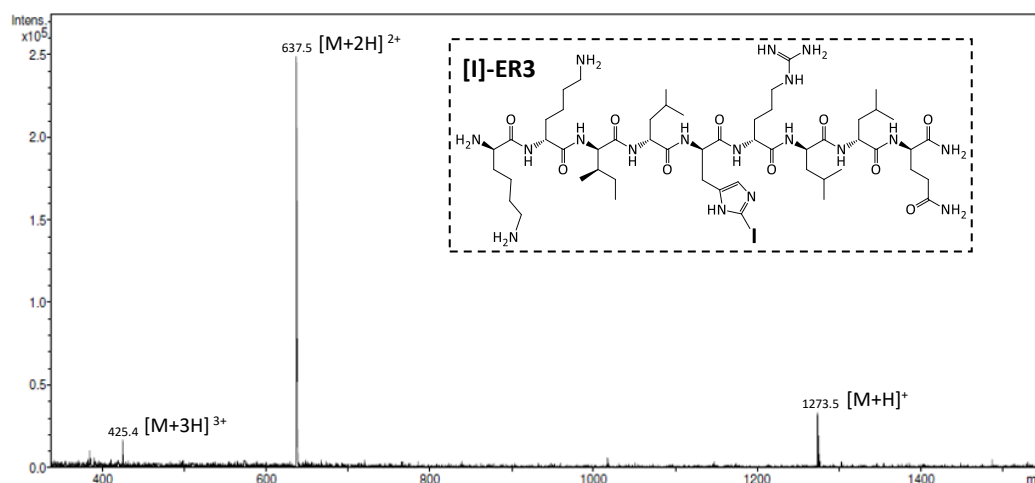


Figure 3.3. ESI-MS spectrum (m/z calcd for $C_{53}H_{98}N_{18}O_{10}$ $[M+H]^+$: 1273.68, found: 1273.5 $[M+H]^+$, 637.5 $[M+2H]^{2+}$, 425.4 $[M+3H]^{3+}$) and chemical structure of **[I]-ER3**.

3.2.2. Peptide Radioiodination with I-125

Radioiodination of the **ER3** peptide was also performed by the CAT method at pH 7.4 using the radioactive Na¹²⁵I. The radioiodination efficiency was evaluated by HPLC with γ detection and by instant thin layer chromatography in silica gel (ITLC-SG).

The most important parameter that was adjusted during the optimization of the radioiodination reaction was the **ER3** peptide concentration. As previously explained, high specific activity is required to achieve optimal binding of the radiotracer to the target receptor *in vivo*. Indeed, the CAT method has been known to be effective in the radiolabelling of proteins and peptides with high specific activities between 9.25 and 33.3 MBq/ μ g [266]. Therefore, aiming to maximize the specific activity of the radiolabelled product, low amounts of peptide, in the 3-6 μ g range, were used for the reactions with Na¹²⁵I (10.91 to 27.57 MBq) in the first radiolabelling experiments. However, using these peptide amounts, the radioiodination yields obtained in different experiments (while keeping all the other conditions) were not reproducible. This was probably due to adsorption of the peptide (which was stored in aqueous solution) to the reaction vial which led to significant variations in the amount of the peptide available for iodination. Therefore, to circumvent that problem, a higher amount of peptide, 20 μ g, had to be used in each radioiodination experiment along with low-protein binding vials (Eppendorf® LoBind). Since CAT is known to be a strong and fast oxidizing agent, the reaction mixture containing Na¹²⁵I, CAT (in a fixed amount of 50 μ g) and **ER3** was left to react for only 60 seconds after which the oxidation was terminated by the addition of the reducing agent sodium metabisulfite. These optimized conditions led to radiochemical yields ranging from 88 to 96%, as determined by HPLC with γ detection. Interestingly, extending the reaction time for 5 minutes led to a reduction of the radioiodinated peptide in 66%, as verified by ITLC, which suggests the occurrence of degradation.

The purification of the radioiodinated peptide, [¹²⁵I]-**ER3**, was accomplished by solid-phase extraction using a C-18 Sep-Pak cartridge. Thus, the radioiodination mixture was applied in the Sep-Pak cartridge and eluted with 2 to 4 mL of water to discard the radioiodide species and salts. The purified [¹²⁵I]-**ER3** was then obtained by eluting the cartridge with a mixture of CH₃OH with 0.1% TFA. After removal of the organic solvent under nitrogen, the radiolabelled peptide was reconstituted in a NaCl 0.9% solution containing 2% of DMSO (to decrease the adsorption to the vial) for the following *in vitro* and *in vivo* studies. In the end, [¹²⁵I]-**ER3** was obtained with a radiochemical purity higher than 98%, as evaluated by HPLC. As previously explained, this is an important parameter to ensure that the biological behaviour of the

radioiodinated peptide is not affected by the presence of radiochemical impurities. The inactive **[I]-ER3** was used to establish the chemical identity of **[¹²⁵I]-ER3** by comparing the chromatographic behaviours through a co-injection of the ¹²⁵I-labelled peptide (γ detection) with the non-radioactive **[I]-ER3** (UV detection, $\lambda = 220$ nm), as shown in Figure 3.4.

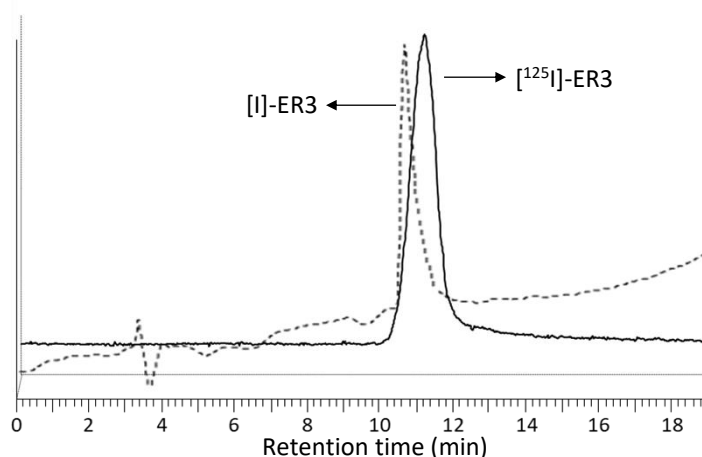


Figure 3.4. Representative chromatograms of **[¹²⁵I]-ER3** (full line, Rt= 11.2 min) obtained by gamma-detection and **[I]-ER3** (dashed line, Rt= 10.6 min) obtained by UV-detection ($\lambda = 220$ nm). HPLC, Method F (Eluents: A- 0.1% aq. TFA; B- 0.1% TFA/CH₃CN. Gradient (%): 90 A/10 B to 100 B in 15 min, 15 min 100 B).

3.3. Evaluation of the Binding Affinity towards ER α

The binding affinity of **[I]-ER3** to the ER α LBD was tested by the fluorescence polarization (FP) assay by measuring the ability of the monoiodinated peptide to displace a fluorescein-labelled coactivator (FL-SRC1B2) from the agonist-bound ER α , as previously described (Section 2.1.3).

It is known that leucines in the LXXLL sequence are important for the interactions with the hydrophobic pocket in the coactivator-binding site of the receptor LBD whereas the XX core amino acids (where histidine is included in **ER3**) are thought to be solvent exposed and thus are not expected to contribute for the ER specificity [57]. Therefore, although the iodide was introduced within the LXXL recognition motif, the iodination was not expected to change significantly the binding affinity of the peptide towards ER α . Indeed, results of the FP binding assay demonstrated that **[I]-ER3** kept a binding affinity towards the ER α LBD in the nanomolar

range presenting an IC_{50} value of $0.543 \pm 0.02 \mu\text{M}$ (Figure 3.5). The histidine iodination led to a 3.5-fold decrease in the potency of the (non-iodinated) **ER3** peptide most probably due to steric effects (Table 3.2). On the other hand, in comparison with the [In]DOTA complex of the same peptide sequence ($IC_{50} = 1.72 \mu\text{M}$), the binding affinity of the iodinated peptide was 3-fold higher which could lead to higher *in vivo* specificity. Therefore, based on the high binding affinity, [^{125}I]-**ER3** was considered a promising ER targeting probe.

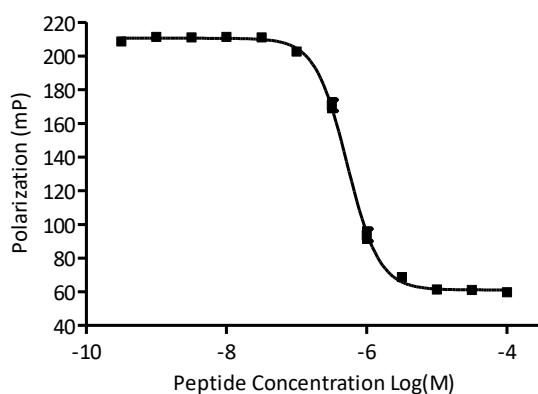


Figure 3.5. FP curves of FL-SRC1B2SRC with increasing concentrations (Log(M)) of [I]-ER3.

Table 3.2. Comparison between the binding affinities of ER3 and [I]-ER3 towards ER α .

Peptide	IC_{50} (μM)
ER3	0.157 ± 0.008
[I]-ER3	0.543 ± 0.021

3.4. *In Vitro* Evaluation of the Radioiodinated Peptide

Lipophilicity Evaluation

The lipophilicity of [^{125}I]-**ER3** was assessed using the octanol/NaCl 0.9% distribution coefficients ($\log P_{o/w}$). The $\log P_{o/w}$ value found for the radioiodinated **ER3** was -1.97 ± 0.01 , showing that [^{125}I]-**ER3** is highly hydrophilic. However, the radioiodinated peptide was found to be less hydrophilic than the ^{111}In -labelled **DOTA-ER3** (described in Chapter 2) most probably due to the lipophilic nature of iodide. This fact is expected to have a positive effect on the cellular internalization of [^{125}I]-**ER3** compared with [^{111}In]**DOTA-ER3** ($\log P_{o/w} = -3.09 \pm 0.06$).

***In Vitro* Stability of [¹²⁵I]-ER3**

The *in vitro* stability of a radioiodinated compound under physiological conditions is a very important factor to be taken into account in the evaluation of its clinical potential. Dehalogenation is the primary degradation pathway of radioiodinated probes leading to free iodide which may cause an undesirable biodistribution of the radioactivity [274]. Actually, the release of radioiodide from the radiolabelled ligand can lead to high activity uptakes in the thyroid and in the salivary glands which also express the NIS transporter [275].

In the performed stability testing studies, [¹²⁵I]-ER3 demonstrated high stability in saline solution at 4°C up to 20 days. The incubation at 37°C in the same medium revealed that the labelled peptide was radiochemically stable up to 48 hours demonstrating the formation of just 2% of free iodide at that time point.

The stability of the radioiodinated peptide was also studied in human blood serum (at 37°C) at different time points up to 24 hours. The proteolytic activity in the serum not only has the potential to cause peptide cleavage but can also cause deiodination [276]. After 1 hour of incubation in serum (Figure 3.6), [¹²⁵I]-ER3 accounted for approximately 40% of the total activity, while most of the radioactivity was associated with more hydrophilic radiochemical species with the same retention time as free radioiodide (Rt = 4 min). Comparing to [¹¹¹In]DOTA-ER3, the degradation rate of the radioiodinated ER3 peptide was significantly faster which corroborates the strong contribution of deiodination for the verified instability. The deiodination rate became slower in the following hours, and after 24 hours of incubation there was still 16% of the intact [¹²⁵I]-ER3 in serum.

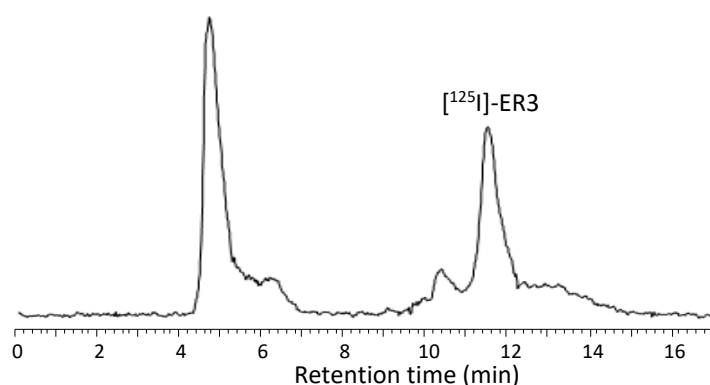


Figure 3.6. Radiochromatogram of an aliquot of human serum after incubation for 1 h with [¹²⁵I]-ER3 at 37°C. HPLC, Method F (Eluents: A- 0.1% aq. TFA; B- 0.1% TFA/CH₃CN. Gradient (%): 90 A/10 B to 100 B in 15 min, 15 min 100 B).

3.5. Biological Evaluation of the ^{125}I -labelled Peptide

3.5.1. Cell Studies

Cellular uptake of [^{125}I]-ER3 was studied in two breast carcinoma cell lines: MCF-7 and MDA-MB-231, which are, respectively, ER(+) and ER(-). The results of the study are shown in Figure 3.7. As seen in the graph, a fast uptake was verified in both cell lines, although in MCF-7 cells the [^{125}I]-ER3 uptake was significantly higher. The maximum uptake of the radioiodinated peptide in MDA-MB-231 cells was about 7.2% (of total activity) and was reached after 30 min of incubation. On the other hand, in MCF-7 cells, [^{125}I]-ER3 demonstrated a maximum uptake of approximately 12% between 30 minutes and 1 hour of incubation. However, after incubation for 1 hour in MCF-7 and after 30 minutes in MDA-MB-231 cells, the [^{125}I]-ER3 retention within the cells demonstrated a prominent decline. This washout cannot be attributed to the deiodination of the peptide in the cellular medium since stability studies on the culture medium (at 37°C) showed high stability of [^{125}I]-ER3 up to 4 hours of incubation with the release of less than 5% of free radioiodide. However, the release of activity from the cells might be attributed to proteolytic catabolism in the internal lysosomes as others have reported with radioiodinated peptides and antibodies [257, 277, 278]. Nevertheless, the higher initial uptake and higher retention of the radioiodinated peptide in the ER(+) MCF-7 cells compared with the ER(-) MDA-MB-231 cells suggest a role of the receptor in the cellular behaviour of [^{125}I]-ER3.

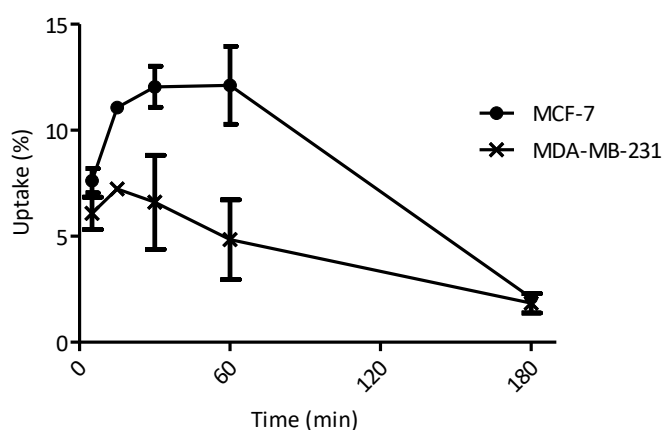


Figure 3.7. Cellular uptake (% of total applied activity \pm SD) of [^{125}I]-ER3 in MCF-7 (ER+) cells and in MDA-MB-231 (ER-) cells (n=3).

Internalization of [^{125}I]-ER3 in the nucleus of the MCF-7 cells was also studied along time. This is an important parameter for two main reasons, specifically the location of the biological target (ER) in the nuclear compartment and the potential of I-125 for Auger therapy which requires the emission of the Auger electrons near DNA [41, 279].

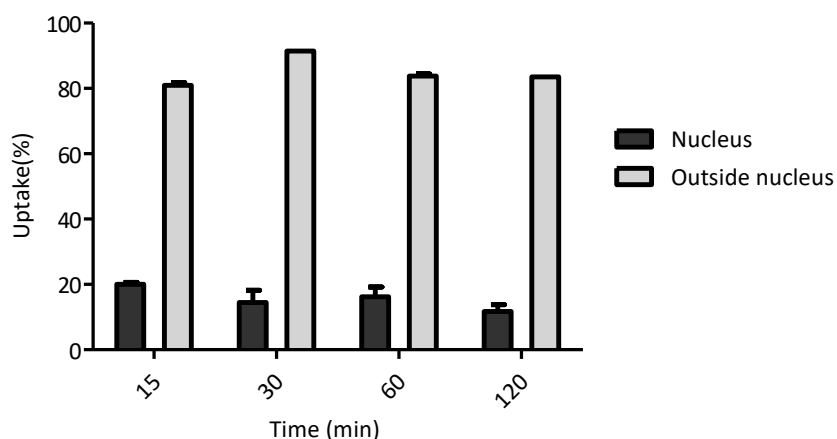


Figure 3.8. Nuclear internalization of [^{125}I]-ER3 in MCF-7 cells expressed as a percentage (average (%) \pm SD, n=3) of cell-associated activity.

As shown in Figure 3.8, uptake in the nucleus (in relation to the total activity associated to the cells) ranged from 19% at 15 minutes to 11% at 2 hours showing the capability of [^{125}I]-ER3 to reach the nuclear compartment of BC cells. For the nuclear targeting ability, the presence of the iodide, which has a more lipophilic character, might have had a significant contribution. As a matter of fact, in comparison to the ^{111}In -labelled ER3 ([^{111}In]DOTA-ER3) which exhibited higher hydrophilicity ($\log P_{o/w} = -3.09 \pm 0.06$), the radioiodinated peptide demonstrated an higher internalization in the cell nucleus. This result represents an important advantage of the radioiodinated peptide for therapeutic applications by the emission of Auger electrons.

3.5.1. Biodistribution and *In Vivo* Stability

Biodistribution in healthy CD-1 mice

Biodistribution of [¹²⁵I]-ER3 was preliminarily studied in healthy female CD-1 mice 1 hour after intravenous injection to assess the *in vivo* stability and the tissue distribution profile. The results, shown in Table 3.3, revealed a fast clearance from the blood stream and an overall radioactivity excretion of approximately 21% (% I.A.) which was significantly lower in comparison with [¹¹¹In]DOTA-ER3 (Section 2.1.6) which demonstrated an excretion of 74% at the same time point and in the same animal model. The high accumulation of radioactivity in the kidneys 1 hour *p.i.* ($15.1 \pm 2.1\%$ I.A./g) suggests that the radioiodinated peptide was eliminated mainly through the renal excretion pathway, which is consistent with its overall hydrophilic character. Thyroid activity ($4.2 \pm 0.7\%$ I.A./g) suggests the presence of some iodide released from the radiolabelled peptide probably due to enzymatic dehalogenation by deiodinases present in the liver. Indeed, the activity found in the liver ($4.2 \pm 0.1\%$ I.A./g) revealed some contribution of the hepatobiliary pathway for the excretion of [¹²⁵I]-ER3.

Following the kidneys, most of the activity was found in the ovaries which is an ER α -rich organ. The ratios of the radioactivity found in the ovaries and in the uterus to the radioactivity in blood at 1 hour *p.i.* were 2.3 and 1.8, respectively, suggesting selective targeting of ER-rich organs.

Table 3.3. Biodistribution data (I.A./g (%) \pm SD) of [¹²⁵I]-ER3 in female CD-1 mice at 60 min *p.i.* (n=3).

Organ	% I.A./ g
Blood	2.3 ± 0.9
Liver	3.6 ± 1.2
Intestine	3.7 ± 1.8
Spleen	2.7 ± 0.4
Heart	2.4 ± 0.2
Lung	2.9 ± 0.9
Kidney	15.1 ± 2.1
Muscle	3.5 ± 0.6
Skeletal	2.5 ± 0.3
Stomach	3.1 ± 0.5
Ovaries	4.3 ± 1.0
Uterus	3.4 ± 0.5
Thyroid	4.2 ± 0.7
Adrenals	2.6 ± 0.3
Excretion (% I.A.)	21.2 ± 2.5

In Vivo Stability

Analysis by HPLC (with γ detection) of the mice blood serum 1 hour *p.i.* revealed the preponderant presence of the intact [^{125}I]-ER3 which accounted for approximately 77% of the detected activity (Figure 3.9). The remaining activity was associated with radiochemical species with the same retention time as the free radioiodide, corroborating the enzymatic dehalogenation. However, proteolytic degradation of the peptide itself could have also contributed for the formation of the degradation products. Furthermore, the radiochromatogram of mice urine demonstrated the presence of hydrophilic radioproducts, probably resulting from renal metabolism.

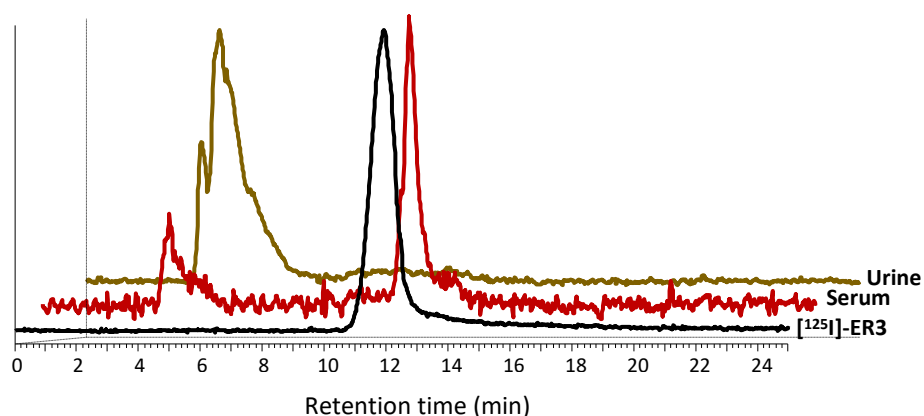


Figure 3.9. HPLC radiochromatograms of mice serum and mice urine 1 h after injection of [^{125}I]-ER3 in CD-1 mice. The radiochromatogram of the injected [^{125}I]-ER3 is also shown. HPLC, Method F (Eluents: A- 0.1% aq. TFA; B- 0.1% TFA/ CH_3CN . Gradient (%): 90 A/10 B to 100 B in 15 min, 15 min 100 B).

Biodistribution in tumor-bearing BALB/c mice

Biodistribution studies in tumor-bearing mice were performed in MCF-7 xenografted BALB/c nude female mice over 3 hours *p.i.*. The results, displayed in Figure 3.10, confirmed the fast clearance of [^{125}I]-ER3 from the blood stream predominantly by renal excretion. However, the uptake in the liver, intestine and stomach suggests some contribution of the hepatobiliary excretion pathway. The uptake in the thyroid ($8.8 \pm 2.2\%$ I.A./g at 1h *p.i.* and $3.5 \pm 0.7\%$ I.A./g at 3h *p.i.*) revealed the presence of free radioiodine derived from the enzymatic dehalogenation of [^{125}I]-ER3.

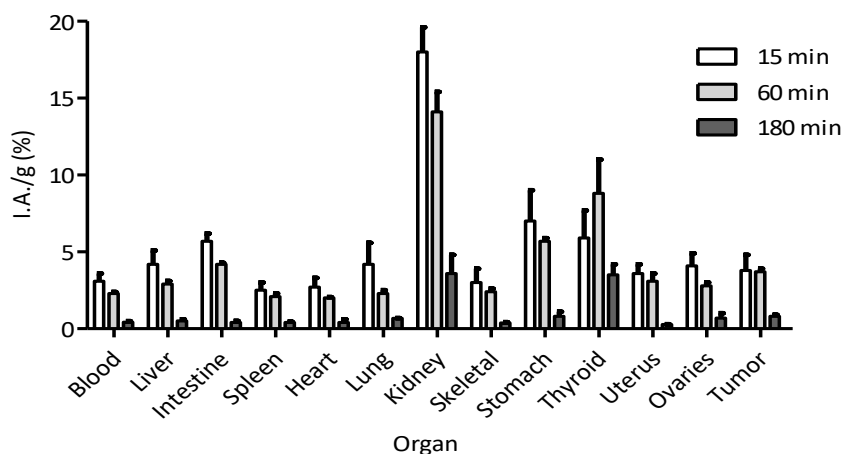


Figure 3.10. Biodistribution profile (I.A./g (%) \pm SD) of [¹²⁵I]-ER3 in MCF-7 xenografted BALB/c nude female mice at 15, 60 and 180 min *p.i.* (n=3).

At 1 hour *p.i.* and at 3 hours *p.i.* the radioactivity uptake in the tumor ($3.7 \pm 2.2\%$ and $0.8 \pm 0.1\%$ I.A./g, respectively) were the highest following the uptake in the thyroid and in the excretory organs. Interestingly the tumor-to-background radioactivity ratios (Figure 3.11) increased over time suggesting some specific accumulation of the radioactivity in the tumor tissue which highlights the potential of this radioiodinated probe for tumor imaging.

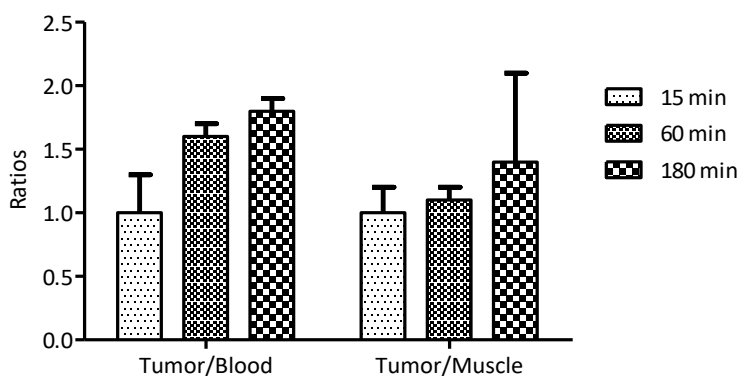


Figure 3.11. Tumor/Blood and Tumor/Muscle radioactivity ratios (\pm SD) of [¹²⁵I]-ER3 at 15, 60 and 180 min *p.i.*.

3.6. Conclusions

The LXXLL peptide **ER3** was successfully iodinated at the histidyl residue using the CAT method. The iodinated peptide [**I**]-**ER3** demonstrated nanomolar affinity towards the ER α LBD which validates its use for ER targeting. Furthermore, the result of the FP binding assay suggests that the peptide could tolerate the introduction of iodide in the XX core of the LXXLL motif without strongly affecting its ability to bind to the ER α LBD.

The radioiodinated peptide [¹²⁵I]-**ER3** showed fast uptake in ER-positive breast cancer cells and a biodistribution profile characterized by fast clearance from blood and some preferential accumulation in ER-rich organs. Furthermore, studies in tumor-bearing mice showed a slightly increase of the radioactivity accumulation in the tumor over time. However, release of the activity from the cells and accumulation of activity in the thyroid were indicators of dehalogenation occurrence along time, fact that was further confirmed in the *in vivo* stability studies. This dehalogenation could have a negative impact on the ability of the radiopeptide to more effectively target the ER-rich tissues (including the tumor) *in vivo*.

Interestingly, [¹²⁵I]-**ER3** demonstrated ability to be internalized in the nucleus of BC cells. Indeed, the nuclear internalization values of [¹²⁵I]-**ER3** in MCF-7 cells are encouraging for the potential application of the radioiodinated peptide for Auger therapy. This property is particularly relevant due to the fact that I-125 is one of the most potent Auger emitters.

Overall, the high affinity towards ER α (demonstrated by the inactive [**I**]-**ER3**) and the moderate nuclear internalization shown by the ¹²⁵I-labelled peptide in BC cells, make the radioiodinated ER3 an attractive candidate for BC theranostics. However, dehalogenation and enzymatic degradation revealed to be important drawbacks for the *in vivo* application of [¹²⁵I]-**ER3** and therefore these issues should be addressed in the future development of this radioiodinated probe.

Chapter 4

Dual-targeting ¹¹¹In-labelled Probes

4. Dual-targeting ¹¹¹In-labelled Probes

Theranostics is a topic of increasing research interest in the field of nuclear medicine, as previously explained. The radionuclide In-111 is valuable for the preparation of radiotheranostic agents due to the simultaneous emission of γ -radiation for diagnosis and Auger electrons for therapy. However, the Auger-mediated therapeutic effect requires the delivery of the Auger electrons into the cell's nucleus near DNA. Furthermore, the theranostic agent should be specific for the target receptor of choice in order to show *in vivo* selectivity. Therefore, these properties must be taken into account in the design of novel radiotheranostic agents.

In this Chapter, a multi-targeting approach was adopted for the preparation of ¹¹¹In-based theranostic agents capable of targeting the ER and reaching the nucleus of BC cells. The work described in this Chapter represents an effort to optimize the theranostic value of previously studied ¹¹¹In-labelled ER-targeting moieties (such as LXXLL-based peptides) by potentiating the location of the radionuclide in close proximity to DNA in BC cells.

4.1. Dual-targeting Radiolabelled Probes

Dual- or multiple-targeting probes using radiolabelled metal chelates conjugated to different biomolecules have potential advantages over single-targeting probes as they can recognize multiple targets thus leading to better sensitivity for imaging and systemic radiotherapy, particularly when tumor heterogeneity is present [280, 281].

Multivalency approaches involving peptide homo- and heterodimers have been described recently with the aim of targeting either two different domains of one cancer-related receptor or two different receptors simultaneously. This dual-targeting strategy has generated heterobivalent probes that have demonstrated greater affinity for tumor cells compared to the monovalent ones [280, 281]. Radioconjugates comprising two different molecular moieties in the same agent have also been designed in order to combine different imaging modalities such as SPECT and NIR (near infrared) optical imaging or to associate the therapeutic effect of cytotoxic drugs with imaging ability [270,282]. Diverse multifunctional radioconjugates have also been prepared to enhance cellular retention and internalization and to potentiate their uptake in specific subcellular localizations such as the nucleus and the mitochondria [138, 283, 284].

The enhancement of nuclear uptake has been particularly important in the design of radioconjugates intended for Auger electron therapy (AET) since nuclear localization of the Auger electron-emitting isotopes is a prerequisite for inducing DNA damage. Introducing a peptidic nuclear localizing sequence (NLS) or a small molecule that acts as DNA intercalator such as acridine orange (AO) or doxorubicin have been strategies used in AET agents for achieving close proximity of the radionuclide to the DNA [138, 285, 286].

The synthetic pathway to achieve multivalent probes can be very challenging and has usually involved complex chemical modifications in biomolecules, such as peptides, prior to the attachment of the appropriate chelator which is usually monofunctionalized with the multivalent construct [280, 287, 288]. Although site-specific bifunctionalization of pirazolyldiamine chelating moieties for ^{99m}Tc labelling have been described, the selective dual vectorization of DOTA- and DTPA-based chelators intended for labelling with several medically relevant radioisotopes such as ¹¹¹In, ⁶⁸Ga, ¹⁷⁷Lu and ⁶⁴Cu, has remained largely unexplored [289]. Therefore, since popularity of dual-targeting probes is increasing, new chemical strategies for the straightforward synthesis of multivalent probes are needed.

The aim of the work discussed in this chapter was the construction of bivalent probes for labelling with In-111 to be studied as potential agents for BC theranostics. To achieve that goal the probes were designed in order to integrate three components:

- i) a DTPA- or DOTA-like chelator for appropriate In(III) complexation;
- ii) a nuclear/DNA targeting molecule to improve the nuclear internalization of the ¹¹¹In-complex;
- iii) a targeting molecule with affinity towards ER α for specific accumulation in ER(+) cancer cells.

The chemical strategies explored for the synthesis of the three components are presented in the following sections with particular focus on the development of prochelators that can be selectively functionalized with two different molecules. The synthesis, radiolabelling and biological evaluation of the final dual-targeting radioconjugates is subsequently discussed.

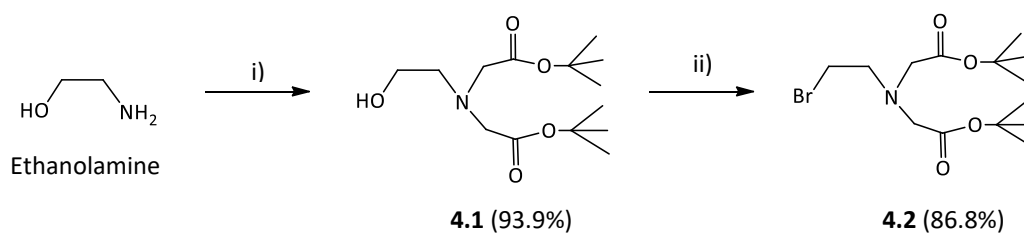
4.2. Synthesis and Characterization of Prochelators for Dual-vectorization of In(III) Complexes

As previously stated, the bifunctional chelators used for In(III) complexation fall in two main categories: acyclic and macrocyclic, with the two most important representatives of these two types being DTPA and DOTA, respectively. Therefore, the chemical structures of these chelators were the starting point for the design of the prochelators for dual-vectorization of In(III) complexes. These prochelators, after modification with the targeting-(bio)molecules and removal of the protecting groups, should render heptadentate or octadentate chelating spheres capable of strong In(III) complexation. As previously discussed, the high stability of the ^{111}In -labelled probes is a critical pre-requisite for clinical application.

4.2.1. Acyclic “DTPA-like” Prochelator

L-glutamic acid has been shown to be a useful building block for the synthesis of DTPA-like chelators through a N-bisalkylation strategy involving the intermediate di-*tert*-butyl 2,2'-((2-bromoethyl)azanediyl)diacetate (**4.2**, Scheme 4.1). However, until now this strategy has only been used for the preparation of DTPA-based chelators intended for monofunctionalization with a targeting biomolecule [147]. Therefore, based on this strategy, a synthetic pathway was designed for the construction of an acyclic chelator suitable for coordinating trivalent metals (such as ^{111}In) and able to be doubly vectorized in a site-specific manner with two different molecules.

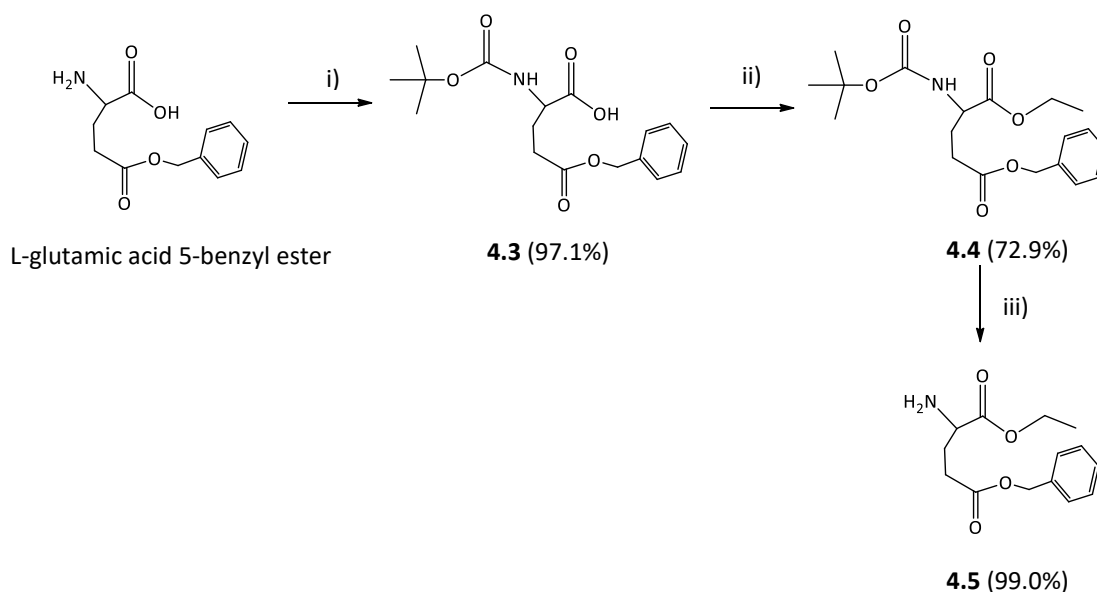
The versatile intermediate **4.2** was synthesized using a procedure already described in literature (Scheme 4.1) that involved the reaction of ethanolamine with *tert*-butyl bromoacetate giving the bis *N*-alkylated alcohol **4.1** that was subsequently converted to the corresponding bromide by treatment of the product with tetrabromomethane (CBr_4) and triphenylphosphine (PPh_3) [149]. The bromination was corroborated by $^1\text{H-NMR}$ by following the chemical shift of the protons of the $-\text{CH}_2$ directly attached to the modified chemical function. Product **4.2** was obtained with an overall yield of about 81%.



Scheme 4.1. Synthesis of the bromide intermediate 4.2.

i) *tert*-butylbromoacetate, K_2CO_3 , DMF, RT, 72 h; *ii)* CBr_4 , PPh_3 , CH_2Cl_2 , RT, 18 h.

In order to accomplish the proposed goal, the commercially available L-glutamic acid 5-benzyl ester was modified to comprise two orthogonally protected carboxylic acids using the synthetic route depicted in Scheme 4.2. Aiming to avoid unwanted reactions in the free amine of the amino acid derivative, the α -amine was first protected with the bulky Boc group using di-*tert* butyl dicarbonate in aqueous 1,4-dioxane in the presence of triethylamine. The reaction yielded the Boc-protected amino acid **4.3** with an almost quantitative yield (97.1%).



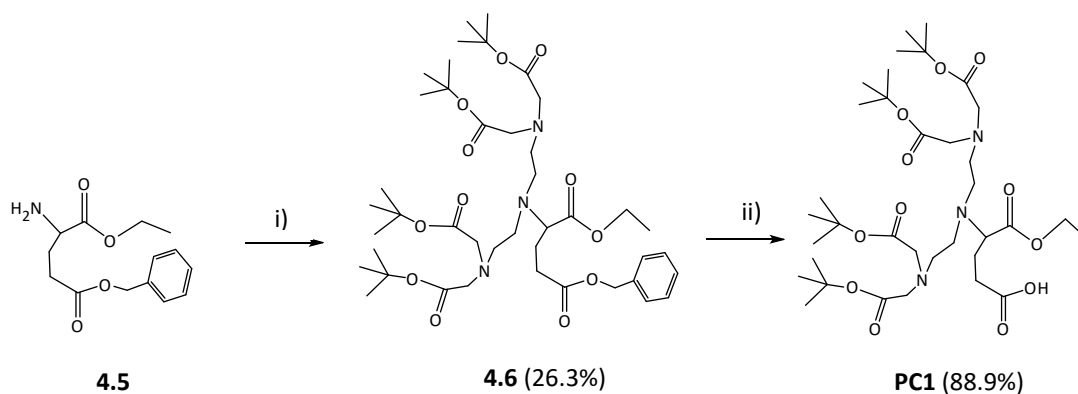
Scheme 4.2. Synthesis of the orthogonally protected amino acid 4.5.

i) di-*tert*-butyl dicarbonate, triethylamine, 1,4-dioxane, RT, 18 h; *ii)* iodoethane, $NaHCO_3$, DMF, RT, 48 h; *iii)* TFA, CH_2Cl_2 , $0^\circ C \rightarrow RT$, 12 h.

The next step was the protection of the free carboxylic acid with an orthogonal group relatively to the benzyl ester. Ethyl ester was the selected protecting group since it should be

unaffected by the removal of the benzyl ester by catalytic hydrogenation while it can be selectively removed in the presence of the *tert*-butyl protected carboxylic acids that will be introduced in a later stage of the synthetic pathway [290]. Protection of the carboxylic acid was performed using iodoethane in DMF in the presence of sodium bicarbonate (NaHCO_3). The ethyl ester **4.4** was obtained with a 72.9% yield. Aiming to restore the free amine, the Boc protecting group was then removed in acidic conditions using diluted TFA in CH_2Cl_2 giving the orthogonally protected amino acid **4.5** in a quantitative yield. The removal of the Boc group was confirmed by the disappearance of the signal associated with the $\text{C}(\text{CH}_3)_3$ protons in the $^1\text{H-NMR}$ spectrum and further confirmed by $^{13}\text{C-NMR}$.

The bisalkylation of the free amine of the glutamic acid derivative **4.5** with the bromide intermediate **4.2** was the most challenging step of the synthesis. The first attempt was performed using 2 equivalents of **4.2** in the presence of DIPEA (2.2 equiv) in CH_3CN at a temperature just below reflux (50 °C). However, these conditions failed to give the desired product. Therefore, a two-phase strategy involving a mixture of CH_3CN and 2 M phosphate buffer with pH 8.0, first reported by Rapoport et al., was employed (Scheme 4.3) [149]. The replacement of the phosphate buffer layer with fresh one (after 2 and 14 hours) was aimed to ensure the most efficient deprotonation of the amine. Moreover, extra 2 equivalents of **4.2** were added after 14 hours to promote the bisalkylation and to account for the easy lactamization of the derivative **4.5**. After purification by column chromatography, the bisalkylated product **4.6** was isolated with a modest yield of 26.3%. The integration of the $^1\text{H-NMR}$ signals corresponding to the methyl protons of the *tert*-butyl groups along with the methylene protons of the prochelator skeleton attached to the glutamic acid derivative corroborated the occurrence of the bisalkylation. The $^{13}\text{C-NMR}$ (Figure 4.1) spectrum showed three distinct carbonyl carbons (173.12, 172.63 and 170.42 ppm) accounting for the three different carboxyl protecting groups.



Scheme 4.3. Synthesis of the acyclic prochelator PC1.

i) 4.2, CH₃CN/ 2 M phosphate buffer pH=8.0, RT, 38 h; ii) H₂, Pd/C, CH₃OH, 6 h.

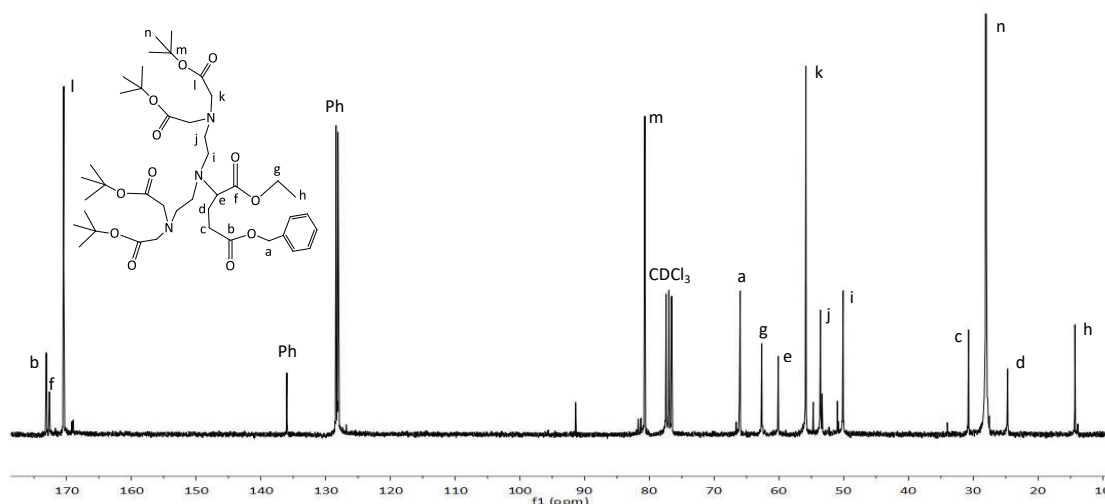


Figure 4.1. Representative ^{13}C -NMR spectrum (CDCl_3) of the bisalkylated product 4.6.

The benzyl group was then selectively removed by classic hydrogenolysis giving prochelator **PC1** in high yield. The removal of this group was confirmed by the disappearance of the corresponding signals from the ^1H -NMR and ^{13}C -NMR spectra. The carbon of the carboxylic acid generated a signal (in the ^{13}C -NMR spectra) at 175.4 ppm corresponding, as expected, to a shift to lower field compared to the carbonyl of the benzyl ester. The compound was further characterized by ESI-MS with the spectrum showing the peaks corresponding to the singly protonated molecule and to the single sodium adduct, both with the expected isotopic distribution (Figure 4.2).

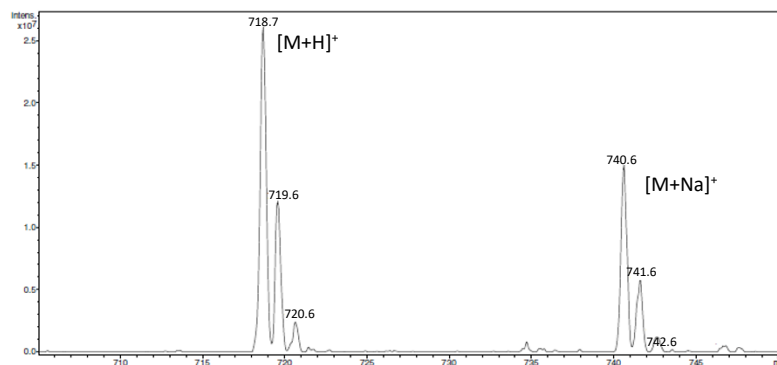


Figure 4.2. ESI-MS spectrum of the acyclic prochelator PC1 in the positive ion mode (m/z calcd for $C_{35}H_{64}N_3O_{12}$ $[M+H]^+$: 718.45, found: 718.7 $[M+H]^+$, 740.6 $[M+Na]^+$).

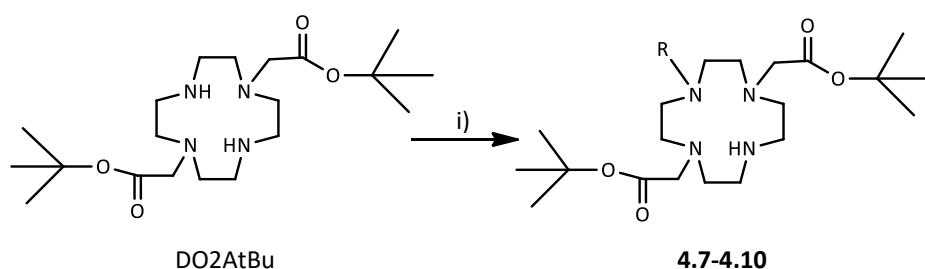
The generated compound has a reactive carboxylic acid that can be used for the coupling of a biomolecule and therefore represents a ready-to-use bifunctional prochelator that upon selective cleavage of the ethyl ester in basic conditions can be further vectorized with a different targeting moiety. This prochelator is also fully compatible with solid-phase synthesis and can be directly applied for the coupling to a resin-bound peptide. When doubly-vectorized, after *tert*-butyl deprotection, four carboxylate groups and three nitrogens will have the ability to coordinate trivalent radiometals such as ^{111}In , ^{68}Ga , ^{90}Y and ^{177}Lu that are known to have important clinical applications. In fact, this heptadentate chelating moiety has already proved to form ^{111}In complexes that demonstrate high *in vivo* stability [88]. However, the low yield of the bisalkylation step and the laborious synthetic route made the macrocyclic prochelators (presented in the next section) more attractive for the synthesis of the final dual-targeting probes. Nevertheless, it is noteworthy that for probes containing thermolabile biomolecules the “DTPA-like” chelator is preferable since it allows the radiolabelling with In-111 at room temperature.

4.2.2. Macrocyclic “DOTA-like” Prochelators

The complexation chemistry of functionalized cyclen (1,4,7,10-tetraazacyclododecane) derivatives has been extensively studied in recent years due to the coordination ability of these macrocycles towards a wide range of metal and lanthanide ions with relevant clinical applications [156, 209, 249, 291, 292]. Selective mono *N*-alkylation has been an important step in the preparation of functionalized macrocycles, particularly for the synthesis of DOTA-like

bifunctional chelators. Tetraazamacrocycles have been typically monoalkylated with different alkyl bromides with reaction yields that are strongly dependent on the nature of the alkylating agents and on the reaction conditions (solvent, temperature and stoichiometry) [249, 292]. DO2A (1,4,7,10-tetraazacyclododecane-1,7-diacetic acid) is a cyclen derivative that allows synthetic transformations on two secondary amines on the macrocyclic ring. The commercially available DO2AtBu (Scheme 4.4) possesses two *tert*-butyl protected acetic arms at position 1,7 (*N-trans*) and can be a valuable precursor for the preparation of multifunctional DOTA-like chelators [291].

Aiming to obtain a DOTA-based prochelator able to be selectively functionalized with two different targeting moieties, the first synthetic step was the monoalkylation of DO2AtBu with an appropriate alkylating agent (Scheme 4.4). Envisioning distinct synthetic strategies for the dual vectorization, different bromide alkylating arms (Table 4.1) were reacted with DO2AtBu. In order to avoid the unwanted bisalkylation, DO2AtBu was used in slight excess ranging from 1.1 to 1.5 molar equivalents relatively to the alkylating reagent. The reaction was performed in dry acetonitrile, which was found to be the best solvent for the *N*-monoalkylation of cyclen in the work done by Li and Wong [292]. The alkylating reagents were added dropwise to the macrocycle over 15 to 20 min and the addition was performed at 0°C to potentiate selectivity. The presence of anhydrous K₂CO₃ as a base was needed to ensure a reasonable yield for the *N*-monoalkylation with the bromo-alkyl-dicarboxylic acid diester **2.3**. The reactions were all carried out at room temperature under inert atmosphere and were monitored by TLC.



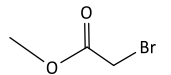
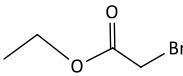
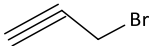
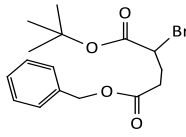
Scheme 4.4. Monoalkylation of DO2AtBu.

i) Alkylating agent R-Br, CH₃CN, RT, 24-48h.

In Table 4.1 the yields of the DO2AtBu monoalkylation reactions are shown. The methyl (**4.7**) and ethyl (**4.8**) acetate arms were selectively introduced in the macrocycle with high yields (77.0% and 65.1%, respectively) as well as the propargyl function (**4.9**, 68.7% yield). However,

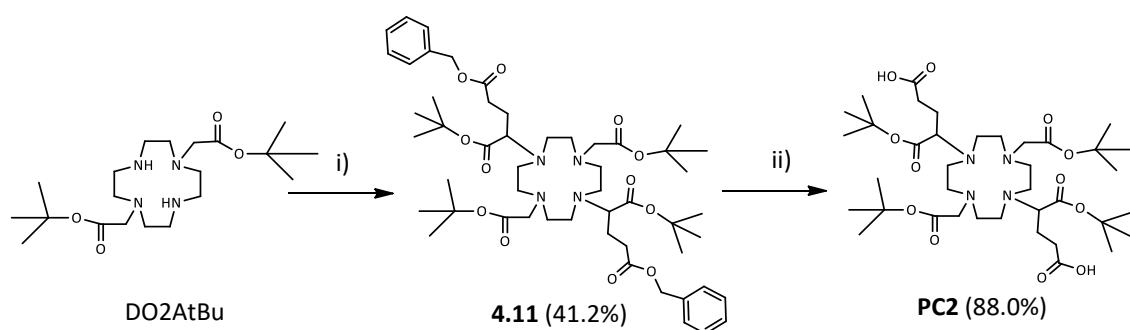
the monoalkylation yield with the glutamic acid derivative (**4.10**) was very low (13.4%). This alkylating molecule, in these reaction conditions, demonstrated to be less reactive and less selective yielding a similar percentage of bisalkylated product (11.2%). The $^1\text{H-NMR}$ spectra (CDCl_3) of the *N*-monoalkylated DO2AtBu derivatives characteristically exhibited a broad singlet between 9 and 10 ppm corresponding to the proton of the remaining free nitrogen of the macrocycle ring. The products were further characterized by ESI-MS.

Table 4.1. Alkylating agents and monoalkylation yields for the synthesis of compounds 4.7-4.10.

Alkylating agent (R-Br)	Product	Monoalkylation yield (%)
	4.7	77.0
	4.8	65.1
	4.9	68.7
 (2.3)	4.10	13.4

For the construction of the final double-vectorized prochelators, the L-glutamic acid derivative is an important building block. However, due to the lower yield found with the *N*-monoalkylation of DO2AtBu with the corresponding bromide derivative it was decided to introduce this moiety in the ring as the final *N*-alkylating agent. However, it should be noted that compound **4.10** itself can be a valuable prochelator since it can be specifically *N*-alkylated with a biomolecule containing an alkyl halide function. Following the alkylation, hydrogenolysis of the benzyl group can render a free carboxylic acid able to react with a different biomolecule via amide bond formation. In the end, after *tert*-butyl deprotection, three carboxylates and the four macrocycle nitrogens can yield a heptadentate chelator. Furthermore, the bisalkylation of DO2AtBu with the bromo-alkyl-dicarboxylic acid diester **2.3** yielded a derivative that after

selective benzyl deprotection can be conjugated to amine-containing biomolecules providing hetero- or homodimeric ligands. Given the interest of this prochelator, the alkylation reaction conditions were optimized to yield the bisalkylated product. The reaction was performed at 50°C, for 48 hours, using 3 equivalents of the bromide arm **2.3** and 2 equivalents of K₂CO₃. In these conditions, the fully alkylated DO2AtBu derivative was obtained with a 41.2% yield.



Scheme 4.5. Synthesis of the symmetric prochelator **PC2**.

i) 2.3, K₂CO₃, CH₃CN, 50°C, 48h; ii) H₂, Pd/C, CH₃OH, 8 h.

After catalytic hydrogenation, the dicarboxylic acid prochelator **PC2** was successfully obtained and characterized by ¹H-NMR, ¹³C-NMR and ESI-MS. As expected due to the symmetry of the molecule, the ¹³C-NMR spectrum (Figure 4.3) showed three different carbonyl carbons corresponding to the six carbonyl groups present in the molecule: the carboxylic acid carbons with higher chemical shift (176.7 ppm) and the *tert*-butyl ester carbonyl carbons of the glutamic acid and acetate arms (174.7 and 173.1 ppm). This prochelator, although valuable for the construction of multivalent probes, does not allow the site-specific vectorization with two different biomolecules even though heterobivalent probes can be obtained by stoichiometric control.

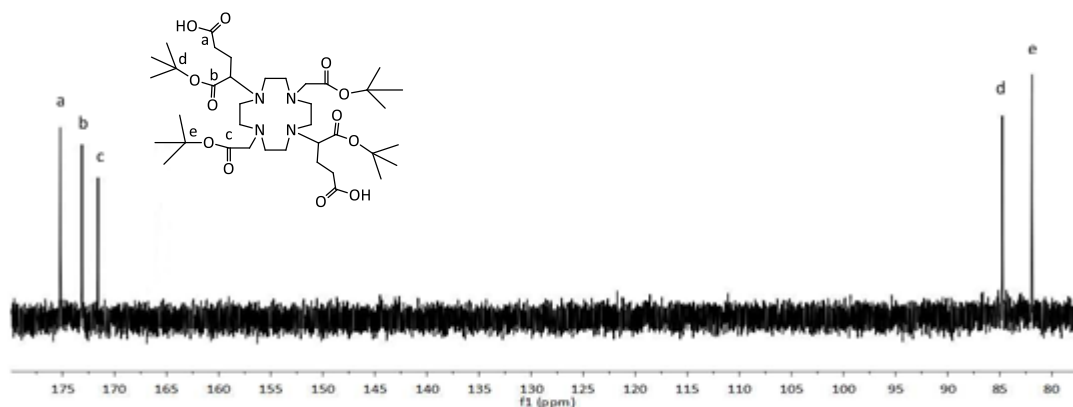
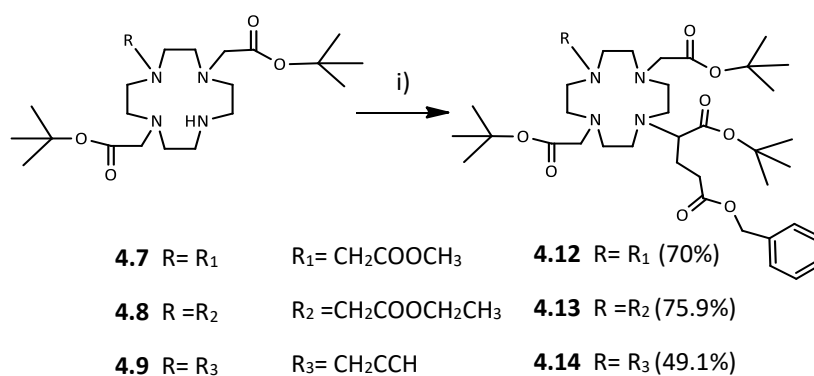


Figure 4.3. Zoom of a representative ^{13}C -NMR spectrum (CD_3OD) of PC2 in the region between 77.5 and 180 ppm.

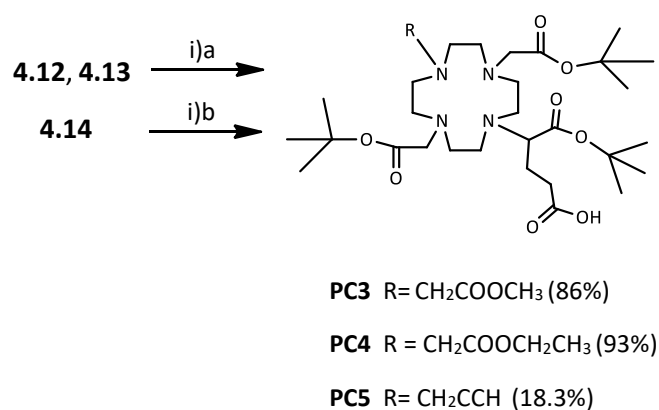
In accordance to the proposed strategy for the synthesis of selectively vectorizable DOTA-like prochelators, the remaining free amine of the macrocycle ring of derivatives **4.7**, **4.8** and **4.9** was then alkylated with the bromo-alkyl-dicarboxylic acid diester **2.3** which was used in a 1.2-1.5 molar excess (Scheme 4.6). The reactions were left for 48 hours in the presence of an excess of K_2CO_3 . The yield was lower for the synthesis of **4.14** (49.1%) compared with **4.12** and **4.13** (70.0% and 75.9%, respectively) probably due to differences in the solubility of the cyclen-based precursors. The formation of the asymmetrical products was corroborated by NMR and ESI-MS.



Scheme 4.6. Synthesis of the asymmetric derivatives **4.12**, **4.13** and **4.14**.

i) **2.3**, K_2CO_3 , CH_3CN , 50°C , 48h.

For the selective deprotection of the benzyl group in order to yield prochelators with the ability of being monofunctionalized with a targeting vector via amide bond formation, two different strategies were adopted (Scheme 4.7). For the methyl and ethyl *tert*-butyl acetate derivatives (**4.12** and **4.13**), the classic palladium-catalysed hydrogenation was employed. This method proved to be very selective and gave almost quantitatively the mono-carboxylic acid prochelators **PC3** and **PC4**. The deprotection was confirmed by NMR by the disappearance of the signals corresponding to the benzyl group while the signals assigned to the *tert*-butyl and methyl/ethyl esters remained intact. Furthermore, in accordance to the assymetrical character of the molecules, the ¹³C-NMR spectra (Figure 4.4) showed five different carbonyl carbons with the carboxylic carbons generating signals with the highest chemical shifts (around 175 ppm). Prochelators **PC3** and **PC4** can be readily coupled to amine containing biomolecules and are fully compatible with the Fmoc-chemistry used in solid phase peptide synthesis. After being monofunctionalized, selective methyl- or ethyl- deprotection should be achieved in basic conditions yielding another reactive carboxylic acid able to be coupled to a different targeting moiety thus providing the bivalent prochelator.



Scheme 4.7. Deprotection of the benzyl ester to yield **PC3**, **PC4** and **PC5**.

i)a H₂, Pd/C, CH₃OH, 8 h; **i)b** 0.5 M NaOH, THF, RT, 6 h.

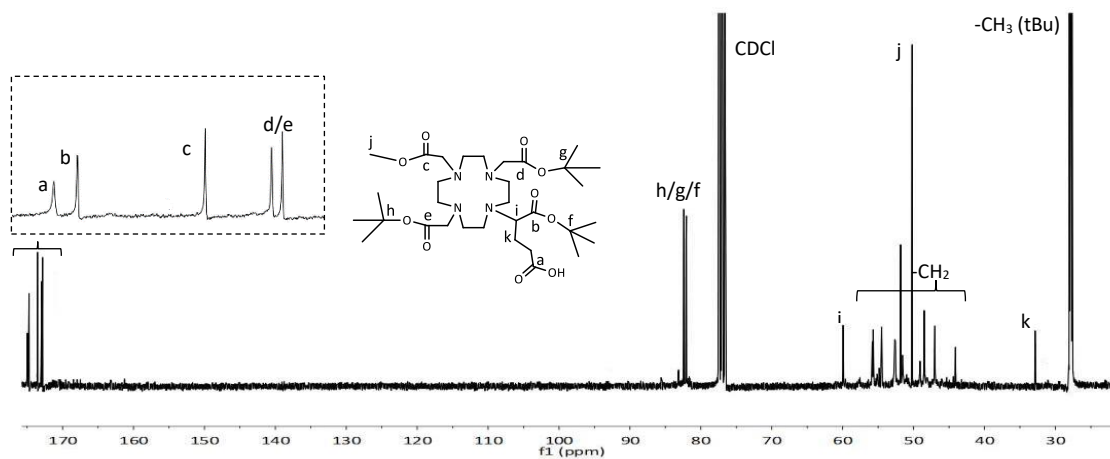


Figure 4.4. Representative ^{13}C -NMR spectrum (CDCl_3) of PC3 with a zoom of the region between 170 and 176 ppm.

On the other hand, for the benzyl deprotection in compound **4.14** different conditions had to be used due to the susceptibility of the alkyne function towards reduction by hydrogenation. Therefore, the removal of this group was performed in basic conditions using a solution of 0.5 M NaOH that was mixed with an equal volume of THF intended to solubilize the product. The progress of the reaction was monitored by TLC and after 6 hours the starting product appeared to have been fully converted to more polar (with lower R_f) products. Therefore, after THF evaporation the crude product was extracted using CHCl_3 . The ^1H -NMR analysis of the organic phase corroborated the removal of the benzyl group and revealed the presence of the byproduct benzyl alcohol. The ESI-MS analysis (Figure 4.5) confirmed the presence of the desired product **PC5** as the most intense peak of the spectrum. However, the removal of the benzyl group in these conditions was not selective since the ESI-MS spectrum showed that partially *tert*-butyl deprotected products were also present. The total deprotection of the three *tert*-butyl esters, although not verified in this analysis, could have occurred since the deprotected product is expected to be water-soluble and therefore could have been effectively washed during the extraction step. Due to the presence of these side products, the compound was purified through a C18 Sep-Pak cartridge eluted with increasing concentrations of acetonitrile in water. The desired *tert*-butyl protected prochelator **PC5** was eluted with the mixture water: CH_3CN 50%:50%. After lyophilization, the product was obtained with a 18.3% yield. For this low yield, besides the partial deprotection of the *tert*-butyl esters during the benzyl removal, some retention in the Sep-Pak cartridge might have also contributed.

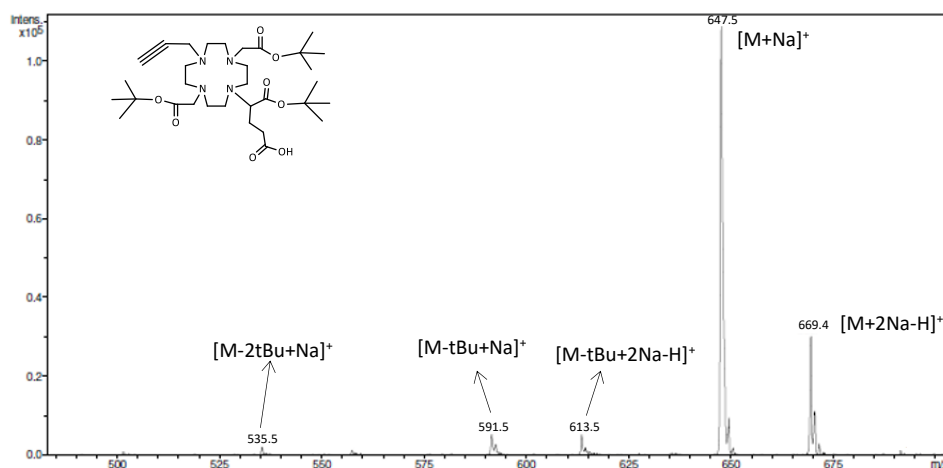


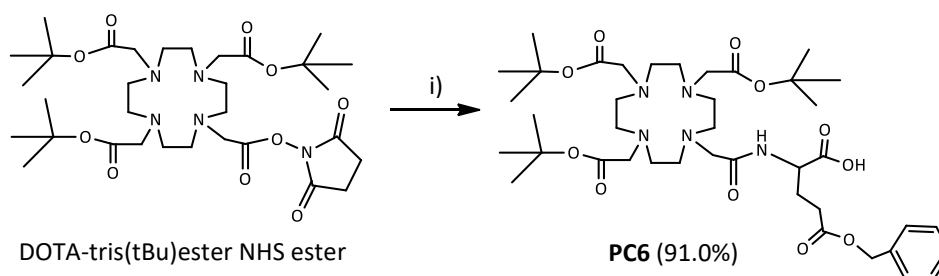
Figure 4.5. ESI-MS spectrum (positive mode) of the crude product of PC5 (m/z calcd for $C_{32}H_{57}N_4O_8$ $[M+H]^+$: 625.42, found: 647.5 $[M+Na]^+$, 669.4 $[M+2Na-H]^+$).

In spite of the synthetic difficulties, **PC5** constitutes an attractive prochelator since it is ready to be bisfunctionalized in a specific manner with two different biomolecules: one containing an azide function intended for a click-chemistry reaction with the alkyne arm, and another one that can be coupled to the free carboxylic acid via amide bond formation. After *tert*-butyl deprotection, a DOTA-like heptadentate chelator is expected.

Alternative Synthetic Approach

The prochelators reported until now allow the introduction of targeting molecules in opposite sides of the macrocycle ring which can be convenient to reduce the potential deleterious effect of the steric hindrance in the biological activities/targeting abilities of each biomolecule. However, the L-glutamic acid building block can also be used in the construction of a prochelator that allows the selective introduction of two different targeting molecules in the same arm of the macrocycle. To accomplish that goal, the commercially available DOTA-tris(*t*Bu)ester NHS ester (1,4,7,10-tetraazacyclododecane-1,4,7-tris-*tert*-butyl acetate-10-succinimidyl acetate) was used as precursor. This protected DOTA derivative has a single carboxylic acid activated as a N-hydroxysuccinimidyl ester which gives specificity to the coupling reaction with an amine-containing molecule. Therefore, the intermediate L-glutamic acid 5-

benzyl ester can be used for the coupling without the need of protecting its free α carboxylic acid. The two reagents were combined in practically equimolar quantities in the presence of the base DIPEA in DMF and the reaction was monitored by HPLC (Scheme 4.8). After reacting for 4 hours, a new major peak with a retention time of 31.2 min had appeared in the HPLC chromatogram, while the peak corresponding to the L-glutamic acid 5-benzylester (Rt= 20.8 min) had completely disappeared which was assumed as an indication of the reaction completion. After DMF evaporation under vacuum, the prochelator **PC6** was isolated by extraction and characterized by NMR and ESI-MS. In the ^{13}C -NMR spectrum of this derivative the three *tert*-butyl ester carbonyl carbons did not give origin to different signals probably because the glutamic acid pendant arm is not directly attached to the macrocycle ring. Remarkably, this synthetic pathway provided a doubly-vectorizable prochelator with high yield (91.0%) in just one step.



Scheme 4.8. Synthesis of the prochelator PC6.

i) L-glutamic acid 5-benzylester, DIPEA, DMF, RT, 6 h.

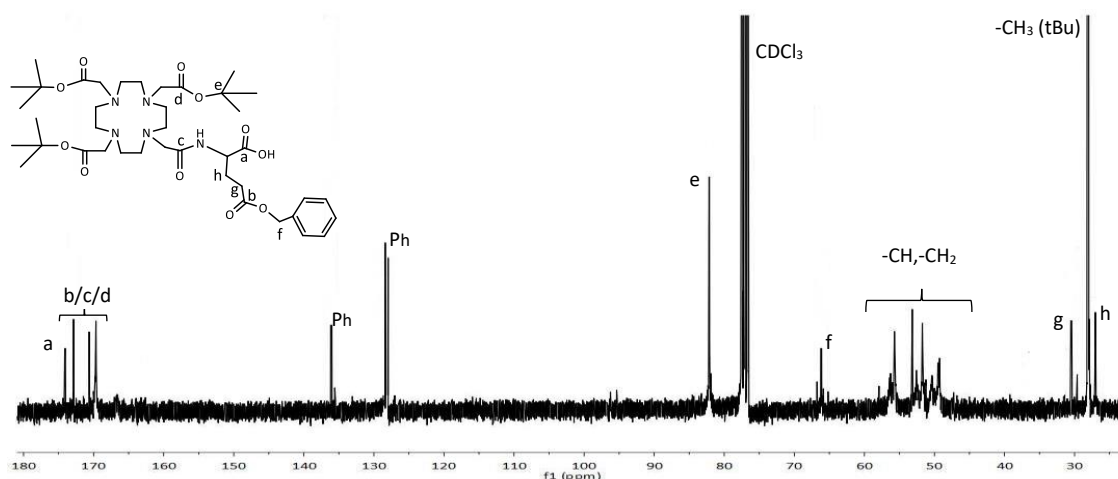


Figure 4.6. Representative ^{13}C -NMR spectrum (CDCl₃) of PC6.

4.3. Molecular Vectors for Nuclear Targeting

As explained in Chapter 1, the therapeutic effect of Auger electrons is maximized when the decay of the Auger-emitting radionuclides occurs in the close vicinity of DNA. Therefore, in the design of radioprobes for Auger therapy, a DNA-targeting moiety should be included to potentiate the internalization of the radioisotope in the cell nucleus. In this regard, most of the DNA-targeting strategies found in the literature have relied in DNA intercalating molecules or in peptide sequences with nuclear localization ability [145, 286, 289, 293, 294]. In this thesis, both approaches have been explored and are thoroughly discussed in the next sections. Therefore, a DNA-intercalating polyaromatic molecule, acridine orange (**AO**), and a peptide containing a nuclear localizing sequence (**NLS**) that is recognized by the cellular nuclear import system, were selected to integrate the targeted radioconjugates prepared in this work. As explained in the following sections, the differences in the chemical nature of the two DNA-targeting vectors have impact in the chemical strategies employed for the construction of the final conjugates and are also expected to influence the biological profiles of the radiolabelled probes.

4.3.1. DNA Intercalating Unit: Acridine Orange

Certain planar polycyclic aromatic small molecules can be inserted between adjacent base pairs of double helical DNA forming a “sandwich-like” structure, a mode of DNA binding named intercalation (Figure 4.7). This insertion has the potential to significantly perturb the double stranded DNA structure and as a result may also perturb DNA-dependent biological processes such as transcription, replication and repair. Therefore, DNA intercalators have been explored as chemotherapeutic agents [295, 296].

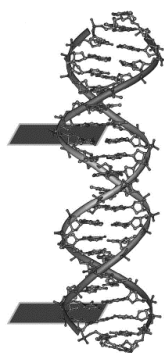


Figure 4.7. Schematic representation of DNA intercalation (the planar bar represents the intercalator). Adapted from [297].

Acridine (Figure 4.8) and derivatives represent a dye class whose interactions with DNA have been extensively studied. Acridines are protonated at the nitrogen atom under neutral conditions and the resulting cationic aromatic compounds constitute a promising class of intercalators. The cytotoxic potential of these molecules has been explored for clinical applications as anti-bacterial, anti-malarial and anti-cancer agents [298].

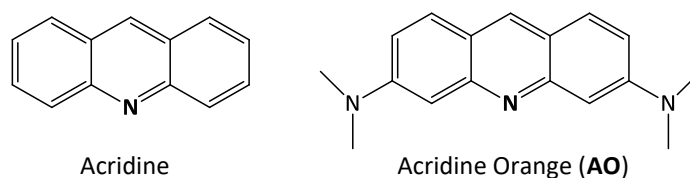


Figure 4.8. Chemical structures of acridine and acridine orange (AO).

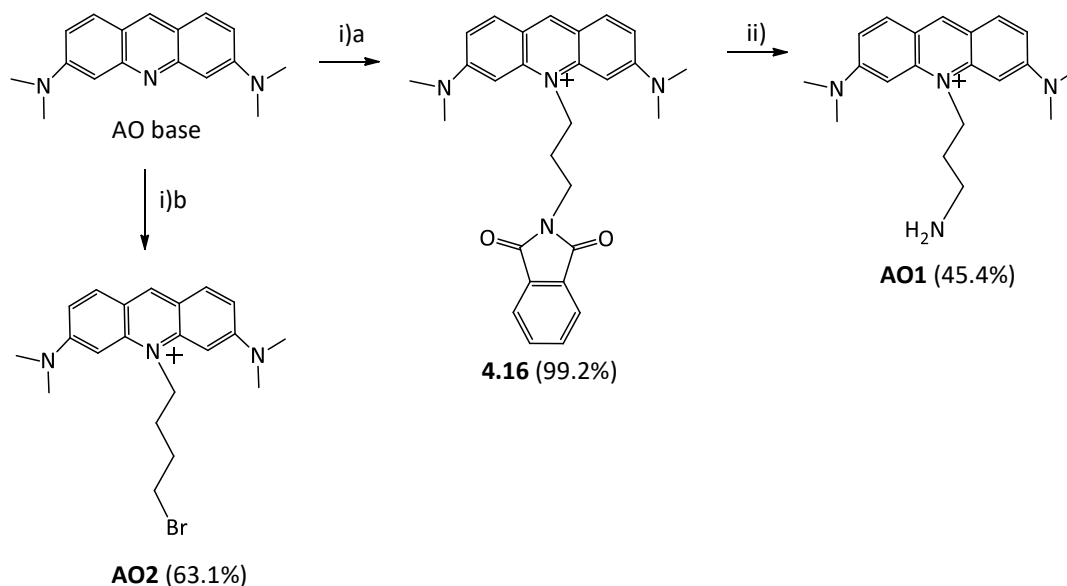
The diamino-substituted derivative acridine orange (**AO**) is a classical representative of this dye class and its DNA intercalating properties have been studied in detail. **AO** intercalates with its long molecular axis virtually parallel to the mean plan passing through the base pairs on either side of the double helix. The intercalator assumes an asymmetric position with the dimethylamino group protruding out away from the helix on one side while being largely confined within the helix on the other [299]. The intercalation modifies the UV/vis absorption properties of the molecule and thus the DNA-binding ability can be evaluated by performing spectrophotometric titrations [300]. Interestingly, intercalation of **AO** into DNA enhances the dye's fluorescence emission and therefore this property has been explored by using **AO** for DNA staining, *e.g.* in gel electrophoresis, or for the detection of cellular DNA. In fact, due to the small size and lipophilic character, **AO** can diffuse into cells within few seconds to bind to nucleic acids in the nuclear compartment [301].

In addition to the clinical applications already mentioned for acridine derivatives, in recent years **AO** has been explored as photosensitizer in photodynamic therapy and as radiosensitizer in radiodynamic therapy for the treatment of oncologic diseases [302, 303]. Acridine rings have also been used in more complex molecules to bring particular functionalities which do not bind to DNA themselves into the close vicinity of the nucleic acids or to increase the binding constant and/or selectivity when the other part of the molecule also binds to nucleic acids [295]. In this regard, **AO** has been linked to platinum complexes to increase selectivity and to overcome the resistance to platinum anticancer agents [304]. Furthermore, **AO** derivatives

have been integrated into ligands intended for radiolabelling with Auger electron emitting radioisotopes such as ¹²⁵I and ^{99m}Tc [125, 300]. The presence of the acridine moiety has shown to potentiate nuclear internalization of the radioconjugates in cancer cells while keeping the ability to interact closely with DNA by intercalation [305]. This DNA-binding ability has potentiated the Auger-induced DNA damage as studies with plasmid DNA have shown. The extent of the damage has been related to the distance between the **AO** moiety and the emitting radionuclides, with greater cytotoxic effects being achieved by using shorter linkers between these two units which leads to the emission of the Auger electrons in closer contact with DNA [125]. However, the use of **AO** derivatives in ¹¹¹In-labelled conjugates has been unexplored until now, despite the relevance of this radionuclide for Auger therapy and theranostic applications.

4.3.1.1. Synthesis and Characterization of Acridine Orange Derivatives

In this work, the **AO** moiety was derivatised in order to be attached as a pendant arm in a prochelator. The resulting monofunctionalized prochelators should be able to be further functionalized by a targeting biomolecule to accomplish target-specific ligands capable of DNA-binding. **AO** derivatives bearing an amine or a bromide function were synthesized using previously reported strategies with modifications (Scheme 4.9) [294, 304]. Alkyl linkers with 3- and 4-carbons were introduced in the heterocyclic nitrogen by alkylation with the corresponding alkyl halide using harsh reaction conditions. The attachment of shorter methylenic linkers (2 carbons) was tried, although difficulties in the synthesis (mainly due to the occurrence of elimination reactions) prevented the achievement of that goal.



Scheme 4.9. Synthesis of the AO derivatives AO1 and AO2.

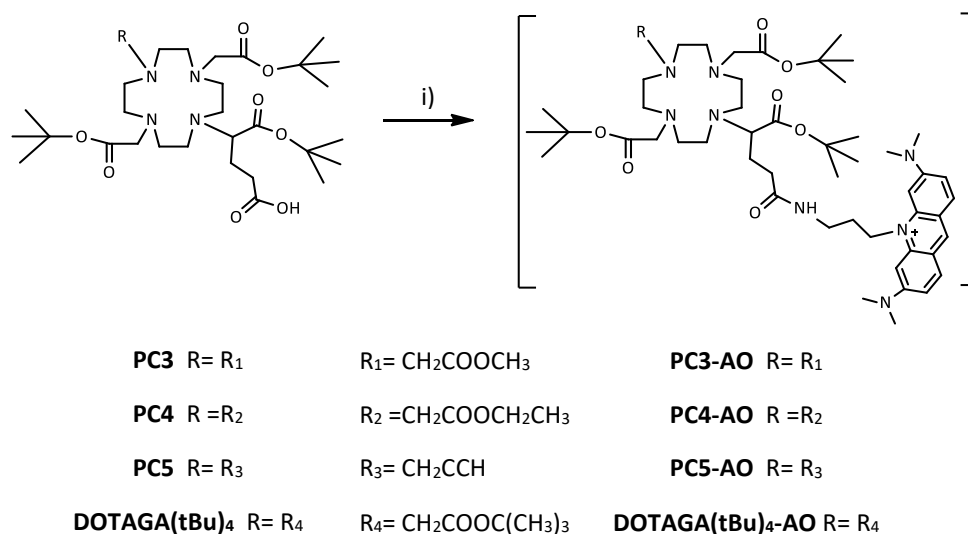
i)a iodopropyl phthalimide (**4.15**), K_2CO_3 , *p*-xylene, reflux, 5 days; *ii*) hydrazine monohydrate, CH_3OH , reflux, 48 h; *i)b* 1,4-dibromobutane, toluene, reflux, 24 h.

For the synthesis of the amine-bearing **AO** derivative **AO1**, bromopropyl phthalimide was used as the starting alkylating agent. Phthalimide is a well-known protecting group for primary amines and after deprotection should yield the desired free amine with a 3-carbon methylenic linker attached to the polyaromatic moiety [306]. Prior to the alkylation reaction, bromide was replaced by iodide (**4.15**) thus providing a better leaving group for the N-alkylation. The conjugation to the **AO** free base was performed in *p*-xylene at reflux (140°C) for 5 days to ensure complete alkylation. The product **4.16** was isolated by precipitation with high yield (99.2%). The next step was the phthalimide deprotection using a large excess of hydrazine (9:1) at reflux (65°C) in dry methanol. In order to release the free amine (as a salt), concentrated HCl was then added. After filtration to remove the precipitate (the byproduct phthalhydrazide), the amine-containing **AO1** was extracted to chloroform after basification with NaOH. The derivative was obtained with a 45.4% yield. The deprotection was confirmed by the disappearance of the signals of the phthalimide protons (7.72-7.82 ppm) and by the shift for higher field (3.03 ppm) of the methyl protons attached to the primary amine in the 1H -NMR spectrum.

On a different approach, the alkyl-halide **AO2** derivative was synthesized by alkylation with a large excess of 1,4-dibromobutane under reflux in toluene. These conditions led to the obtention of a bromide derivative with a 4-carbon alkyl chain as confirmed by NMR.

4.3.1.2. Synthesis and Characterization of Macrocyclic Prochelators with Acridinium Pendant Arms

The free amine of **AO2** was used for the conjugation to the free carboxylic acid present in the prepared cyclen derivatives. The conjugation was first tested with **DOTAGA(tBu)₄** prior to the reaction with the doubly-vectorizable prochelators. Attempts to perform the coupling employing the classic DCC/NHS system to pre-activate the carboxylic acid failed to yield the desired conjugate even in a 5-days reaction. Long reaction times for the coupling of amine-bearing **AO** derivatives have already been reported in previous studies [304, 305]. Therefore, *in situ* activation using the more effective coupling agent HATU was employed. In fact, the high coupling efficiencies and fast reaction rates usually associated with this agent are thought to arise from a neighbouring group effect brought about by the pyridine nitrogen atom which can stabilize the incoming amine through a hydrogen-bonded 7-membered cyclic transition state [307]. For this approach, the carboxylic acid was activated with an equimolar amount of HATU in the presence of DIPEA for a few minutes (3-10 min) before being added to the **AO** solution in DMF (Scheme 4.10). The reaction was monitored by HPLC and after 12 hours the same amounts of HATU and DIPEA were added to the mixture to ensure maximum coupling yield. After additional 24 hours, the solvent was evaporated and the product was isolated by extraction from water to chloroform. The organic phase was analysed by HPLC and the chromatogram presented a major compound that was identified by ESI-MS analysis as the desired conjugate. Purification by column chromatography on silica gel (CH₂Cl₂:CH₃OH, 9:1 with 1% of NH₄OH) was attempted but extensive product degradation and adsorption were verified. Therefore, to minimize losses, the adopted approach was to purify the product at a later stage using a C18 Sep-Pak column or by HPLC. This optimized coupling strategy was then successfully applied with prochelators **PC3**, **PC4** and **PC5**, with the formation of the AO conjugations being corroborated by HPLC and ESI-MS (a representative spectrum is shown in Figure 4.9).



Scheme 4.10. Conjugation of AO2 to PC3, PC4, PC5 and DOTAGA(tBu)₄.

i) AO2, HATU, DMF, DIPEA, RT, 48 h

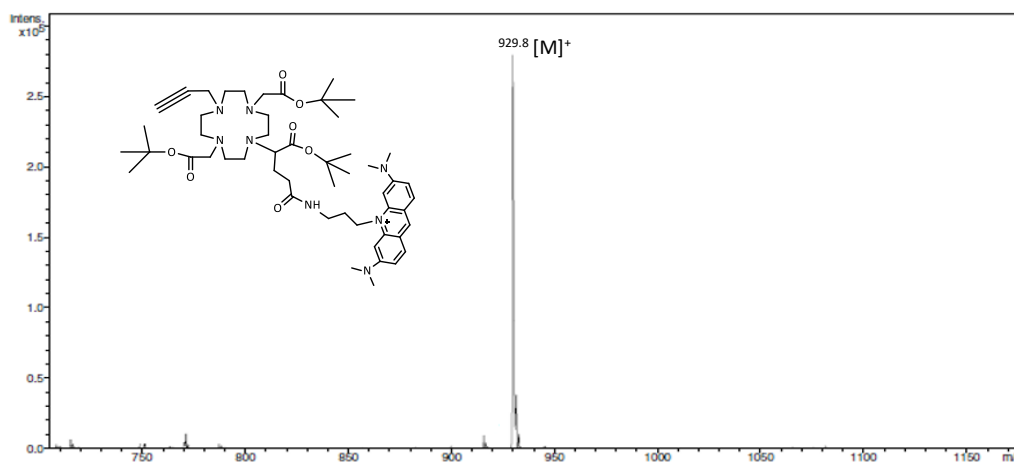
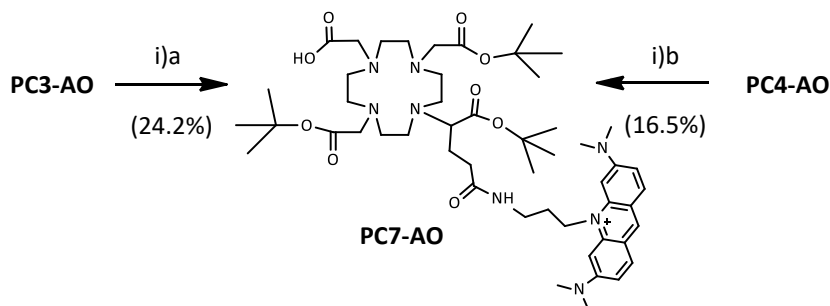


Figure 4.9. ESI-MS spectrum (positive mode) of the crude product of PC5-AO (m/z calcd for [C₅₂H₈₁N₈O₇]⁺: 929.62, found: 929.8 [M]⁺).

The selective deprotections of the ethyl and methyl esters to yield another reactive carboxylic acid were carried out using the crude products present in the organic phases of the extractions. Different conditions were used for the basic hydrolysis of the two esters as depicted in Scheme 4.11. Therefore, the ethyl ester was treated with a solution of 1.0 M KOH in THF, while the methyl ester was dissolved in a mixture of THF:CH₃OH:water and combined with an excess of LiOH [308, 309]. The progress of the reactions was monitored by the appearance in

the HPLC chromatograms of a peak with lower retention time (a difference of approximately two minutes) relatively to the parent compounds (Figure 4.10). After stirring for 5-6 hours both reactions were completed with almost total conversion of the starting products.



Scheme 4.11. Deprotection of the methyl- (PC3-AO) or the ethyl- (PC4-AO) ester to yield PC7-AO.

i)a LiOH, THF:CH₃OH:water, RT, 6 h; **i)b** KOH (1 M), THF, RT, 6 h

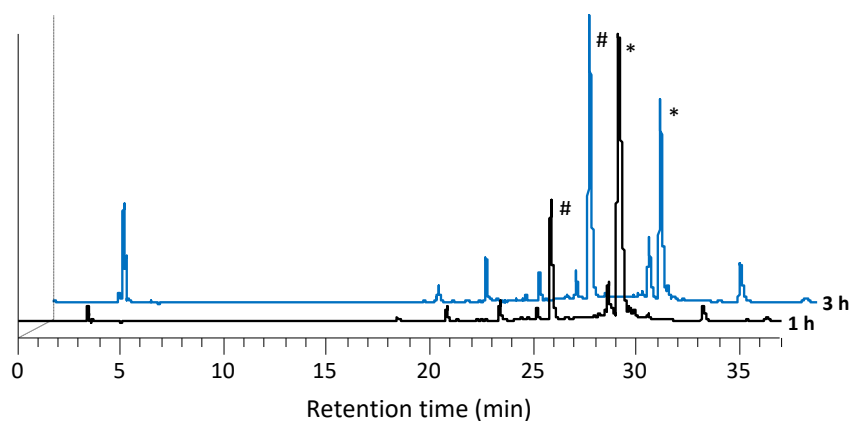


Figure 4.10. HPLC chromatograms ($\lambda=254$ nm) of the reaction mixture of the methyl ester deprotection at 1 and 3 hours after the addition of LiOH. * = PC3-AO, # = PC7-AO.

Both hydrolyses were effective and generated the desired compound as the major product, although evidence of *tert*-butyl deprotection was shown in the ESI-MS spectrum and in the HPLC chromatogram of the crude mixture of the ethyl ester deprotection. These results suggest that LiOH provided a smoother and more selective hydrolysis and therefore this synthetic pathway allowed the obtention of the desired product in slightly higher yield. After purification through a C18 Sep-Pak cartridge, the new cyclen-based prochelator **PC7-AO** bearing a free carboxylic acid and an acridinium pendant arm on opposite sides was characterized by NMR and ESI-MS. In the ¹H-NMR spectra was clearly visible the absence of the methyl (or ethyl)

ester signal(s) while the *tert*-butyl protons were still present along with the characteristic signals associated with the acridine aromatic rings and *N*-dimethyl protons (Figure 4.11). Additionally, the ESI-MS spectrum clearly showed the presence of the molecular ion ($[M]^+$) with the expected isotopic distribution. This compound, along with **PC5-AO**, represents a versatile building block for the construction of targeting probes with potential DNA-binding and nuclear internalization abilities.

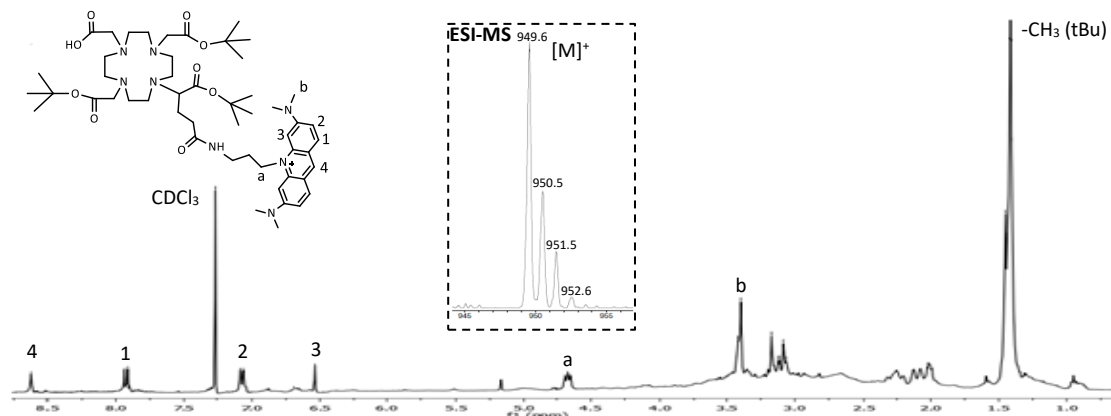
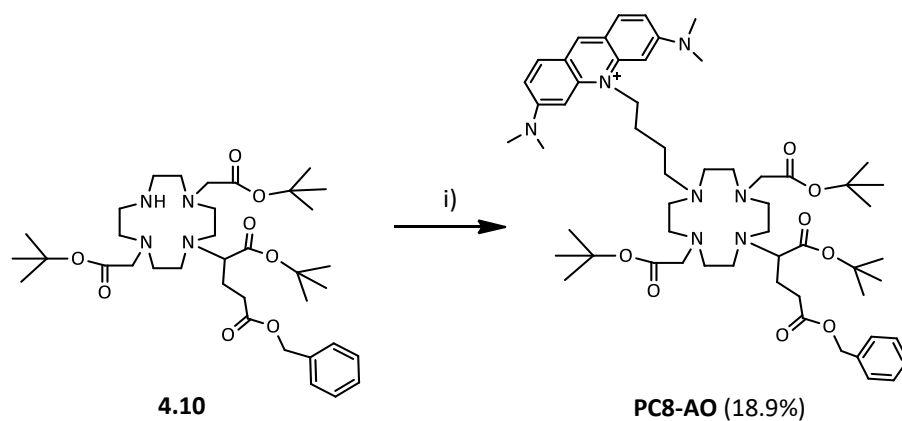


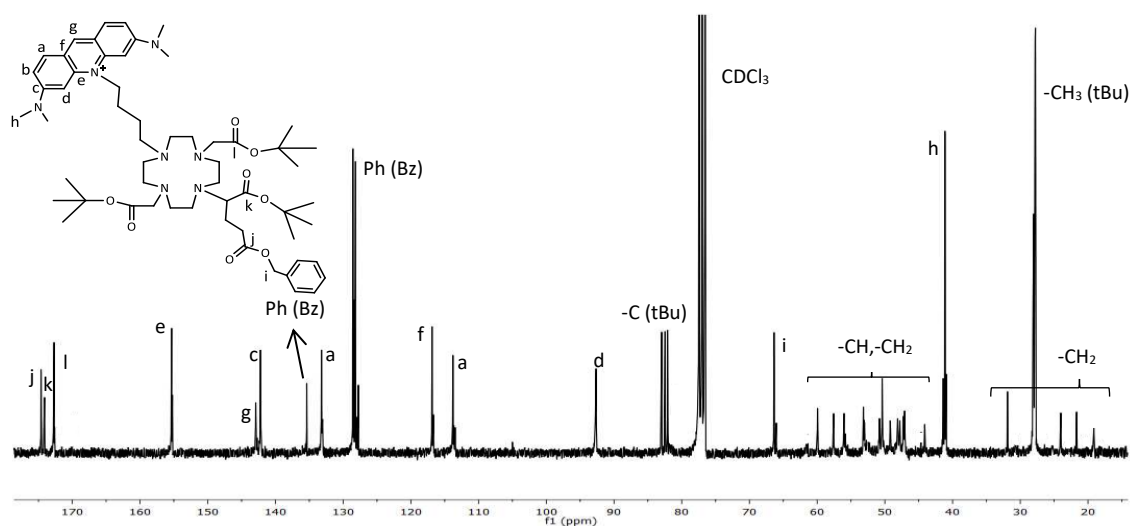
Figure 4.11. Representative ¹H-NMR spectrum (CDCl₃) and zoom of ESI-MS spectrum of **PC7-AO** (m/z calcd for $[C_{51}H_{81}N_8O_9]^+$: 949.61, found: 949.6 $[M]^+$).

In a different synthetic approach (Scheme 4.12), the bromide derivative **AO2** was used for the *N*-alkylation of the derivative **4.10**. The reaction was done at 60°C for 48 hours in DMF in the presence of an excess (4 equivalents) of K₂CO₃. Despite some degradation during the purification through a silica gel column, the alkylated product **PC8-AO** was isolated (19% yield) and characterized by NMR and ESI-MS. The NMR spectra (Figure 4.12) showed the simultaneous presence of the characteristic signals associated with the **AO** moiety and with the benzyl group. To generate a free carboxylic acid on the opposite side of the macrocycle, the benzyl ester was then removed using the standard catalytic hydrogenation with Pd/C. However, these conditions despite causing the removal of the benzyl ester also led to the degradation of the product with the ¹H-NMR spectrum showing the duplication of the signals corresponding to the protons of the **AO** aromatic rings. Furthermore, the ESI-MS analysis did not indicate the presence of the desired product corroborating the susceptibility of the compound to degradation by hydrogenation. For this reason and taking also into account the low yield of the *N*-alkylation, this synthetic approach was not further explored.



Scheme 4.12. Alkylation of 4.10 with the AO derivative AO2 to yield PC8-AO.

i) AO2, K₂CO₃, DMF, 60°C, 48 h

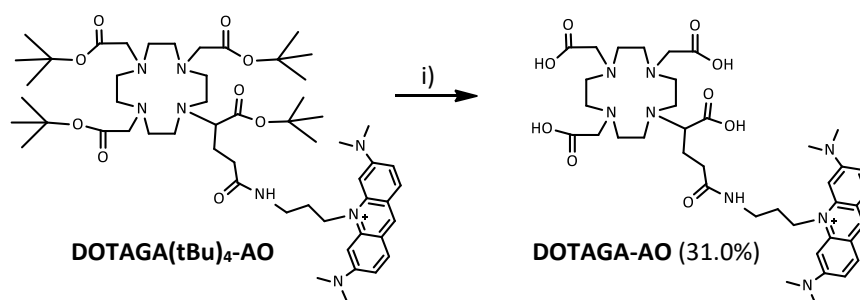


4.3.1.2.1. Validation of DOTAGA-AO as a DNA-binding Unit

Synthesis and Characterization of DOTAGA-AO

The prochelator **PC7-AO** which bears an acridinium pendant arm is intended to be a building block for the construction of dual-targeting probes with ability to interact with DNA. Therefore, it was relevant to study the properties of the totally deprotected **DOTAGA-AO** conjugate derived from **PC7-AO** as DNA-intercalator, since this ligand will correspond to an important unit integrating the final bivalent probe.

DOTAGA-AO was prepared from **DOTAGA(tBu)₄-AO** by deprotecting the four *tert*-butyl esters with neat TFA for 24 hours (Scheme 4.13). The final deprotected conjugate was then purified by semi-preparative HPLC. The shift of the carbonyl carbons signals for lower field and the disappearance of the protons and carbons signals associated with the *tert*-butyl groups corroborated the deprotection in the NMR spectra (Figure 4.13).



Scheme 4.13. Synthesis of DOTAGA-AO.

i) TFA, RT, 24 h.

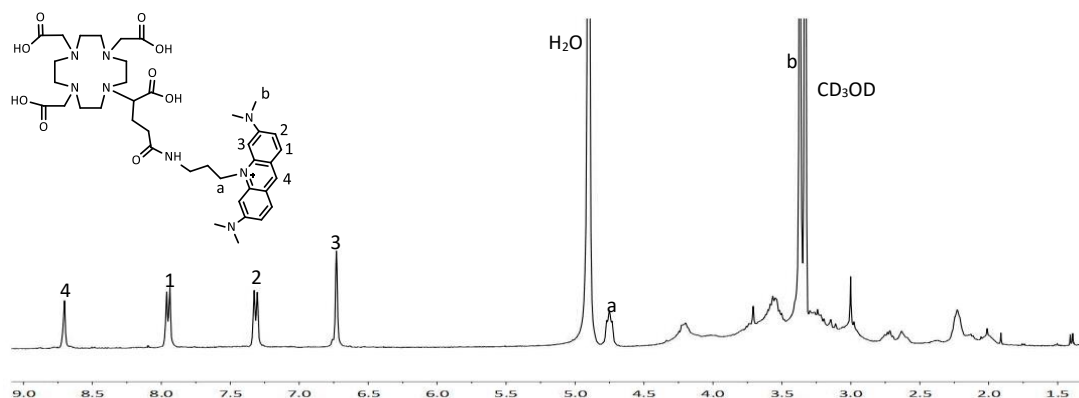
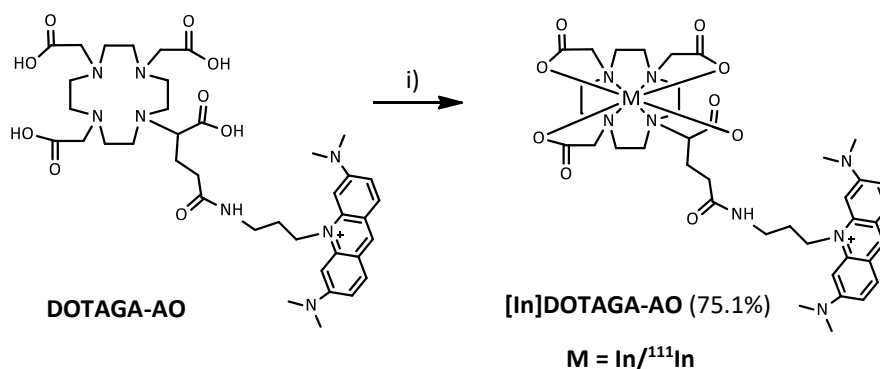


Figure 4.13. Representative ¹H-NMR spectrum (CD₃OD) of DOTAGA-AO.

Synthesis and Characterization of $[\text{In}/^{111}\text{In}]\text{DOTAGA-AO}$

The inactive Indium complex was prepared by reacting the **DOTAGA-AO** ligand with anhydrous InCl_3 at 95°C for 25 min at pH 5.5 (Scheme 4.14). The Indium complex, $[\text{In}]\text{DOTAGA-AO}$, was then purified by semi-preparative HPLC. The shift for higher field of the carbonyl carbons signals in the ^{13}C -NMR spectrum (in comparison to **DOTAGA-AO**) along with the detection of the singly protonated ion in the ESI-MS analysis (Figure 4.14) of the purified product confirmed the formation of the In-complex.

Radiolabelling with ^{111}In was performed at the conditions previously described in Chapter 2, using the ligand at a concentration of 10^{-5} M. The radiolabelling efficiency was evaluated by HPLC with γ -detection and by ITLC to assess the presence of colloidal hydroxides. The radiochromatogram revealed the presence of $[\text{In}/^{111}\text{In}]\text{DOTAGA-AO}$ with a RCP of 97%.



Scheme 4.14. Preparation of $[\text{In}/^{111}\text{In}]\text{DOTAGA-AO}$.

i) InCl_3 , NaOAc pH 5.5, 95°C , 25 min.

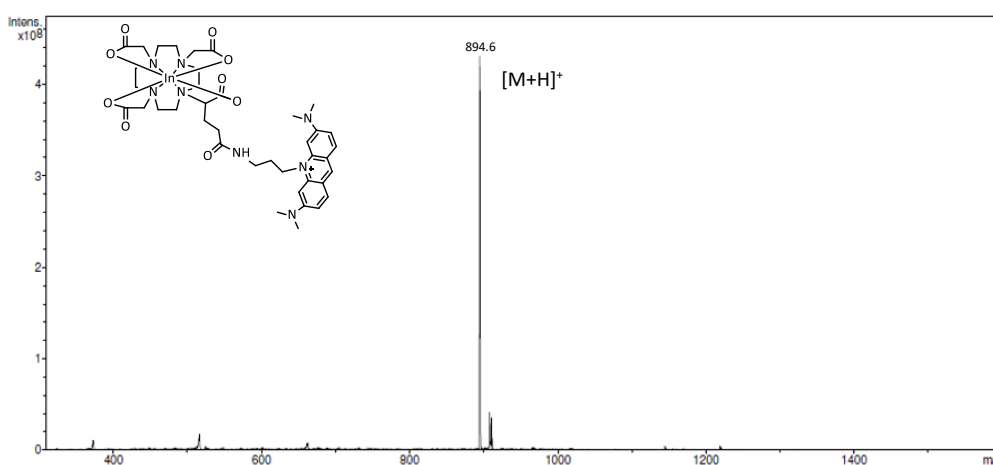


Figure 4.14. ESI-MS spectrum of $[\text{In}]\text{DOTAGA-AO}$ (m/z calcd for $\text{C}_{39}\text{H}_{55}\text{InN}_8\text{O}_9$ $[\text{M}+\text{H}]^+$: 894.31, found: 894.6 $[\text{M}+\text{H}]^+$).

DNA Interaction Studies

The ability of **[In]DOTAGA-AO** to interact with DNA was qualitatively evaluated in an agarose gel mobility shift assay using plasmid DNA. The binding of a compound to the supercoiled (SC) DNA is expected to change the electrophoretic mobility of the corresponding band [310]. For comparison with the prepared complex and as a positive control, **AO** was also incubated with the plasmid in the same concentrations of **[In]DOTAGA-AO**. A plasmid sample with no added compound but incubated at the same conditions (24 h, 37°C, 0.1 M phosphate buffer pH 7.4) was used as control (C).

As it can be seen in Figure 4.15, the addition of **[In]DOTAGA-AO** led to a decrease in the mobility of the SC band in the agarose gel. This decrease was verified in a concentration-dependent manner from 50 to 250 μM and the pattern observed was very similar to the one caused by the addition of **AO** itself. These results suggest that the attachment of the **AO** moiety to the glutamic arm of the macrocycle through a 3-carbon spacer and the presence of the coordinated In(III) did not affect the ability of the polyaromatic moiety to interact with DNA and to modify the DNA topology.

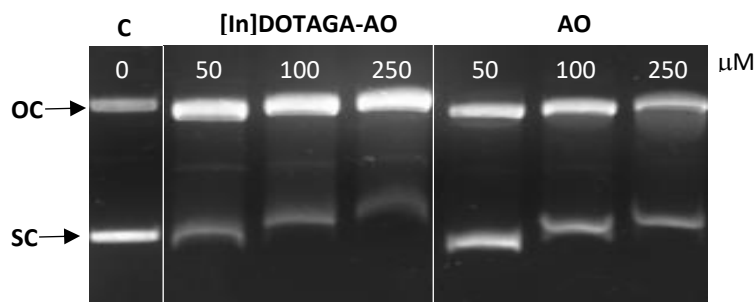


Figure 4.15. Agarose gel electrophoresis of plasmid DNA incubated with **[In]DOTAGA-AO** and **AO** at the indicated concentrations for 24 h at 37°C in phosphate buffer. A control (C) with no added compound was also tested. OC- open circular, SC- supercoiled.

The interaction of **[In]DOTAGA-AO** with calf thymus DNA (CT DNA) was also studied using UV-visible (UV-vis) and fluorescence spectroscopies by monitoring the spectral changes in the presence of increasing amounts of DNA. Therefore, the UV-Vis spectra of the complex with the addition of increasing amounts of CT DNA (up to a 7:1 molar ratio) were measured in the range between 350 and 700 nm (Figure 4.16-a). The free **[In]DOTAGA-AO** Uv-vis spectrum demonstrated an absorbance maximum at 498 nm and a shoulder at 470 nm assigned to the presence of dimeric species in solution resulting from the self-association of the AO rings. Upon

addition of CT DNA, a red shift of the stronger band to a new maximum at 504 nm ($\Delta\lambda = 6$ nm) and a hypochromic effect expressed by a reduction of 10% of the absorption intensity were verified. This behaviour has been observed for other compounds containing **AO** moieties and is consistent with interaction with DNA through intercalation which leads to the interaction of transition moments of **AO** with parallelly oriented non-degenerate transition moments of neighbour purine and pyrimidine bases [125, 300, 311]. The intensity of the shoulder band also exhibited a reduction since the formation of dimers becomes less significant when **AO** is bound to the DNA [300].

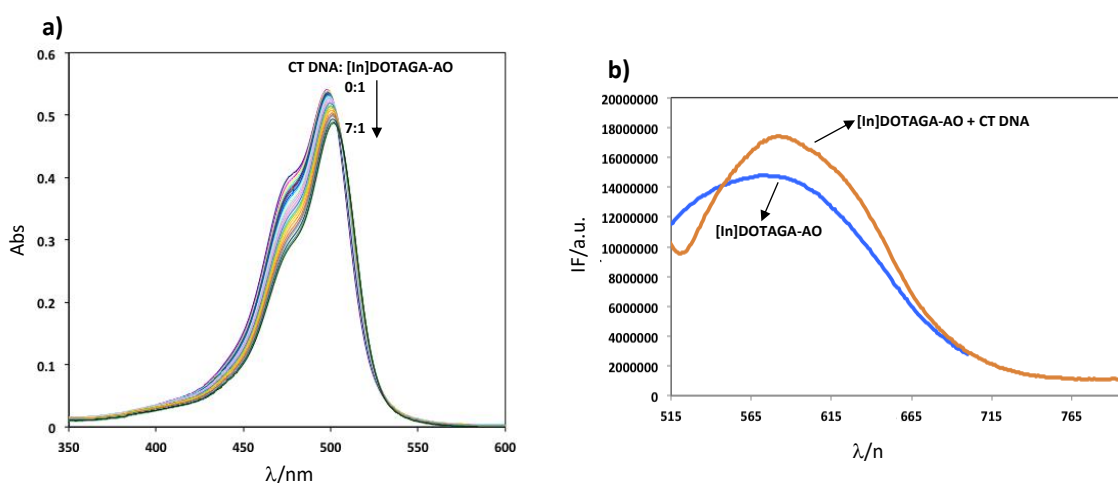


Figure 4.16. Spectroscopic evaluation of DNA interaction. a) UV-Vis absorption spectra measured for solutions of [In]DOTAGA-AO (ca. 65 μ M) and increasing amounts of CT-DNA. b) Fluorescence emission spectra for solutions containing [In]DOTAGA-AO (ca. 8 μ M) and increasing amounts of CT-DNA.

In order to determine intrinsic binding constants several models can be applied to evaluate the UV-Vis absorption data. The Scatchard model is usually applied for UV-Vis data, using equation (5), in which D is the DNA concentration in base pairs, $\Delta\epsilon_{ap} = [\epsilon_a - \epsilon_f]$ and $\Delta\epsilon = [\epsilon_B - \epsilon_f]$ [300, 312]. The ϵ_a value corresponds to the ratio between the measured absorbance and the concentration of the studied compound ($Abs_{obs}/[compound]$); ϵ_B and ϵ_f are the molar absorptivities of the DNA bound complex (in saturation conditions) and the free complex, respectively. From the plot of $D/\Delta\epsilon_{ap}$ vs D , the value of K , the binding constant can be obtained, being the ratio of the slope to the intercept.

$$D/\Delta\epsilon_{ap} = D/\Delta\epsilon + 1/(\Delta\epsilon K) \quad (\text{Equation 5})$$

For **[In]DOTAGA-AO** a binding constant, K , of $1.6 \times 10^{-3} \text{ M}^{-1}$ was obtained from this study. This value indicates a weaker binding affinity towards DNA compared with **AO** itself ($K = 3.9 \times 10^{-4} \text{ M}^{-1}$) and also in comparison with other **AO** conjugates reported in the literature [300, 313]. The bulky macrocycle could have impacted negatively the ability of the polyaromatic moiety to bind to DNA.

Regarding the fluorometric titration, the fluorescence emission of **[In]DOTAGA-AO**, upon excitation at 505 nm, was enhanced by the addition of CT DNA (Figure 4.16-b). This fluorescence enhancement has also been regarded as a relevant spectroscopic fingerprint of the intercalation of **AO** into DNA which is thought to stabilize the dye's excited state [300, 314].

Overall, these results present evidence of the ability of the complex **[In]DOTAGA-AO** to interact with DNA through intercalation, further corroborating its use as a DNA-binding unit for a theranostic approach.

Evaluation of DNA Damage

The distance within the radioconjugate between the DNA-binding moiety and the Auger-emitting radioisotope has been considered an important factor affecting the ability of the radiolabelled probes to induce DNA damage. Therefore, besides testing the DNA-binding properties of **[In]DOTAGA-AO**, it was considered relevant to test if the **[¹¹¹In]DOTAGA-AO** probe could induce DNA damage *in vitro* thus validating the spacer used between the **AO** moiety and the coordinated ¹¹¹In. For that purpose, samples of **[¹¹¹In]DOTAGA-AO** with different activities were incubated with double-stranded plasmid DNA for the time corresponding to approximately two times the In-111 radioactive half-life (140 hours). Under agarose gel electrophoresis, the increase of the open circular (OC) and linear (L) DNA isoforms were used as indicators of the Auger electrons ability to induce, respectively, single strand breaks (SSB) and double strand breaks (DSB) in the parental SC DNA. To allow the distinction between the effects derived from the direct ionization of the DNA backbone produced by Auger electrons and the indirect damaging effects caused by the radical oxygen species in the medium, DMSO was used as a radical scavenger [126, 315-317]. The interaction of ¹¹¹In-labelled DOTA with plasmid DNA was used as comparison since the complex is known to prevent ¹¹¹In from direct binding to DNA [318]. DOTA was prepared from the deprotection of the commercially available DOTA-tris(tBu)ester with TFA and **[¹¹¹In]DOTA** was obtained by employing the standard radiolabelling

conditions used for [^{111}In]DOTAGA-AO. A representative image of the gel after the incubation with the radiolabelled compounds is shown in Figure 4.17.

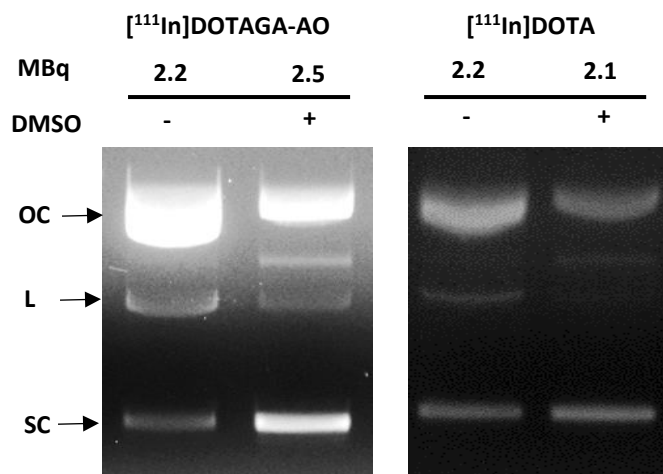


Figure 4.17. Representative gel of plasmid DNA incubated with [^{111}In]DOTAGA-AO and [^{111}In]DOTA (activities used are shown on the top), in the absence and in the presence of DMSO. DNA isoforms are indicated as OC - open circular, L – linear and SC – supercoiled.

The quantification of the pixel intensity of the DNA bands in the experiments performed in the absence of DMSO (Figure 4.18, left column) revealed the increase of the L isoform with increasing activities for both [^{111}In]DOTAGA-AO and [^{111}In]DOTA while the inverse trend was observed with respect to the SC isoform. The formation of L DNA was more notorious for the **AO** conjugate which demonstrated, for the highest activity, the formation of approximately 21% of this isoform. On the other hand, when the incubation was performed in the presence of DMSO (Figure 4.18, right column) the appearance of the L isoform was practically suppressed for [^{111}In]DOTA regardless of the activity. In contrast, for [^{111}In]DOTAGA-AO it was still possible to verify an increase in the L isoform (up to 9%) suggesting that the **AO**-based radioconjugate can induce DSB even under scavenging conditions.

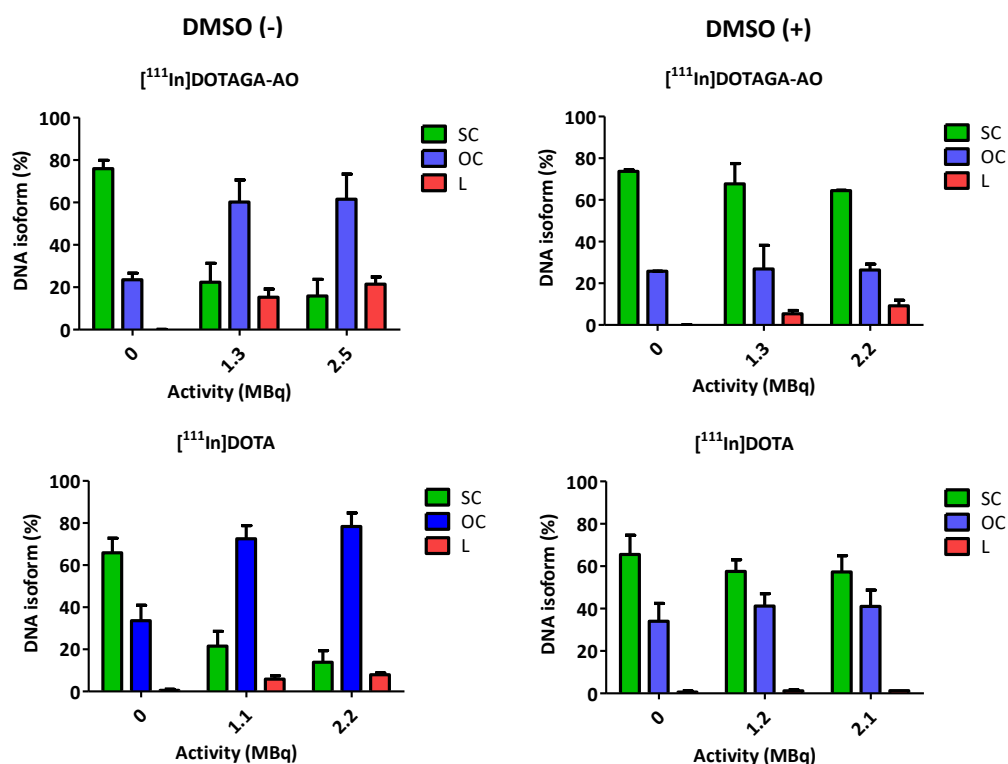


Figure 4.18. Quantitative analysis of the proportion (average (%) \pm SD, $n=3$) of each DNA isoform (OC – open circular, L – linear and SC – supercoiled) after incubation of the plasmid DNA with 2 different activities of $[^{111}\text{In}]\text{DOTAGA-AO}$ and $[^{111}\text{In}]\text{DOTA}$, in the absence (left columns) and in the presence (right columns) of DMSO.

These results indicate that the $[^{111}\text{In}]\text{DOTA}$ effects in DNA are predominantly mediated by indirect mechanisms associated with the radiolysis of water, whereas $[^{111}\text{In}]\text{DOTAGA-AO}$ causes DNA damage by a combination of both direct and indirect mechanisms. The direct effect can be attributed to the presence of the **AO** moiety that leads to a tight interaction between the Auger electron emitter and the DNA, as others have previously shown [300]. The demonstrated ability to cause DNA damage validates the use of **DOTAGA-AO** as a DNA-binding unit in a dual-targeting probe with potential to be used in Auger-electron therapy.

4.3.2. Nuclear Targeting Peptide: Nuclear Localization Sequence

Fusion proteins containing a nuclear localization sequence (**NLS**) have been widely used to exploit intracellular transport mechanisms and promote the translocation of macromolecules into the cell nucleus. **NLS**-containing macromolecules specifically interact with importin (karyopherin) α - β -transport factors that function as carrier molecules and facilitate the passage of cargo proteins through the nuclear pore complex. The best characterized **NLS** is a short amino acid sequence, Pro-Lys-Lys-Lys-Arg-Lys-Val, required for nuclear accumulation of the SV40 large T-antigen [319, 320]. This 7-mer **NLS**-motif was first conjugated to a variety of macromolecules that are excluded from the nucleus, such as bovine serum albumin, ferritin, IgG and IgM proteins and as a result of the **NLS** conjugation these proteins gained the ability of nuclear translocation [145, 319]. This strategy has also been explored for promoting the nuclear internalization of probes radiolabelled with Auger electron emitters such as ¹¹¹In. In this respect, the **NLS** sequence has been conjugated to antibodies and peptides targeting relevant cancer-related targets with the aim of achieving close proximity to the DNA of the final radioconjugates. Ginj et al. verified a 6-fold increase in cellular retention and a 45-fold higher accumulation of In-111 in the cell nuclei after conjugation of a DOTA-somatostatin derivative to a **NLS**-motif in comparison with the unconjugated probe [138]. Constantini et al. further demonstrated that the inclusion of a **NLS** sequence into a ¹¹¹In-labelled probe can effectively potentiate the Auger-induced cytotoxicity [145].

Synthesis and Characterization of the NLS motif

Therefore, for the construction of ¹¹¹In-labelled dual targeting probes capable of reaching the cell nucleus and inducing DNA damage, a **NLS** motif was synthesized. A flexible GlyGly linker was included in the N-terminal of the core **NLS** sequence to act as a spacer and to facilitate the conjugation to the prochelator by reducing the steric hindrance. Although the prochelators are fully compatible with the standard chemistry used in SPPS, it was decided to perform the coupling reaction in solution. Carrying out the reaction in solution offers the advantages of allowing the analysis of the reaction progress by HPLC and the use of stoichiometric amounts of peptide and functionalized chelator while in SPPS the molecule to be coupled is usually employed in large excess (from 3 to 10 equiv). However, the functional groups present in the side chains of the amino acid residues of the peptide sequence could potentially react with the activated free carboxylic acid of the prochelators thus giving different undesired

byproducts. Consequently, in order to achieve a selective coupling reaction in solution, the peptide had to be used in the fully protected form with just one single amine group available to react.

For the obtention through SPPS of fully protected peptides with a C-terminal amide, the Sieber amide resin, which contains a hyper acid-labile xanthenyl linker, has been used as solid support. This resin allows the cleavage of peptides in very mild acidic conditions (1-3% TFA) while retaining the standard side chain protecting groups which subsequently may be removed in solution at higher acid concentrations [321]. The **GGNLS** sequence (H-Gly-Gly-Pro-Lys-Lys-Lys-Arg-Lys-Val-NH₂) was therefore assembled on a Sieber amide resin in a microwave-assisted peptide synthesizer. Double couplings were applied to Val, Arg (at 50 °C) and Pro as well as to the residues immediately attached to these amino acids. The final Fmoc-group was removed to render a free amino group able to be coupled to the prochelator via amide bond formation. After the synthesis was completed, the resin was treated with 3% TFA in CH₂Cl₂ for 10 minutes. This procedure was repeated until no peptide was detected in the HPLC chromatograms of the obtained fractions. The peptide-containing fractions were then combined and since the HPLC chromatogram showed the presence of several chemical entities (most probably corresponding to partially deprotected peptide forms), the peak with highest retention time (presumably the fully protected peptide) was purified by semi-preparative HPLC. These results suggest that milder cleavage conditions (in terms of time and % of TFA) should have been used to preserve all the side chain protecting groups. The ESI-MS analysis (Figure 4.19) of the purified peak revealed the presence of the desired **GGNLSprot**, which is intended to act as precursor of a nuclear targeting vector (the deprotected **GGNLS**) in dual-targeting probes.

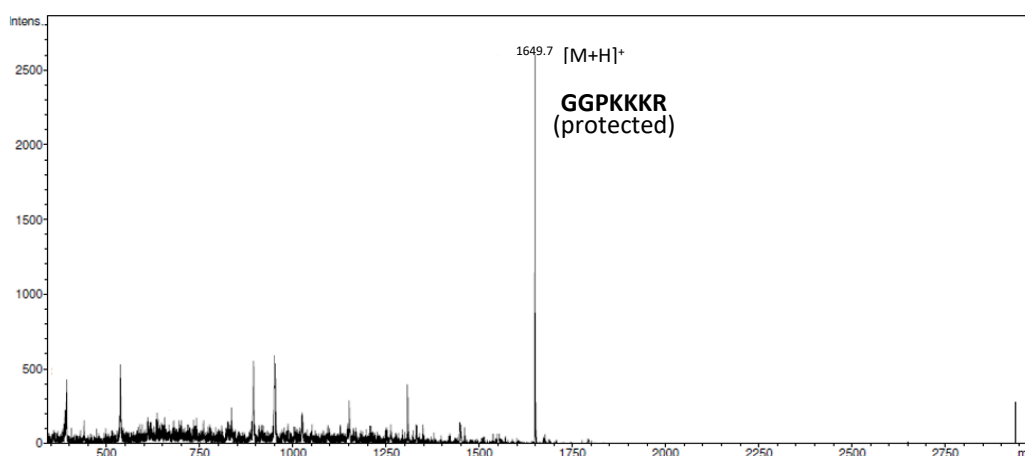


Figure 4.19. ESI-MS spectrum and amino acid sequence of GGNLSprot (m/z calcd for C₇₇H₁₃₄N₁₇O₂₀S [M+H]⁺: 1648.97, found: 1649.7 [M+H]⁺).

4.4. Molecular Units for ER Binding

The synthesis of targeted radioprobes for ER imaging has relied predominantly in estradiol analogues, as previously stated. However, small peptides containing the LXXLL sequence have also shown potent binding affinities towards ER and therefore are putative targeting vectors for the construction of ER-targeting probes. In this thesis, both types of targeting moieties were explored for the synthesis of the ER-targeting dual-vectorized probes. The chemical approaches employed for the synthesis of each ER-binding unit are discussed in the following sections.

4.4.1. Synthesis and Characterization of the LXXLL-based Peptide

To construct a heterobivalent probe capable of targeting ER(+) breast cancer cells, the LXXLL peptide **ER3** was selected as biological vector to be coupled to an appropriate prochelator. This peptide sequence has previously shown to bind the ER with high affinity and have demonstrated moderate *in vivo* stability.

Aiming to perform the coupling reaction with the prochelator in solution, the **ER3** peptide had to be used in the fully protected form with just one reactive amine group. Therefore, the **ER3** peptide was assembled on a Sieber amide resin in a microwave-assisted peptide synthesizer using the same method previously applied on the Rink amide resin. However, in this synthetic approach, the N-terminal Lys (Lys¹) was protected in the ϵ -amine with the methyltrityl group (Mtt) instead of the standard *tert*-butyloxycarbonyl (Boc) group used to protect the second Lys (Lys²). Mtt is a hyper acid-sensitive group that can be removed quantitatively upon treatment with 1-3% of TFA in CH₂Cl₂ in 15-30 min while the other protecting groups of the *tert*-butyl type remain intact under these conditions [322]. Furthermore, the N-terminal Lys was acetylated using acetic anhydride after removal of the Fmoc group. In previous experiments, the coupling in solution of small molecules to the N-terminal amine of the fully protected peptide failed to give the desired conjugates most probably due to steric hindrance. Therefore, in this approach, the amine in the N-terminus (α -amine) was protected with an acetyl group while the ϵ -amine in the end of the four-carbon chain was selected to form an amide bond with the prochelator. Besides being less sterically hindered, the ϵ -amine of Lys has a higher pK_a compared to the α -amine which makes it a stronger nucleophile.

After the automated synthesis was completed, the resin was treated with a solution of 3% TFA in CH_2Cl_2 for 10 min and the obtained fraction was analyzed by HPLC. This procedure was repeated until no peptide was detected in the HPLC chromatograms which was an indication of the complete cleavage from the resin. The HPLC analysis of the combined fractions revealed the presence of a chemical entity with a degree of purity around 85%, which was considered appropriate for the use in the next synthetic step with no need for purification. Analysis by ESI-MS (Figure 4.20) confirmed the presence of the fully protected peptide bearing one single free amine, **ER3prot**.

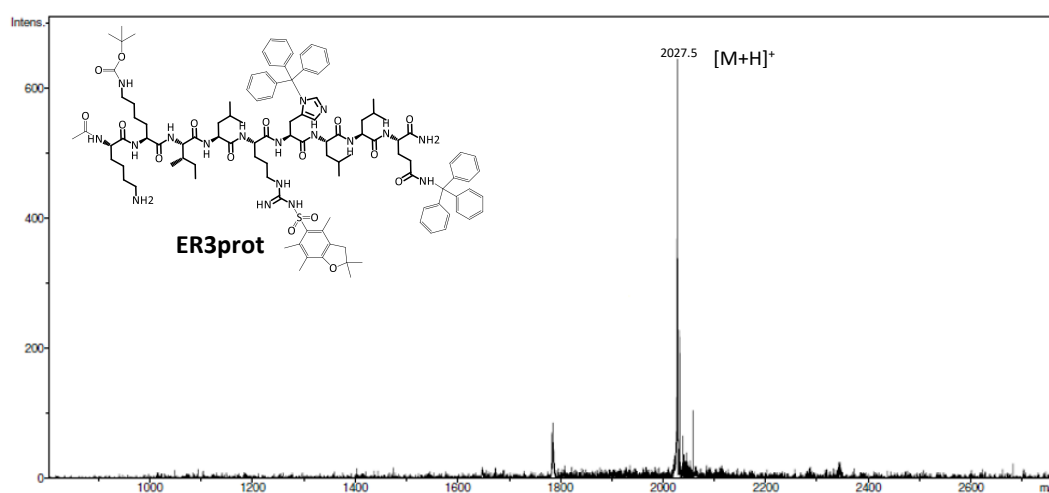


Figure 4.20. ESI-MS spectrum and chemical structure of ER3prot (m/z calcd for $\text{C}_{111}\text{H}_{153}\text{N}_{18}\text{O}_{16}\text{S}$ $[\text{M}+\text{H}]^+$: 2027.15, found: 2027.5 $[\text{M}+\text{H}]^+$).

4.4.2. Synthesis and Characterization of Estradiol Derivatives

Estradiol (17 β -estradiol, **E2**, Figure 4.21) is the most active endogenous estrogen and its derivatives are of great clinical importance. **E2** strongly binds to the ER, demonstrating a binding affinity for the receptor in the 0.1-0.4 nM range. The aromatic ring (A ring), the phenolic OH group (in position 3) and the 17 β -hydroxyl group are known to contribute greatly for receptor binding.

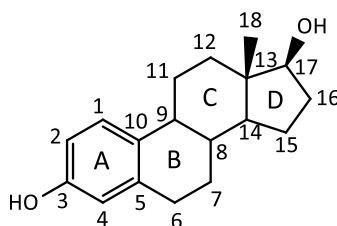


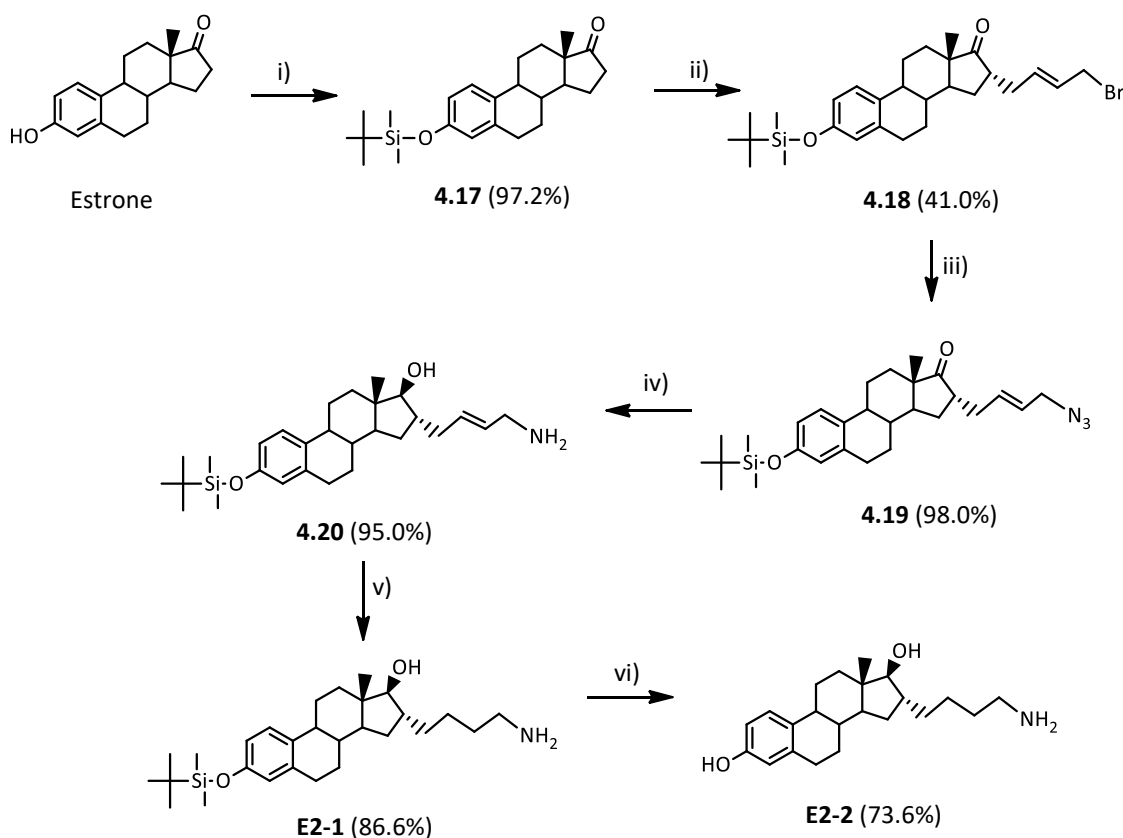
Figure 4.21. Chemical structure of 17β-estradiol (E2).

Synthesis of functionalized derivatives have focused on positions 7 α , 11 β , 16 α and 17 α . However, these positions have usually demonstrated limited tolerance to polar and large substituents which have compromised the ability to find new derivatives with good ER binding affinity [323]. For the development of ER-targeting ¹¹¹In-based radiotheranostic probes this is particularly challenging due to the need of attachment of a bulky chelator to the steroid ring [88]. Despite the challenges, Saha et al. were able to synthesize doxorubicin conjugates at the 16 α position of the steroid ring using linkers of variable length with the final compounds showing affinity towards ER α [324]. These results along with others of previous works suggest that the 16 α position can in fact have some tolerance to larger substituents [325]. Therefore, for the introduction of the steroid ring as an ER-targeting vector in a dual-targeting probe, **E2** derivatives functionalized at the 16 α -position were synthesized.

The synthetic pathway employed towards the intended **E2** derivatives was based on the stereoselective procedure described by Fevig and Katzenellenbogen starting from the commercially available estrone (Scheme 4.15) [326]. In the first step, aiming to avoid undesired side reactions at this critical position, the phenolic -OH was protected as a *tert*-butyldimethylsilyl ether (**4.17**). Subsequently, in order to induce deprotonation at the 16 position, the strong base lithium diisopropylamide (LDA) was formed *in situ* by adding *n*-butyllithium to a cooled solution of diisopropylamine in THF. After forming the lithium enolate of the protected estrone, the activated electrophile 1,4-dibromo-2-butene was added to alkylate the 16 α position of the D steroid ring. The angular methyl group (C18) is known to provide facial selectivity in the alkylation reaction but control of the reaction temperature (between -35°C and -45°C) was also important to ensure stereoselectivity and to avoid bisalkylation. After purification, the bromo ketone **4.18** was obtained with a yield of 41.0%.

The bromide function was then converted into an azide (**4.19**) by using sodium azide (NaN₃) in a reaction that proceeded with high yield. The simultaneous reduction of the azide function and of the 17-ketone was performed using lithium aluminium hydride (LiAlH₄). The

reaction was first carried out at -78°C to ensure the formation of the 17β -alcohol while minimizing the formation of the 17α congener. Once the reduction was completed, the amine **4.20** was obtained. The appearance of the 17-proton signal in the $^1\text{H-NMR}$ spectrum corroborated the reduction of the ketone function. Goto et. al. described that the coupling constant of the 17C-proton (J_{16-17}) is typically between 6 and 8 when the stereochemistry of the protons is $16\beta\text{H}$ and $17\alpha\text{H}$ [327]. Therefore, the stereoselectivity was supported by the presence of the 17α -proton signal as a doublet at 3.75 ppm with $J=6.6$ Hz, confirming that the 4-carbon linker was at the 16α position of the steroid and that the alcohol had formed at the 17β position as it appears in the endogenous **E2**. The presence of a distinct C13-methyl protons signal corroborated the formation of a single product.



Scheme 4.15. Synthesis of the E2 derivatives functionalized at the 16α position with a four-carbon chain.

i) TBDMS-Cl, imidazole, DMF, RT, 2 h; **ii)** LDA, *trans*-1,4-dibromo-2-butene, THF, $0^{\circ}\text{C} \rightarrow -45^{\circ}\text{C}$, 4.5 h; **iii)** NaN_3 , DMSO:THF:H₂O, RT, 18 h; **iv)** LiAlH_4 , THF, $-78^{\circ}\text{C} \rightarrow -10^{\circ}\text{C}$, 4 h; **v)** Pd/C, H₂, RT, 12 h, **vi)** 2% HCl, CH₃OH, RT, 6 h

The double bond in the linker was then removed by catalytic hydrogenation yielding the amine **E2-1** which was characterized by NMR (Figure 4.22) and ESI-MS. This amine can be conjugated to a prochelator bearing a free carboxylic acid through the formation of an amide bond. Furthermore, since the phenolic hydroxyl group is not expected to react in the standard conjugation conditions, the *tert*-butyldimethylsilyl protecting group was removed under mild acidic conditions yielding the derivative **E2-2**.

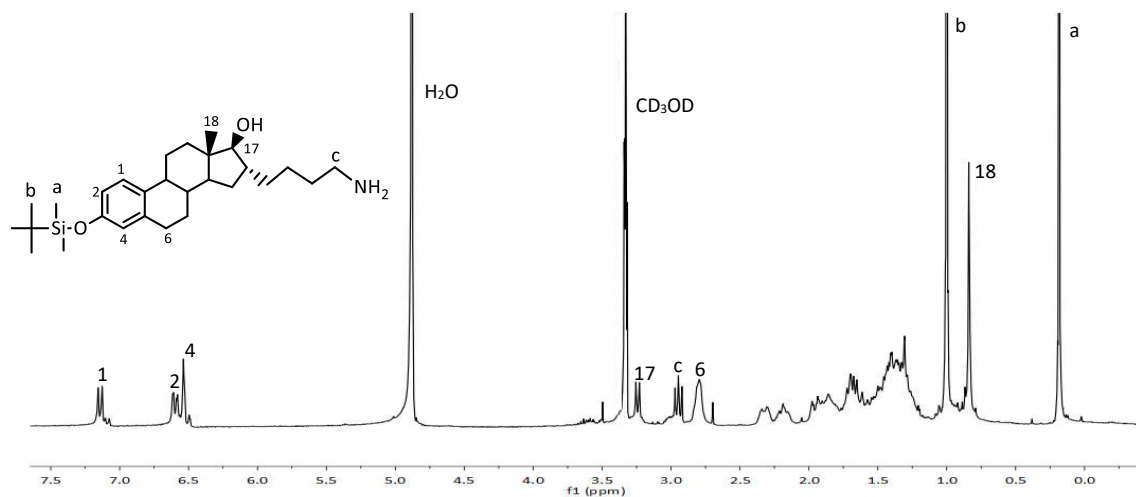


Figure 4.22. Representative ¹H-NMR spectrum (CDCl₃) of **E2-1**.

4.5. Dual-targeting Probes

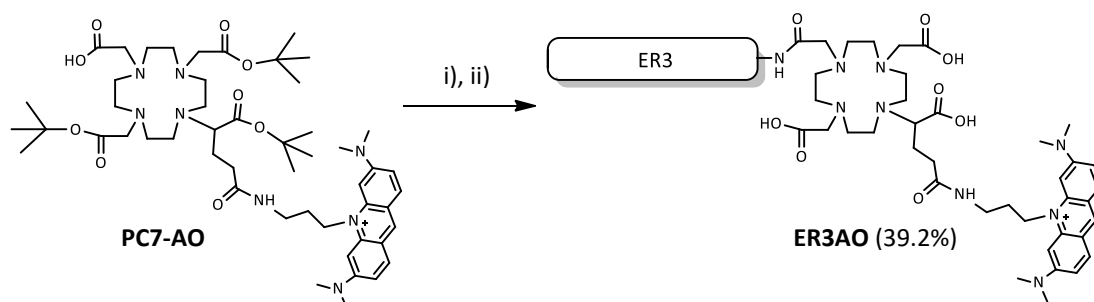
In order to target ER-positive BC cells, an LXXLL motif or a E2 derivative was included in the synthesized dual-targeting probes in addition to the nuclear targeting moiety. As previously explained, the conjugation of the two different targeting molecules in the same chemical agent is expected to potentiate the theranostic value of the corresponding ^{111}In -radioconjugates.

The prepared dual-targeting probes are described in the following sections. The description of the synthetic pathways towards the bivalent probes and the discussion regarding the biological evaluation of the ^{111}In -labelled conjugates were divided according to the type of ER-targeting molecule integrated in the probe.

4.5.1. Synthesis and Biological Evaluation of a LXXLL-based Dual-targeting Radioconjugate

Synthesis and Characterization of ER3AO

A dual-targeting probe comprising an LXXLL peptide (**ER3**) with known affinity towards $\text{ER}\alpha$ and a DNA intercalating unit (**AO**) was synthesized starting from the “DOTA-like” prochelator bearing an acridinium pendant arm **PC7-AO** (Section 4.3.1.2). Therefore, to the free carboxylic acid of this prochelator, the partially protected **ER3** peptide, **ER3prot**, was conjugated in solution through the ϵ -amine of Lys^1 using HATU as coupling agent and DIPEA as base (Scheme 4.16). The progress of the reaction was monitored by HPLC for 18 hours. The fully protected intermediate that resulted from the conjugation was not isolated and therefore the crude product (after removing the volatiles) was treated directly with a high percentage of TFA (95%) to promote the complete deprotection of the side chain protecting groups along with the *tert*-butyl esters attached to the macrocycle. After purification, the ESI-MS analysis confirmed the presence of the bivalent **ER3AO** (m/z calculated for $[\text{C}_{94}\text{H}_{155}\text{N}_{26}\text{O}_{19}]^+$ = 1952.20) with the MS spectrum showing the peaks corresponding to the singly ($m/z = 977.1 [\text{M}+\text{H}]^{2+}$), doubly ($m/z = 651.9 [\text{M}+2\text{H}]^{3+}$) and triply ($m/z = 489.3 [\text{M}+3\text{H}]^{4+}$) protonated conjugate. **ER3AO** was obtained with a final yield of 39% and the HPLC analysis revealed a 97% degree of purity.

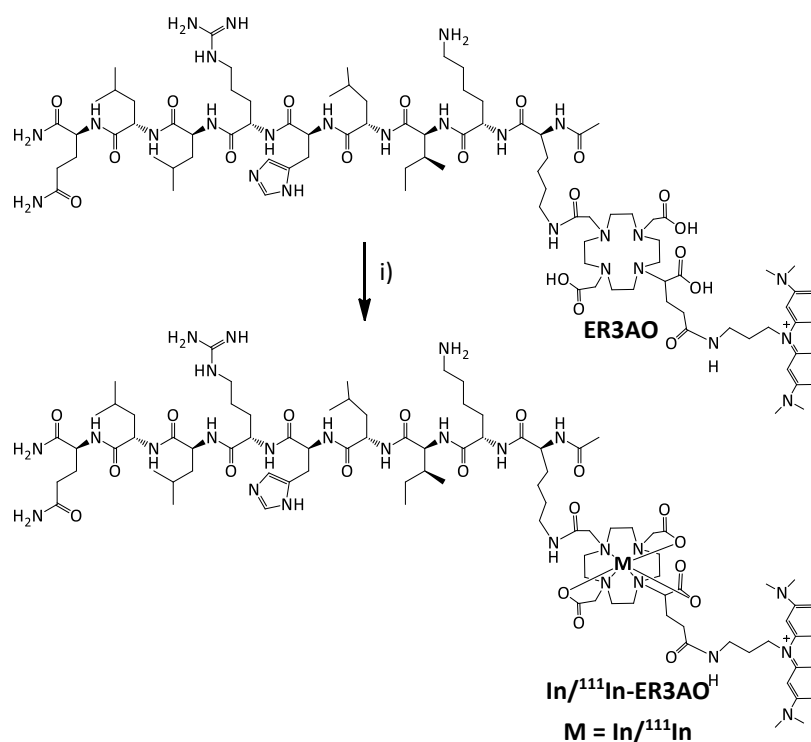


Scheme 4.16. Synthesis of ER3AO.

i) ER3prot, HATU, DIPEA, DMF, RT, 18 h; ii) TFA:TIS:water, RT, 24 h.

Synthesis and Characterization of [In]ER3AO

The coordination ability of the novel dual-targeting probe was then proved by the preparation of the In(III) complex by the reaction between **ER3AO** with InCl₃ at high temperature (95°C) as depicted in Scheme 4.17. After purification of the product by HPLC, MS analysis supported the formation of [In]ER3AO with the isotopic pattern observed in the ESI-MS spectrum of the purified product being consistent with Indium complexation as shown in Figure 4.23.



Scheme 4.17. Preparation of [In/¹¹¹In]ER3AO.

i) InCl₃/¹¹¹InCl₃, 0.1 M NaOAc pH=5.5, 95°C, 25 min

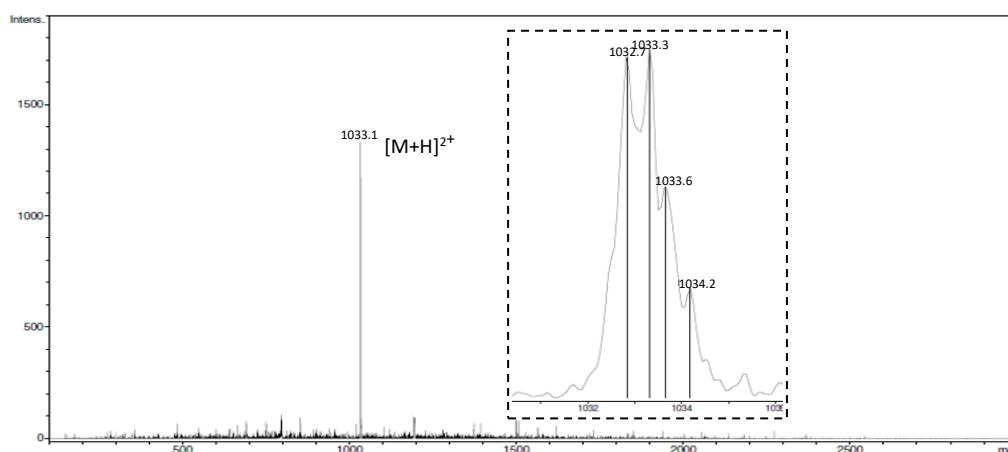


Figure 4.23. Representative ESI-MS spectrum of [In]ER3AO with a zoom showing the isotopic pattern. ESI(+)-MS m/z calcd for $[C_{94}H_{152}N_{26}O_{19}In]^+$: 2064.09, found 1033.1 [M+H]²⁺.

Radiolabelling and In Vitro Evaluation

The doubly vectorized chelator **ER3AO** was successfully radiolabelled with ¹¹¹In with high radiochemical yield and purity (> 96%) using the standard radiolabelling conditions (Scheme 4.13) and the chemical identity of [¹¹¹In]ER3AO was ascertained by comparing the HPLC gamma chromatogram with the HPLC UV chromatogram of [In]ER3AO.

The lipophilicity of [¹¹¹In]ER3AO was evaluated by the shake-flask method and the log $P_{o/w}$ (octanol/saline) value determined was -1.79 ± 0.03 . This partition coefficient revealed the hydrophilic character of the radioconjugate, although in comparison with [¹¹¹In]DOTA-ER3 (log $P_{o/w} = -3.09 \pm 0.06$), which bears the same peptide sequence, there was a decrease in the hydrophilicity most probably due to the contribution of the **AO** moiety.

In vitro stability studies revealed a high stability (> 95%) of [¹¹¹In]ER3AO at 37°C in saline and in the presence of an excess of apo-transferrin up to 48 hours. On the other hand, studies in human blood serum demonstrated the presence of the intact radioconjugate with a purity of approximately 70% after 6 hours of incubation. Since the challenging test did not show transchelation towards apotransferrin, the main factor governing the stability of [¹¹¹In]ER3AO should be the susceptibility of the peptide sequence towards proteolytic degradation by serum peptidases. This was confirmed by the fact that [¹¹¹In]ER3AO showed a similar behaviour in blood comparing to the monovalent probe [¹¹¹In]DOTA-ER3 (Section 2.1.4).

Cell Studies

Cellular uptake of [^{111}In]ER3AO was studied in human BC cell lines: MCF-7 (ER+) and MDA-MB-231 (ER-). As shown in Figure 4.24, the dual-targeting radioconjugate demonstrated a fast and high uptake in both cell lines reaching a maximum value of 20.7% in MCF-7 cells at 1 hour of incubation after which a steady decrease was verified up to 3 hours. This release, already verified with the monovalent peptide-based probe, could be related with lysosomal degradation of the peptide skeleton yielding radiolabelled fragments that readily exit the cells [328]. Although throughout the 3 hours of the assay the uptake values of [^{111}In]ER3AO in MCF-7 cells were higher than in MDA-MB-231 cells, the radioconjugate did not considerably show specific accumulation in the ER-positive cells. In fact, the presence of the AO unit might drive the uptake of the radiolabelled probe to the cells regardless of their receptor status which can hamper the achievement of specificity with this dual-targeting approach.

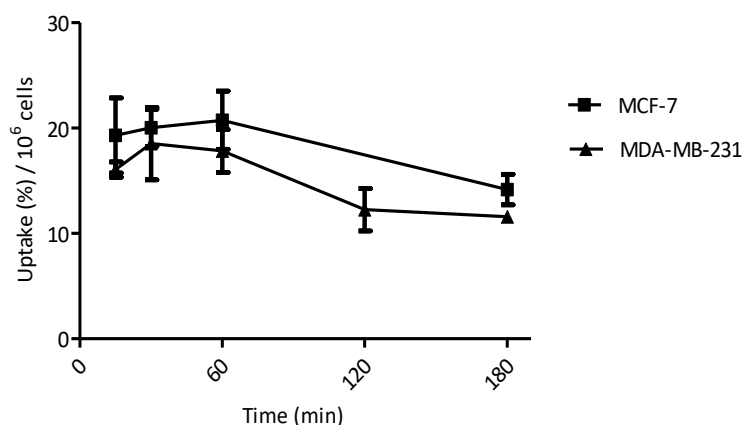


Figure 4.24. Cellular uptake of [^{111}In]ER3AO in MCF-7 and MBA-MB-231 cells expressed as a percentage (average (%) \pm SD, n=3) of the total applied activity normalized per 10^6 cells.

Nevertheless, the ability of [^{111}In]ER3AO to reach the nuclear compartment of MCF-7 cells was also studied due to the relevance of this property for Auger electron therapy. As depicted in Figure 4.25, most of the activity was found in the nuclear compartment of the BC cells at the three time points under study. Remarkably, after 3 hours of incubation approximately 80% of the cell-associated activity was found in the nuclear compartment of MCF-7 cells, demonstrating the efficacy of the double vectorized probe to deliver the Auger emitter In-111 to the nucleus of BC cells.

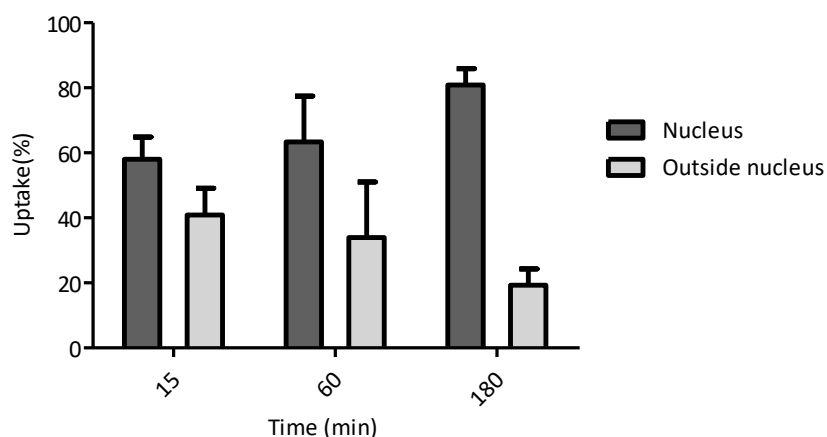


Figure 4.25. Nuclear internalization of [^{111}In]ER3AO in MCF-7 cells expressed as a percentage (average (%) \pm SD, n=3) of cell-associated activity.

DNA Damage

The high nuclear internalization of [^{111}In]ER3AO encouraged the study of the ability of the radioconjugate to cause DNA damage *in vitro*. Although the monofunctionalized [^{111}In]DOTAGA-AO has already proved to be able to induce DSB in plasmid DNA (Section 4.3.1.2.1.), it was relevant to verify if the double-vectorization has affected the ability of the probe to bring In-111 close to the DNA and cause direct damage. For that purpose, different activities of [^{111}In]ER3AO were incubated with double-stranded plasmid DNA for the time corresponding to approximately two times the In-111 radioactive half-life (140 hours) in the absence (DMSO (-)) and in the presence (DMSO (+)) of the radical scavenger DMSO. After gel electrophoresis, the percentage of each DNA isoform (SC, L or OC) was quantified. A representative image of the agarose gel showing the bands corresponding to the different DNA isoforms after the incubation with [^{111}In]ER3AO is shown in Figure 4.26.

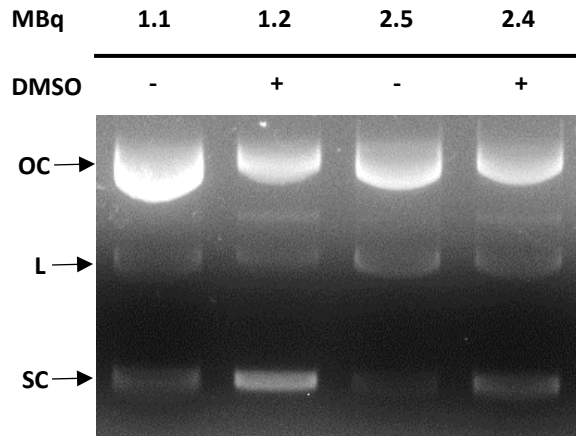


Figure 4.26. Representative gel of plasmid DNA incubated with [¹¹¹In]ER3AO (activities used are shown on the top), in the absence (-) and in the presence (+) of DMSO. DNA isoforms are indicated as OC - open circular, L - linear and SC - supercoiled.

Results from the quantification of the DNA isoforms are displayed in Figure 4.27. In the absence of DMSO there was an increase both in the L and OC isoforms and a decrease of the SC DNA with increasing activities. After incubation with the highest activity, the L isoform accounted for 14% of the total DNA. On the other hand, in the presence of the scavenger, incubation with [¹¹¹In]ER3AO also led to an increase of the OC (from 34% to 61%) and of the L (up to 7%) DNA isoforms. These results suggest that as verified for [¹¹¹In]DOTAGA-AO, [¹¹¹In]ER3AO is able to cause DNA damage by a combination of indirect and direct mechanisms. Combined with the high nuclear internalization, this property reinforces the potential of this probe for Auger electron therapy.

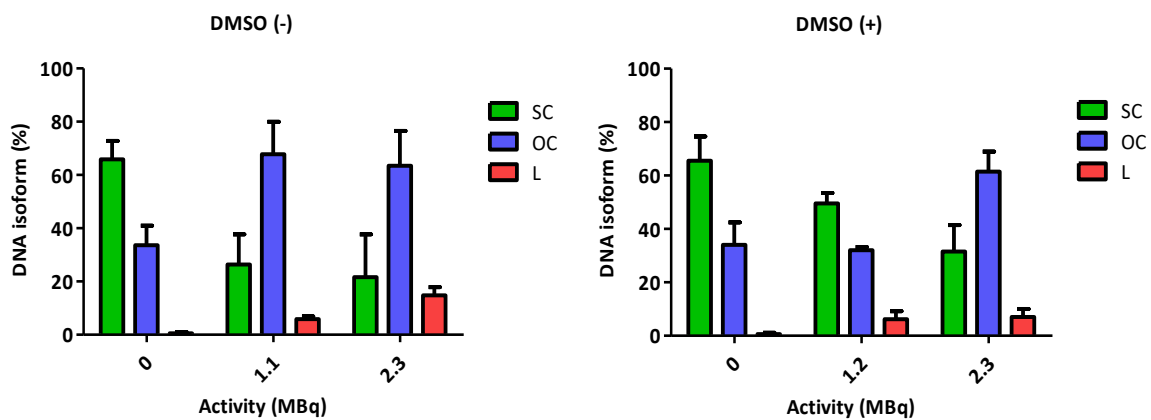


Figure 4.27. Quantitative analysis of the proportion (average (%) \pm SD, n=3) of each DNA isoform (OC - open circular, L - linear and SC - supercoiled) after incubation of the plasmid DNA with 2 different activities of [¹¹¹In]ER3AO, in the absence (-) and in the presence (+) of DMSO.

In Vivo Studies in Tumor-bearing BALB/c Mice

The *in vivo* behaviour of [^{111}In]ER3AO was preliminarily studied in Balb/c nude mice bearing MCF-7 xenografts and the biodistribution data is displayed in Figure 4.28-a. One hour after injection most of the activity (32% I.A./g) was found in the kidneys suggesting that the [^{111}In]ER3AO excretion was performed mainly by the urinary tract. However, there was a significant activity uptake in the intestines and in the liver demonstrating that the hepatobiliary system also played an important role in the elimination of the radioconjugate. In fact, this represented a major difference between the bivalent [^{111}In]ER3AO and the monovalent [^{111}In]DOTA-ER3 since the latter was almost exclusively eliminated by the kidneys (Section 2.16). Furthermore, the elimination of [^{111}In]ER3AO was significantly slower with an excretion of about 39% at 1 hour *p.i.* in comparison with 78% for [^{111}In]DOTA-ER3 at the same time point. The higher lipophilicity and the presence of the AO moiety might explain this shift towards the hepatobiliary system and the slower clearance. Nevertheless, there was some accumulation in the tumor and in the ER-rich organs (ovaries and uterus) as demonstrated by the target/non-target ratios displayed in Figure 4.28-b.

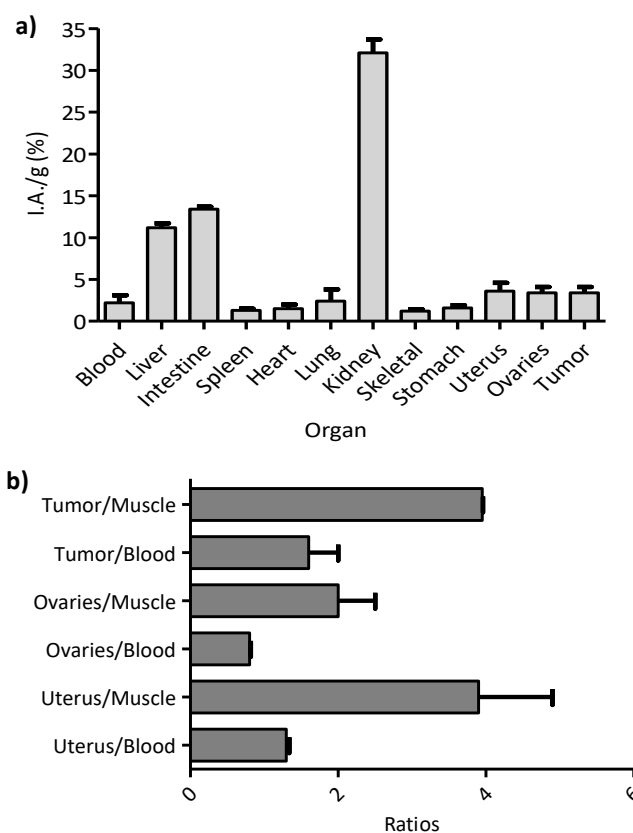


Figure 4.28. Biodistribution studies of [^{111}In]ER3AO in female BALB/c nu/nu mice bearing MCF-7 xenografts at 60 min *p.i.* (n=3). a) Biodistribution profile (I.A./g (%) ± SD). b) Target/Non-target ratios (± SD).

Analysis by HPLC of the mice blood revealed the preponderant presence of the intact [¹¹¹In]ER3AO confirming the high stability *in vivo* of the radiolabelled dual probe at 1 h *p.i.* (Figure 4.29).

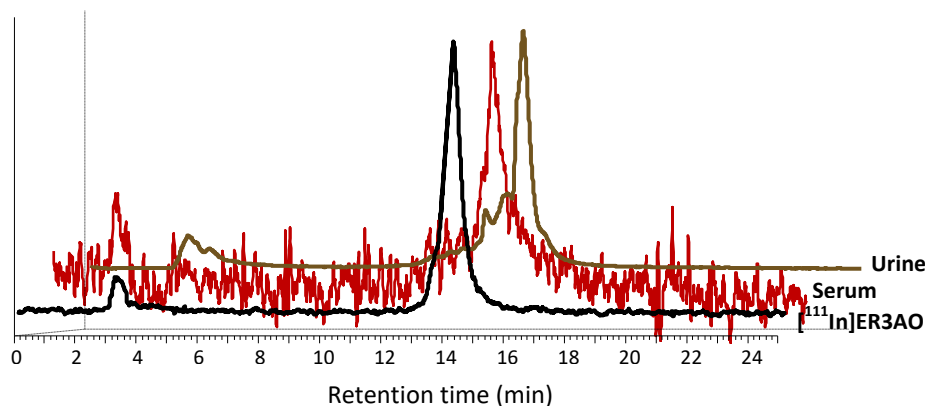


Figure 4.29. HPLC radiochromatograms (Method C) of mice serum and mice urine of [¹¹¹In]ER3AO in Balb/C nu/nu mice bearing MCF-7 xenografts 1 h *p.i.*.

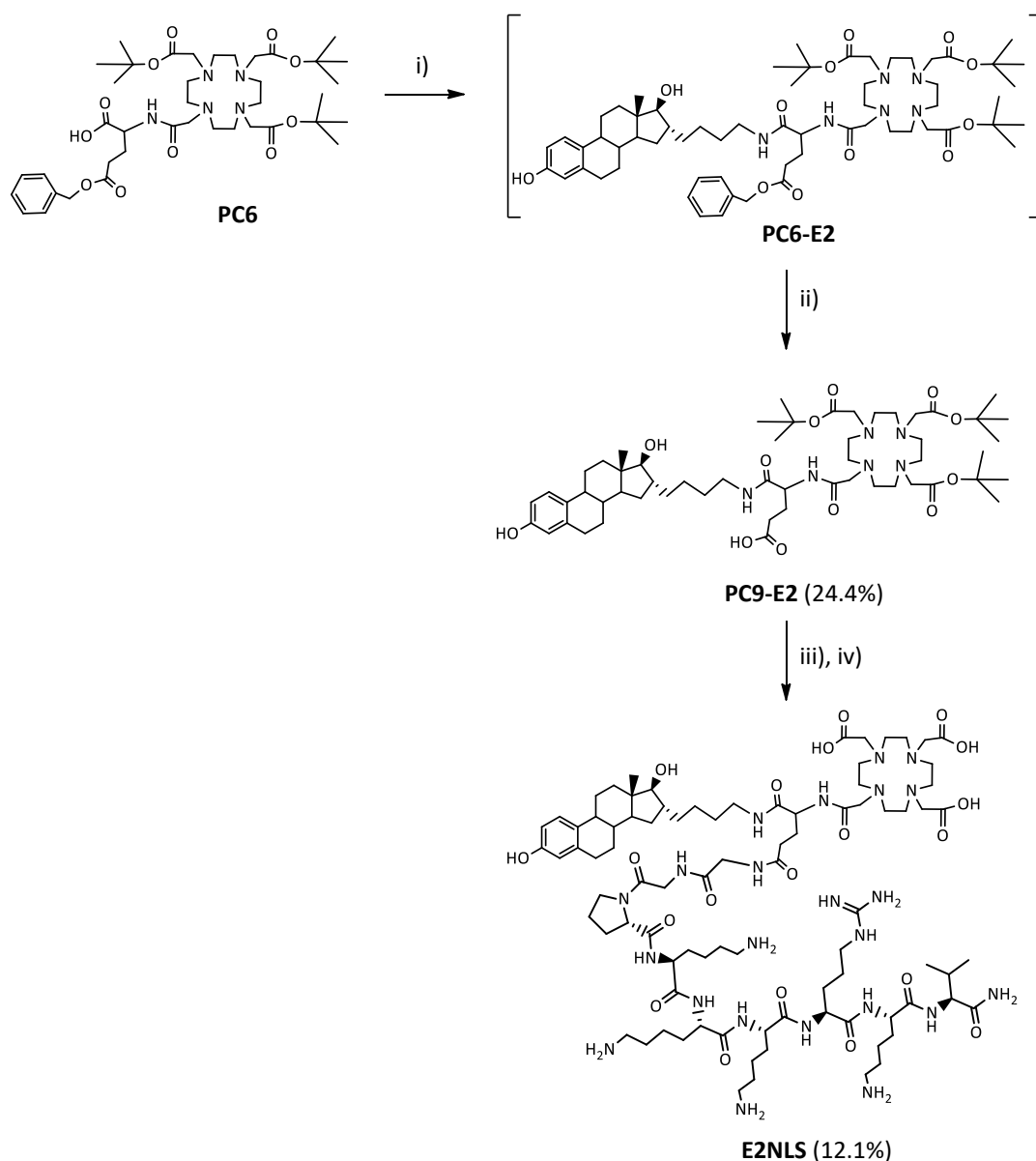
4.5.2. Synthesis and Biological Evaluation of Estradiol-based Dual-targeting Radioconjugates

Synthesis and Characterization of E2NLS and E2AO

Bivalent probes towards the nucleus of ER(+) BC cells comprising a steroid targeting moiety were also prepared. The amine **E2-2** with a 4-carbon linker in the 16 α position of estradiol (Section 4.4.2) was used as a building block to construct dual-targeting probes containing different molecular units for nuclear targeting.

In the first approach (Scheme 4.18), **E2-2** was coupled to the free carboxylic acid of **PC6** (Section 4.2.2). The reaction was followed by HPLC and proceeded for 48 hours. The crude product was analysed by ESI-MS and the product **PC6-E2** was identified in the reaction mixture. After removing the volatiles and washing with water, the crude product was used for the next step without further purification in order to minimize losses. The deprotection of the benzyl ester was then performed by catalytic hydrogenation with Pd/C and the product **PC9-E2** was purified through a C-18 Sep-Pak column. The disappearance of the ¹H-NMR signals associated

with the benzyl ester along with the ESI-MS analysis confirmed the deprotection. Moreover, the triplet corresponding to the two protons of the methylene group attached to the amine in the **E2-2** precursor was absent in the $^1\text{H-NMR}$ spectrum confirming the conjugation to the prochelator. The presence of a single C18-methyl protons signal corroborated the formation of a single product.

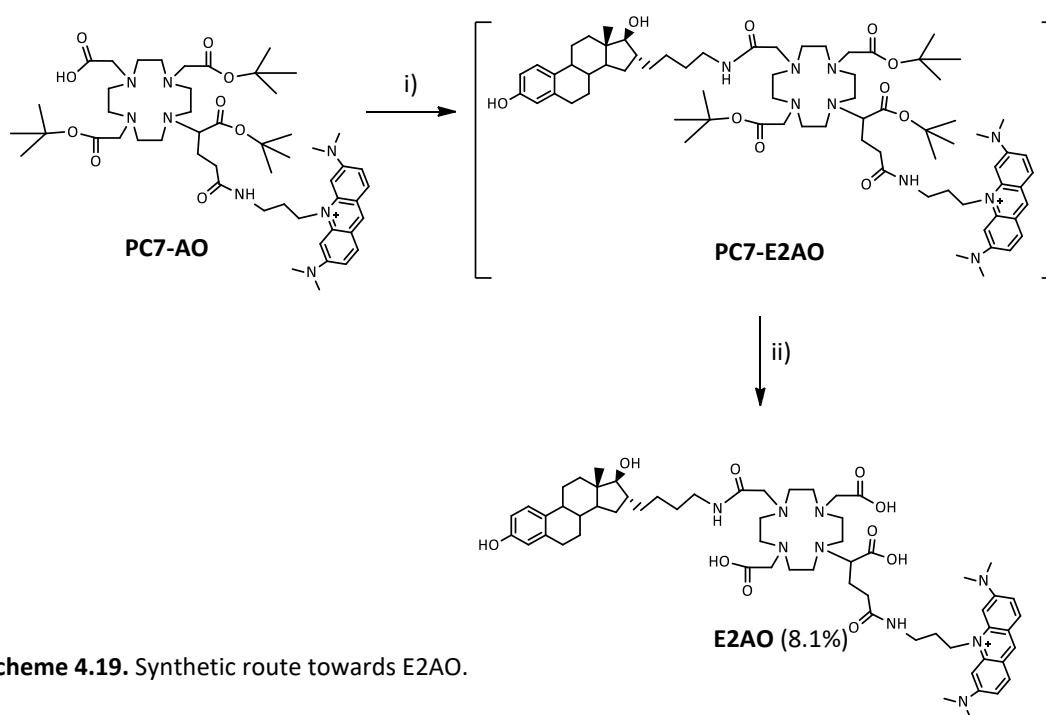


Scheme 4.18. Synthetic route towards E2NLS.

i) E2-2, HATU, DIPEA, DMF, RT, 48 h; **ii)** H₂, Pd/C, CH₃OH, RT, 6 h; **iii)** GGNSprot, HATU, DIPEA, DMF, RT, 24 h; **iv)** TFA, TIS, H₂O, 12 h, RT.

The free carboxylic acid of **PC9-E2** was then conjugated in solution with the fully protected peptide **GGNLSprot**. The conjugation proceeded for 24 hours and after removing the volatiles and washing the residue with water, the crude was treated with the standard cleavage cocktail (TFA 95%, TIS 2.5%, H₂O 2.5%) for 12 hours to allow complete deprotection of the *tert*-butyl esters along with the peptide's side chain protecting groups. After purification, the bivalent probe **E2NLS** was obtained with a high degree of purity (> 96%) and its chemical identity was fully elucidated by ESI-MS with the spectrum showing the doubly protonated molecule as the most intense peak. However, the final yield of **E2NLS** was very low (approximately 12%) most probably due to the steric hindrance caused by the presence of the steroid ring in the vicinity of the free carboxylic acid.

In a second approach depicted in Scheme 4.19, **AO** was used as nuclear targeting moiety for the construction of a E2-based bivalent probe. Therefore, the estradiol derivative **E2-2** was conjugated to the acridinium-containing prochelator **PC7-AO**. The reaction was monitored by HPLC and proceeded for 72 hours although with low yield of the product **PC7-E2AO** (about 12%, as determined through the HPLC chromatogram). In fact, the difficulty of the reaction of **E2-2** with the carboxylic acid of **PC7-AO** promoted the occurrence of guanylation at the primary amine of the estradiol derivative by the coupling agent HATU. Nevertheless, the crude product was deprotected in acidic conditions, and the dual conjugate **E2AO** was purified by HPLC and obtained with high chemical purity (>95%) as evaluated by HPLC.



Scheme 4.19. Synthetic route towards E2AO.

i) E2-2, HATU, DIPEA, DMF, RT, 72 h; ii) TFA, CH₂Cl₂, RT, 12 h.

Despite the complexity of the NMR spectrum, the characteristic signals associated with the **AO** and **E2** aromatic rings were clearly identified, along with a single C18-methyl protons signal. However, for the complete elucidation of the chemical identity of **E2AO**, the ESI-MS analysis was decisive with the spectrum showing as most intense peaks the singly and the doubly protonated **E2AO**.

The characterization of **E2NLS** and **E2AO** by HPLC and ESI-MS is summarized on Table 4.2.

Table 4.2. Characterization of E2NLS and E2AO by HPLC and ESI-MS.

Conjugate	HPLC	ESI-MS		Molecular Formula
	Rt (min)/Method	Calculated (m/z)	Found (m/z)	
E2NLS	18.16/G	919.57 [M+2H] ²⁺	919.7 [M+2H] ²⁺	C ₈₇ H ₁₄₄ N ₂₃ O ₂₀
E2AO	12.49/H	1106.66 [M] ⁺	1106.6 [M] ⁺	[C ₆₁ H ₈₈ N ₉ O ₁₀] ⁺

Preparation of the In/¹¹¹In-complexes

The corresponding inactive In(III) complexes were prepared with high yield using the standard conditions previously described. After HPLC purification, the two complexes were obtained with a degree of purity higher than 95% as verified by HPLC analysis. Characterization of **[In]E2AO** by NMR was hampered by the very low solubility of the complex in the common NMR solvents (CD₃OD, CD₃CN, and even in DMSO-d₆), which along with the low yield verified in the preparation of the ligand **E2AO**, determined the acquisition of NMR spectrum of poor quality. Therefore, the identity of complexes **[In]E2AO** and **[In]E2NLS** was fully elucidated by ESI-MS analysis as exemplified in Figure 4.30.

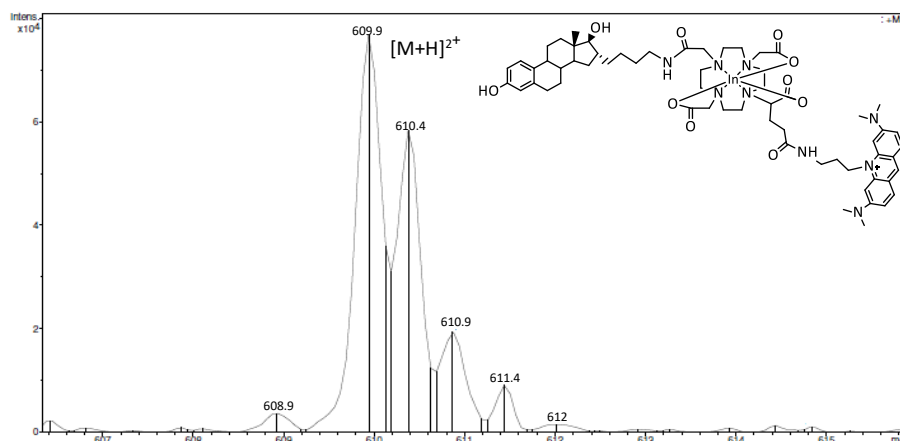


Figure 4.30. Zoom of the ESI-MS spectrum of [In]E2AO. ESI(+)-MS m/z calcd for $[C_{61}H_{85}InN_9O_{10}]^+$: 1218.5, found 609.9 $[M+H]^{2+}$.

The radiolabelled $[^{111}\text{In}]E2\text{NLS}$ and $[^{111}\text{In}]E2\text{AO}$ were then prepared using the same conditions. Both dual-targeting probes were radiolabelled at a concentration of 10^{-5} M and the radioconjugates were obtained with high radiochemical yield and purity (> 95%). Table 4.3 summarizes the characterization of both In- and ^{111}In -conjugates.

Table 4.3. Characterization of $[\text{In}/^{111}\text{In}]E2\text{NLS}$ and $[\text{In}/^{111}\text{In}]E2\text{AO}$.

Conjugate	HPLC	Lipophilicity $\log P_{o/w}$	ESI-MS		Molecular Formula
	Rt (min)/ Method		Calculated (m/z)	Found (m/z)	
[In]E2NLS	18.27/K	-	975.52 $[M+2H]^{2+}$	975.7 $[M+2H]^{2+}$	$C_{87}H_{146}InN_{23}O_{20}$
$[^{111}\text{In}]E2\text{NLS}$	19.07/K	-1.84 ± 0.03	-	-	-
[In]E2AO	11.23/L	-	609.78 $[M+H]^{2+}$	609.9 $[M+H]^{2+}$	$[C_{61}H_{85}InN_9O_{10}]^+$
$[^{111}\text{In}]E2\text{AO}$	11.96/L	0.018 ± 0.02	-	-	-

Estradiol itself has been known to present a very lipophilic character. In fact, Palmer et al. estimated the **E2** $\log P_{o/w}$ value to be 3.261 [329]. However, $[^{111}\text{In}]E2\text{NLS}$ demonstrated a highly hydrophilic character due to the contribution of the hydrophilic amino acids in the peptide sequence (Lys and Arg) and of the DOTA-based chelating sphere. On the other hand, $[^{111}\text{In}]E2\text{AO}$ was able to retain a slightly lipophilic character as suggested by the positive $\log P_{o/w}$ value.

Regarding the *in vitro* stability of the radioconjugates, both [^{111}In]E2NLS and [^{111}In]E2AO demonstrated high stability (> 95%) in saline and in the presence of an excess of apotransferrin (at 37°C) up to 48 hours, demonstrating the ability of the dual-targeting probes to form highly stable complexes with In(III).

Cell Studies

Cellular uptake of both E2-based dual-targeting probes was studied in the BC cell lines MCF-7 (ER+) and MDA-MB-231 (ER-) and the results are displayed in Figure 4.31.

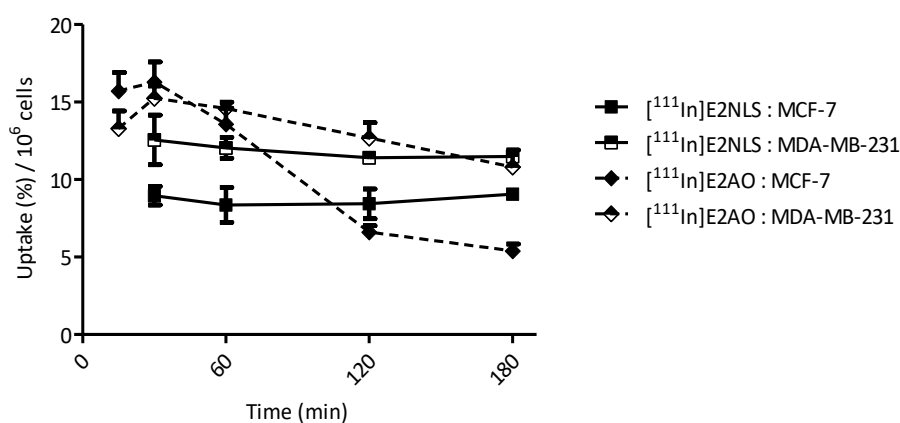


Figure 4.31. Cellular uptake of [^{111}In]E2NLS and [^{111}In]E2AO in MCF-7 and MDA-MB-231 cells expressed as a percentage (average (%) \pm SD, n=3) of the total applied activity normalized per 10^6 cells.

Both radioconjugates demonstrated a high and fast uptake in both cell lines. Interestingly, the radiolabelled AO-containing conjugate although showing a higher initial uptake (about 15% at 30 min in both cell lines) demonstrated some release from the cells over time, while [^{111}In]E2NLS presented steady uptake values of approximately 9% in MCF-7 and 11% in MDA-MB-231 cells along the 3 hours. It is noteworthy that in previous works E2-DOTA conjugates did not present significant uptake values in both cell lines most probably due to the size and hydrophilicity of the DOTA chelating moiety [330]. Therefore, the inclusion of NLS and AO was effective in enhancing the cellular uptake. However, both [^{111}In]E2NLS and [^{111}In]E2AO showed higher uptake in the ER-negative cells MDA-MB-231. These uptake profiles demonstrate that the doubly-vectorized probes were not retained in the cells in an ER-dependent manner

which strongly suggests that the probes did not keep the ER α -binding affinity of **E2**. For this lack of specificity, the inclusion of the non-selective **AO** and **NLS** moieties should have had an important contribution.

Nevertheless, the ability of both ¹¹¹In-labelled probes to reach the nucleus of the MCF-7 cells was studied in a nuclear internalization assay (Figure 4.32). The nuclear uptake values after 15, 60 and 180 minutes showed that [¹¹¹In]**E2NLS** and [¹¹¹In]**E2AO** were able to reach the cell nucleus at high percentages. After 3 hours of incubation approximately 56% and 76% of the activity was found in the nuclear compartment for, respectively, [¹¹¹In]**E2NLS** and [¹¹¹In]**E2AO**. The **AO**-containing conjugate demonstrated a higher uptake in the nuclear compartment corroborating the effectiveness of **AO** in potentiating nuclear targeting.

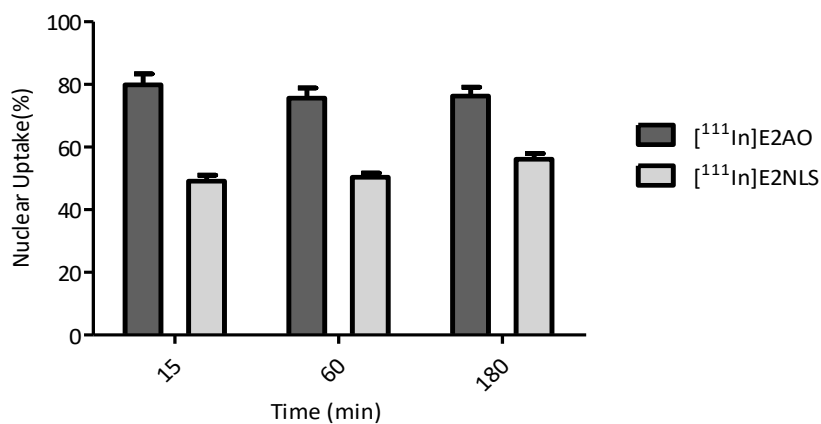


Figure 4.32. Nuclear internalization of [¹¹¹In]E2AO and [¹¹¹In]E2NLS in MCF-7 cells expressed as a percentage (average (%) \pm SD, n=3) of cell-associated activity.

4.6. Conclusions

Versatile synthetic strategies were described for the preparation of acyclic and macrocyclic prochelators for the dual-vectorization of radioconjugates. The chemical approaches reported in this Chapter were based on an orthogonal protection strategy starting from commercial available “building-blocks”, among which the partially protected amino acid L-glutamic acid 5-benzyl ester and the cyclen derivative DO2AtBu assumed particular importance. This orthogonal strategy allowed the synthesis of prochelators that could be selectively functionalized with two different (bio)molecules, small molecules or peptides, in a straightforward manner. Furthermore, after dual-vectorization and total deprotection, the prepared chelating moieties were capable of forming highly stable ^{111}In -complexes at high specific activities. Therefore, the chemical approaches discussed in this Chapter are of interest for the design of multi-targeting radioprobes for clinical applications.

The dual-targeting approach was employed in this work for the construction of ^{111}In -labelled conjugates with potential theranostic value by combining in the same probe a ER-binding molecule intended for the selective targeting of ER-positive BC cells, and a nuclear-targeting moiety for the delivery of the radioisotope in close proximity to DNA. To achieve the latter goal, the polyaromatic acridine orange (**AO**) was explored and the In-complex of the monofunctionalized DOTAGA derivative, **DOTAGA-AO**, showed ability to interact with DNA most probably by intercalation. Furthermore, the radiolabelled analogue, [^{111}In]**DOTAGA-AO**, showed ability to induce DNA damage *in vitro* by a combination of indirect and direct mechanisms, which corroborated the use of this unit in the design of radioconjugates for Auger electron therapy.

Aiming to target the ER, an LXXLL peptide (**ER3**) or a estradiol derivative was included in the dual-vectorized conjugates. Furthermore, in addition to **AO**, a peptide with a nuclear localizing sequence (**NLS**) was also explored as nuclear-targeting moiety. The dual-targeting conjugates were successfully synthesized despite the low yield of the estradiol-containing bivalent probes **E2NLS** and **E2AO**. Studies with the radiolabelled LXXLL-containing bivalent conjugate, [^{111}In]**ER3AO**, demonstrated that the double-vectorization did not affect the ability of the radioconjugate to induce DNA damage *in vitro* in comparison with the monovalent [^{111}In]**DOTAGA-AO**. The potential for Auger electron therapy was further corroborated by the high nuclear internalization in BC cells of the three dual-targeting radioconjugates, showing the effectiveness of the employed nuclear-targeting strategies. However, the three bivalent radioprobes did not show specific uptake in the ER-positive cells compared to the ER-negative BC cells, which suggests that the strategies for ER-targeting failed to confer the desired specificity to the final conjugates. One hypothesis for this result is that the **AO** and **NLS** moieties

might have driven the uptake of the dual-vectorized probes into the cells in a non-specific manner. Therefore, this lack of specificity compromises the utility of the reported bivalent probes for the selective targeting of ER-positive BC. Furthermore, these results highlight the difficulty in designing multivalent probes with specific multitargeting properties.

Chapter 5

DNA-binding Peptide for Radiotheranostics

5. DNA-binding Peptide for Radiotheranostics

As already discussed in previous Chapters, Auger therapy requires the emission of Auger electrons in the vicinity of DNA. Therefore, DNA-targeting moieties have been explored to deliver Auger-emitting radionuclides, such as In-111, to the cell nucleus. In this context, a DNA-binding peptide based on the amino acid sequence of a transcription factor (GCN4) is introduced in this Chapter. Besides providing a DNA-targeting moiety able to deliver In-111 to the DNA for theranostic applications, this approach can also offer the possibility of targeting specific DNA sequences, which could be of potential value for gene therapy.

5.1. DNA-binding Peptides

The interaction of transcription factors (TFs) with specific DNA sites is key for the regulation of gene expression. Therefore, the development of non-natural agents that can reproduce the DNA-binding properties of natural TFs has been a challenging goal in chemical biology. Besides contributing for the understanding of the involved molecular mechanisms, the “miniature” versions of TFs may also have important applications in gene-based medicine [331, 332]. In this regard, peptides have received a special focus. Synthetic small peptides with DNA-recognition properties have been designed by following the DNA interaction of certain TFs [332-334]. However, this has been a major challenge since high-affinity DNA binding usually requires the full protein domain or the concerted action of multiple binding components [335, 336].

The basic-region leucine-zipper (bZIP) motif is one of the simplest of all DNA-binding motifs of TFs as it consists of a dimer of α -helices. As shown in Figure 5.1, in each helix there are two different subdomains: a C-terminal leucine-rich area which mediates the dimerization through a parallel coiled-coil, and the basic region (BR) which is a domain of approximately 20 amino acids located at the N-terminus. This region is rich in basic amino acids and is responsible for most of the direct contacts with the DNA bases and phosphates [331, 332].

Over the last years, short DNA-binding peptides based on dimeric bZIP basic regions have been synthesized. In these synthetic constructs, the natural C/C-terminal leucine zipper has been replaced by artificial dimerizers such as disulfide bridges (Figure 5.1), azo-benzene linkers, cyclodextrin inclusion complexes and metal complexes. The resulting peptide scaffolds

have demonstrated high-affinity recognition of specific double stranded DNA sequences [337-340].

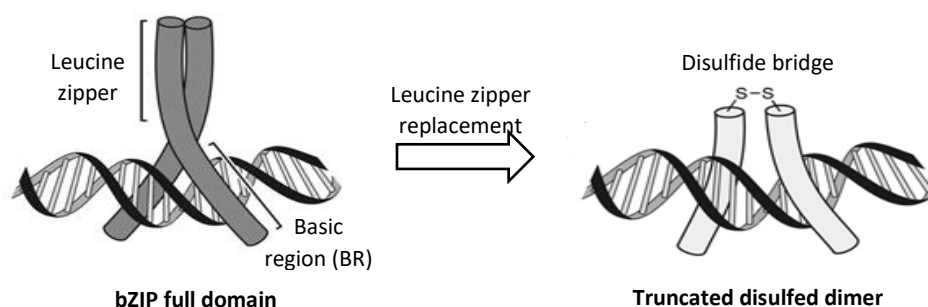


Figure 5.1. Representation of the full bZIP DNA-binding domain (on the left) and of a truncated artificial peptide dimer (on the right). Adapted from [331].

Regarding the specific peptide sequences required for strong DNA binding, Talanian et al., in 1992, demonstrated that dimers of peptides containing as few as 20 residues of the BR of the yeast transcriptional activator GCN4 were capable of binding to DNA with sequence specificity similar to that of the intact protein [341]. Moreover, the truncated 23-amino acid Asp226-Gln248 sequence of the GCN4 BR was identified as the core sequence required to achieve strong DNA binding. Therefore, this peptide sequence has been used as starting point for the design of DNA-binding peptide-based constructs [337, 342, 343].

DNA-targeting Radiotherapeutic Agents

DNA-targeted radiotherapeutic agents have been designed for the delivery of Auger emitting radioisotopes to DNA. Radioiodinated thymidine analogues which could directly incorporate the radionuclide into the DNA sequence were among the first agents to demonstrate the DNA damaging effects of Auger electrons in mammalian cells [120]. Since then, other molecules such as DNA intercalators have been used for the delivery of Auger electrons to DNA, as previously described. More recently, peptide nucleic acids (PNAs), which are DNA mimics with a neutral peptide backbone, have been used to deliver In-111 to designated DNA-sites causing sequence-specific single- and double-strand breaks [316]. Despite the interest of this approach for gene therapy, PNAs have demonstrated important drawbacks related to the poor cell uptake and the difficult and laborious chemical synthesis [344]. Therefore, the search

for novel targeting vectors for the design of DNA-targeted radiotherapeutic agents has been an important task.

The general aim of the work described in this Chapter was to explore the use of the GCN4 BR peptide sequence (Asp226-Gln248) as targeting vector to deliver the radioisotope In-111 to the DNA, in order to maximize its Auger therapy potential. This would represent an innovative approach of targeting DNA with peptide-based radioconjugates and could be especially relevant for gene therapy if specific DNA sequences could be targeted with the Auger-emitting radionuclide.

5.2. Synthesis of the DNA-binding Dimeric Peptide

Design of the DNA-binding construct

The proposed DNA-binding dimeric peptide construct is represented in Figure 5.2. The starting point for the design of the conjugate was the 23-amino acid sequence Asp226-Gln248 of GCN4 BR. As previously stated, a dimerization strategy for the peptide sequence was needed to mimic the natural TF. In this work, we proposed the DProPro dipeptide as a unit to induce a rigid turn structure (hairpin) that could set the two sequences as anti-parallel strands. This strategy has been previously applied with success for the synthesis of β -hairpin peptidomimetics [345-347]. In addition, flexible 2-amino acid linkers were added between the turn inducer and the DNA-binding amino acid sequences. For the formation of highly stable In-¹¹¹In-complexes, a DOTA chelator was attached to one of the linkers.

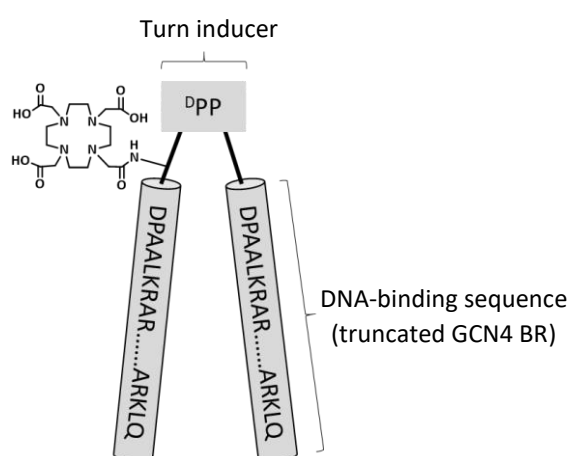


Figure 5.2. Representation of the proposed final DNA-binding dimeric construct. The full sequence of the GCN4 basic region peptide is D²²⁶PAALKRRARNTAARRSRARKLQ²⁴⁸.

For the synthesis of the final construct, a convergent strategy was employed. The convergent approach involves the conjugation of several small peptide segments in order to synthesize the intended final peptide and is aimed to improve the synthesis efficiency for long peptides [348]. Therefore, two peptide fragments were synthesized by microwave-assisted solid-phase automatic synthesis, both containing the core Asp226-Gln248 sequence synthesized in the same direction, followed by the linker and/or the turn-inducing unit which was included in one of the fragments. Furthermore, a DOTA chelator was attached to the side-chain of a Lys residue in the linker region of the same fragment.

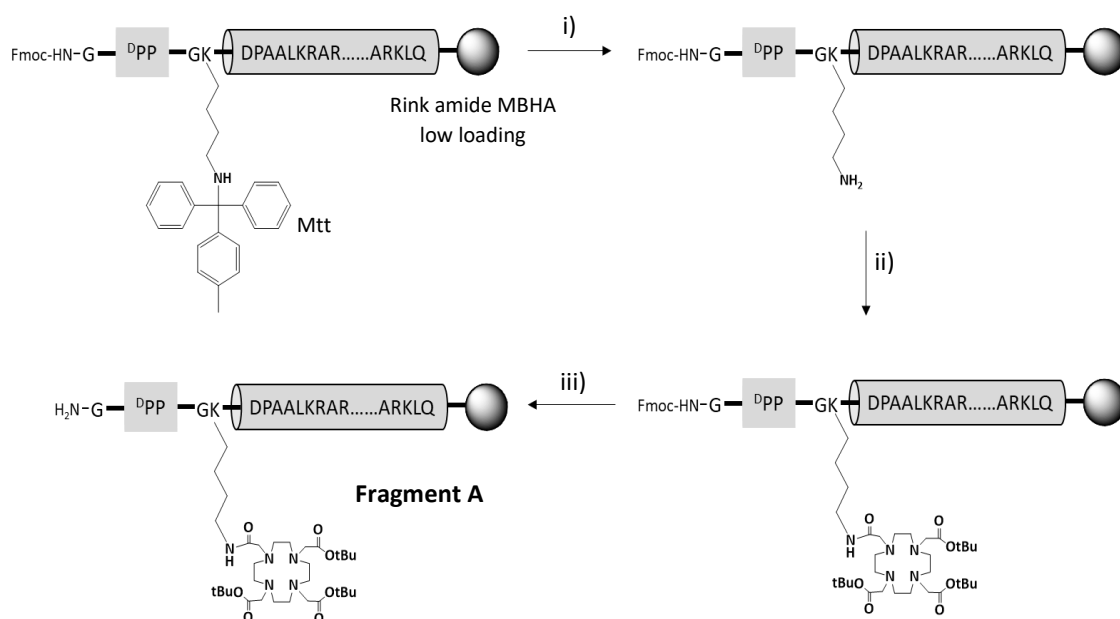
The conjugation of the two fragments was carried out using two different approaches: solid-phase fragment condensation and fragment condensation in solution. These two strategies have also determined the specific procedures used for the synthesis of the individual fragments, as discussed in the following sections.

5.2.1. Synthesis by Solid-Phase Fragment Condensation

In the solid-phase fragment condensation (SPFC) approach, a protected peptide fragment is conjugated to a resin-bound fragment. The obvious advantage of this approach is the easy removal of excess peptide fragment by simple washing of the resin [349, 350]. Gatos and Tzavra, in 2001, were able to synthesize the 32-amino acid salmon I calcitonin with 71% of purity using this approach. More recently, the SPFC methodology has also been used for the synthesis of longer peptides [351, 352].

Synthesis and Characterization of Fragment A

The synthetic pathway for the preparation of the first fragment, **Fragment A**, is depicted in Scheme 5.1. The 28-amino acid peptide sequence of this fragment included the DProPro unit connected through a GlyLys linker to the GCN4 BR sequence. The Lys of the linker was protected with the hyper-acid labile group Mtt. Furthermore, **Fragment A** also included a Gly residue to link the DProPro turn unit to the second peptide fragment (**Fragment B**).



Scheme 5.1. Synthesis of Fragment A.

i) TFA, CH_2Cl_2 , 5 min (5x); **ii)** DOTA-tris(*t*Bu), HATU, DIPEA, DMF, 4 h **iii)** Piperidine, DMF, 30 min

For the synthesis of the peptide sequence of **Fragment A**, Rink Amide MBHA low loading resin was selected as solid support. This resin has a lower substitution (0.38 mmol/g) and therefore is particularly suited for the synthesis of long sequences that are prone to aggregation [353].

In the first attempt to synthesize the peptide sequence in the automatic synthesizer, the standard coupling and Fmoc-deprotection microwave methods were applied. However, taking into account the long length of the sequence, double couplings were performed from the 14th residue forward regardless of the amino acid type. This synthetic protocol yielded a very impure crude in which, after ESI-MS analysis, the desired peptide sequence was not detected. Instead, truncated forms of the peptide sequence were identified, namely sequences lacking the final 3 ($m/z = 761.8$ [$\text{M}+4\text{H}$]⁴⁺) and the final 5 ($m/z = 952.2$ [$\text{M}+3\text{H}$]³⁺) amino acids.

Therefore, in view of the synthetic difficulties, a new synthetic procedure was employed for the synthesis of the peptide sequence of **Fragment A**. In this regard, from the 17th residue onward the microwave-assisted coupling time was extended from 5 to 10 minutes. Furthermore, a capping protocol was added after each amino acid coupling. During the capping step, the free amines on the resin (in which the coupling of the subsequent amino acid failed) are blocked by acetylation with an excess of acetic anhydride. Therefore, this is expected to ensure a higher

degree of purity while the peptide chain is growing [180]. However, the introduction of these modifications to the synthetic protocol had the disadvantages of extending significantly the synthesis total time and of increasing reagents and solvent waste. Nevertheless, it is noteworthy that for the success of the proposed SPFC strategy, the purity of **Fragment A** is of particular importance since this resin-bound fragment cannot be purified prior to the coupling to the second fragment (**Fragment B**).

Indeed, the new protocol successfully produced the desired peptide sequence as confirmed by ESI-MS analysis (Figure 5.3) of the crude product obtained after cleavage and deprotection of a small aliquot of resin. According to the HPLC chromatogram, the peptide was present in the crude with a 74% of purity.

After confirmation of the synthesis of the intended peptide sequence, the work on the resin-bound peptide proceeded with the selective deprotection of the Mtt group in the Lys residue of the linker region using highly diluted TFA (3%) in CH_2Cl_2 . Since the N-terminal Fmoc was not removed, this procedure was expected to render the only free amine of the resin-bound peptide. The presence of the free amine on the resin was confirmed by the Kaiser test.

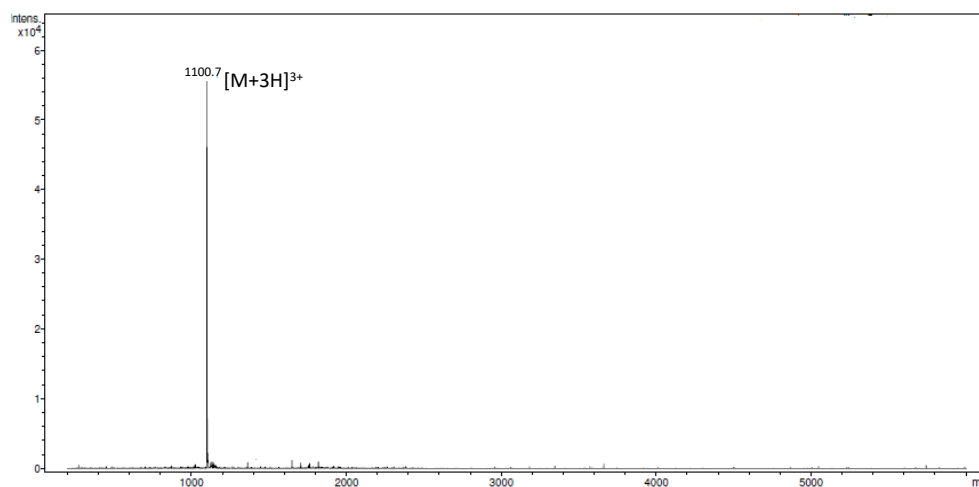


Figure 5.3. ESI-MS spectrum of the crude product obtained after cleavage and deprotection of the peptide-bound resin obtained by automated-synthesis of the sequence: Fmoc-GPPGKDP AALKRARNTAARRSRARKLQ. ESI(+)-MS m/z calcd for $\text{C}_{143}\text{H}_{239}\text{N}_{52}\text{O}_{38}$ $[\text{M}+\text{H}]^+$: 3293.84, found: 1100.7 $[\text{M}+3\text{H}]^{3+}$.

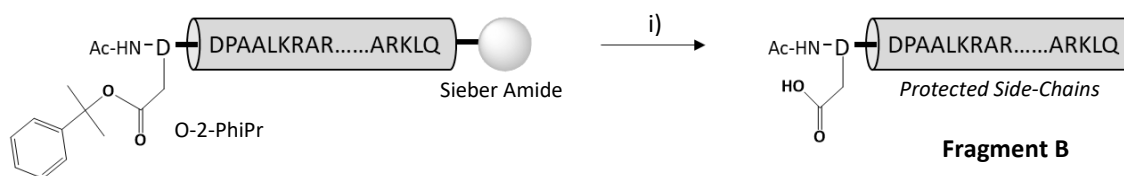
The next step was the conjugation of the commercial prochelator DOTA-tris(*tert*-butyl ester) to the generated free amine, after activation of the single carboxylic acid with HATU. Once the coupling reaction was performed, the amine on the N-terminus of the peptide was finally deprotected by the cleavage of the Fmoc group in basic conditions. These chemical

modifications were confirmed by ESI-MS after peptide cleavage from a small amount of resin. In fact, due to difficulties in obtaining an ESI-MS spectrum of the crude peptide, a purification by HPLC was performed in order to isolate the fully deprotected form of **Fragment A**. The HPLC analysis of the crude revealed that the DOTA-peptide conjugate was present with a 66% purity. The resin-bound **Fragment A** bearing a reactive N-terminal amine and a DOTA chelator on the side-chain was then ready to be conjugated to the second fragment, **Fragment B**.

To assess the ^{111}In -labelling feasibility of the DOTA-bearing **Fragment A**, the purified fraction was radiolabelled with $^{111}\text{InCl}_3$ at a 1.0×10^{-5} M concentration in a reaction performed at 95°C for 25 minutes. Indeed, the radiolabelling was successfully accomplished yielding a single radiochemical species in high radiochemical yield (96%).

Synthesis and Characterization of Fragment B

To be conjugated to the resin-bound **Fragment A**, the chemical strategy employed to prepare **Fragment B** had to yield the peptide in solution. Furthermore, the peptide had to be obtained in the fully protected form to avoid unwanted side reactions during the conjugation reaction. Consequently, the solid support of choice for the peptide synthesis was the hyper-acid labile Sieber amide resin. As depicted in Scheme 5.2, the peptide sequence of **Fragment B** included an additional Asp residue besides the GCN4 sequence. The side-chain carboxylic acid of this Asp residue was protected with a 2-phenylisopropyl ester (O-2-PhiPr) which can be removed by mild acidolysis with 2-3% of TFA without affecting the other side-chain protecting groups of the *tert*-butyl type [354]. Indeed, when used in conjugation with the Sieber amide resin this protected Asp residue is particularly useful since the removal of the O-2-PhiPr protecting group can be performed simultaneously with the cleavage of the partially protected peptide from the resin [355]. The N-terminal amine of **Fragment B** was protected by an acetyl group since this amine will not participate in the conjugation to **Fragment A**.



Scheme 5.2. Synthesis of Fragment B.

i) TFA, CH₂Cl₂, 5 min (5x)

As in the case of **Fragment A**, the synthesis of the peptide sequence of **Fragment B** in the automatic synthesizer was challenging. The initial attempt using the same protocol that was successfully applied for the synthesis of **Fragment A** gave the desired sequence with a purity of approximately 12%, which was considered inadequate. Although it was not possible to identify the other amino acid sequences present in the crude of the totally deprotected peptide, it was hypothesized that side-reactions could have occurred during the synthesis thus compromising the final purity and yield. Therefore, a new protocol was employed in which the amino acid couplings were all performed at 50°C instead of the standard 70°C, while keeping both the double couplings with extended times and the capping procedures as in the synthesis of **Fragment A**. These new conditions gave the desired peptide sequence (identified by ESI-MS) with a purity of approximately 88%, as determined by HPLC after cleavage from an aliquot of resin and total deprotection of the side-chain protecting groups.

The cleavage of the protected peptide along with the selective removal of the O-2-PhiPr was then performed using diluted TFA (3%) in CH₂Cl₂. Although in the HPLC analysis the protected peptide presented a high degree of purity (Figure 5.4), it was not possible to confirm the selective deprotection of the Asp residue and consequently the presence of a reactive carboxylic acid group in the fragment, since the ESI-MS analysis of the high molecular weight (MW) protected peptide (MW=5211.62) was not conclusive.

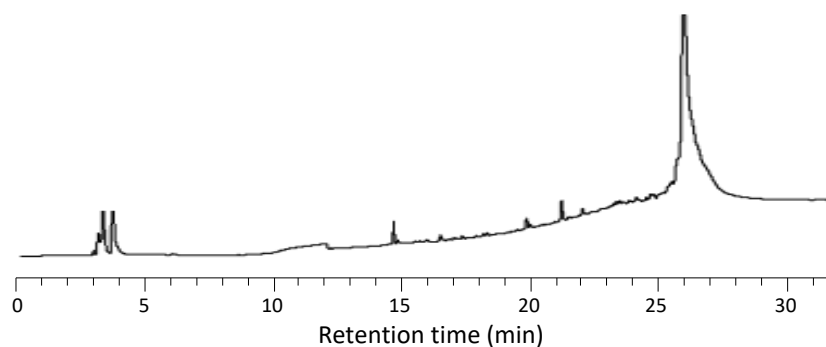


Figure 5.4. HPLC chromatogram of the protected peptide (Fragment B) obtained after cleavage from Sieber amide resin. Method H (Eluents: A- 0.1% aq. TFA; B- 0.1% TFA/CH₃CN. Gradient (%): 90 A/10 B to 100 B in 15 min, 20 min 100 B).

The characterization of the two peptide fragments by HPLC and ESI-MS is summarized in Table 5.1.

Table 5.1. Characterization of the final peptide fragments by HPLC and ESI-MS.

Fragment	HPLC	ESI-MS		Molecular
	Rt (min)*	Calculated (m/z)	Found (m/z)	Formula
A**	14.32	1737.96 [M+2H] ²⁺	1739.0 [M+2H] ²⁺	C ₁₄₄ H ₂₅₄ N ₅₆ O ₄₄
B**	13.13	931.19 [M+3H] ³⁺ 698.64 [M+4H] ⁴⁺ 559.12 [M+5H] ⁵⁺ 466.10 [M+6H] ⁶⁺	931.9 [M+3H] ³⁺ 698.9 [M+4H] ⁴⁺ 559.3 [M+5H] ⁵⁺ 466.3 [M+6H] ⁶⁺	C ₁₁₄ H ₂₀₃ N ₄₇ O ₃₅

*Method C (Eluents: A- 0.1% aq. TFA; B- 0.1% TFA/CH₃CN. Gradient (%): 5 min 95 A/5 B, 95 A/5 B to 100 B in 18 min, 10 min 100 B).

**Fully deprotected

Conjugation of the Peptide Fragments

Fragment B was used without further purification for the conjugation to the resin-bound **Fragment A**. Activation of the carboxylic acid with HATU was performed prior to the addition of **Fragment B** to the resin. In total, 4 equivalents of **Fragment B** were added for the coupling to the resin-bound peptide. In fact, the waste of peptide is one of the major disadvantages of the SPFC methodology.

After a reaction time of 8 hours, the peptide product was cleaved from the resin and the total deprotection was performed in acidic conditions. Subsequent HPLC analysis of the crude product revealed a chromatogram presenting multiple peaks with similar retention times (Figure 5.5). Therefore, the purification of the crude product was very challenging. Nevertheless, a purification by preparative HPLC was attempted by dividing the chromatogram into defined fractions. Nevertheless, the intended dimeric peptide construct was not detected by ESI-MS in any of the collected fractions.

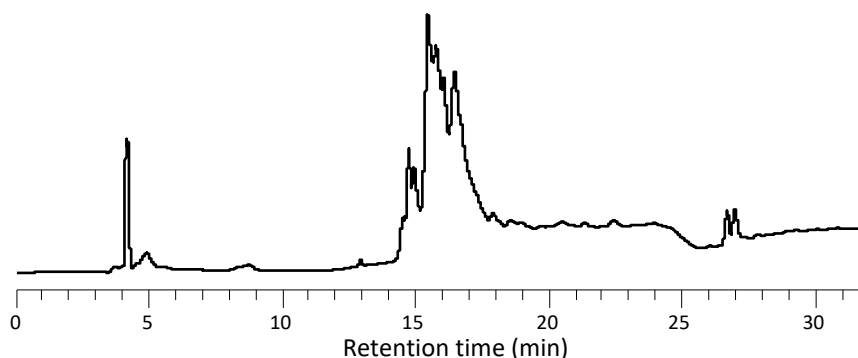


Figure 5.5. HPLC chromatogram (Method C) of the crude (deprotected) peptide after the coupling reaction by SPFC.

The presence of impurities (about 44%) in the peptide-bound resin (**Fragment A**) might have contributed for the lack of purity of the final crude product. Furthermore, the fact that it was not possible to confirm the deprotection of the Asp residue and the integrity of all other protecting groups in **Fragment B** was a major limitation. Indeed, the incomplete deprotection of Asp could have hampered the conjugation reaction with **Fragment A** while the undesired deprotection of one or several amino acid side chains of **Fragment B** could have led to multiple side reactions.

It should be mention that the possible presence of the desired final dimeric peptide conjugate in the crude product, even though with very low yield, should not be completely discarded since the fractions collected during the HPLC purification and subsequently analyzed by ESI-MS were not completely pure, which might have limited the ability of the MS technique to detect all the chemical species present. Nevertheless, for all the reasons discussed, this synthetic approach proved to be inadequate for the synthesis of the final DNA-binding construct.

5.2.2. Synthesis by Fragment Condensation in Solution

Synthesis and Characterization of Fragment A2

The second approach used for the convergent synthesis of the dimeric GCN4-based construct was fragment condensation in solution. This strategy has the advantages of minimizing peptide waste and allowing the purification, if required, of both fragments prior to the conjugation in solution. Moreover, as the conjugation occurs in solution, it is possible to monitor the reaction by HPLC.

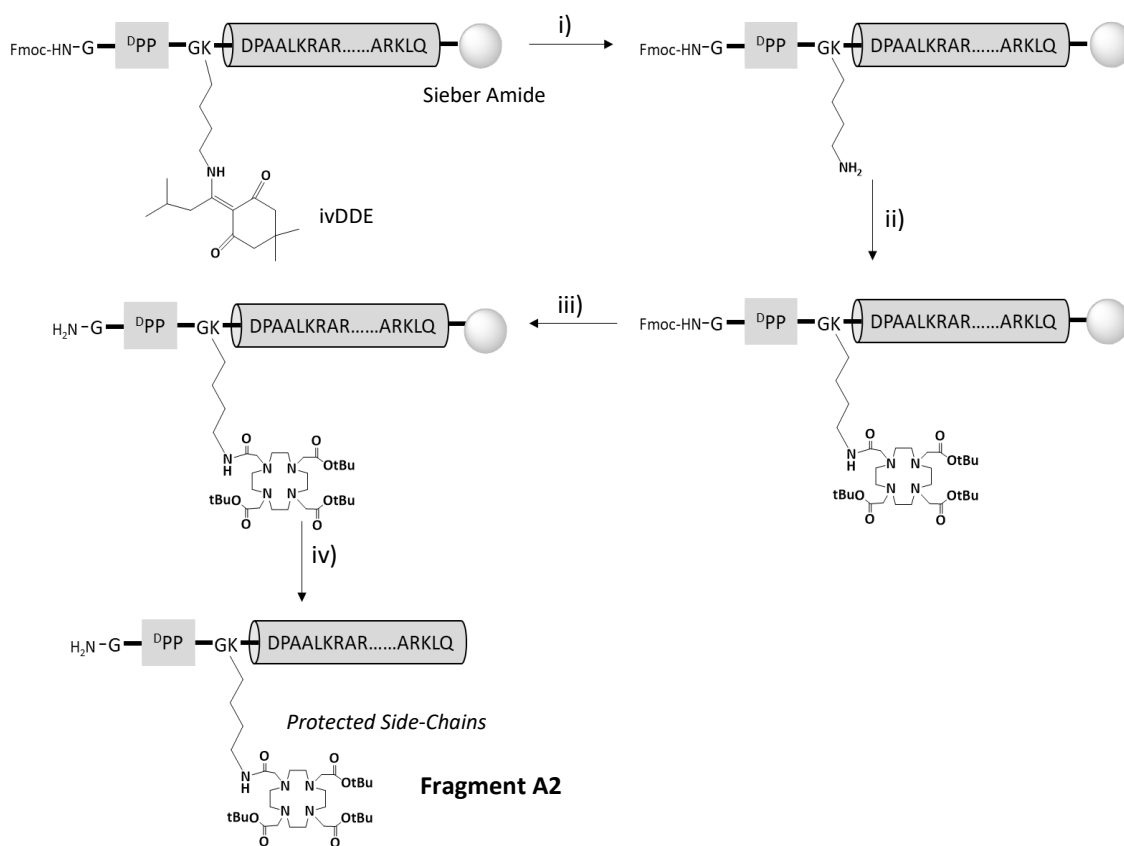
To apply this solution-phase strategy, both peptide fragments were obtained in the fully protected form. Therefore, the Sieber amide resin was employed for the automatic syntheses of both sequences. In this approach, the second fragment, **Fragment B**, was the same that was used in the SPFC strategy, while the first fragment, now named **Fragment A2**, was modified according to the specificities of the solution-phase approach.

As depicted in Scheme 5.4, the Mtt group that was protecting the ϵ -amine of the Lys residue of Fragment A (for the SPFC strategy) was replaced by the ivDDE group (1-(4,4-Dimethyl-2,6-dioxocyclohexylidene)-3-methylbutyl) in the synthetic pathway towards **Fragment A2**. The reason for this replacement was the need for a protecting group that on one hand could be removed in basic conditions (due to the acid liability of the Sieber amide linker) and that, on the other hand could be cleaved under conditions completely orthogonal to the Fmoc-group. Diaz-Mochon et al. showed that ivDDE could fulfil these two requirements when deprotected using a mixture of hydroxylamine hydrochloride ($\text{NH}_2\text{OH}\cdot\text{HCl}$) and imidazole [356].

The synthesis was performed in the automated synthesizer using extended coupling times, at 50°C, and applying capping and double couplings for the last 7 amino acids. After cleavage and deprotection of an aliquot of resin, the desired peptide sequence (with the N-terminal Fmoc and the ivDDE group) was identified by ESI-MS (m/z calculated for $\text{C}_{156}\text{H}_{256}\text{N}_{51}\text{O}_{41}$ $[\text{M}+\text{H}]^+$: 3500.95, found: 876.0 $[\text{M}+4\text{H}]^{4+}$, 701.0 $[\text{M}+5\text{H}]^{5+}$, 584.4 $[\text{M}+6\text{H}]^{6+}$). The peptide sequence was obtained with a purity of 89% as evaluated by HPLC analysis.

After confirming the synthesis of the desired amino acid sequence, the peptide was modified on solid-phase by treatment with a solution of $\text{NH}_2\text{OH}\cdot\text{HCl}$ and imidazole in a mixture of NMP and DMF. The reaction time needed for the complete deprotection of the ivDDE group was monitored by cleaving and deprotecting small aliquots of the resin at specific time points (2, 5 and 8 hours) and analysing the crude products by HPLC. In fact, the removal of the lipophilic

ivDDE group caused a change in the retention time of the peptide from 21.4 min (ivDDE protected) to 15.7 min (free NH_2). After 8 hours of reaction, the complete removal of the ivDDE group was accomplished while the N-terminal Fmoc group remained intact as confirmed by ESI-MS (m/z calculated for $\text{C}_{143}\text{H}_{239}\text{N}_{52}\text{O}_{38}$ $[\text{M}+\text{H}]^+$: 3293.84, found: 659.7 $[\text{M}+5\text{H}]^{5+}$, 549.8 $[\text{M}+6\text{H}]^{6+}$). The prochelator DOTA-tris(*tert*-butyl ester) was then conjugated to the generated free amine using the HATU/DIPEA system, in a reaction that proceeded almost quantitatively. Fmoc-deprotection using the standard basic conditions rendered **Fragment A2** with a reactive free amine in the N-terminal. The fully deprotected peptide (equivalent to the deprotected peptide derived from Fragment A) was characterized by HPLC, showing a 78% degree of purity, and properly identified by ESI-MS.



Scheme 5.3. Synthesis of Fragment A2.

i) NH₂OH.HCl, Imidazole, NMP:DMF, 8 h ii) DOTA-tris(tBu), HATU, DIPEA, DMF, 4 h iii) Piperidine, DMF, 30 min iv) TFA, CH₂Cl₂, 5 min (5x).

The fully protected peptide was cleaved from the Sieber amide resin using diluted TFA (3%) in CH₂Cl₂ and the collected fractions were analysed by HPLC. The HPLC analysis revealed a high degree of purity (around 80%), and therefore the peptide was used in the next step without further purification.

Conjugation of the Peptide Fragments

For the conjugation of the two fragments, PyBOP was used as coupling agent. In comparison with HATU, PyBOP has the advantage of not causing guanylation of primary amines and therefore can be used in excess and for longer reaction times [200]. For the conjugation reaction, the two fragments were used in equimolar amounts and 4 equivalents of PyBOP were added for the activation of the free carboxylic acid of Fragment B. The reaction proceeded for 14 hours.

Although there were modifications in the HPLC profile of the mixture during the course of the reaction, the formation of a new product was not clear. It should be mentioned that the distinction by HPLC of fully protected long peptide segments with similar amino acid sequences revealed to be a very difficult task. Therefore, after full deprotection of the reaction mixture with concentrated TFA, the crude product was analysed by HPLC and ESI-MS.

The solution-phase strategy rendered a much cleaner crude product compared with the SPFC approach as shown in the chromatogram in Figure 5.6. However, the MALDI-TOF/TOF analysis of the purified fractions did not reveal the presence of the desired dimeric peptide. Interestingly, one of the major species found in the MALDI-TOF/TOF analysis presented an m/z that could be attributed to a loss of water (-18 Da) from the deprotected **Fragment B** ($m/z = 2772.9$). This might have resulted from an intramolecular reaction involving one of the Asp residues. In fact, aspartimide formation is a common side-reaction associated with the synthesis of peptides containing Asp [353]. Furthermore, chemical species with m/z values slightly lower in comparison to the deprotected **Fragment A2** were also detected ($m/z = 3317.1, 3278.0$). Although it was not possible to attribute these m/z values to exact sequences or chemical modifications, these results also suggest the occurrence of intramolecular reactions in this peptide fragment. Therefore, the results demonstrated that this approach was also not effective in yielding the desired GCN4-based dimeric construct.

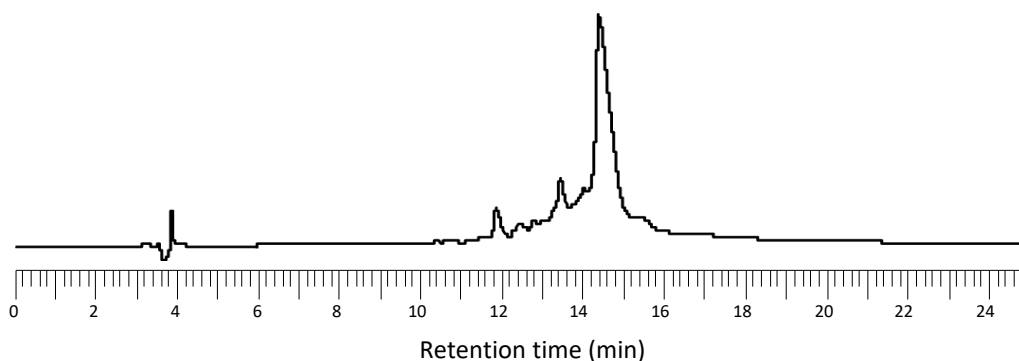


Figure 5.6. HPLC chromatogram (Method C) of the crude (deprotected) peptide after the coupling reaction in solution.

5.3. Conclusions

For the convergent synthesis of a dimeric peptide construct with DNA-binding ability, two peptide fragments containing the BR of the GCN4 TF were successfully synthesized after optimization of the microwave-assisted synthetic protocols. A DOTA chelator was conjugated to the side-chain of a Lys residue contained in one of the fragments, giving the possibility of In-111 radiolabelling.

Two different strategies were adopted for the conjugation of the two peptide fragments: in solid-phase and in solution. However, both approaches failed to give the desired dimeric construct, thus proving to be inadequate for the synthesis of the proposed peptide-based dimeric probe. The long length of the two peptide fragments and the presence within the sequence of amino acids (such as Asp) that are prone to intra-molecular reactions might have contributed for the failure of the conjugation reactions. Furthermore, the difficulties in identifying (by ESI-MS) and monitoring (by HPLC) the fully protected sequences synthesised on the Sieber Amide resin revealed to be major drawbacks that hampered the full control of the reactions.

For all the reasons mentioned above, the synthetic strategy for the preparation of this DNA-binding peptide should be reviewed in order to involve smaller and well-characterized peptide fragments. Nevertheless, due to the potential of Auger therapy and the increasing interest in gene-based medicine, this novel approach should be pursued and ^{111}In -labelled peptides based on TF sequences should be evaluated as potential theranostic probes.

Chapter 6

Conclusions and Future Perspectives

6. Conclusions and Future Perspectives

Breast cancer is the most diagnosed cancer among women worldwide and represents an important societal and economic burden for today's societies [3, 5]. Therefore, this disease has been the subject of intense research in the last decades which has resulted in the development of targeted therapeutic options that have significantly improved the survival rate and the quality of life of BC patients [7, 15]. However, the heterogeneity of the disease has posed a challenge for the selection of the best therapeutic approach for each patient [9, 10]. Moreover, there are still no targeted therapeutic options available for more aggressive BC subtypes which remain largely incurable [18].

In the last years it has been increasingly clear that the molecular characterization of BC is crucial for effective therapeutic decisions and prognostic evaluation in the clinical setting. Indeed, there is a pressing need for a personalized approach for BC management [75, 77]. Nuclear medicine has been addressing this need through the study and development of new target-specific radiopharmaceuticals for the non-invasive characterization of the disease at the molecular level [78]. Furthermore, the integration of therapeutic modalities into the imaging agent has constituted a further step for the real-time personalized monitoring of BC through a theranostic approach [112].

ER, the most studied BC biomarker, has been a preferential target for the development of radiolabelled probes for both imaging and therapy. This research has been focused mainly on radiolabelled steroid analogues which usually present slow clearance from the blood stream and high liver uptake *in vivo* due to their highly lipophilic character [76, 93-95]. Furthermore, the attachment to the steroid ring of bulky chelators for the coordination of SPECT radioisotopes, such as In-111, usually leads to the loss of the ER-binding affinity, which compromises the targeting-specificity of the resulting radiolabelled probes [88]. Therefore, the search for the ideal ER-targeting radiopharmaceutical is still an unmet need. In this context, new radiolabelled ER-targeting probes were developed and studied in this thesis. The increasing knowledge on the structure and mechanisms of action of ER has led to the discovery of new types of ligands, such as peptides, that bind to the receptor with high binding affinity and that have not been explored until now for the design of ER-specific radioprobes [190, 215]. Therefore, in this thesis, small peptides were selected as targeting vectors towards ER. Besides the high ER-binding affinity which is a pre-requisite for the preparation of ER-specific radiopharmaceuticals, the choice of

ligands of peptidic nature can offer pharmacokinetic-related advantages, specifically fast clearance from the blood stream and high accumulation in the target tissues [161, 165, 166]. The theranostic potential of the new probes was explored by selecting Auger-emitting radionuclides, namely In-111 and I-125, for the radiolabelling of the ER-targeting moieties. Furthermore, the importance of the radioisotopes delivery in the close vicinity of DNA for achieving the Auger-therapeutic effect was also taken into account in the design of the radiolabelled probes. In this regard, a dual-targeting strategy was explored for the design of ER-targeting radioprobes capable of reaching the nucleus of BC cells. Finally, a DNA-binding peptide construct based on a naturally occurring transcription factor was also proposed in this thesis for the development of ^{111}In -based radiotheranostic agents.

In short, the general aim of the work presented in this thesis was the synthesis and pre-clinical evaluation of new peptide-based radiolabelled conjugates intended for BC management through a theranostic approach.

The advent of solid-phase peptide synthesis and the later automation of the synthetic process have made the synthesis of small peptide sequences more accessible and convenient [181, 182]. In this thesis, four small peptides (from 6 to 9 amino acids), named **ER1**, **ER2**, **ER3** and **pY**, were successfully synthesized by microwave-assisted automated solid phase synthesis and conjugated to a bifunctional chelator (DOTA, DOTAGA or DTPA) on the N-terminus, in reactions that proceeded with high yield (>90%). The peptide conjugates were radiolabelled with In-111 and obtained with high radiochemical purity (>95%), high stability and high specific activity, which are important parameters to maximize the radiotracers binding to the biological target *in vivo*. The non-radioactive peptide-based In(III) complexes were also prepared and fully characterized.

cER1 (the disulfide-bridge analogue of **ER1**), **ER2** and **ER3** peptides were selected from the literature due to the reported high binding affinities towards ER α . Indeed, these peptides contain an LXXLL sequence intended to mimic the interaction of the natural coactivators with the receptor LBD [190, 191]. The selected LXXLL peptides were successfully conjugated to DOTA and the corresponding In/ ^{111}In -complexes were evaluated. Regarding the binding affinity towards ER α , a fluorescence polarization assay demonstrated that the three peptide-based In-complexes were capable of binding *in vitro* to the ER α LBD, showing IC₅₀ values between 1.20 and 1.72 μM . Although the found binding affinities were still promising for the development of ER-targeting probes, these IC₅₀ values revealed a significant decrease in potency in comparison to the unconjugated peptide sequences (IC₅₀ values between 0.157 to 0.560 μM). Considering

the expected disturbing steric effect of the attachment of the bulky macrocycle to the LXXLL sequence, the introduction of a spacer between the two units should be considered in the future for the optimization of the binding affinity of the LXXLL-based In-complexes.

Cellular uptake studies performed with the radiolabelled peptides in ER-positive MCF-7 cells demonstrated a significantly higher uptake for [¹¹¹In]DOTA-ER3 (up to 23%) in comparison with [¹¹¹In]DOTA-cER1 and [¹¹¹In]DOTA-ER2. Furthermore, the [¹¹¹In]DOTA-ER3 cellular uptake also demonstrated selectivity towards ER-positive cells in detriment of ER-negative BC cells. However, most of the activity of [¹¹¹In]DOTA-ER3 was found in association with the cells membrane and cytosol. In fact, the internalization of the radiolabelled probes into the cells, and in particular into the nuclear compartment, would be highly desirable due to the nuclear localization of the target receptor and in order to maximize the Auger therapy potential of In-111. Nevertheless, the found results suggest that the hydrophilic character of the ¹¹¹In-labelled conjugates hindered a high rate of internalization of the radioprobes into BC cells. Therefore, aiming to potentiate cellular and nuclear internalization of the radiolabelled peptides, the introduction of cell-penetrating sequences or lipophilic moieties are strategies that should be considered in the future.

It is well-known that the susceptibility towards degradation by plasmatic peptidases is one of the most critical factors that can limit the use of peptides for medical applications [161, 165, 166]. Therefore, the resistance towards proteolytic degradation was studied both *in vitro*, by incubation of the radiopeptides in human blood, and *in vivo*, in animal studies, with the obtained results revealing a distinct behavior of the three ¹¹¹In-labelled LXXLL peptides. Indeed, [¹¹¹In]DOTA-ER3 and [¹¹¹In]DOTA-cER1 showed a considerable higher metabolic stability compared to [¹¹¹In]DOTA-ER2 which was rapidly degraded in blood. This fast degradation severely compromises the ability of the ¹¹¹In-labelled ER2 to reach the target organs *in vivo*. Therefore, the ER2 peptide was not considered a promising compound to proceed for biological evaluation, unless structural modifications are introduced into the sequence to increase resistance towards peptidases.

Biodistribution studies of [¹¹¹In]DOTA-ER3 and [¹¹¹In]DOTA-cER1 in healthy and tumor-bearing female mice revealed a fast clearance from the blood stream, predominantly by urinary excretion. This finding is in accordance with the highly hydrophilic character of the radiolabelled peptides. Furthermore, the radiopeptides showed accumulation in ER-rich organs (uterus and ovaries) and in the breast tumor xenograft, suggesting ER-mediated uptake. The verified fast clearance and the accumulation in the target tissues represent favourable properties for imaging

purposes that should be further explored, specifically by performing microSPECT imaging in tumor-bearing animals injected with [^{111}In]DOTA-ER3 and [^{111}In]DOTA-cER1.

Considering the *in vitro/in vivo* stability and selectivity of the ^{111}In -labelled ER3, this peptide was radiolabelled with another radioisotope with known value for the development of radiopharmaceuticals for Auger-therapy: I-125 [103, 125, 254]. Taking advantage of the presence of a histidine residue in the peptide sequence, a direct (radio)iodination approach was successfully applied for the preparation of [^{125}I]-ER3. Interestingly, the iodinated ER3 peptide revealed a nanomolar affinity ($\text{IC}_{50} = 0.543 \mu\text{M}$) towards the ER α LBD, showing higher potency in comparison with [^{111}In]DOTA-ER3. This finding highlights the advantage for the preservation of the peptide's biological activity of the direct introduction of the radioisotope into the sequence, in comparison to the conjugation of a bulky chelator to the N-terminus as in the In-based probe. The [^{125}I]-ER3 cellular studies in MCF-7 cells, demonstrated a significant internalization in the cell nucleus (up to 19%), which also represents an important advantage in comparison with [^{111}In]DOTA-ER3. In fact, the higher nuclear internalization might be related with the lipophilic character of iodide. This finding is particularly important since I-125 is a more potent Auger emitter than In-111, and therefore the ability of [^{125}I]-ER3 to reach the nuclear compartment in high percentages is a relevant property for therapeutic applications [123].

Biodistribution studies in female mice demonstrated selective uptake of [^{125}I]-ER3 in ER-rich organs and MCF-7 xenografts (tumor/blood radioactivity ratio: 3.0 ± 0.2 and tumor/muscle radioactivity ratio: 8.9 ± 1.7 , at 3 h *p.i.*). However, dehalogenation by blood deiodinases was verified both *in vitro* and *in vivo*. Indeed, in the animal model this degradation pathway led to a relevant accumulation of activity in the thyroid one hour after injection. Nevertheless, a high percentage of radioiodinated ER3 remained in circulation allowing its delivery to target tissues. The radioiodination of ER3 through the conjugation of a prosthetic group, such as SIB, might be considered in the future with the aim of achieving a radioiodinated probe presenting less susceptibility towards proteolytic dehalogenation [270, 271]. Furthermore, in the recent years attention has been given to the development of residualizing agents for the radioiodination of peptides and proteins. The introduction of residualizing groups is aimed to increase the retention of radioiodide inside the tumor cells [357-359]. Since the cellular uptake studies performed with [^{125}I]-ER3 revealed a prominent efflux from the BC cells after three hours of incubation, the residualizing strategy should be considered in the future for this radioiodinated peptide. Although these approaches could potentially increase the *in vivo* target/non-target ratios, the eventual negative effect of the conjugation of a prosthetic/residualizing group on the binding affinity towards ER α must be evaluated. Therefore, these chemical modifications should

be carefully studied taking into account all the factors that can affect the *in vivo* performance of a targeted radioiodinated peptide.

Overall, the radiolabelled LXXLL peptides showed promising properties for imaging and for therapy (in the case of the radioiodinated peptide) of ER-expressing BC tumors. Furthermore, this preliminary evaluation corroborated the potential of this ER-targeting strategy for the development of radiopharmaceuticals for BC management, as alternative to the conventional radiofluorinated and radioiodinated estradiol analogues.

In a different approach, another targeting moiety consisting of a small peptide sequence containing a phosphorylate tyrosine, the **pY** peptide, was explored for the design of ^{111}In -labelled probes for BC management. The biological target of this peptide-based vector was the tyrosine kinase Src which is overexpressed in BC and is strongly associated with the non-genomic effects mediated by ER [66]. Due to the importance of these effects for the development of resistance to endocrine therapies and for the most aggressive phenotypes of the disease, imaging of Src could be valuable both for diagnostic and prognostic reasons [239, 240].

Thus, [^{111}In]DTPA-**pY** and [^{111}In]DOTAGA-**pY** were successfully prepared and the two radiopeptides were compared evaluating the influence of the bifunctional chelator on their properties. However, the presence of the phosphorylated tyrosine revealed to be a major drawback for the *in vitro/in vivo* stability of the radiolabelled probes towards proteolytic degradation. Indeed, both ^{111}In -labelled peptides demonstrated rapid degradation in blood, which compromises their potential for *in vivo* applications by hindering their ability to reach and bind to the biological target. The issue of the *in vivo* resistance of phosphorylated amino acids has been addressed before and phosphotyrosine mimetics, such as phenylalanine derivatives, have been described [360]. Therefore, the replacement of the phosphorylated tyrosine in the **pY** peptide by one phosphotyrosine mimetic should be evaluated in the future with the aim of achieving peptide-based probes of higher metabolic stability providing that the binding affinity towards Src is retained. Indeed, due to the potential clinical value of Src imaging for BC personalized management this targeting strategy should be pursued.

The heterogeneity and complexity of cancer diseases have led to the development of multi-targeting agents capable of recognizing different disease-related biomarkers. In the context of Auger therapy, the inclusion of a DNA- or nuclear-targeting moiety in the design of

targeted radiopharmaceuticals has been an effective strategy to potentiate the delivery of the Auger-emitting radionuclides near DNA [138, 285]. However, the integration in the same chemical entity of different targeting vectors is challenging from the synthetic point of view [280, 287, 288]. In this thesis, convenient synthetic pathways were described for the synthesis of DTPA- and DOTA-based prochelators for the dual-vectorization of ^{111}In -labelled probes. A special focus was made on the development of cyclen derivatives for selective functionalization with different biological targeting vectors (namely **PC3**, **PC4**, **PC5** and **PC6**) due to the high thermodynamic and kinetic stabilities of In-DOTA complexes [141]. In fact, the prochelators described in this thesis can also be valuable for the synthesis of dual-targeting radiopharmaceuticals based on diverse biomolecules and other medically relevant radionuclides such as $^{68/67}\text{Ga}$, ^{177}Lu and ^{64}Cu [139].

To bring the radioisotope In-111 in close proximity to DNA, the DNA intercalator **AO** was evaluated as DNA-targeting moiety. *In vitro* studies with [**In**]DOTAGA-**AO** proved that after conjugation to the macrocycle and In-complexation, the **AO** moiety kept the ability to interact with DNA. Furthermore, studies with the ^{111}In -labelled analogue corroborated that the **AO** derivative was effective in promoting the Auger-mediated DNA damage caused by In-111. This evaluation represented an important validation of this approach since it is known that the Auger therapeutic effect is strongly dependent on the distance between the DNA intercalator and the metal centre [120, 125].

The synthesis of bivalent conjugates comprising an ER-targeting moiety (LXXLL peptide or estradiol derivative) and a nuclear-targeting agent (an **AO** derivative or a **NLS**) was successfully achieved by following an orthogonal strategy with the prepared prochelators. The In-/ ^{111}In - complexes of the hybrid conjugates were successfully prepared and the radiolabelled conjugates demonstrated high stability, proving the convenience of this approach for the preparation of dual-targeting ^{111}In -based radiopharmaceuticals. The prepared dual-targeting radiolabelled probes [^{111}In]ER3**AO**, [^{111}In]E2**NLS** and [^{111}In]E2**AO** demonstrated high nuclear internalization (higher than 50%) in BC MCF-7 cells, proving the efficacy of the applied nuclear-targeting approaches. Moreover, [^{111}In]ER3**AO** demonstrated ability to cause direct damage in DNA proving that the double-vectorization did not affect the ability of the **AO** moiety to bring In-111 close to DNA in order to induce single- and double-strand breaks. Indeed, these results represent promising properties for the development of ^{111}In -based radiopharmaceuticals for Auger therapy. However, cellular uptake studies performed with the bivalent probes suggested that the introduction of the non-specific nuclear-targeting moieties (**AO** and **NLS**) led to a loss of selectivity towards ER-positive cells. In fact, these results highlight the difficulties in designing

multi-targeting radiopharmaceuticals with high *in vivo* selectivity. Nevertheless, *in vitro* ER-binding affinity studies should be performed with the inactive In-complexes as these studies can provide an indication about the ER-targeting ability of the ¹¹¹In-labelled dual-targeting probes. Overall, the preliminary results described in this thesis suggest that the chemical design of the bivalent probes should be reviewed in order to achieve radioconjugates with selectivity and specificity towards ER α while keeping the high nuclear internalization.

In the context of the development of DNA-targeting radiopharmaceuticals, a DNA-binding peptide based on the amino acid sequence of the GCN4 transcription factor was also proposed in this thesis. Due to the long length of the proposed dimeric construct, a convergent synthetic strategy was adopted. The automatic synthesis of the individual peptide fragments was challenging due to the long length of the sequences (between 24 and 28 amino acids) proving the importance of the optimization of the synthetic protocol for each peptide sequence. The conjugation of the individual fragments to yield the desired dimeric peptide was not successful, even though two different coupling strategies were explored, specifically solid-phase fragment condensation and fragment condensation in solution. A strategy involving smaller peptide fragments and more selective conjugation procedures should be implemented in the future. In this regard, native chemical ligation might be a good alternative for the synthesis of the desired dimeric construct since it involves the selective coupling of unprotected peptide fragments [361]. In fact, in the era of personalized medicine and gene therapy, the development of radiolabelled probes able to target specific DNA regions represents a research area of great interest and therefore this approach should be further pursued in the future.

In conclusion, the work developed in this thesis represented an effort for the development of radiopharmaceuticals intended for the personalized management of BC through a theranostic approach. In fact, this thesis explored new targeting ligands for the preparation of ER-targeted radiopharmaceuticals. Thus, novel In-based LXXLL probes with demonstrated ER α -binding affinity were achieved and the biological evaluation of the radiolabelled peptides demonstrated promising biological properties. Furthermore, the radioiodination of a LXXLL peptide was able to generate a radioprobe of potential clinical interest, in particular for targeted Auger therapy. Due to the importance of the multi-targeting approach in the development of new radiopharmaceuticals for cancer theranostics, this thesis also introduced convenient synthetic strategies for the double vectorization of ¹¹¹In-based

probes. Moreover, in the context of Auger therapy, targeting moieties capable of potentiating the nuclear internalization and the DNA damaging effect of In-111 were described. Overall, the findings presented in this thesis constitute important contributions for the development of novel targeted radiotheranostic probes that should be further explored with the aim of achieving more selective and effective agents for BC management.

Chapter 7

Experimental Section

7. Experimental Section

7.1. Solvents and Reagents

Handling of air- and/or moisture-sensitive compounds was performed in an inert atmosphere, using vacuum lines and Schlenk techniques.

All commercially acquired chemical reagents and solvents were pro-analysis quality, and were used without any additional purification.

Solvents were dried and distilled in accordance to literature [362]. Briefly:

- THF was distilled in the presence of sodium/benzophenone and immediately used;
- CH₂Cl₂ and CH₃CN were distilled in the presence of calcium hydride and stored under N₂ atmosphere and kept over 4 Å and 3 Å molecular sieves, respectively;
- CH₃OH was distilled in the presence of metallic magnesium and molecular iodine and stored under N₂ atmosphere and kept over 4 Å molecular sieves;
- DMF was used after drying with 4 Å molecular sieves.

All chemicals were purchased from Sigma-Aldrich and used as received, unless otherwise specified.

Rink Amide resin, Sieber Amide resin, HATU, HBTU and all Fmoc-protected amino acids were Novabiochem (UK) products.

DOTA(tBu)₃, DOTA(tBu)₃ NHS, DO3At, DO2At and mDTPA, were purchased from Chematech (France).

InCl₃ (anhydrous 99%) was acquired from Alfa Aesar (Germany). ¹¹¹InCl₃ (370 MBq/mL in HCl) was obtained from Mallinckrodt Medical B.V. (Netherlands).

Carrier-free Na¹²⁵I was obtained from Amersham Biosciences (UK).

ER α -LBD(302-553) and FL-SRC1B2 were kindly provided by Professor Luc Brunsveld of Eindhoven University of Technology (TU/e).

7.2. Purification and Characterization Techniques

7.2.1. Thin Layer Chromatography (TLC)

TLC analyses of reaction mixtures were done on silica-gel coated with fluorescent indicator F254 (Merck). The chromatograms were revealed by exposure to UV radiation at a wavelength of 254 nm, or in an iodine chamber.

7.2.2. Column Chromatography

This technique was used to purify some of the synthesized compounds with silica gel (60 Å with granulometry of 70-230 mesh ASTM (Merck)) as chromatographic support. This support was prepared with the appropriate eluent and filled into glass columns with the proper dimensions. The choice of the eluents depended on the characteristics of the compounds to separate, and the column glass size on the amount used for the purification. The compounds were applied on the top of the column and eluted through gravity effect, and then collected as several small fractions. Those fractions were analysed by TLC and separated in different sets according to the respective retardation factor (R_f). The purified compounds were dried under reduced pressure and characterized by common analytical techniques.

7.2.3. High Performance Liquid Chromatography (HPLC)

The HPLC analyses were performed using solvents HPLC grade and H₂O bidistilled and filtered through 0.22 µm milipore filters. Different systems and methods were used in the HPLC analyses as described above.

Systems

System I: Perkin Elmer Series 200 analytical HPLC instrument, equipped with a UV/Vis detector (LC 290).

System II: Perkin-Elmer LC 200 analytical HPLC coupled to a LC 290 UV/Vis detector and to a Berthold LB-507 A radiometric detector

System III: Perkin Elmer Series 200 analytical HPLC instrument coupled to a LC 290 UV/Vis detector and to a Berthold LB-509 radiometric detector

System IV: Waters semi-preparative HPLC instrument (Waters 2535 Quaternary Gradient Module), equipped with a diode array detector (Waters 2996)

Analytical Methods

Method A

System: I

Column: Supelco Analytical Discovery BIO WidePore C18 column (250 x 4.6 mm, 5 μ m particle size)

Eluents: A- TFA 0.1% aq; B- CH₃CN with 0.1% TFA

Flow: 1 mL/min

Detection: 220 nm

Gradient:

Step	Time (min)	%A	%B	Curve
0	5	90	10	
1	10	70	30	1,0
2	30	55	45	1,0

Method B

System: II

Column: Supelco Analytical Discovery BIO WidePore C18 column (250 x 4.6 mm, 5 μ m particle size)

Eluents: A- TFA 0.1% aq; B- CH₃CN with 0.1% TFA

Flow: 1 mL/min

Detection: 220 nm and γ -detection

Gradient:

Step	Time (min)	%A	%B	Curve
0	5	90	10	
1	30	50	50	1,0
2	10	0	100	1,0

Method C**System:** II**Column:** Supelco Analytical Discovery BIO WidePore C18 column (250 x 4.6 mm, 5 µm particle size)**Eluents:** A- TFA 0.1% aq; B- CH₃CN with 0.1% TFA**Flow:** 1 mL/min**Detection:** 220 nm and γ -detection

Gradient:	Step	Time (min)	%A	%B	Curve
	0	5	95	5	
	1	5	95	5	
	2	18	0	100	1,0
	3	10	0	100	
	4	5	95	5	1,0

Method D**System:** II**Column:** Supelcosil LC-3DP column (250 x 4.6 mm, 5 µm particle size)**Eluents:** A- TFA 0.1% aq; B- CH₃CN with 0.1% TFA**Flow:** 1 mL/min**Detection:** 220 nm

Gradient:	Step	Time (min)	%A	%B	Curve
	0	5	90	10	
	1	1	90	10	
	2	17	0	100	1,0
	3	10	0	100	

Method E**System:** I**Column:** Supelco Analytical Discovery BIO WidePore C18 column (250 x 4.6 mm, 5 µm particle size)**Eluents:** A- TFA 0.1% aq; B- CH₃CN with 0.1% TFA**Flow:** 1 mL/min**Detection:** 220 nm**Gradient:**

Step	Time (min)	%A	%B	Curve
0	5	90	10	
1	30	60	40	1,0
2	5	0	100	1,0

Method F**System:** III**Column:** Supelco Analytical Discovery BIO WidePore C18 column (250 x 4.6 mm, 5 µm particle size)**Eluents:** A- TFA 0.1% aq; B- CH₃CN with 0.1% TFA**Flow:** 1 mL/min**Detection:** 220 nm and γ-detection**Gradient:**

Step	Time (min)	%A	%B	Curve
0	5	90	10	
1	15	0	100	1,0
2	15	0	100	

Method G**System:** I**Column:** Supelco Analytical Discovery BIO WidePore C18 column (250 x 4.6 mm, 5 µm particle size)**Eluents:** A- TFA 0.1% aq; B- CH₃CN with 0.1% TFA**Flow:** 1 mL/min

Detection: 254 nm

Gradient:

Step	Time (min)	%A	%B	Curve
0	5	90	10	
1	45	15	85	1,0
2	5	0	100	1,0

Method H

System: I

Column: Supelco Analytical Discovery BIO WidePore C18 column (250 x 4.6 mm, 5 µm particle size)

Eluents: A- TFA 0.1% aq; B- CH₃CN with 0.1% TFA

Flow: 1 mL/min

Detection: 220 nm

Gradient:

Step	Time (min)	%A	%B	Curve
0	5	90	10	
1	15	0	100	1,0
2	20	0	100	

Method I

System: I

Column: Supelco Analytical Discovery BIO WidePore C18 column (250 x 4.6 mm, 5 µm particle size)

Eluents: A- TFA 0.1% aq; B- CH₃CN with 0.1% TFA

Flow: 1 mL/min

Detection: 220 nm

Gradient:

Step	Time (min)	%A	%B	Curve
0	5	90	10	
1	35	0	100	1,0

Method J**System:** I**Column:** Supelco Analytical Discovery BIO WidePore C18 column (250 x 4.6 mm, 5 µm particle size)**Eluents:** A- TFA 0.1% aq; B- CH₃CN with 0.1% TFA**Flow:** 1 mL/min**Detection:** 254 nm**Gradient:**

Step	Time (min)	%A	%B	Curve
0	5	85	15	
1	1	85	15	
2	15	0	100	1,0
3	7	0	100	

Semi-Preparative Methods**Method SP1****System:** IV**Column:** Supelco Discovery BIO WidePore C18 column (250 x 10 mm, 10 µm particle size)**Eluents:** A- TFA 0.1% aq; B- CH₃CN with 0.1% TFA**Flow:** 3 mL/min**Detection:** 220 nm**Gradient:**

Step	Time (min)	%A	%B	Curve
0	5	90	10	
1	3	90	10	
2	45	40	60	1,0

Method SP2**System:** I**Column:** Supelco Discovery BIO WidePore C18 column (250 x 10 mm, 10 µm particle size)**Eluents:** A- TFA 0.1% aq; B- CH₃CN with 0.1% TFA**Flow:** 2 mL/min**Detection:** 220 nm**Gradient:**

Step	Time (min)	%A	%B	Curve
0	5	90	10	
1	3	90	10	
2	30	35	65	1,0

Method SP3**System:** IV**Column:** Supelco Discovery BIO WidePore C18 column (250 x 10 mm, 10 µm particle size)**Eluents:** A- TFA 0.1% aq; B- CH₃CN with 0.1% TFA**Flow:** 3 mL/min**Detection:** 220 nm**Gradient:**

Step	Time (min)	%A	%B	Curve
0	5	80	20	
1	5	80	20	
2	65	65	35	1,0

Method SP4**System:** IV**Column:** Supelco Discovery BIO WidePore C18 column (250 x 10 mm, 10 µm particle size)**Eluents:** A- TFA 0.1% aq; B- CH₃CN with 0.1% TFA**Flow:** 3 mL/min

Detection: 254 nm

Gradient:

Step	Time (min)	%A	%B	Curve
0	5	80	20	
1	45	55	45	1,0

Method SP5

System: IV

Column: Supelco Discovery BIO WidePore C18 column (250 x 10 mm, 10 µm particle size)

Eluents: A- TFA 0.1% aq; B- CH₃CN with 0.1% TFA

Flow: 3 mL/min

Detection: 220 nm

Gradient:

Step	Time (min)	%A	%B	Curve
0	5	80	20	
1	20	0	100	1,0
2	20	0	100	

7.2.4. Instant Thin Layer Chromatography (ITLC)

Radiolabelling yields and radiochemical purity were evaluated by ITLC using silica-gel layers (ITLC-SG, Agilent). The radioactivity distribution in the chromatograms was detected in a Raytest γ -miniGITA TLC scanner.

7.2.5. Nuclear Magnetic Resonance Spectroscopy (NMR)

¹H- and ¹³C-NMR spectra were recorded on a Bruker Avance III 400 MHz or 300 MHz spectrometers (IST, Lisbon, Portugal). The chemical shifts (δ) are given in ppm and were

referenced to the solvent resonances relative to tetramethylsilane (SiMe₄). Coupling constants (*J*) are given in Hz.

7.2.6. Mass Spectrometry: Electrospray Ionization

Mass spectra were acquired in an electrospray ionization/quadrupole ion trap (ESI/QITMS) Bruker HCT mass spectrometer. Samples were injected in mixtures of water:CH₃CN and injected at a flow rate of 150 μL.h⁻¹.

Tandem mass spectrometry (MS/MS) experiments were performed by collision induced dissociation (CID) using helium buffer gas as the collision partner. The isolation mass, the isolation and the fragmentation amplitude were adjusted for each peptide.

7.2.7. Mass Spectrometry: Matrix-Assisted Laser Desorption/Ionization – Time of Flight

MALDI-TOF spectra were provided by the Mass Spectrometry Unit (UniMS) of ITQB/iBET (Oeiras, Portugal). Data was acquired in Linear Low Mass mode (positive mode) using a 4800*plus* MALDI-TOF/TOF (ABSciex) mass spectrometer and using 4000 Series Explorer Software v.3.5.4. (Applied Biosystems).

7.3. Synthesis and Characterization of Peptides and Peptide Conjugates

Peptides were synthesized by Fmoc-based solid phase synthesis on a Liberty 12-channel automated peptide synthesizer coupled with a Discover SPS microwave peptide synthesizer platform (CEM).

General Method

The following amino acid side chain protecting groups were used: Trt for His, Gln and Cys; Boc for Lys, Pbf for Arg and tBu for Asp. Tyrosine was introduced as Tyr(PO₃H₂). Couplings were performed using 5-fold molar excesses of the corresponding Fmoc-protected amino acids and 2-(1H-benzotriazol-1-yl)-1,1,3,3-tetramethyluronium hexafluorophosphate (HBTU) in the presence of 10 equivalents of N,N-diisopropylethylamine (DIPEA). The standard microwave program used for the couplings was: 25W, 75°C, for 5 min. For Arg coupling, a two-stage program was used: 1) 0W, RT, 25 min; 2) 25W, 75°C, 5 min. His and Cys residues were coupled at lower temperature using the following two-stage program: 1) 0W, RT, 2 min; 2) 25W, 50°C, 4 min. Double couplings were applied to Gln, Arg, Ile and for the residues attached to Ile and His. Fmoc deprotection was achieved using 20% of piperidine in DMF (7 mL) with a 3 min microwave irradiation (42W) at 75°C.

7.3.1. Synthesis of ER1, ER2, ER3 and pY

Amino acids were coupled to a Rink Amide MBH resin (degree of substitution between 0.59 and 0.65 mmol/g) using a 0.1 mmol scale (150 to 170 mg of resin, approximately). The final Fmoc group was removed to yield resin-bound peptides with a free terminal amine. After the synthesis was completed, 25 mg of the resin was treated with cleavage cocktail A (94% TFA, 2.5% water, 2.5% EDT, 1% TIS) in the case of peptides ER1 and ER2 or cleavage cocktail B (95% TFA, 2.5% water, 2.5% TIS) in the case of peptides ER3 and pY. After stirring for 4 hours, the solutions were concentrated under nitrogen to 5% of the initial volume and ice-cooled diethyl ether (10 volumes) was added yielding a white precipitate that was further isolated by centrifugation. The precipitate was redissolved in a mixture of water:CH₃CN (3:1) and purified by semi-preparative HPLC (Method SP1 - ER1, ER2 and ER3; Method SP2- pY) giving the desired peptides with a degree of purity > 95% (assessed by analytical HPLC – Method A). The peptide sequences were identified by ESI-MS and MS/MS.

ER1 (HArgDCysIleLeuCysArgLeuLeuGlnNH₂)

Rt (HPLC, Method A) = 17.10 min

ESI(+)-MS *m/z* calcd for C₄₇H₉₀N₁₇O₁₀S₂ [M+H]⁺: 1116.65, found: 1116.5 [M+H]⁺, 559.1 [M+2H]²⁺

MS/MS:

Fragment ion	<i>m/z</i>	Sequence
y ₈	962.5	R[CILCRLLQ]
b ₇	860.2	[RCILCRL]LQ
y ₆	745.4	RCI[LCRLLQ]
y ₅	633.3	RCIL[CRLQ]
b ₅	589.3	[RCILC]RLLQ
b ₄	486.4	[RCIL]CRLQ

ER2 (HArgIleLeuArgCysLeuLeuGlnNH₂)

Rt (HPLC, Method A) = 14.61 min

ESI(+)-MS *m/z* calcd for C₄₄H₈₅N₁₆O₉S [M+H]⁺: 1013.64, found: 1013.6 [M+H]⁺, 507.7 [M+2H]²⁺

MS/MS:

Fragment ion	<i>m/z</i>	Sequence
y ₇	857.7	R[ILRCLLQ]
b ₆	755.6	[RILRCL]LQ
y ₆	745.2	RI[LRCLLQ]
b ₅ -NH ₃	625.8	[RILRC]LLQ

ER3 (HLysLysIleLeuHisArgLeuLeuGlnNH₂)

Rt (HPLC, Method A) = 12.43 min

ESI(+)-MS *m/z* calcd for C₅₃H₉₉N₁₈O₁₀ [M+H]⁺: 1147.78, found: 1148.3 [M+H]⁺, 574.8 [M+2H]²⁺

MS/MS:

Fragment ion	<i>m/z</i>	Sequence
M+H-NH ₃	1130.7	[KKILHRLLQ]
y ₈	1019.7	K[KILHRLLQ]
b ₈ -NH ₃	985.8	[KKILHRLL]Q
b ₇ -NH ₃	872.7	[KKILHRL]LQ
b ₆	776.6	[KKILHR]LLQ
y ₅	665.6	KKIL[HRLLQ]
y ₄	528.5	KKILH[RLLQ]
y ₃	373.4	KKILHR[LLQ]

pY (HLeupTyrAspLeuLeuLeuNH₂)

Rt (HPLC, Method A) = 17.32 min

ESI(-)-MS *m/z* calcd for C₃₇H₆₁N₇O₁₂P: 826.41 [M-H]⁻, found: 826.6 [M-H]⁻

MS/MS:

Fragment ion	<i>m/z</i>	Sequence
M+H-NH ₃	811.4	[LpYDLLL]
b ₅	698.3	[LpYDLL]L
b ₄	585.2	[LpYDL]LL
Y ₄ / b ₃	472.5	LpY[DLLL] [LpYD]LLL
b ₂	357.3	[LpY]DLLL

7.3.2. Synthesis of DOTA-ER1, DOTA-ER2 and DOTA-ER3

100 mg of the resin bound peptide were swelled with DCM for 1 hour. A solution of 86 mg (0.15 mmol) of DOTA-tris(tert-butyl ester), 57 mg (0.15 mmol) of HATU and 52 μ L (0.30 mmol) of DIPEA in 5 mL of DMF was mixed for 2 min. The solution was then added to the pre-swelled resin and left reacting for 2 hours. After washing the resin with DCM, another coupling cycle with 5 mL of a fresh solution with the same composition was performed for additional 2 hours. The coupling efficiency was evaluated by the Kaiser test on a sample of a few beads. The resin was then treated with cleavage cocktail A (ER1 and ER2) or cleavage cocktail B (ER3) for 10 hours. The solutions obtained were concentrated under nitrogen to 5% of the initial volume and a precipitate was formed upon addition of 10 volumes of cold diethyl ether. The precipitate was redissolved in a mixture of water:ACN (3:1) and purified by semi-preparative HPLC (Method SP1) giving the desired peptide-DOTA conjugates (identified by ESI-MS) with a degree of purity > 95% (assessed by HPLC – Method A).

DOTA-ER1

Rt (HPLC, Method A) = 17.23 min

ESI(+)-MS *m/z* calcd for C₆₃H₁₁₆N₂₁O₁₇S₂ [M+H]⁺: 1502.83, found: 1502.6 [M+H]⁺, 751.9 [M+2H]²⁺

DOTA-ER2

Rt (HPLC, Method A) = 15.48 min

ESI(+)-MS *m/z* calcd for C₆₀H₁₁₁N₂₀O₁₆S [M+H]⁺: 1399.82, found: 1400.5 [M+H]⁺, 700.7 [M+2H]²⁺

DOTA-ER3

Rt (HPLC, Method A) = 12.66 min

ESI(+)-MS m/z calcd for $C_{69}H_{125}N_{22}O_{17}$ $[M+H]^+$: 1533.96, found: 1533.8 $[M+H]^+$

7.3.3. Synthesis of cER1 and DOTA-cER1

3 mg of ER1 or DOTA-ER1 were dissolved in 3 mL of a 1:1 mixture of ammonium acetate buffer (0.1 M pH=8) and DMSO in a plastic flask. The solution was stirred for 12 hours and the cyclized peptide was obtained after purification by semi-preparative HPLC (Method SP1) with a degree of purity > 95% (assessed by analytical HPLC – Method A).

cER1 (HArgDCys*IleLeuCys*ArgLeuLeuGlnNH₂)

*disulfide bridge

Rt (HPLC, Method A) = 17.58 min

ESI(+)-MS m/z calcd for $C_{47}H_{88}N_{17}O_{10}S_2$: 1114.63 $[M+H]^+$, found: 1114.9 $[M+H]^+$, 558.2 $[M+2H]^{2+}$

MS/MS:

Fragment ion	m/z	Sequence
b ₈ -H ₂ O	952.5	[RC*ILC*RL]Q
b ₇ -NH ₃	839.5	[RC*ILC*RL]LQ
b ₆ -NH ₃	726.4	[RC*ILC*R]LLQ
b ₅	587.3	[RC*ILC*]RLLQ
M+2H-NH ₃	549.4	[RC*ILC*RLLQ]
b ₄	486.4	[RCIL]CRLQ

DOTA-cER1

Rt (HPLC, Method A) = 17.49 min

ESI(+)-MS m/z calcd for $C_{63}H_{114}N_{21}O_{17}S_2$ $[M+H]^+$: 1500.81, found: 1500.4 $[M+H]^+$, 751.3 $[M+2H]^{2+}$

7.3.4. Synthesis of DTPA-pY and DOTAGA-pY

100 mg of the resin-bound peptide was swelled with DCM for 1 hour. To a solution of 91 mg of mDTPA or 103 mg of DOTAGA(tBu)₄ (2.5 equiv, 0.15 mmol) in DMF (5 mL), PyBOP (77 mg, 0.15 mmol) and HOBt (20 mg, 0.15 mmol) were added. The solution was vortexed for 2 min and was added to the pre-swelled resin. After agitation (by a nitrogen flow) for 3 hours at RT, the resin was washed with DCM and a fresh solution containing the pro-chelator and the activators (2.5 equiv, 0.15 mmol) was added. The second coupling reaction was left for additional 3 hours. The coupling efficiency was evaluated by performing the Kaiser test on a sample of a few beads. After coupling completion, the resin was washed with DCM and then treated with 10 mL of a mixture of 95% TFA, 2.5% water and 2.5% TIS for 3 hours. After filtration, the acidic solution was concentrated under nitrogen to 5% of the initial volume and ice-cooled diethyl ether (10 volumes) was added yielding a pale-brown precipitate that was further isolated by centrifugation. The precipitate was redissolved in a mixture of water:ACN (3:1) and purified by semi-preparative HPLC (Method SP2). The peptide conjugates were identified by ESI-MS and the purity degree (higher than 95%) was ascertained by HPLC (Method A).

DTPA-pY

Rt (HPLC, Method A) = 17.40 min

ESI(-)-MS m/z calcd for C₅₁H₈₂N₁₀O₂₁P [M-H]⁻: 1201.54, found: 1201.9 [M-H]⁻, 600.5 [M-2H]²⁻

DOTAGA-pY

Rt (HPLC, Method A) = 18.14 min

ESI(-)-MS m/z calcd for C₅₆H₉₁N₁₁O₂₁P [M-H]⁻: 1284.61, found: 1284.3 [M-H]⁻, 642.1 [M-2H]²⁻

7.3.5. Synthesis of GGNLS and ER3 peptides with protected side chains

General Method

Peptides were synthesized by Fmoc-based solid phase synthesis on a Liberty 12-channel automated peptide synthesizer coupled with a Discover SPS microwave peptide synthesizer platform (CEM). Amino acids were coupled to a Sieber Amide resin (0.178 g, substitution: 0.59 mmol/g) using a 0.1 mmol scale. Couplings were performed using 5-fold molar excesses of the

corresponding Fmoc-protected amino acids and 2-(1H-benzotriazol-1-yl)-1,1,3,3-tetramethyluronium hexafluorophosphate (HBTU) in the presence of 10 equivalents of N,N-diisopropylethylamine (DIPEA). The standard microwave program used for the couplings was: 25W, 75°C, for 5 min. For Arg coupling, a two-stage program was used: 1) 0W, RT, 25 min; 2) 25W, 75°C, 5 min. Fmoc deprotection was achieved using 20% of piperidine in DMF (7 mL) with a 3 min microwave irradiation (42W) at 75°C. After the syntheses were completed, resins were treated with a solution of 3% TFA in CH₂Cl₂ during 5-6 cycles of 10 minutes. The fractions collected in each cycle were analysed by HPLC (Method H) and the ones containing peptide were combined. The solutions were concentrated under nitrogen to 5% of the initial volumes and ice-cooled diethyl ether was added (10 volumes) giving the desired peptides that were further isolated by centrifugation.

GGNLSprot (HGlyGlyProLysLysLysArgLysValNH₂): The following amino acid side chain protecting groups were used: Boc for Lys and Pbf for Arg. Double couplings were applied to Val, Arg, and Pro as well as to the residues immediately attached to these amino acids. The final Fmoc group was removed rendering a free terminal amine. The crude peptide was further purified by semi-preparative HPLC (Method SP5).

Rt (HPLC, Method H) = 18.62 min

ESI(+)-MS *m/z* calcd for C₇₇H₁₃₄N₁₇O₂₀S [M+H]⁺: 1648.97, found: 1648.8 [M+H]⁺

ER3prot (AcLysLysIleuLeuHisArgLeuLeuGlnNH₂): The following side chain protecting groups: Trt for His and Gln, Boc for Lys², Mtt for Lys¹ and Pbf for Arg. Double couplings were applied to Gln, Arg, Ile, Lys¹ and for the residues attached to Ile, His and Arg. After removing the final Fmoc group, acetylation of the N-terminus was performed using acetic anhydride (10% in DMF, 7 mL) using the microwave program: 40 W, 65°C, 2 min.

Rt (HPLC, Method H) = 19.41 min

ESI(+)-MS *m/z* calcd for C₁₁₁H₁₅₃N₁₈O₁₆S [M+H]⁺: 2027.15, found: 2027.5 [M+H]⁺

7.3.6. Synthesis of GCN4-based Peptides

7.3.6.1. Synthesis of Fragment A

Peptide Synthesis

(FmocGlyDProProGlyLysAspProAlaAlaLeuLysArgAlaArgAsnThrGluAlaAlaArgArgSerArgAla-ArgLysLeuGlnNH₂)

Amino acids were coupled to a Rink Amide MBHA resin low loading (0.210 g, substitution: 0.38 mmol/g) on a Liberty 12-channel automated peptide synthesizer coupled with a Discover SPS microwave peptide synthesizer platform (CEM). The following side chain protecting groups were used: Trt for Gln and Asn, Boc for Lys¹¹ and Lys²⁶, Mtt for Lys⁵, Pbf for Arg, OtBu for Glu and Asp, tBu for Ser and Thr. Couplings were performed using 5-fold molar excesses of the corresponding Fmoc-protected amino acids and HBTU, in the presence of 10 equiv of DIPEA. The standard microwave program used for the couplings of the first 16 amino acids was: 25W, 75°C, for 5 min. For Glu coupling, a lower temperature (50°C) was employed. For Arg coupling, a two-stage program was used: 1) 0W, RT, 25 min; 2) 25W, 75°C, 5 min. From the 17th amino acid onwards, the following microwave program was used for the amino acid couplings: 25W, 75°C, 10 min. Double couplings were applied for all the final amino acids followed by a capping step with acetic anhydride (10% (v/v) in DMF, 7 mL) for 2 min (40W, 65°C). Fmoc deprotection was achieved using 20% of piperidine in DMF (7 mL) with a 3-min microwave irradiation (42W) at 75°C. The Fmoc group on the N-terminus was not removed.

After the synthesis was completed, an aliquot (10 mg) of the resin was treated with the mixture TFA:water:TIS (95%:2.5%:2.5%). After stirring for 4 hours, the solution was filtered and concentrated under nitrogen to 5% of the initial volume and ice-cooled diethyl ether (10 volumes) was added. The precipitate was isolated and analysed by HPLC and the deprotected peptide was identified by ESI-MS.

Rt (HPLC, Method C) = 16.60 min

ESI(+)-MS *m/z* calcd for C₁₄₃H₂₃₉N₅₂O₃₈ [M+H]⁺: 3293.84, found: 1100.7 [M+3H]³⁺

Deprotection of the Lys(Mtt) side-chain and DOTA(tBu)₃ coupling

The resin was treated with a solution of 3% TFA in CH₂Cl₂ during 5-6 cycles of 10 minutes. Kaiser test was used for monitoring the Mtt deprotection. After washing with CH₂Cl₂, a solution of DOTA-tris(tert-butyl ester) (4 equiv), HATU (4 equiv) and DIPEA (8 equiv) in 5 mL of DMF was added to the resin, after a 2-min pre-activation. The reaction was left (under nitrogen bubbling) for 4 hours. After washing the resin with CH₂Cl₂, another coupling cycle with 5 mL of a fresh solution with the same composition was performed for additional 4 hours. After washing, the resin was then treated with a solution of 20% of piperidine in DMF for 1 hour (2 x).

An aliquot (5-10 mg) of the resin treated with the mixture TFA:water:TIS (95%:2.5%:2.5%). After stirring for 4 hours, the solution was filtered and concentrated under nitrogen to 5% of the initial volume and ice-cooled diethyl ether (10 volumes) was added. The precipitate was isolated and purified by HPLC and the purified fractions were analysed by ESI-MS and HPLC.

Rt (HPLC, Method C) = 14.32 min

ESI(+)-MS *m/z* calcd for C₁₄₄H₂₅₅N₅₆O₄₄ [M+H]⁺: 3473.95, found: 1739.0 [M+2H]²⁺

7.3.6.2. Synthesis of Fragment B**(AcAspAspProAlaAlaLeuLysArgAlaArgAsnThrGluAlaAlaArgArgSerArgAla-ArgLysLeuGlnNH₂)**

Amino acids were coupled to a Sieber Amide resin (0.178 g, substitution: 0.59 mmol/g) on a Liberty 12-channel automated peptide synthesizer coupled with a Discover SPS microwave peptide synthesizer platform (CEM). The following side chain protecting groups were used: Trt for Gln and Asn, Boc for Lys, Pbf for Arg, OtBu for Glu and Asp², O-2-PhiPr for Asp¹, tBu for Ser and Thr. Couplings were performed using 5-fold molar excesses of the corresponding Fmoc-protected amino acids and HBTU, in the presence of 10 equiv of DIPEA. The standard microwave program used for the couplings was: 25W, 50°C, for 720 sec. Double couplings and capping procedures (with acetic anhydride 10% (v/v)) were applied for the last 12 amino acids. After removing the final Fmoc group, acetylation of the N-terminus was also performed using acetic anhydride (40 W, 65°C, 2 min).

The resin was treated with a solution of 3% TFA in CH₂Cl₂ during 5-6 cycles of 10 minutes. The fractions collected in each cycle were analysed by HPLC (Method H) and the ones containing peptide were combined. The solutions were concentrated under nitrogen to 5% of the initial volumes and ice-cooled diethyl ether was added (10 volumes) giving the desired peptide (Fragment B) that was further isolated by centrifugation and dried under vacuum. An aliquot of the crude protected peptide (10 mg) was treated with a solution of TFA:water:TIS (95%:2.5%:2.5%) for 5 hours. After that, the solution was concentrated under nitrogen and the product was precipitated with ice-cooled diethyl ether (10 volumes). The peptide was purified by HPLC and characterized by HPLC and ESI-MS.

Rt (HPLC, Method C) = 13.13 min

ESI(+)-MS *m/z* calcd for C₁₁₄H₂₀₄N₄₇O₃₅ [M+H]⁺: 2792.57, found: 931.9 [M+3H]³⁺, 698.9 [M+4H]⁴⁺, 559.3 [M+5H]⁵⁺, 466.3 [M+6H]⁶⁺

7.3.6.3. Conjugation by Solid Phase Fragment Condensation

A solution of Fragment B (2 equiv), HATU (2 equiv) and DIPEA (4 equiv) in DMF was stirred for 5 minutes under nitrogen. This solution was then added to the pre-swelled resin-bound Fragment A and the mixture was left reacting for 4 hours under nitrogen bubbling. After removing the reagents and washing the resin with CH₂Cl₂, a fresh solution of Fragment B, HATU and DIPEA was added to the resin and left reacting for additional 4 hours. After washing, the resin was then treated with the mixture TFA:water:TIS (95%:2.5%:2.5%) for 6 hours. After filtration, the solution was concentrated under nitrogen to 5% of the initial volume and ice-cooled diethyl ether (10 volumes) was added. The precipitate was isolated and purified by HPLC and the purified fractions were analysed by HPLC and ESI-MS.

7.3.6.4. Synthesis of Fragment A2

Peptide Synthesis

(FmocGlyDProProGlyLysAspProAlaAlaLeuLysArgAlaArgAsnThrGluAlaAlaArgArgSerArgAla-ArgLysLeuGlnNH₂)

Amino acids were coupled to a Sieber Amide resin (0.362 g, substitution: 0.69 mmol/g) on a Biotage Initiator + Alstra automated microwave peptide synthesizer. The following side chain protecting groups were used: Trt for Gln and Asn, Boc for Lys¹¹ and Lys²⁶, ivDDE for Lys⁵ and Pbf for Arg, OtBu for Glu and Asp, tBu for Ser and Thr. Couplings were performed using 2-fold molar excesses of the corresponding Fmoc-protected amino acids and HBTU, in the presence of 4 equiv of DIPEA. The standard microwave program used for the couplings of the first 14 amino acids was: 125W, 50°C, for 390 sec. Starting from the 15th amino acid, the following program was used: 125W, 50°C, for 780 secs, followed by capping with acetic anhydride (20 equiv) at room temperature (10 minutes). Double couplings were applied to Arg, Gln and for the last 7 amino acids. Fmoc deprotection was achieved using 20% of piperidine in DMF (36 equiv) at room temperature for 13 minutes (first 14 amino acids) or 20 minutes (last amino acids). The Fmoc group on the N-terminus was not removed.

After the synthesis was completed, an aliquot (5-10 mg) of the resin was treated with the mixture TFA:water:TIS (95%:2.5%:2.5%). After stirring for 3 hours, the suspension was filtered and the obtained solution was concentrated under nitrogen to 5% of the initial volume and ice-cooled diethyl ether (10 volumes) was added. The precipitate was isolated and analysed by HPLC and the deprotected peptide was identified by ESI-MS.

Rt (HPLC, Method C) = 18.01 min

ESI(+)-MS *m/z* calcd for C₁₅₆H₂₅₆N₅₁O₄₁ [M+H]⁺: 3501.96, found: 876.0 [M+4H]⁴⁺, 701.0 [M+5H]⁵⁺, 584.4 [M+6H]⁶⁺

Deprotection of the Lys(ivDDE) side-chain

The resin-bound peptide was treated with a solution of NH₂OH.HCl (1.25 g) and Imidazole (0.92 g) in a mixture of NMP (5 mL) and DMF (2 ML) for 8 hours, based on a procedure

previously described [356]. After washing with CH_2Cl_2 , an aliquot (5-10 mg) of the resin was treated with the mixture TFA:water:TIS (95%:2.5%:2.5%). After stirring for 3 hours, the solution was filtered and concentrated under nitrogen to 5% of the initial volume and ice-cooled diethyl ether (10 volumes) was added. The precipitate was isolated and analysed by HPLC and the deprotected peptide was identified by ESI-MS.

Rt (HPLC, Method C) = 16.66 min

ESI(+)-MS m/z calcd for $\text{C}_{143}\text{H}_{238}\text{N}_{52}\text{O}_{38}$ $[\text{M}+\text{H}]^+$: 3292.83, found: 659.7 $[\text{M}+5\text{H}]^{5+}$, 549.8 $[\text{M}+6\text{H}]^{6+}$

Conjugation to DOTA(tBu)₃

A solution of DOTA-tris(tert-butyl ester) (4 equiv), HATU (4 equiv) and DIPEA (8 equiv) in 5 mL of DMF was added to the resin, after a 2-min pre-activation. The reaction was left stirring for 5 hours. After washing the resin with CH_2Cl_2 , another coupling cycle with 5 mL of a fresh solution with the same composition was performed for additional 5 hours. After washing, the resin was then treated with a solution of 20% of piperidine in DMF for 1 hour (2 x).

An aliquot (5-10 mg) of the resin treated with the mixture TFA:water:TIS (95%:2.5%:2.5%). After stirring for 3 hours, the solution was filtered and concentrated under nitrogen to 5% of the initial volume and ice-cooled diethyl ether (10 volumes) was added. The precipitate was isolated and purified by HPLC and the purified fractions were analysed by HPLC and identified by ESI-MS (same as Fragment A).

Cleavage from the resin

The resin was treated with a solution of 3% TFA in CH_2Cl_2 during 5-6 cycles of 10 minutes. The fractions collected in each cycle were analysed by HPLC (Method H) and the ones containing peptide were combined. The solutions were concentrated under nitrogen to 5% of the initial volumes and ice-cooled diethyl ether was added (10 volumes) giving the desired peptide (Fragment A2) that was further isolated by centrifugation and dried under vacuum.

Rt (HPLC, Method H) = 28.04 min

7.3.6.5. Conjugation by Fragment Condensation in Solution

A solution of Fragment B, PyBOP (2 equiv) and DIPEA (4 equiv) in DMF was stirred for 10 minutes under nitrogen. Fragment A2 (1 equiv) in DMF was added to the solution and the mixture was left stirring for 2 hours. Additional PyBOP (2 equiv) and DIPEA (4 equiv) were then added to the reaction mixture. After stirring for 12 hours under nitrogen, DMF was removed under vacuum and the residue was washed with water. The precipitate was then treated for 6 hours with a mixture of TFA:water:TIS (95%:2.5%:2.5%). The crude product was analysed by HPLC, ESI-MS and MALDI-TOF/TOF.

7.4. Synthesis of the Peptide-based In(III) Complexes

7.4.1. Synthesis of [In]DOTA-cER1, [In]DOTA-ER2 and [In]DOTA-ER3

1.5 μmol of the peptide conjugates were dissolved in 0.5 mL of acetate buffer (0.1 M, pH 5.5) and 1.8 μmol of InCl_3 (0.4 mg) were added. The solutions were heated to 95°C and left for 30 min. The mixtures were then purified by semi-preparative HPLC (Method SP1) and the purified complexes were identified by ESI-MS and further characterized by analytical HPLC (Method A).

[In]DOTA-cER1

Rt (HPLC, Method A) = 17.61 min

ESI(+)-MS m/z calcd for $\text{C}_{63}\text{H}_{111}\text{InN}_{21}\text{O}_{17}\text{S}_2$ $[\text{M}+\text{H}]^+$: 1612.69, found: 807.0 $[\text{M}+2\text{H}]^{2+}$

[In]DOTA-ER2

Rt (HPLC, Method A) = 15.49 min

ESI(+)-MS m/z calcd for $\text{C}_{60}\text{H}_{108}\text{InN}_{20}\text{O}_{16}\text{S}$ $[\text{M}+\text{H}]^+$: 1511.70, found: 1511.8 $[\text{M}+\text{H}]^+$

[In]DOTA-ER3

Rt (HPLC, Method A) = 12.78 min

ESI(+)-MS m/z calcd for $\text{C}_{69}\text{H}_{122}\text{InN}_{22}\text{O}_{17}$ $[\text{M}+\text{H}]^+$: 1645.84, found: 1645.7 $[\text{M}+\text{H}]^+$, 823.7 $[\text{M}+2\text{H}]^{2+}$

7.4.2. Synthesis of [In]DTPA-pY

2.1 mg (1.7 μmol) of DTPA-pY were dissolved in 1 mL of acetate buffer (0.1 M, pH 5.5) and 2.0 μmol of InCl_3 (0.4 mg) were added. The solution was stirred for 30 min at room temperature. The mixture was then purified by HPLC (Method SP2) and the purified complex was identified by ESI-MS and further characterized by analytical HPLC (Method A).

[In]DTPA-pY

Rt (HPLC, Method A) = 17.56 min

ESI(+)-MS m/z calcd for $[\text{C}_{51}\text{H}_{79}\text{InN}_{10}\text{O}_{21}\text{P}]^-$: 1313.42, found: 1337.42 $[\text{M}+\text{H}+\text{Na}]^+$

7.4.3. Synthesis of [In]DOTAGA-pY

2.5 mg (1.9 μmol) of DOTAGA-pY were dissolved in 1 mL of acetate buffer (0.1 M, pH 5.5) and 2.3 μmol of InCl_3 (0.5 mg) were added. The solution was heated at 90°C for 15 min. The mixture was then purified by HPLC (Method SP2) and the purified complex was identified by ESI-MS and further characterized by analytical HPLC (Method A).

[In]DOTAGA-pY

Rt (HPLC, Method A) = 18.80 min

ESI(-)-MS m/z calcd for $[\text{C}_{56}\text{H}_{88}\text{InN}_{11}\text{O}_{21}\text{P}]^-$: 1396.49, found: 1396.4 $[\text{M}]^-$

7.5. Synthesis of the Iodinated ER3 Peptide

To a solution of ER3 (4 mg, 3.49 mmol) in phosphate buffer 0.1 M pH 7.4 (100 μL), a solution of sodium iodide (0.8 mg, 5.24 mmol) in the same buffer (50 μL) was added followed by a solution (50 μL , phosphate buffer) of chloramine-T (1.9 mg, 6.99 mmol). The reaction was allowed to proceed for 30 min and the progress was monitored by HPLC (Method E). The iodination was then quenched by the addition of a solution of sodium metabisulphite (4 mg, 2.10 mmol) in phosphate buffer (100 μL). The resulting mixture was purified by HPLC (Method

E) and the purified fractions were lyophilized and [I]-ER3 was identified by ESI-MS and characterized by HPLC (Methods E and F).

[I]ER3

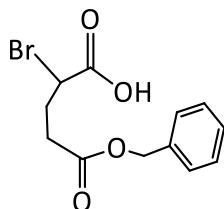
Rt (HPLC, Method E) = 16.78 min

Rt (HPLC, Method F) = 10.62 min

ESI(+)-MS m/z calcd for $C_{53}H_{98}IN_{18}O_{10}$ $[M+H]^+$: 1273.68, found: 1273.5 $[M+H]^+$, 637.5 $[M+2H]^{2+}$, 425.4 $[M+3H]^{3+}$

7.6. Synthetic Protocols and Characterization of Prochelators

2.1. 5-(benzyloxy)-2-bromo-5-oxopentanoic acid [249]

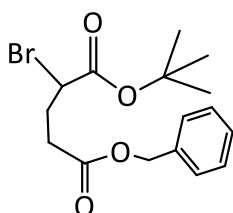


A solution of 6 g (25.9 mmol) of L-glutamic acid 5-benzylester and 9.1 g (88.5 mmol) of sodium bromide in 45 mL of a hydrobromic acid solution (1 M) was cooled at 0°C. To the solution 3.175 g (46 mmol) of sodium nitrite was added portionwise and the mixture was left stirring in an ice-bath. After 3 hours, 2.25 mL of sulfuric acid (99.9%) was added followed by 50 mL of diethyl-ether. The water phase was then extracted three times with diethyl-ether and the organic phases were combined and extracted with brine. After drying the organic phase with anhydrous Na₂SO₄, the solvent was removed using rotatory evaporation. The crude product (yellow oil) was then purified by column chromatography on silica gel using as eluents petroleum ether and ethyl acetate in a 7:3 proportion. After evaporation of the solvents under vacuum, the product was obtained as a pale yellow oil.

Yield: 41.6% (3.23 g, 10.8 mmol)

¹H-NMR (300 MHz, CDCl₃) δ 10.76 (br, 1H, COOH), 7.37 (m, 5H, Ar), 5.15 (s, 2H, CH₂-Ph), 4.41 (dd, *J* = 8.1 Hz, *J* = 6.0 Hz, 1H, CHBr), 2.61 (t, *J* = 6.9 Hz, 2H, CH₂COOBz), 2.40-2.32 (m, 2H, CHBrCH₂CH₂)

2.2. 5-benzyl 1-*tert*-butyl 2-bromopentanedioate [249]

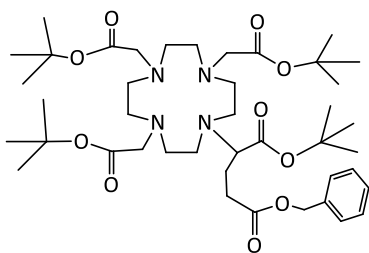


To a solution of 3.23 g (10.7 mmol) of 2.1 in chloroform, a solution of 3.83 mL (21.4 mmol) of *tert*-butyltrichloroacetimidate (TBTA) in 10 mL of cyclohexane was added dropwise for 15 min. To dissolve the white precipitate formed, 5 mL of dimethylacetamide (DMA) was added followed by 320 μL of boron trifluoride ethyl etherate (BF₃OEt₂). The reaction mixture was stirred for 4 days at room temperature. The solvents were evaporated under vacuum and the remaining DMA phase was extracted three times with 20 mL of hexane. The hexane phase was evaporated and the crude product (yellow oil) was purified by column chromatography (silica gel 60) using petroleum ether and ethyl acetate in a 20:1 proportion, and then in a 15:1 proportion. The product was obtained as a colorless oil.

Yield: 67.3% (2.56 g, 7.19 mmol)

¹H-NMR (300 MHz, CDCl₃) δ 7.38 (m, 5H, Ar), 5.14 (s, 2H, CH₂-Ph), 4.26 (dd, *J* = 8.1 Hz, *J* = 6.3 Hz 1H, CHBr), 2.58 (t, *J* = 6.9 Hz, 2H, CH₂COOBz), 2.38-2.25 (m, 2H, CHBrCH₂CH₂), 1.49 (s, 9 H, C(CH₃)₃)

2.3. 1-*tert*-butyl 5-(2-oxo-2-phenylethyl) 2-(4,7,10-tris(2-(*tert*-butoxy)-2-oxoethyl)-1,4,7,10-tetraazacyclododecan-1-yl)pentanedioate



To a solution of 220 mg (0.43 mmol) of tri-*tert*-butyl 2,2',2''-(1,4,7,10-tetraazacyclododecane-1,4,7-triyl)triacetate (DO3AtBu) in dry acetonitrile, was added 154 mg (0.43 mmol) of 2.2 and 60 mg (0.43 mmol) of K₂CO₃. The reaction was left stirring at room temperature under inert atmosphere for 16 hours. The mixture was then filtered and

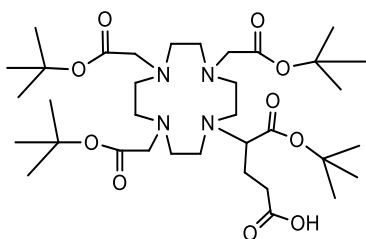
the acetonitrile was evaporated from the filtrate. The crude product (dark yellow oil) was then purified by column chromatography (silica gel) using the mixture CH₂Cl₂/MeOH (9:1). The product was obtained as a colourless oil after evaporation of the solvents under vacuum.

Yield: 68.3% (232 mg, 0.29 mmol)

¹H-NMR (300 MHz, CDCl₃) δ 7.32 (m, 5H, Ar), 5.03 (s, 2H, CH₂-Ph), 3.36-2.03 (m, 27 H, CHN, NCH₂, CH₂COOBz, CHNCH₂CH₂, CH₂COOtBu), 1.37 (s, 36 H, C(CH₃)₃)

¹³C-NMR (75 MHz, CDCl₃) δ 174.5 (COOBz), 172.8, 172.7 (COOC(CH₃)₃), 135.4 (CH₂C(Ar)), 128.45, 128.23, 128.11 (Ar), 82.35, 81.74, 81.70 (C(CH₃)₃), 66.19 (OCH₂Ar), 57.81, 55.64, 55.56, 55.31, 52.46, 52.23, 48.39, 47.95, 47.01, 44.12 (13C, HCNCH₂, NCH₂CH₂N, CH₂COOtBu, CH₂COOBz), 32.31 (NCHCH₂CH₂), 27.96, 27.67, 27.52 (C(CH₃)₃)

DOTAGA(tBu)₄. 5-(*tert*-butoxy)-5-oxo-4-(4,7,10-tris(2-(*tert*-butoxy)-2-oxoethyl)-1,4,7,10-tetraazacyclododecan-1-yl)pentanoic acid [249]



232 mg (0.29 mmol) of 2.3 was dissolved in dry methanol (10 mL) and 20 mg of Pd/C was added. The mixture was hydrogenated for 8 hours, filtered over Celite and evaporated to dryness under vacuum. The product was obtained as a pale yellow oil.

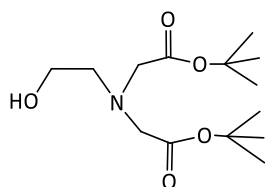
Yield: 94.2% (194 mg, 0.27 mmol)

¹H-NMR (300 MHz, CDCl₃) δ 3.62-2.05 (m, 27 H, CHN, NCH₂, CH₂COOH, CHNCH₂CH₂, CH₂COOC(CH₃)₃), 1.35 (m, 36 H, C(CH₃)₃)

¹³C-NMR (75 MHz, CDCl₃) δ 175.0 (COOH), 172.9, 172.6, 172.5, 171.4 (COOtBu), 82.22, 81.75, 81.71 (C(CH₃)₃), 57.82, 55.64, 55.58, 55.32, 52.44, 52.34, 48.38, 48.30, 46.96, 44.07 (13C, NCHCOOtBu, HCNCH₂, NCH₂CH₂N, CH₂COOtBu, CH₂COOH), 33.02 (NCHCH₂CH₂), 27.88, 27.67, 27.52 (C(CH₃)₃)

ESI(+)-MS *m/z* calcd for C₃₅H₆₅N₄O₁₀ [M+H]⁺: 701.47, found: 723.8 [M+Na]⁺

4.1. di-*tert*-butyl 2,2'-((2-hydroxyethyl)azanediyl)diacetate



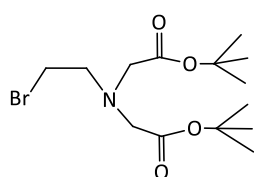
Ethanolamine (0.42 mL, 7 mmol), *tert*-butyl bromoacetate (2.21 mL, 15.4 mmol) and K₂CO₃ (6.4 g, 46.2 mmol) were mixed in DMF (10 mL) and the suspension was stirred for 72 hours. The mixture was filtered and the filtrate was evaporated under vacuum giving the product as

a yellow oil.

Yield: 93.9% (1.9 g, 6.57 mmol)

¹H-NMR (300 MHz, CDCl₃) δ 3.48 (t, *J* = 4.2 Hz, 2H, CH₂OH), 3.41 (s, 4H, NCH₂COOtBu), 2.82 (t, *J* = 4.4 Hz, 2H, NCH₂CH₂OH), 1.42 (s, 18 H, C(CH₃)₃)

4.2. di-*tert*-butyl 2,2'-((2-bromoethyl)azanediyl)diacetate



4.1 (1.9 g, 6.57 mmol) was dissolved in dry CH₂Cl₂ (10 mL) and tetrabromomethane (4.8 g, 14.53 mmol) was added. After mixing for 10 min, 4 g (15.2 mmol) of triphenylphosphine dissolved in 10 mL of CH₂Cl₂ were added dropwise to the mixture for 20 min. The reaction

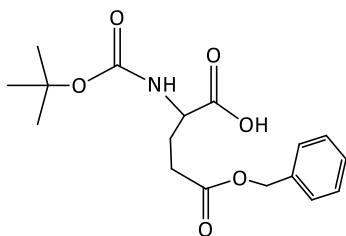
was left stirring overnight at RT and, after filtration and evaporation, the crude product was purified through column chromatography (silica gel) using a mixture of petroleum ether (70%) and ethyl acetate (30%). The product was obtained as a dark brown oil.

Yield: 86.8% (2.0 g, 5.70 mmol)

¹H-NMR (300 MHz, CDCl₃) δ 3.47 (s, 4H, NCH₂COOtBu), 3.39 (t, *J* = 7.2 Hz, 2H, CH₂Br), 3.12 (t, *J* = 7.2 Hz, 2H, NCH₂CH₂Br), 1.37 (s, 18 H, C(CH₃)₃)

$^{13}\text{C-NMR}$ (75 MHz, CDCl_3) δ 169.33 (COOtBu), 81.83 ($\text{C}(\text{CH}_3)_3$), 55.35 (CH_2N), 56.05 ($\text{NCH}_2\text{COOtBu}$), 29.56 (CH_2Br), 27.87 ($\text{C}(\text{CH}_3)_3$)

4.3. 5-(benzyloxy)-2-((tert-butoxycarbonyl)amino)-5-oxopentanoic acid

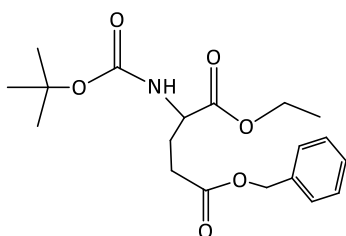


L-glutamic acid 5-benzylester (350 mg, 1.48 mmol), di-*tert*-butyl dicarbonate (356 mg, 1.63 mmol) and triethylamine (248 μL , 1.78 mmol) were dissolved in a 1:1 mixture of water and 1,4-dioxane (14 mL). After stirring for 18 hours at RT, 15 mL of water were added and the pH of the solution was adjusted to 4 using an appropriate volume of HCl (5 N). The product was then extracted (3x) using ethyl acetate, and the combined organic phase was washed with brine. After evaporating under vacuum, the product was obtained as a pale-yellow oil.

Yield: 97.1% (486 mg, 1.44 mmol)

$^1\text{H-NMR}$ (300 MHz, CDCl_3) δ 10.83 (br, 1H, COOH), 7.32 (m, 5H, Ar), 5.09 (s, 2H, $\text{CH}_2\text{-Ph}$), 4.31 (m, 1H, CH), 2.56-2.15 (m, 4H, CHCH_2CH_2), 1.43 (s, 9 H, $\text{C}(\text{CH}_3)_3$)

4.4. 5-benzyl 1-ethyl 2-((tert-butoxycarbonyl)amino)pentanedioate

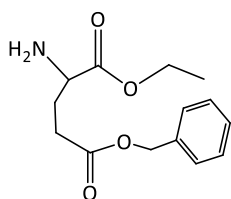


A solution of **4.3** (486 mg, 1.44 mmol), iodoethane (270 mg, 1.73 mmol) and NaHCO_3 (250 mg, 2.96 mmol) in DMF (10 mL) was stirred at RT for 48 hours. After this time, 40 mL of water were added and an extraction was made with diethyl ether (3 x). After washing the organic phase with brine, the solvent was evaporated under vacuum and the product was obtained as a yellow oil.

Yield: 72.9% (383 mg, 1.05 mmol)

$^1\text{H-NMR}$ (300 MHz, CDCl_3) δ 7.33 (m, 5H, Ar), 5.09 (s, 2H, $\text{CH}_2\text{-Ph}$), 4.29 (m, 1H, CH), 4.15 (q, $J=7.2$ Hz, 2H, $\text{COOCH}_2\text{CH}_3$), 2.47-1.94 (m, 4H, CHCH_2CH_2), 1.40 (s, 9 H, $\text{C}(\text{CH}_3)_3$), 1.21 (t, $J=7.2$ Hz, 3H, $\text{COOCH}_2\text{CH}_3$)

4.5. 5-benzyl 1-ethyl 2-aminopentanedioate



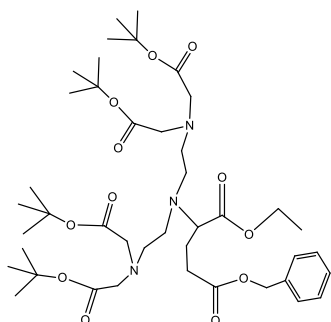
To a solution of **4.4** (383 mg, 1.05 mmol) in CH_2Cl_2 (10 mL), at 0°C , trifluoroacetic acid (3 mL) was added. The solution was stirred at RT for 12 hours and after that the acid and the solvent were removed under vacuum. After evaporation, the product was obtained as a yellow oil.

Yield: 99% (264 mg, 1.04 mmol)

$^1\text{H-NMR}$ (300 MHz, CDCl_3) δ 7.22 (m, 5H, Ar), 5.01 (s, 2H, $\text{CH}_2\text{-Ph}$), 4.12-3.98 (m, 3H, CH, $\text{COOCH}_2\text{CH}_3$), 2.52-2.18 (m, 4H, CHCH_2CH_2), 1.09 (t, $J = 6.9$ Hz, 3H, $\text{COOCH}_2\text{CH}_3$)

$^{13}\text{C-NMR}$ (75 MHz, CDCl_3) δ 172.59 (COOBz), 169.49 (COOEt), 135.3 ($\text{CH}_2\text{C(Ar)}$), 128.53, 128.34, 128.21 (Ar), 66.46 (OCH_2Ar), 63.12 ($\text{COOCH}_2\text{CH}_3$), 52.31 (CH), 29.60 (CHCH_2CH_2), 25.12 (CHCH_2CH_2), 13.58 ($\text{COOCH}_2\text{CH}_3$)

4.6. 5-benzyl 1-ethyl 2-(bis(2-(bis(2-(tert-butoxy)-2-oxoethyl)amino)ethyl)amino)pentanedioate



4.5 (264 mg, 1.04 mmol) and **4.2** (730 mg, 2.08 mmol) were suspended in a mixture of acetonitrile and phosphate buffer pH=8 (2 M) in a 1:1 proportion (8 mL, total volume). After stirring for 2 hours at RT, the phosphate layer was removed and replaced by fresh phosphate buffer. The reaction was left stirring for 12 hours and after that time the phosphate buffer was again replaced and additional 730 mg (2.08 mmol) of **4.2** were added

to the mixture. The reaction was left for additional 24 hours, after which 20 mL of water were added and the organic phase was separated and concentrated using a rotary evaporator. The crude product was purified through silica gel using petroleum ether and ethyl acetate in a 7:3 proportion. After purification and solvent evaporation under vacuum, the product was obtained as a yellow oil.

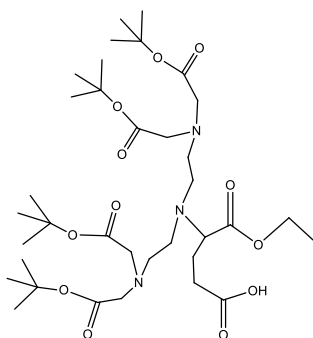
Yield: 26.3% (221 mg, 0.27 mmol)

$^1\text{H-NMR}$ (300 MHz, CDCl_3) δ 7.28 (m, 5H, Ar), 5.05 (s, 2H, $\text{CH}_2\text{-Ph}$), 4.07-4.02 (m, 3H, CH, $\text{COOCH}_2\text{CH}_3$), 3.33 (s, 8H, $\text{NCH}_2\text{COOtBu}$), 2.65 (m, 8H, $\text{NCH}_2\text{CH}_2\text{N}$), 2.35 (m, 2H, CH_2COOBz), 2.08-1.78 (m, 2H, CH_2CHN), 1.37 (m, 36 H, $\text{C}(\text{CH}_3)_3$), 1.18 (t, $J = 7.2$ Hz, 3H, $\text{COOCH}_2\text{CH}_3$)

¹³C-NMR (75 MHz, CDCl₃) δ 173.12 (COOBz), 172.63 (COOEt), 170.42 (COOtBu), 135.9 (CH₂C(Ar)), 128.46, 128.08, 128.03 (Ar), 80.71 (C(CH₃)₃), 65.99 (OCH₂Ar), 62.66 (COOCH₂CH₃), 60.11 (CH), 55.84 (NCH₂COOtBu), 53.60, 50.10 (NCH₂CH₂N), 30.73 (CH₂COOBz), 28.03 (C(CH₃)₃), 24.70 (CHCH₂CH₂), 14.30 (COOCH₂CH₃)

ESI(+)-MS *m/z* calcd for C₄₂H₇₀N₃O₁₂ [M+H]⁺: 808.50, found: 808.9 [M+H]⁺, 830.6 [M+Na]⁺

PC1. 4-(bis(2-(bis(2-(tert-butoxy)-2-oxoethyl)amino)ethyl)amino)-5-ethoxy-5-oxopentanoic acid



To a solution of **4.6** (221 mg, 0.27 mmol) in dry methanol (10 mL), Pd/C (30 mg) was added and the suspension was hydrogenated for 6 hours. After filtration through Celite, the filtrate was evaporated under vacuum giving the product as a yellow oil.

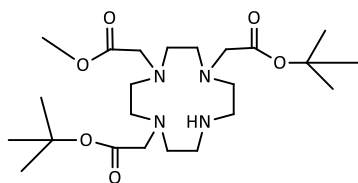
Yield: 88.9% (172 mg, 0.24 mmol)

¹H-NMR (300 MHz, CDCl₃) δ 4.21-4.09 (m, 3H, CH, COOCH₂CH₃), 3.43 (s, 8H, NCH₂COOtBu), 2.82 (m, 8H, NCH₂CH₂N), 2.62 (m, 2H, CH₂COOH), 2.08-1.97 (m, 2H, CH₂CHN), 1.41 (m, 36 H, C(CH₃)₃), 1.23 (t, *J* = 6.0 Hz, 3H, COOCH₂CH₃)

¹³C-NMR (75 MHz, CDCl₃) δ 175.36 (COOH), 171.14 (COOEt), 170.25 (COOtBu), 81.22 (C(CH₃)₃), 62.93 (COOCH₂CH₃), 60.83 (CH), 55.42 (NCH₂COOtBu), 52.14, 49.83 (NCH₂CH₂N), 31.15 (CH₂COOH), 27.84 (C(CH₃)₃), 23.54 (CHCH₂CH₂), 13.95 (COOCH₂CH₃)

ESI(+)-MS *m/z* calcd for C₃₅H₆₄N₃O₁₂ [M+H]⁺: 718.45, found: 718.7 [M+H]⁺, 740.6 [M+Na]⁺

4.7. di-tert-butyl 2,2'-(4-(2-methoxy-2-oxoethyl)-1,4,7,10-tetraazacyclododecane-1,7-diyl)diacetate



To a solution of 300 mg (0.749 mmol) of di-tert-butyl 2,2'-(1,4,7,10-tetraazacyclododecane-1,7-diyl)diacetate (DO2AtBu) in dry acetonitrile (5 mL) cooled to 0°C, 76.5 mg (0.5 mmol) of methyl 2-bromoacetate in dry acetonitrile (4 mL) was added dropwise. The reaction was stirred for 48 hours at room temperature and concentrated under vacuum. The crude product was purified by column chromatography on silica gel (CH₂Cl₂:MeOH, 9:1) yielding 4.7 as a pale yellow oil.

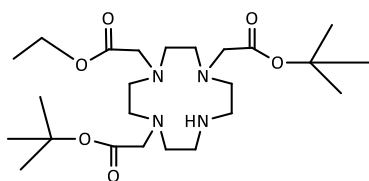
Yield: 77.0% (182 mg, 0.38 mmol)

¹H NMR (300 MHz, CDCl₃) δ 9.72 (br, 1H, NH), 3.61 (s, 3H, COOCH₃), 3.31-2.12 (m, 22H, NCH₂, NCH₂COOtBu, NCH₂COOMe, NHCH₂), 1.36 (s, 18H, C(CH₃)₃)

¹³C NMR (75 MHz, CDCl₃) δ 173.2 (COOMe), 170.7 (COOtBu), 82.5 (C(CH₃)₃), 58.0, 55.9, 54.7, 52.1, 49.2, 47.5 (NCH₂CH₂N, NCH₂CH₂NH, CH₂COOMe, CH₂COOCH₃, CH₂COOtBu), 28.3 (C(CH₃)₃)

ESI(+)-MS *m/z* calcd for C₂₃H₄₅N₄O₆ [M+H]⁺: 473.33, found: 495.3 [M+Na]⁺

4.8. di-tert-butyl 2,2'-(4-(2-ethoxy-2-oxoethyl)-1,4,7,10-tetraazacyclododecane-1,7-diyl)diacetate



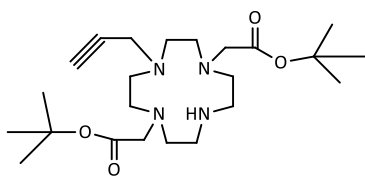
A solution of 500 mg (1.25 mmol) of DO2AtBu in 5 mL of dry acetonitrile was cooled at 0°C. To this solution, ethyl bromoacetate (92 μL, 0.832 mmol) and K₂CO₃ (115 mg, 0.83 mmol) were added. The reaction was left under stirring overnight at room temperature. After filtration, the solvent was evaporated from the filtrate and the crude was purified on silica gel using CH₂Cl₂:MeOH in a 95:5 proportion. The purified product was obtained as a pale yellow oil.

Yield: 65.1% (263 mg, 0.54 mmol)

¹H-NMR (300 MHz, CDCl₃) δ 9.88 (br, 1H, NH), 4.11 (q, *J* = 7.2 Hz, 2H, NCH₂COOCH₂CH₃), 3.40-2.74 (m, 22H, NCH₂COOtBu, NCH₂COOCH₂CH₃, NCH₂CH₂N, CH₂NHCH₂), 1.39 (s, 16 H, C(CH₃)₃), 1.21 (t, *J* = 7.2 Hz, 3H, NCH₂COOCH₂CH₃)

ESI(+)-MS *m/z* calcd for C₂₄H₄₇N₄O₆ [M+H]⁺: 487.35, found 487.3 [M+H]⁺

4.9. di-tert-butyl 2,2'-(4-(2-ethoxy-2-oxoethyl)-1,4,7,10-tetraazacyclododecane-1,7-diyl)diacetate



A solution of 400 mg (0.99 mmol) of DO2AtBu in dry acetonitrile (15 mL) was cooled to 0°C. To this solution, 92.5 μ L (0.83 mmol) of propargyl bromide (80 wt.%) in 5 mL of dry acetonitrile were added dropwise over 10 min and the reaction was left at room temperature for 48 hours. After evaporating the solvent, the crude product was purified by column chromatography (silica gel) using CH₂Cl₂:CH₃OH (9:1). The purified product was obtained as a yellow oil after evaporation under vacuum.

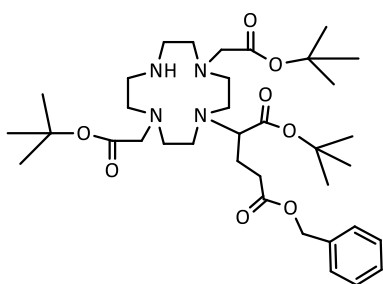
Yield: 68.7% (252 mg, 0.57 mmol)

¹H-NMR (300 MHz, CDCl₃) δ 3.41 (d, J = 2.1 Hz, 2H, CH₂CCH), 3.35 (s, 4H, CH₂COOtBu), 3.17-2.66 (m, 16H, NCH₂CH₂N, CH₂NHCH₂), 2.19 (t, J = 2.3 Hz, 1H, (CCH), 1.44 (s, 16 H, C(CH₃)₃)

¹³C-NMR (75 MHz, CDCl₃) δ 170.8 (COOC(CH₃)₃), 81.99 (C(CH₃)₃), 76.69 (CCH), 74.63 (CCH), 58.81 (CH₂COOtBu), 51.50, 50.32, 49.57, 48.14 (8C, CH₂NHCH₂, CH₂NCH₂), NCH₂CH₂N, CH₂COOtBu), 35.79 (NCH₂CCH), 28.48 (C(CH₃)₃)

ESI(+)-MS m/z calcd for C₂₃H₄₃N₄O₄ [M+H]⁺: 439.33, found 439.5 [M+H]⁺

4.10. 5-benzyl 1-tert-butyl 2-(4,10-bis(2-(tert-butoxy)-2-oxoethyl)-1,4,7,10-tetraazacyclododecan-1-yl)pentanedioate



To a solution of 294 mg (0.73 mmol) of DO2AtBu in dry acetonitrile (5 mL) was added dropwise 200 mg (0.66 mmol) of **2.3** in dry acetonitrile (2 mL). To this solution, 100 mg (0.73 mmol) of K₂CO₃ were added and the reaction was stirred for 18 hours at room temperature under inert atmosphere. The reaction mixture was then filtered and the acetonitrile was evaporated in the rotatory evaporator. The crude product was purified on a silica gel column using CH₂Cl₂/MeOH (9:1). The purified product was obtained as a colourless oil.

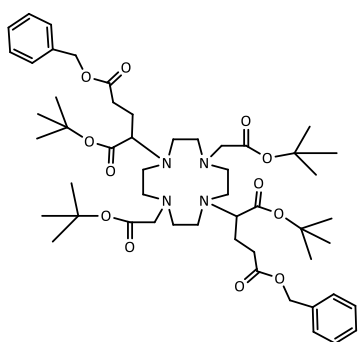
Yield: 13.4% (60 mg, 0.09 mmol)

¹H-NMR (300 MHz, CDCl₃) δ 9.21 (br, 1H, NH), 7.34 (m, 5H, Ar), 5.12 (s, 2H, CH₂-Ph), 3.33-1.92 (m, 26 H, CHN, NHCH₂, NCH₂, CH₂COOBz, CHNCH₂CH₂, CH₂COOC(CH₃)₃), 1.42 (s, 27 H, C(CH₃)₃)

$^{13}\text{C-NMR}$ (75 MHz, CDCl_3) δ 172.8 (COOBz), 171.3, 170.2 (COOC(CH₃)₃), 135.8 (CH₂C(Ar)), 128.54, 128.31, 128.24 (Ar), 82.09, 81.56 (C(CH₃)₃), 66.46 (OCH₂Ar), 60.68, 56.30, 51.42, 50.59, 49.50, 46.27 (12C, CH₂NHCH₂, HCNCH₂, NCH₂CH₂N, CH₂COOtBu), 30.67 (CH₂COOBz), 28.22, 28.13 (C(CH₃)₃), 27.72 (NHCHCH₂CH₂)

ESI(+)-MS m/z calcd for C₃₆H₆₁N₄O₈ [M+H]⁺: 677.45, found: 677.6 [M+H]⁺

4.11. 5-dibenzyl 1-di-tert-butyl 2,2'-(4,10-bis(2-(tert-butoxy)-2-oxoethyl)-1,4,7,10-tetraazacyclododecane-1,7-diyl)dipentanedioate



To a solution of 242 mg (0.60 mmol) of DO2AtBu in dry acetonitrile (10 mL), 648 mg (1.81 mmol) of 5-benzyl 1-*tert*-butyl 2-bromopentanedioate and 166 mg (1.2 mmol) of K₂CO₃. The mixture was stirred for 48 hours at 50°C under inert atmosphere. After filtration, the solvent was evaporated and the crude was purified on silica gel using CH₂Cl₂:MeOH (9:1). After evaporating the solvents under vacuum, the product was

obtained as a pale-yellow oil.

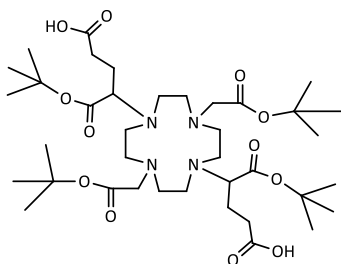
Yield: 41.2% (235 mg, 0.25 mmol)

$^1\text{H-NMR}$ (300 MHz, CDCl_3) δ 7.27 (m, 10H, Ar), 5.08 (s, 4H, CH₂-Ph), 3.28-2.05 (m, 30 H, CHN, NCH₂, CH₂COOBz, CHNCH₂CH₂, CH₂COOtBu), 1.38 (s, 36 H, C(CH₃)₃)

$^{13}\text{C-NMR}$ (75 MHz, CDCl_3) δ 172.8 (COOBz), 171.3, 170.3 (COOC(CH₃)₃), 135.8 (CH₂C(Ar)), 128.57, 128.33, 128.28 (Ar), 82.41, 82.08 (C(CH₃)₃), 66.49 (OCH₂Ar), 59.85, 56.28, 52.49, 50.69, 49.58, 46.35 (14C, HCNCH₂, NCH₂CH₂N, CH₂COOtBu, CH₂COOBzl), 32.46 (NCHCH₂CH₂), 28.24, 28.16 (C(CH₃)₃)

ESI(+)-MS m/z calcd for C₅₂H₈₁N₄O₁₂ [M+H]⁺: 953.59, found: 953.9 [M+H]⁺, 976.0 [M+Na]⁺

PC2. 2-(4,10-bis(2-(tert-butoxy)-2-oxoethyl)-7-(1-(tert-butoxy)-4-carboxy-1-oxobutan-2-yl)-1,4,7,10-tetraazacyclododecan-1-yl)pentanedioic acid



235 mg (0.25 mmol) of **4.11** was dissolved in dry methanol and 20 mg of Pd/C were added. The suspension was hydrogenated for 8 hours and then filtered over Celite. The solvent was evaporated under vacuum and the product was obtained as a colourless oil.

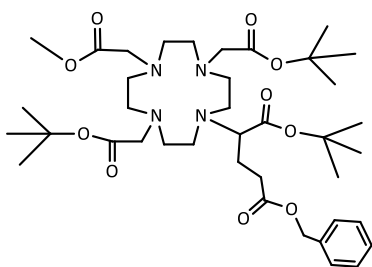
Yield: 88.0% (157 mg, 0.22 mmol)

¹H-NMR (300 MHz, CD₃OD) δ 3.52-2.50 (m, 30 H, CHN, NCH₂, CH₂COOH, CHNCH₂CH₂, CH₂COOC(CH₃)₃), 1.56 (s, 18 H, C(CH₃)₃), 1.47 (s, 18 H, C(CH₃)₃)

¹³C-NMR (75 MHz, CD₃OD) δ 176.7 (COOH), 174.7, 173.1 (COOC(CH₃)₃), 86.30, 83.46, (C(CH₃)₃) 61.70, 59.66, 56.75, 54.59, 52.30, 46.19, 43.76 (14C, NCHCOOtBu, NCH₂CH₂N, CH₂COOtBu, CH₂COOH), 32.05 (NCHCH₂CH₂), 28.75, 28.66 (C(CH₃)₃)

ESI(+)-MS *m/z* calcd for C₃₈H₆₉N₄O₁₂ [M+H]⁺: 773.49, found 796.5 [M+Na]⁺

4.12. 5-benzyl 1-tert-butyl 2-(4,10-bis(2-(tert-butoxy)-2-oxoethyl)-7-(2-methoxy-2-oxoethyl)-1,4,7,10-tetraazacyclododecan-1-yl)pentanedioate



136 mg (0.38 mmol) of **2.3** was added to a suspension of **4.7** (150 mg, 0.32 mmol) and dry K₂CO₃ (100 mg, 0.73 mmol) in dry acetonitrile (10 mL). The reaction was heated to 50.°C and stirred for 48 hours. The reaction mixture was filtered and the filtrate was concentrated under vacuum. The crude product was purified by column chromatography on silica gel

(CH₂Cl₂:MeOH, 95:5) yielding the compound as a yellow oil.

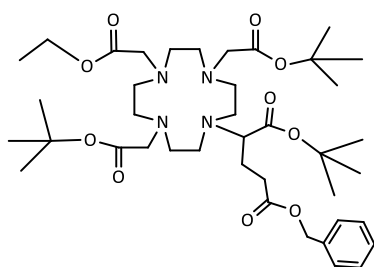
Yield: 70.0% (167 mg, 0.22 mmol)

¹H NMR (300 MHz, CDCl₃) δ 7.30 (m, 5H, Ar), 5.04 (s, 2H, CH₂Ph), 3.64 (s, 3H, COOCH₃) 3.4-1.9 (m, 27H, NCH₂, CH₂COOBzl, NCH₂COOMe, NCH, NCHCH₂CH₂, CH₂COOBz), 1.42 (s, 27H, C(CH₃)₃)

^{13}C NMR (75 MHz, CDCl_3) δ 174.9 (COOBzl) 174.3 (COOMe), 173.4, 173.0 (COOtBu), 135.4 ($\text{CH}_2\text{C}(\text{Ar})$), 128.8, 128.6, 128.5 ($\text{C}(\text{Ar})$) 82.5, 82.1 ($\text{C}(\text{CH}_3)_3$), 66.6 (OCH_2Ar) 60.2, 56.1, 54.8, 56.2, 53.1, 52.7, 51.2, 49.0, 48.5, 47.4, 44.6 ($\text{NCH}_2\text{CH}_2\text{N}$, CH_2COOMe , $\text{CH}_2\text{COOCH}_3$, CH_2COOtBu , CH_2COOBzl , NCH), 32.7 ($\text{NCHCH}_2\text{CH}_2$), 28.1, 27.9 ($\text{C}(\text{CH}_3)_3$)

ESI(+)-MS m/z calcd for $\text{C}_{39}\text{H}_{65}\text{N}_4\text{O}_{10}$ $[\text{M}+\text{H}]^+$: 749.47, found: 749.6 $[\text{M}+\text{H}]^+$, 771.8 $[\text{M}+\text{Na}]^+$, 787.5 $[\text{M}+\text{K}]^+$

4.13. 5-benzyl 1-tert-butyl 2-(4,10-bis(2-(tert-butoxy)-2-oxoethyl)-7-(2-methoxy-2-oxoethyl)-1,4,7,10-tetraazacyclododecan-1-yl)pentanedioate



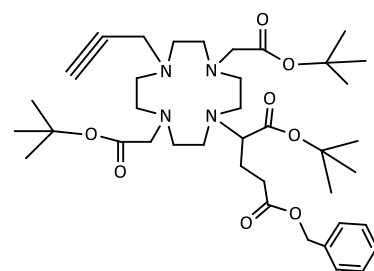
To a solution of 263 mg (0.54 mmol) of **4.8** in dry acetonitrile (5mL), **2.3** (232 mg, 0.65 mmol) was added dropwise at 0°C . The mixture was left stirring for 48 hours at room temperature. After filtration and solvent evaporation, the crude was purified by column chromatography on silica gel (CH_2Cl_2 :MeOH, 9:1). The product was obtained as a yellow oil.

Yield: 75.9% (310 mg, 0.41 mmol)

^1H -NMR (300 MHz, CDCl_3) δ 7.32 (m, 5H, Ar), 5.07 (s, 2H, CH_2 -Ph), 4.10 (m, 2H, $\text{NCH}_2\text{COOCH}_2\text{CH}_3$), 3.53-1.96 (m, 27H, $\text{NCH}_2\text{COOtBu}$, $\text{NCH}_2\text{COOCH}_2\text{CH}_3$, $\text{NCH}_2\text{CH}_2\text{N}$, CHN, NCH_2 , CH_2COOBzl , $\text{CHNCH}_2\text{CH}_2$, CH_2COOtBu), 1.41 (m, 27H, $\text{C}(\text{CH}_3)_3$), 1.24 (t, $J = 5.4$ Hz, 3H, $\text{NCH}_2\text{COOCH}_2\text{CH}_3$)

ESI(+)-MS m/z calcd for $\text{C}_{40}\text{H}_{67}\text{N}_4\text{O}_{10}$ $[\text{M}+\text{H}]^+$: 763.49, found 785.3 $[\text{M}+\text{Na}]^+$

4.14. 5-benzyl 1-tert-butyl 2-(4,10-bis(2-(tert-butoxy)-2-oxoethyl)-7-(prop-2-yn-1-yl)-1,4,7,10-tetraazacyclododecan-1-yl)pentanedioate



252 mg (0.57 mmol) of **4.9** were dissolved in dry acetonitrile (5 mL). To the solution, 306 mg (0.86 mmol) of **2.3** were added along with 118 mg (0.86 mmol) of K_2CO_3 . The reaction was left under nitrogen at room temperature for 48 hours. After filtration and solvent evaporation, the crude product was purified through a silica gel column (CH_2Cl_2 :MeOH, 95:5). The

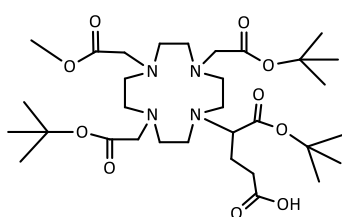
compound was obtained as a yellow oil.

Yield: 49.1% (198 mg, 0.28 mmol)

¹H-NMR (300 MHz, CDCl₃) δ 7.32 (m, 5H, Ar), 5.07 (s, 2H, CH₂-Ph), 3.47-1.85 (m, 30H, NCH₂COOtBu, CH₂CCH, CCH, NCH₂CH₂N, CHN, NCH₂, CH₂COOBzl, CHNCH₂CH₂, CH₂COOtBu), 1.42 (m, 27H, C(CH₃)₃)

ESI(+)-MS *m/z* calcd for C₃₉H₆₃N₄O₈ [M+H]⁺: 715.46, found 715.5 [M+H]⁺, 737.5 [M+Na]⁺

PC3. 4-(4,10-bis(2-(tert-butoxy)-2-oxoethyl)-7-(2-methoxy-2-oxoethyl)-1,4,7,10-tetraaza-cyclododecan-1-yl)-5-(tert-butoxy)-5-oxopentanoic acid



167 mg (0.22 mmol) of **4.12** was dissolved in methanol (20 mL) and 20 mg of Pd/C was added. The mixture was hydrogenated for 1 day, filtered through celite and the filtrate was concentrated using a rotary evaporator providing **PC3** as pale yellow oil.

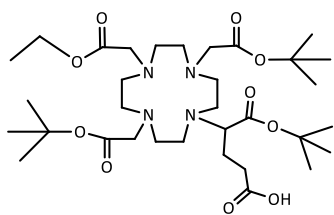
Yield: 86.0% (125 mg, 0.19 mmol)

¹H-NMR (300 MHz, CDCl₃) δ 3.68 (s, 3H, COOCH₃) 3.6-1.9 (m, 27H, NCH₂, CH₂COOH, CH₂COOMe, NCH, NCHCH₂CH₂), 1.43 (m, 27H, C(CH₃)₃)

¹³C-NMR (75 MHz, CDCl₃) δ 175.3 (COOH) 174.3 (COOMe), 173.9, 173.5, 173.3 (COOtBu), 82.8, 82.5, 82.4 (C(CH₃)₃), 60.3, 56.2, 54.9, 53.0, 52.2, 50.8, 48.9, 47.5, 44.5 (NCH₂CH₂N, CH₂COOMe, CH₂COOCH₃, CH₂COOtBu, CH₂COOH, NCH), 33.5 (NCHCH₂CH₂) 28.3, 28.2, 28.1 (C(CH₃)₃)

ESI(+)-MS *m/z* calcd for C₃₂H₅₉N₄O₁₀ [M+H]⁺: 659.42, found 659.5 [M+H]⁺, 681.4 [M+Na]⁺

PC4. 4-(4,10-bis(2-(tert-butoxy)-2-oxoethyl)-7-(2-ethoxy-2-oxoethyl)-1,4,7,10-tetraazacyclododecan-1-yl)-5-(tert-butoxy)-5-oxopentanoic acid



310 mg (0.41 mmol) of **4.13** were dissolved in methanol (10 mL) and Pd/C (30 mg) was added. The suspension was hydrogenated for 8 hours, after which the mixture was filtered over Celite. After evaporation under vacuum, the product was obtained as a yellow oil.

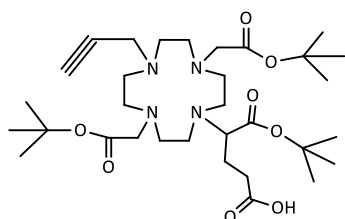
Yield: 93.0% (255 mg, 0.38 mmol)

¹H-NMR (300 MHz, CDCl₃) δ 4.12 (m, 2H, NCH₂COOCH₂CH₃), 3.55-1.89 (m, 27H, NCH₂COOtBu, NCH₂COOCH₂CH₃, NCH₂CH₂N, CHN, NCH₂, CH₂COOH, CHNCH₂CH₂, CH₂COOtBu), 1.39 (m, 27H, C(CH₃)₃), 1.21 (t, *J* = 6.9 Hz, 3H, NCH₂COOCH₂CH₃)

¹³C-NMR (75 MHz, CDCl₃) δ 175.35 (COOH), 173.45, 173.19, 173.12, 173.10 (COOtBu, COOEt), 82.70, 82.26, 82.21 (C(CH₃)₃), 61.43, 60.23, 56.08, 55.02, 52.93, 50.50, 48.82, 48.41, 47.35, 44.43 (13C, NCHCOOtBu, HCNCH₂, NCH₂CH₂N, CH₂COOtBu, CH₂COOEt, CH₂COOH), 33.39 (NCHCH₂CH₂), 28.17, 27.99 (C(CH₃)₃), 14.35 (COOCH₂CH₃)

ESI(+)-MS *m/z* calcd for C₃₃H₆₁N₄O₁₀ [M+H]⁺: 673.44, found 695.4 [M+Na]⁺

PC5.4-(4,10-bis(2-(tert-butoxy)-2-oxoethyl)-7-(prop-2-yn-1-yl)-1,4,7,10 tetraazacyclododecan-1-yl)-5-(tert-butoxy)-5-oxopentanoic acid



100 mg (0.14 mmol) of **4.14** were dissolved in a mixture of THF (2 mL) and an aqueous solution of NaOH 0.5 M (1 mL). The mixture was left stirring for 6 hours at room temperature. After evaporation of THF under vacuum, the product was extracted

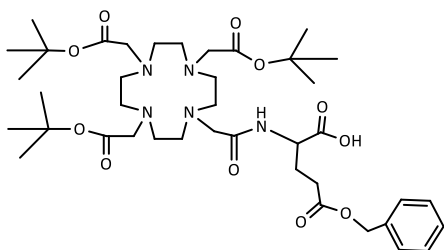
using water and CHCl₃. The organic phase was evaporated and the product was purified through a C18 Sep-Pak cartridge using as eluents water with increasing concentrations of acetonitrile (0, 20, 30, 50, 70, 100%). The product was eluted in the water:ACN (50:50) fraction. After lyophilization the product was obtained as a white powder.

Yield: 18.3% (16 mg, 0.03 mmol)

¹H-NMR (300 MHz, CDCl₃) δ 3.68-2.16 (m, 30H, NCH₂COOtBu, CH₂CCH, CCH, NCH₂CH₂N, CHN, NCH₂, CH₂COOH, CHNCH₂CH₂, CH₂COOtBu), 1.46 (m, 27H, C(CH₃)₃)

ESI(+)-MS *m/z* calcd for C₃₂H₅₇N₄O₈ [M+H]⁺: 625.42, found 625.8 [M+H]⁺, 647.5 [M+Na]⁺

PC6. 5-(benzyloxy)-5-oxo-2-(2-(4,7,10-tris(2-(tert-butoxy)-2-oxoethyl)-1,4,7,10-tetraaza-cyclododecan-1-yl)acetamido)pentanoic acid



200 mg (0.25 mmol) of DOTA-tris(tBu)ester NHS ester were dissolved in dry DMF (5 mL). To the solution, L-glutamic acid 5-benzylester (64 mg, 0.27 mmol) and DIPEA (85 μ L, 0.49 mmol) were added. The reaction was left at room temperature under nitrogen and was followed by HPLC until completion. After DMF

evaporation under vacuum, the crude product was extracted using water and CHCl_3 . The organic phase was evaporated under vacuum, and the product was obtained as a pale yellow oil.

Yield: 91% (180 mg, 0.23 mmol)

Rt (HPLC, Method G) = 31.93 min

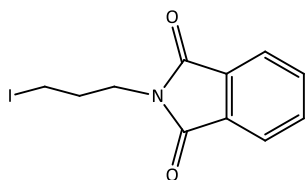
$^1\text{H-NMR}$ (300 MHz, CDCl_3) δ 7.31 (m, 5H, Ar), 5.06 (s, 2H, $\text{CH}_2\text{-Ph}$), 4.46 (dd, $J=12.6$ Hz, $J=6.3$ Hz, 1H, NHCH), 3.97-1.90 (m, 28 H, NCH_2 , CH_2COOBz , $\text{NHCHCH}_2\text{CH}_2$, CH_2COOtBu), 1.43 (m, 27 H, $\text{C}(\text{CH}_3)_3$)

$^{13}\text{C-NMR}$ (75 MHz, CDCl_3) δ 174.4 (COOH), 173.2 (COOBz), 170.9, 170.0 (COOtBu, CONH), 136.4 ($\text{CH}_2\text{C}(\text{Ar})$), 128.83, 128.41, 128.39 (Ar), 82.44, 81.94 ($\text{C}(\text{CH}_3)_3$), 66.48 (OCH_2Ar), 56.68, 56.05, 53.47, 52.88, 52.01, 50.57, 49.59, 47.95, 47.01, 44.12 (13C, HCNCH_2 , $\text{NCH}_2\text{CH}_2\text{N}$, CH_2COOtBu , CH_2COOBzl), 30.77 (CH_2COOBzl), 28.41, 28.37 ($\text{C}(\text{CH}_3)_3$), 27.35 ($\text{NHCHCH}_2\text{CH}_2$)

ESI(+)-MS m/z calcd for $\text{C}_{40}\text{H}_{66}\text{N}_5\text{O}_{11}$ $[\text{M}+\text{H}]^+$: 792.48, found 792.6 $[\text{M}+\text{H}]^+$

7.7. Synthesis and Characterization of Acridine Orange Derivatives

4.15. 2-(3-iodopropyl)isoindoline-1,3-dione



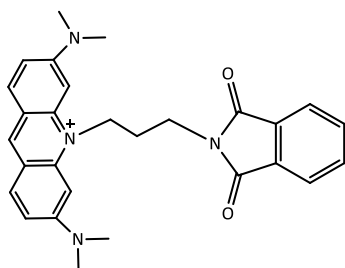
A suspension of 4.0 g (14.9 mmol) of N-(3-Bromopropyl)phthalimide and 4.2 g (25.4 mmol) of KI in dry acetone (20 mL) was heated to reflux and left stirring for 48 hours. After cooling, the mixture was filtered and the filtrate was evaporated under vacuum giving the

product as a brown powder.

Yield: 84.2 % (3.95 g, 12.5 mmol)

¹H-NMR (300 MHz, CDCl₃) δ 7.74-7.59 (m, 4H, Ar), 3.64 (t, *J*= 6.9 Hz, 2H, NCH₂), 3.06 (t, *J*= 7.2 Hz, 2H, CH₂I), 2.13 (quin, *J*= 6.9 Hz, 2H, CH₂)

4.16. 3,6-bis(dimethylamino)-10-(3-(1,3-dioxisoindolin-2-yl)propyl)acridin-10-ium

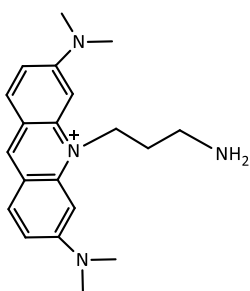


700 mg (2.64 mmol) of 3,6-Bis(dimethylamino)acridine (acridine orange base) were dissolved in dry *p*-xylene (15 mL). To this solution, 4.15 (1.0 g, 3.2 mmol) and K₂CO₃ (360 mg, 2.64 mmol) were added. The suspension was heated to reflux and left stirring for 5 days. After cooling, the mixture was filtered and the solid residue was washed twice with diethyl ether and further

dried under vacuum. The product was obtained as a dark brown powder.

Yield: 99.2 % (1.19 g, 2.62 mmol)

¹H-NMR (300 MHz, CDCl₃) δ 8.67 (s, 1H, CH, Ar), 7.86 (d, *J*= 6.9 Hz, 2H, CH, Ar), 7.82-7.72 (m, 4H, CH, Ar), 7.00 (d, *J*= 6.9 Hz, 2H, CH, Ar), 6.51 (s, 2H, CH, Ar), 4.90 (t, *J*= 6.3 Hz, 2H, CH₂), 4.14 (t, *J*= 5.1 Hz, 2H, CH₂), 3.28 (s, 12H, CH₃), 2.32 (quin, *J*= 6.3 Hz, 2H, CH₂)

AO1. 10-(3-aminopropyl)-3,6-bis(dimethylamino)acridin-10-ium

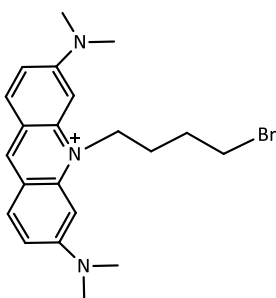
200 mg (0.44 mmol) of **4.16** was dissolved in dry methanol (5 mL). To this solution, 300 μ L (3.96 mmol) of hydrazine monohydrate (64%) were added and the solution was heated to reflux. The reaction was left for 48 hours and after cooling concentrated HCl (3 mL) was added and the mixture was stirred for 15 min leading to the formation of a precipitate.

The mixture was filtered and the pH of the filtrate was adjusted to 11 by adding an appropriate volume of a 3 M NaOH solution. After the basification, an extraction was performed using water and CHCl_3 . After extracting the product from the aqueous phase 3 times with CHCl_3 , the combined organic phases were evaporated under nitrogen to reduce the volume to 2 mL. Then, 20 mL of ice-cooled diethyl ether were added and the precipitate was isolated by centrifugation. After drying under vacuum, the product was obtained as a dark red powder.

Yield: 45.4 % (66 mg, 0.20 mmol)

$^1\text{H-NMR}$ (300 MHz, CD_3OD) δ 8.68 (s, 1H, CH, Ar), 7.93 (d, J = 6.9 Hz, 2H, CH, Ar), 7.29 (d, J = 6.9 Hz, 2H, CH, Ar), 6.79 (s, 2H, CH, Ar), 4.81 (t, J = 6 Hz, 2H, CH_2), 3.36 (s, 12H, CH_3), 3.03 (t, J = 5.1 Hz, 2H, CH_2), 2.17 (quin, J = 6.1 Hz, 2H, CH_2)

ESI(+)-MS m/z calcd for $[\text{C}_{20}\text{H}_{27}\text{N}_4]^+$: 323.22, found: 323.3 $[\text{M}]^+$

AO2. 10-(4-bromobutyl)-3,6-bis(dimethylamino)acridin-10-ium

Acridine orange free base (100 mg, 0.38 mmol) was dissolved in dry toluene (10 mL) and 1,4-dibromobutane (1 mL, 8.44 mmol) was added. The mixture was heated to reflux and was left reacting for 24 hours. After cooling, 20 mL of toluene were added and the precipitate was filtered. The residue was washed with toluene and with toluene with a few drops of ammonia and then dissolved in CH_2Cl_2 . To this

solution hexane was added until a precipitate formed. A few drops of ammonia were added and the mixture was stirred for 10 min. The precipitate was isolated and dried under vacuum giving the product as a dark orange powder.

Yield: 63.1 % (96 mg, 0.24 mmol)

$^1\text{H-NMR}$ (300 MHz, CDCl_3) δ 8.46 (s, 1H, CH, Ar), 7.77 (d, J = 9.3 Hz, 2H, CH, Ar), 7.05 (d, J = 9.3 Hz, 2H, CH, Ar), 6.53 (s, 2H, CH, Ar), 4.63 (t, J = 6.3 Hz, 2H, CH_2), 3.68 (t, J = 6.0 Hz, 2H, CH_2), 3.36 (s, 12H, CH_3), 2.27-2.03 (m, 4H, CH_2)

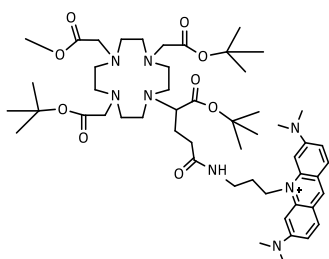
$^{13}\text{C-NMR}$ (75 MHz, CDCl_3) δ 155.67, 142.82, 142.64, 133.11, 116.99, 114.12 (CH(Ar), C(Ar), CN(CH₃)₂), 92.58 (NCH₂), 40.72 (CH₃), 34.13, 29.40, 23.81 (CH₂)

7.8. Synthesis and Characterization of Macrocyclic Prochelators with Acridinium Pendant Arms

General procedure for the conjugation of AO1 to the carboxylic acid-containing macrocycles: PC3, PC4, PC5, DOTAGA(tBu)₄

AO1 (92 mg, 0.28 mmol) was dissolved in dry DMF (5 mL) and DIPEA (100 μL , 0.58 mmol) was added. This solution was stirred for 1 hour. In a separate flask, HATU (76 mg, 0.20 mmol) and DIPEA (70 μL , 0.40 mmol) were added to a solution of the prochelator (0.19 mmol) in dry DMF (5 mL). The activation reaction proceeded for 10 minutes and then this solution was added to the first solution. The mixture was stirred for 12 hours and after that time the same amounts of HATU and DIPEA were added. The progress of the reaction was monitored by HPLC (Method G) and ESI-MS. After additional 24 hours the volatiles were removed and the crude was extracted from water to chloroform (3x). The organic phase was concentrated under vacuum and reserved for the next step.

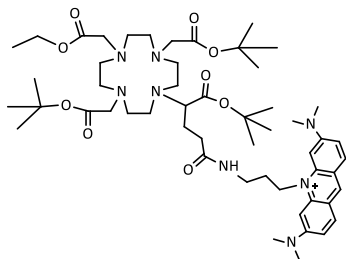
PC3-AO. 10-(3-(4-(4,10-bis(2-(tert-butoxy)-2-oxoethyl)-7-(2-methoxy-2-oxoethyl)-1,4,7,10-tetraaza-cyclododecan-1-yl)-5-(tert-butoxy)-5-oxopentanamido)propyl)-3,6-bis(dimethyl-amino)acridin-10-ium



Rt (HPLC, Method G) = 29.6 min

ESI(+)-MS m/z calcd for $[\text{C}_{52}\text{H}_{83}\text{N}_8\text{O}_9]^+$: 963.63, found: 963.4 $[\text{M}]^+$

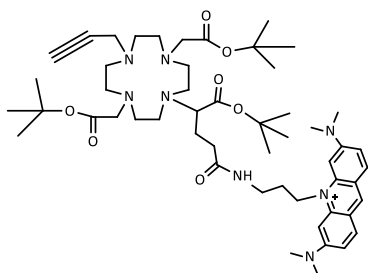
PC4-AO. 10-(3-(4-(4,10-bis(2-(tert-butoxy)-2-oxoethyl)-7-(2-ethoxy-2-oxoethyl)-1,4,7,10-tetraazacyclododecan-1-yl)-5-(tert-butoxy)-5-oxopentanamido)propyl)-3,6-bis(dimethylamino)acridin-10-ium



Rt (HPLC, Method G) = 31.2 min

ESI(+)-MS m/z calcd for $[C_{53}H_{85}N_8O_9]^+$: 977.64, found: 977.5 $[M]^+$

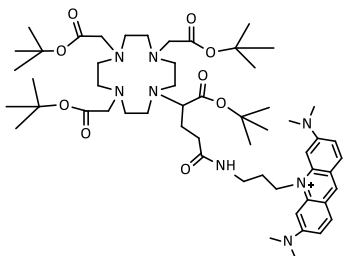
PC5-AO. 10-(3-(4-(4,10-bis(2-(tert-butoxy)-2-oxoethyl)-7-(prop-2-yn-1-yl)-1,4,7,10-tetraazacyclododecan-1-yl)-5-(tert-butoxy)-5-oxopentanamido)propyl)-3,6-bis(dimethylamino)acridin-10-ium



Rt (HPLC, Method G) = 30.4 min

ESI(+)-MS m/z calcd for $[C_{52}H_{81}N_8O_7]^+$: 929.62, found: 929.6 $[M]^+$

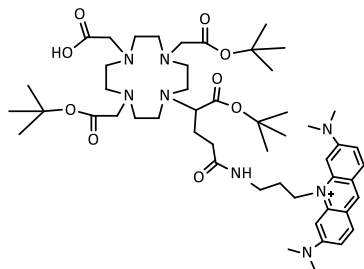
DOTAGA(tBu)₄-AO. 10-(3-(5-(tert-butoxy)-5-oxo-4-(4,7,10-tris(2-(tert-butoxy)-2-oxoethyl)-1,4,7,10-tetraazacyclododecan-1-yl)pentanamido)propyl)-3,6-bis(dimethylamino)acridin-10-ium



Rt (HPLC, Method G) = 31.9 min

ESI(+)-MS m/z calcd for $[C_{55}H_{89}N_8O_9]^+$: 1005.67, found: 1005.8 $[M]^+$

PC7-AO. 10-(3-(4-(4,10-bis(2-(tert-butoxy)-2-oxoethyl)-7-(carboxymethyl)-1,4,7,10-tetraazacyclododecan-1-yl)-5-(tert-butoxy)-5-oxopentanamido)propyl)-3,6-bis(dimethylamino)acridin-10-ium



PC3-AO was redissolved in 7 mL of THF:MeOH:water (3:2:2) and 23 mg (0.95 mmol) of LiOH was added. The reaction mixture was stirred for 5 hours at room temperature and the progress was monitored by HPLC. After the reaction was completed, the crude was concentrated under vacuum. The product was purified by a Sep-Pak C18 cartridge using 0.1% of

TFA in water and increasing concentrations of ACN with 0.1% TFA (0 – 70%). The fractions containing the product (eluted with 40% of ACN 0.1% TFA) were combined and after lyophilization, the desired compound was obtained as a dark orange powder.

Yield: 24 % (43 mg, 0.04 mmol)

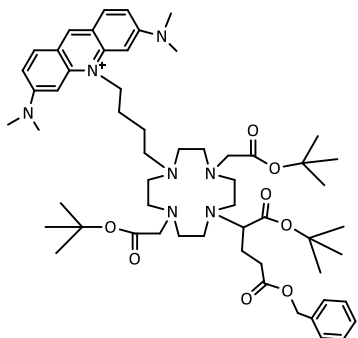
Rt (HPLC, Method G) = 26.1 min

¹H-NMR (300 MHz, CD₃OD) δ 8.75 (s, 1H, CH, Ar), 7.99 (d, *J*=9.0 Hz, 2H, CH, Ar), 7.35 (d, *J*=9.0 Hz, 2H, CH, Ar), 6.78 (s, 2H, CH, Ar), 4.78 (t, *J*=9.0 Hz, 2H, CH₂NCC), 3.6-1.9 (m, 43H, N(CH₃)₂, COONCH₂CH₂, NCH₂, CH₂COOH, NCH₂COOMe, NCH, NCHCH₂CH₂), 1.45 (m, 27H, C(CH₃)₃)

¹³C-NMR (75 MHz, CDCl₃) δ 176.4 (COOH) 174.8 (COONH), 173.6, 170.8, 170.5 (COOtBu), 156.42, 142.92, 133.41, 129.12, 114.17 (CH(Ar), C(Ar), CN(CH₃)₂), 92.58 (NCH₂), 82.1, 79.2 (C(CH₃)₃), 61.02, 56.4, 55.12, 53.63, 52.65, 49.13, 48.02 (NCHCOOtBu, HCNCH₂, NCH₂CH₂N, CH₂COOtBu, CH₂COOH), 41.0 (N(CH₃)₂), 36.5, 30.3, 29.7, 26.5 (CONHCH₂, NCHCH₂CH₂, NCHCH₂CH₂), 28.72, 28.70 (C(CH₃)₃), 26.5 (CH₂CH₂CH₂)

ESI(+)-MS *m/z* calcd for [C₅₁H₈₁N₈O₉]⁺ : 949.61, found 949.7 [M]⁺, 971.6 [M + Na]⁺

PC8-AO. 10-(4-(7-(5-(benzyloxy)-1-(tert-butoxy)-1,5-dioxopentan-2-yl)-4,10-bis(2-(tert-butoxy)-2-oxoethyl)-1,4,7,10-tetraazacyclododecan-1-yl)butyl)-3,6-bis(dimethylamino)-acridin-10-ium



AO2 (120 mg, 0.30 mmol) and **4.10** (200 mg, 0.30 mmol) were dissolved in dry DMF (5 mL) in the presence of 164 mg (1.18 mmol) of K_2CO_3 and the mixture was heated at 60°C. The reaction was left stirring under nitrogen for 48 hours. After cooling, the mixture was filtrated to remove the solids and the solvent was evaporated from the filtrated under vacuum. The crude product was purified by column chromatography (silica

gel) using a mixture of CH_2Cl_2 and EtOH (from 95:5 to 80:20). The product was obtained as a dark orange oil.

Yield: 18.9 % (57 mg, 0.057 mmol)

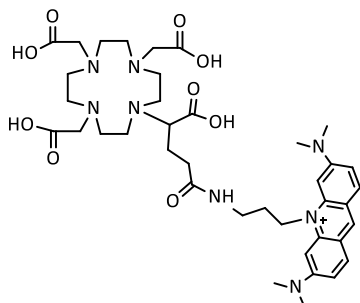
1H -NMR (300 MHz, $CDCl_3$) δ 8.52 (s, 1H, CH, Ar), 7.81 (d, J = 9.3 Hz, 2H, CH, Ar), 7.29 (m, 5H, Ar(Bz)), 7.05 (d, J = 9.0 Hz, 2H, CH, Ar), 6.56 (s, 2H, CH, Ar), 5.05 (s, 2H, CH_2 -Ph(Bz)), 4.76 (t, J = 7.5 Hz, 2H, CH_2), 3.78 (m, 2H, CH_2), 3.26 (s, 12H, CH_3), 3.33-1.92 (m, 30H, CH_2CH_2 , $CHCHN$, NCH_2 , CH_2COOBz , $CHNCH_2CH_2$, $CH_2COOC(CH_3)_3$), 1.40 (m, 27 H, $C(CH_3)_3$)

^{13}C -NMR (75 MHz, $CDCl_3$) δ 174.6 ($COOBz$), 174.1, 172.8 ($COOC(CH_3)_3$), 155.36, 142.93, 142.22 ($CH(Ar)$, $C(Ar)$, $CN(CH_3)_2$), 135.54 ($CH_2C(Ar)$, Bz), 133.11 ($CH(Ar)$), 128.57, 128.40, 128.26 (Ar, Bz), 116.88, 113.81 ($CH(Ar)$), 92.64 ($(Ar)NCH_2$), 82.96, 82.46, 82.11 ($C(CH_3)_3$), 66.38 (OCH_2Ar), 59.95, 57.58, 56.05, 53.18, 50.41, 47.01, 44.14 (12C, CH_2NHCH_2 , $HCNCH_2$, NCH_2CH_2N , $CH_2COOtBu$), 41.14 ($N(CH_3)_2$), 32.00 (CH_2COOBz), 27.82, 27.78, 27.75 ($C(CH_3)_3$), 24.02, 21.71, 19.17 (CH_2)

ESI(+)-MS m/z calcd for $[C_{57}H_{86}N_7O_8]^+$: 996.65, found: 996.8 $[M]^+$, 499.0 $[M+H]^{2+}$

7.9. Synthesis and Characterization of DOTAGA-AO and [In]DOTAGA-AO

DOTAGA-AO. 10-(3-(4-carboxy-4-(4,7,10-tris(carboxymethyl)-1,4,7,10-tetraazacyclododecan-1-yl)butanamido)propyl)-3,6-bis(dimethylamino)acridin-10-ium



The crude product of **DOTAGA(tBu)₄-AO** was treated with neat TFA (4 mL) and the mixture was stirred for 24 hours at room temperature. The volatiles were then removed under vacuum and the residue redissolved in a 1:1 mixture of ACN:water. The product was then purified by semi-preparative HPLC (Method SP4), and after lyophilization the compound was obtained as a

dark orange powder.

Yield: 31.0 % (46 mg, 0.059 mmol)

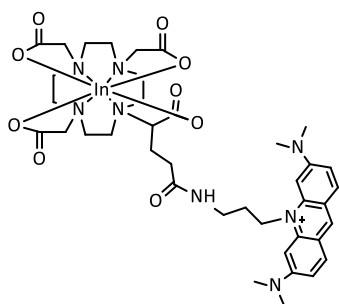
Rt (HPLC, Method G) = 16.4 min

¹H-NMR (400 MHz, CD₃OD) δ 8.68 (s, 1H, CH, Ar), 7.93 (d, *J* = 8.8 Hz, 2H, CH, Ar), 7.29 (d, *J* = 8.8 Hz, 2H, CH, Ar), 6.71 (s, 2H, CH, Ar), 4.73 (t, *J* = 7.6 Hz, 2H, CH₂), 4.21-1.82 (m, 25H, CH₂COOH, NCH₂CH₂N, NCH, CH₂CH₂CONH, CH₂CH₂), 3.35 (s, 12H, CH₃)

¹³C-NMR (75 MHz, CDCl₃) δ 173.81-173.92 (COOH), 172.2 (CONH), 156.12, 143.04, 142.73, 133.06, 117.19, 114.24 (CH(Ar), C(Ar), CN(CH₃)₂), 92.14 (NCH₂), 53.8 (CH), 51.62-50.51 (CH₂COOH), 48.31, 48.09, 47.88, 47.66, 47.45, 45.13, 45.08 (CH₂), 39.48 (N(CH₃)₂), 36.67, 32.56, 25.78, 25.67 (CH₂)

ESI(+)-MS *m/z* calcd for [C₃₉H₅₇N₈O₉]⁺: 781.42, found: 781.9 [M]⁺

[In]DOTAGA-AO



10 mg (0.013 mmol) of **DOTAGA-AO** were mixed with 4.0 mg (0.018 mmol) of anhydrous InCl₃ in a sodium acetate buffer (0.5 M) pH= 5. The solution was heated at 95°C for 25 min. After cooling, the mixture was purified by semi-preparative HPLC (Method SP4). After lyophilization, the complex was obtained as a dark orange powder.

Yield: 75.1 % (8 mg, 0.009 mmol)

Rt (HPLC, Method G) = 16.5 min

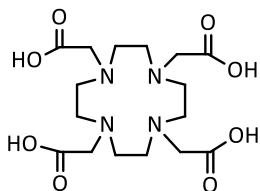
¹H-NMR (300 MHz, CD₃OD) δ 8.68 (s, 1H, CH, Ar), 7.91 (d, *J* = 8.8 Hz, 2H, CH, Ar), 7.28 (d, *J* = 8.8 Hz, 2H, CH, Ar), 6.72 (s, 2H, CH, Ar), 4.78 (m, 2H, CH₂), 3.92-1.25 (m, 25H, CH₂COO, NCH₂CH₂N, NCH, CH₂CH₂CONH, CH₂CH₂), 3.35 (s, 12H, CH₃)

¹³C-NMR (75 MHz, DMSO-d₆) δ 171.32-169.31 (COOH, CONH), 155.32, 141.04, 140.73, 132.16, 117.10, 114.21 (CH(Ar), C(Ar), CN(CH₃)₂), 90.14 (NCH₂), 52.6 (CH), 50.51-48.23 (CH₂COOH), 48.31, 47.99, 43.88, 46.66, 46.26, 45.10, 44.06 (CH₂), 38.42 (N(CH₃)₂), 35.67, 32.56, 25.28, 24.21 (CH₂)

ESI(+)-MS *m/z* calcd for C₃₉H₅₄InN₈O₉ [M+H]⁺: 894.31, found: 894.6 [M+H]⁺

7.10. Synthesis and Characterization of DOTA

DOTA. 1,4,7,10-tetraazacyclododecane-1,4,7,10-tetraacetic acid



DOTA-tris(tBu)ester (15 mg, 0.026 mmol) was treated with neat TFA (1 mL) for 24 hours at room temperature. After evaporating under vacuum, the product was washed with diethyl ether and obtained as a white powder.

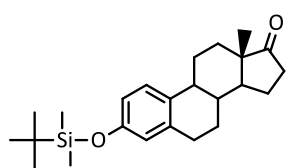
Yield: 92.3 % (10 mg, 0.024 mmol)

¹H-NMR (300 MHz, D₂O) δ 3.92 (CH₂COOH), 3.56 (NCH₂CH₂N)

ESI(+)-MS *m/z* calcd for C₁₆H₂₈N₄O₈ [M+H]⁺: 405.20, found 405.5 [M+H]⁺

7.11. Synthesis and Characterization of Estradiol Derivatives

4.17.3-[(*tert*-Butyldimethylsilyl)oxy]estra-1,3,5(10)-trien-17-one

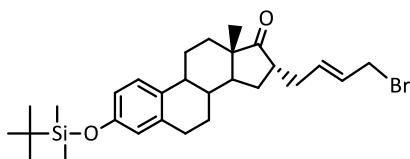


Estrone (0.8 g, 2.96 mmol) and imidazole (605 mg, 8.9 mmol) were dissolved in 4 mL of dry DMF and *tert*-butyldimethylsilyl chloride (TBDMS-Cl, 670 mg, 4.45 mmol) was added. The reaction was stirred at room temperature and after 2 hours 20 mL of ethyl acetate were added. The solution was washed with water (3 times) and then dried with Na₂SO₄. After solvent removal, the product was obtained as a white powder.

Yield: 97.1 % (1.1 g, 2.88 mmol)

¹H-NMR (300 MHz, CDCl₃) δ 7.13 (d, *J* = 8.4 Hz, H1), 6.64 (dd, *J* = 8.4 Hz, *J* = 2.7 Hz, H2), 6.58 (d, 1H, *J* = 2.4 Hz, H4), 2.83-1.44 (m, 15H), 0.99 (s, 9H, C(CH₃)₃), 0.93 (s, 3H, CH₃, C18), 0.20 (s, 6H, Si(CH₃)₂)

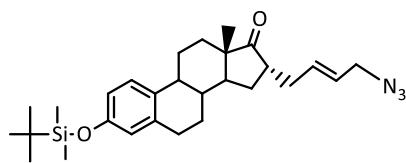
4.18. 16 α -(4-Bromo-2-butenyl)-3-[(*tert*-butyldimethylsilyl)-oxy]estra-1,3,5(10)-trien-17-one



Dry THF (9 mL) and diisopropylamine (0.18 mL, 1.30 mmol) were combined under nitrogen and the solution was cooled to 0°C. *N*-butyllithium (0.72 mL of a 1.55 M hexane solution, 1.12 mmol) was added dropwise and the solution was stirred for 0.5 h at 0°C. **4.17** (474 mg, 1.23 mmol) was added and the stirring was continued at 0°C for 1 h. The solution was then cooled to -45°C, and *trans*-1,4-dibromo-2-butene (780 mg, 3.65 mmol) was added dropwise over 20 min. The reaction mixture was stirred at -45°C for 3 hours, then poured into water and extracted several times with ethyl acetate. After removing the solvent, the crude was purified through column chromatography (silica gel) using hexane:CHCl₃:ether (15:2:1). The product was obtained as a colourless oil.

Yield: 41.0 % (260 mg, 0.50 mmol)

¹H-NMR (300 MHz, CDCl₃) δ 7.09 (d, *J* = 8.4 Hz, H1), 6.60 (dd, *J* = 8.4 Hz, *J* = 2.4 Hz, H2), 6.55 (d, 1H, *J* = 2.4 Hz, H4), 5.75-5.71 (m, 2H, CHCH), 3.94-3.91 (m, 2H, CH₂Br), 2.83-1.40 (m, 15H), 0.95 (s, 9H, C(CH₃)₃), 0.93 (s, 3H, CH₃, C18), 0.17 (s, 6H, Si(CH₃)₂)

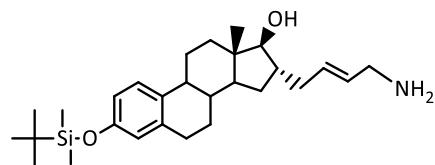
4.19. 16 α -(4-Azido-2-butenyl)-3-[(tert-butyldimethylsilyl)-oxy]estra-1,3,5(10)-trien-17-one

4.18 (260 mg, 0.50 mmol) was combined with NaN₃ (315 mg, 4.85 mmol) and dissolved in a mixture of DMSO (30 mL), THF (12 mL) and water (2 mL). The mixture was stirred at room temperature for 18 h and then poured into 500 mL of

water and extracted several times with CH₂Cl₂. The organic phase was dried with Na₂SO₄ and after evaporation under vacuum, the residue was filtered through silica gel (eluting with CH₂Cl₂) providing the compound as a yellow oil which solidified on standing.

Yield: 98.0 % (236 mg, 0.49 mmol)

¹H-NMR (300 MHz, CDCl₃) δ 7.08 (d, J = 8.4 Hz, H1), 6.60 (dd, J = 8.4 Hz, J = 2.4 Hz, H2), 6.55 (d, 1H, J = 2.4 Hz, H4), 5.70-5.55 (m, 2H, CHCH), 3.70 (d, J = 6.0 Hz, 2H, CH₂N₃), 2.83-1.38 (m, 15H), 0.96 (s, 9H, C(CH₃)₃), 0.94 (s, 3H, CH₃, C18), 0.17 (s, 6H, Si(CH₃)₂)

4.20. 16 α -(4-Amino-2-butenyl)-3-[(tert-butyldimethylsilyl)-oxy]estra-1,3,5(10)-trien-17 β -ol

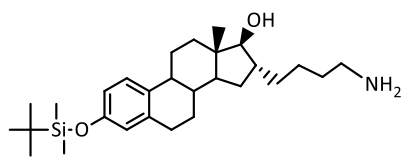
4.19 (236 mg, 0.49 mmol) was treated with LiAlH₄ (57 mg, 1.49 mmol) in 10 mL of dry THF cooled to -78°C. The reaction was stirred for 1 h at this temperature and then the mixture was warmed to -10°C and stirred for

additional 3 h. The reaction was quenched with water and then poured into brine and extracted several times with CH₂Cl₂. The organic phase was dried with Na₂SO₄ and the solvent was removed under vacuum giving the desired compound as a yellow oil.

Yield: 95.1 % (200 mg, 0.44 mmol)

¹H-NMR (300 MHz, CDCl₃) δ 7.09 (d, J = 8.4 Hz, H1), 6.60 (dd, J = 8.4 Hz, J = 2.4 Hz, H2), 6.55 (d, 1H, J = 2.4 Hz, H4), 5.92-5.54 (m, 2H, CHCH), 3.74 (d, J = 6.6 Hz, 17 α H), 3.34-2.81 (m, 2H, CH₂NH₂), 2.79-1.81 (m, 15H), 0.96 (s, 9H, C(CH₃)₃), 0.79 (s, 3H, CH₃, C18), 0.17 (s, 6H, Si(CH₃)₂)

ESI(+)-MS m/z calcd for C₂₈H₄₆NO₂Si [M+H]⁺: 456.33, found: 456.7 [M+H]⁺

E2-1. 16 α -(4-Aminobutyl)-3-[(tert-butyldimethylsilyl)-oxy]estra-1,3,5(10)-trien-17 β -ol

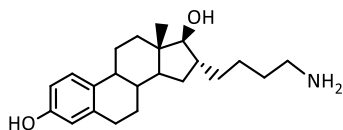
85 mg (0.19 mmol) of **4.20** was dissolved in dry methanol (15 mL) and 15 mg of Pd/C was added. The mixture was hydrogenated for 12 hours, filtered over Celite and evaporated to dryness under vacuum. The product was obtained as a pale yellow oil.

Yield: 86.6% (74 mg, 0.16 mmol)

Rt (HPLC, Method G) = 42.4 min

¹H-NMR (300 MHz, CD₃OD) δ 7.12 (d, J = 8.4 Hz, H1), 6.57 (dd, J = 8.4 Hz, J = 2.4 Hz, H2), 6.51 (d, 1H, J = 2.4 Hz, H4), 3.22 (d, J = 7.8 Hz, 17 α H), 2.93 (t, J = 7.5 Hz, 2H, CH₂NH₂), 2.84-1.21 (m, 15H), 0.96 (s, 9H, C(CH₃)₃), 0.79 (s, 3H, CH₃, C18), 0.17 (s, 6H, Si(CH₃)₂)

ESI(+)-MS m/z calcd for C₂₈H₄₈NO₂Si [M+H]⁺: 458.35, found: 458.5 [M+H]⁺

E2-2. 16 α -(4-Aminobutyl)-estra-1,3,5(10)-trien-3,17 β -diol

50 mg (0.11 mmol) of **E2-1** were dissolved in a solution of methanol containing 2% of HCl. The mixture was stirred at room temperature for 6 hours. The solvent was then evaporated and the residue was extracted with water and ethyl acetate. The organic phase was evaporated under vacuum and the product was obtained as a yellow oil.

Yield: 73.6 % (28 mg, 0.08 mmol)

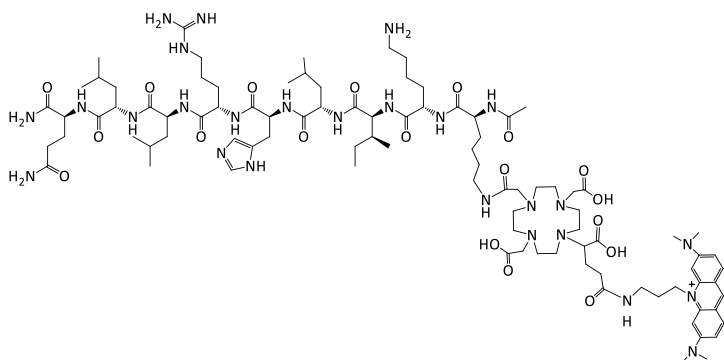
Rt (HPLC, Method G) = 29.6 min

¹H-NMR (300 MHz, CD₃OD) δ 7.06 (d, J = 8.4 Hz, H1), 6.54 (dd, J = 8.4 Hz, J = 2.4 Hz H2), 6.48 (d, 1H, J = 2.4 Hz, H4), 3.22 (d, J = 7.8 Hz, 17 α H), 2.94 (t, J = 7.5 Hz, 2H, CH₂NH₂), 2.77-1.21 (m, 15H), 0.81 (s, 3H, CH₃, C18)

ESI(+)-MS m/z calcd for C₂₂H₃₄NO₂ [M+H]⁺: 344.26, found: 344.5 [M+H]⁺

7.12. Synthesis and Characterization of the Dual-targeting Conjugates and In(III) Complexes

ER3AO



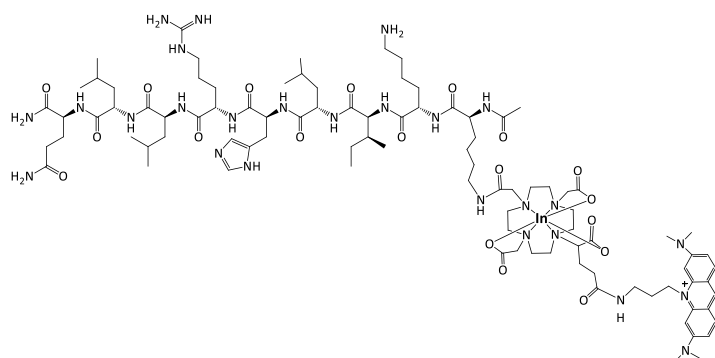
5.0 mg (5.27 μmol) of **PC7-AO** was dissolved in 2 mL of dry DMF. 5.0 mg (13.15 μmol) of HATU and 4.5 μL (26.0 μmol) of DIPEA were added to the solution. After stirring for 15 minutes 12 mg (6.10 μmol) of **ER3prot** peptide was added. The

reaction mixture was left stirring for 18 hours at room temperature and the reaction was followed by HPLC. After removing the volatiles under vacuum, 3 mL of a TFA:water:TIS (95:2.5:2.5) mixture was added to the solid residue and stirred for 12 hours at room temperature. 30 mL of ice-cooled diethyl ether were added to the mixture forming a dark orange precipitate that was isolated by centrifugation. The precipitate was redissolved in a water:ACN (3:1) solution and was purified by semi-preparative HPLC (Method SP3). The desired conjugate was identified by ESI-MS. After lyophilization, **ER3AO** was obtained as a light orange powder (4 mg, 39% yield)

Yield: 39.0 % (4.0 mg, 2.06 μmol)

Rt (HPLC, Method G) = 29.9 min

ESI(+)-MS m/z calcd for $[\text{C}_{94}\text{H}_{155}\text{N}_{26}\text{O}_{19}]^+$: 1952.20, found: 977.1 $[\text{M}+\text{H}]^{2+}$, 651.9 $[\text{M}+2\text{H}]^{3+}$, 489.3 $[\text{M}+3\text{H}]^{4+}$

[In]ER3AO

1.0 mg (0.51 μmol) of **ER3AO** was dissolved in 0.5 mL of 0.1 M sodium acetate buffer pH 5.5 and 0.5 mg (2.26 μmol) of InCl_3 was added. The solution was heated to 95°C and the reaction was left to proceed for 30 min. The

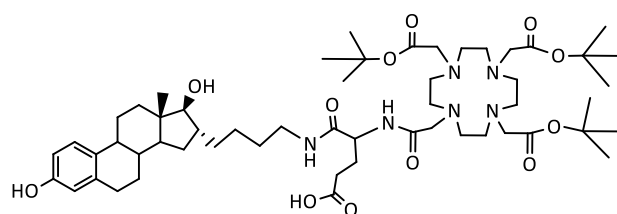
mixture was purified by semi-preparative HPLC (Method SP3) and the complex identified by ESI-MS. After lyophilisation the compound was obtained as a light orange powder.

Yield: 88.0 % (0.9 mg, 0.45 μmol)

Rt (HPLC, Method G) = 30.6 min

ESI(+)-MS m/z calcd for $[\text{C}_{94}\text{H}_{152}\text{InN}_{26}\text{O}_{19}]^+$: 2064.09, found: 1033.1 $[\text{M}+\text{H}]^2$

PC9-E2. 5-((4-(3,17 β -dihydroxyestra-1,3,5(10)-trien-16-yl)butyl)amino)-5-oxo-4-(2-(4,7,10-tris(2-(tert-butoxy)-2-oxoethyl)-1,4,7,10-tetraazacyclododecan-1-yl)acetamido)pentanoic acid



40 mg (0.05 mmol) of **PC6** was dissolved in 5 mL of dry DMF and 29 mg (0.08 mmol) of HATU followed by 26 mL (0.15 mmol) of DIPEA. The mixture was stirred for 5 minutes until the addition of 20 mg

(0.06 mmol) of **E2-2**. The reaction was left stirring for 48 hours and after evaporating the volatiles under vacuum, the crude product was extracted from water to chloroform. The organic phase was evaporated and the residue was dissolved in 10 mL of methanol. To this solution, 20 mg of Pd/C were added and the mixture was hydrogenated for 8 hours. The suspension was then filtered through Celite and the filtrate was evaporated. The residue was then purified through a C-18 Sep-Pak Cartridge by elution with water containing increasing percentages of acetonitrile (increments of 10%). The collected fractions were analysed by HPLC (Method G) and by TLC (silica, CH_2Cl_2 :MeOH 9:1, revelation with 5% H_2SO_4 in ethanol) and the fraction containing the desired conjugate was identified by ESI-MS. After lyophilization, **PC9-E2** was obtained as a pale yellow powder.

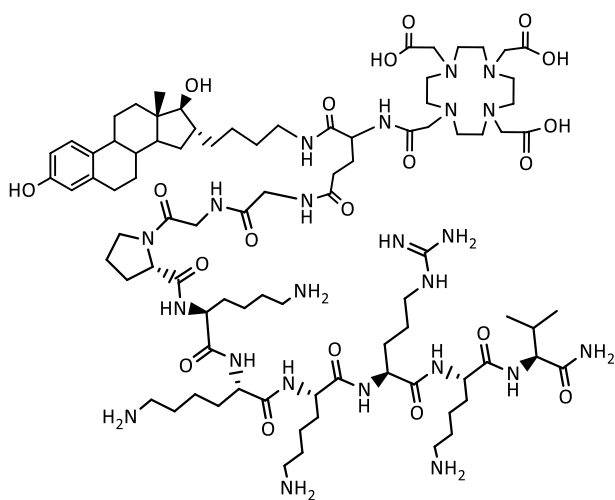
Yield: 24.2 % (13 mg, 0.012 mmol)

Rt (HPLC, Method G) = 30.6 min

¹H-NMR (300 MHz, CD₃OD) δ 7.07 (d, *J* = 8.7 Hz, H1), 6.53 (dd, *J* = 8.4 Hz, *J* = 2.4 Hz, H2), 6.48 (d, 1H, *J* = 2.4 Hz, H4), 4.38 (m, 1H, NHCH), 3.20 (d, *J* = 7.5 Hz, H17α), 3.98-1.21 (m, 43H), 1.47 (m, 27 H, C(CH₃)₃), 0.80 (s, 3H, CH₃, C18)

ESI(+)-MS *m/z* calcd for C₅₅H₉₁N₆O₁₂ [M+H]⁺: 1027.67, found: 1027.4 [M+H]⁺

E2NLS



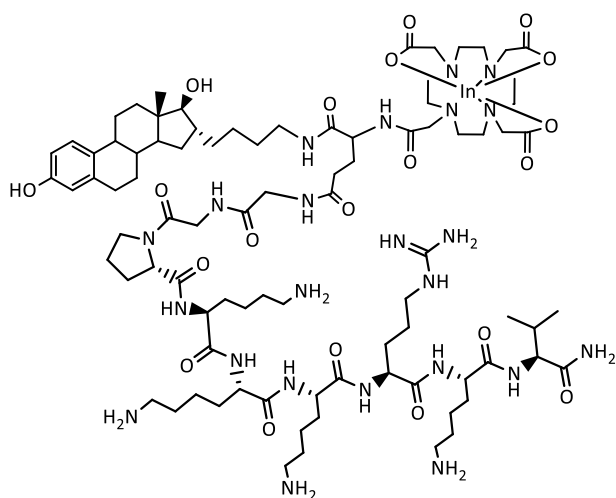
To 13 mg (0.012 mmol) of **PC9-E2** in dry DMF (3 mL), HATU (9 mg, 0.024 mmol) and DIPEA (8 mL, 0.048 mmol) were added. The mixture was stirred for 2 min and **GGNLS** (25 mg, 0.015 mmol) in 0.5 mL of DMF was added. The reaction was stirred for 24 hours after which the volatiles were removed under vacuum and the crude product was washed with water. The residue was treated with the mixture (5 mL) of 95% TFA,

2.5% TIS and 2.5% water, for 12 hours. After evaporating the TFA to reduce the volume in approximately 50%, 25 mL of ice-cooled diethyl ether were added to the mixture forming a white precipitate that was isolated by centrifugation. The precipitate was redissolved in water:acetonitrile (3:1) and was purified by HPLC (Method SP2). After lyophilization, **E2NLS** was obtained as a white powder.

Yield: 12.1 % (2.6 mg, 1.45 μmol)

Rt (HPLC, Method G) = 18.16 min

ESI(+)-MS *m/z* calcd for C₈₇H₁₄₅N₂₃O₂₀ [M+H]⁺: 1832.10, found: 919.7 [M+2H]²⁺

[In]E2NLS

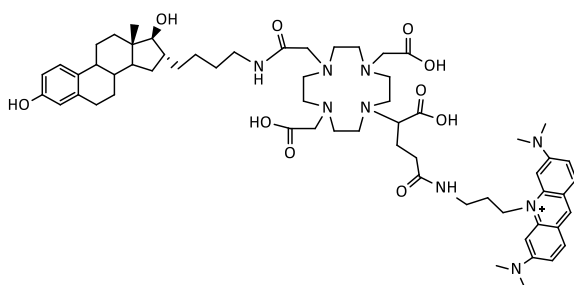
1.0 mg (0.54 μmol) of **E2NLS** was dissolved in 0.5 mL of 0.1 M sodium acetate buffer pH 5.5 and 0.5 mg (2.26 μmol) of InCl_3 was added. The solution was heated to 95°C and the reaction was left to proceed for 30 min. The mixture was purified by semi-preparative HPLC (Method SP2) and the complex identified by ESI-MS. After lyophilization the compound was obtained as a light orange powder.

Yield: 94.4 % (1.0 mg, 0.51 μmol)

Rt (HPLC, Method K) = 18.27 min

ESI(+)-MS m/z calcd for $\text{C}_{87}\text{H}_{147}\text{InN}_{23}\text{O}_{20}$ $[\text{M}+\text{H}]^+$: 1949.02, found: 975.7 $[\text{M}+\text{H}]^{2+}$

E2AO. 10-(3-(4-(4,10-bis(carboxymethyl)-7-(2-((4-(3,17 β -dihydroxyestra-1,3,5(10)-trien-16-yl)butyl)amino)-2-oxoethyl)-1,4,7,10-tetraazacyclododecan-1-yl)-4-carboxybutanamido)-propyl)-3,6-bis(dimethylamino)acridin-10-ium



To 55 mg (0.06 mmol) of **PC7-AO** in 5 mL of dry DMF, HATU (35 mg, 0.09 mmol) and DIPEA (0.12 mmol, 21 μL) were added. The mixture was stirred for 5 minutes and **E2-2** (30 mg, 0.09 mmol) was added. The reaction was stirred for 24 hours and additional

amounts of HATU (35 mg) and DIPEA (21 μL) were added. The mixture was left stirring for additional 72 hours and the volatiles were removed under vacuum. The crude product was washed with water and the solid residue was treated with 40% of TFA in CH_2Cl_2 (10 mL) for 12 hours. After solvent removal, the product was redissolved in a mixture of water:acetonitrile (3:1) and purified by HPLC (Method SP4). After lyophilization of the purified fraction, E2AO was obtained as a dark orange powder.

Yield: 8.3 % (5.0 mg, 4.5 μmol)

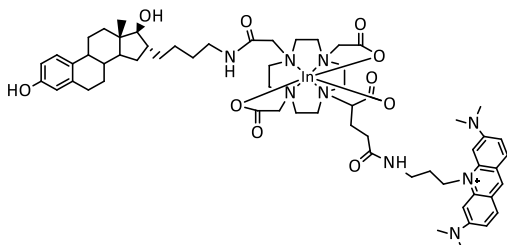
Rt (HPLC, Method H) = 11.7 min

$^1\text{H-NMR}$ (300 MHz, CD_3OD) δ 8.69 (s, 1H, CH, Ar), 7.93 (d, $J=9.3$ Hz, 2H, CH, Ar), 7.35 (d, $J=9.0$ Hz, 2H, CH, Ar), 7.04 (d, $J=8.4$ Hz, 1H, H1), 6.70 (s, 2H, CH, Ar), 6.51 (d, 1H, $J=2.4$ Hz, H4), 4.74 (br, 2H, CH_2NCC), 3.33 (s, 12H, CH_3), 3.87-0.98 (m, 62H), 0.76 (s, 3H, CH_3 , C18)

$^{13}\text{C-NMR}$ (75 MHz, CDCl_3) δ 173.20 - 173.09 (COOH, CONH), 157.52, 155.8, 145.18, 144.09, 138.8, 134.24, 132.7, 127.2, 118.19, 116.04, 115.18, 113.7, (CH(Ar), C(Ar), $\text{CN}(\text{CH}_3)_2$, C1-C6 steroid ring), 94.07 (NCH₂), 88.88 (C17), 52.69-50.44 (CH_2COOH), 48.31, 48.09, 47.88, 47.66, 47.45, 45.39, 45.23, 45.08, 45.13, 45.08, 44.0, 40.79, 40.29 (CH_2), 40.55 ($\text{N}(\text{CH}_3)_2$), 38.12, 36.67, 36.60, 32.56, 31.07, 30.69, 28.49, 27.48, 27.23, 26.82, 25.67, 22.76 (CH_2), 12.59 (C18)

ESI(+)-MS m/z calcd for $[\text{C}_{61}\text{H}_{88}\text{N}_9\text{O}_{10}]^+$: 1106.66, found: 1106.6 $[\text{M}]^+$

[In]E2AO



2.0 mg (1.8 μmol) of **E2AO** were mixed with 0.5 mg (2 μmol) of anhydrous InCl_3 in a 0.5 M sodium acetate buffer with pH 5. The solution was heated at 95°C for 25 min. After cooling, the mixture was purified by HPLC (Method J). After lyophilization, the complex was obtained as a dark orange powder.

Yield: 88.6 % (1.9 mg, 1.6 μmol)

Rt (HPLC, Method H) = 11.9 min

$^1\text{H-NMR}$ (300 MHz, DMSO-d_6) δ 8.73 (s, 1H, CH, Ar), 7.95 (d, $J=9.3$ Hz, 2H, CH, Ar), 7.31 (d, $J=9.0$ Hz, 2H, CH, Ar), 6.99 (d, $J=8.4$ Hz, 1H, H1), 6.72 (s, 2H, CH, Ar), 6.41 (d, 1H, $J=2.4$ Hz, H4), 3.35 (s, 12H, CH_3), 3.99-0.97 (m, 62H), 0.67 (s, 3H, CH_3 , C18)

ESI(+)-MS m/z calcd for $[\text{C}_{61}\text{H}_{85}\text{InN}_9\text{O}_{10}]^+$: 1218.5, found: 609.9 $[\text{M}+\text{H}]^{2+}$

7.13. Evaluation of the *In Vitro* Stability of pY and DOTAGA-pY in Human Serum

2 mg of pY or DOTAGA-pY were incubated in 500 μ L of human serum at 37°C and aliquots (50 μ L) were taken at several time points and directly analysed by HPLC (Method D). To identify the degradation products, fractions were collected from the HPLC and analysed by ESI-MS after lyophilization.

7.14. Fluorescence Polarization Binding Assay

The determination of the binding affinity of the peptide-based ligands and complexes by Fluorescence Polarization was performed in collaboration with Professor Luc Brunsveld of Eindhoven University of Technology (TU/e).

A reaction mixture containing a fluorescein-labelled coactivator (Src1Box2) peptide (FL-CQLLTERHKILHRLQEGSPSD (100 nM), the ER α -LBD553 (500 nM) and 17 β -estradiol (5 μ M) was prepared. Fluorescence polarization inhibition experiments were performed in 384-well plates (Optiplate-384 F, Perkin Elmer) by adding 10 μ L of the reaction mixture to 40 μ L of peptides or peptides derivatives at increasing concentrations. After 1 h incubation at 4°C, the fluorescence polarization of the labelled coactivator peptide was measured on a plate reader (Safire2, Tecan) at room temperature with excitation at 485 nm and emission at 535 nm for fluorescein. The concentration of inhibitor peptide that resulted in a half-maximum decrease in the polarization value of the fluorescent coactivator peptide displayed from the purified ER was defined as IC₅₀ and was determined from 3-4 independent experiments.

7.15. Spectroscopic Studies of the Interaction of [In]DOTAGA-AO with DNA

These studies were performed with the collaboration of Dra. Isabel Correia from Centro de Química Estrutural (IST, Lisbon).

The DNA sodium salt from calf thymus (CT) DNA (1 mg, Sigma) was dissolved in PBS (10 mM, pH=7.2) (1 mL) for a few hours and then quantified per nucleotide, after adequate dilution with the buffer, by absorption spectroscopy at 260 nm ($\epsilon_{260\text{nm}} = 6600 \text{ M}^{-1} \text{ cm}^{-1}$).

The UV-vis spectra were recorded on a Perkin Elmer Lambda 35 UV-vis spectrometer, using quartz cuvettes (1 cm). To solutions of the In-complex or AO in PBS (ca. 65 μ M) increasing amounts of CT-DNA were added and after 1 min equilibration time the UV-Visible spectra between 300 and 700 nm were measured. Equivalent amounts of the CT-DNA solution were added to the reference (PBS) to eliminate possible interferences of DNA absorbance.

The fluorescence spectra were recorded on a Perkin Elmer LS 55 fluorescence spectrometer, using quartz cuvette (1 cm). After each addition of CT-DNA, the mixture was allowed to equilibrate and the absorption at the excitation wavelength was recorded. The In-complex was excited at ca. 505 nm and the emission spectra were recorded from 515 – 800 nm, with a scan speed of 300 nm min⁻¹. Emission and excitation slits were chosen in order to maximize the fluorescence intensity.

7.16. Study of the Interaction of [In]DOTAGA-AO with DNA by Electrophoretic Mobility Shift Assay

The plasmid DNA used was supercoiled ϕ X174 plasmid DNA (Promega). Each reaction mixture was prepared by adding water (6 mL), supercoiled DNA (2 mL, 200 ng), phosphate buffer solution (pH 7.2, 100 mM, 2 mL) and the solution of the In-complex or AO (10 mL). Samples were incubated for 24 h at 37°C in the dark. After incubation, DNA loading buffer (0.25% bromophenol blue, 0.25% xylene cyanol, 30% glycerol in water, AppliChem) was added to each tube and the sample was loaded onto an agarose gel (0.8%) in TAE buffer (Tri-acetate EDTA, AppliChem). Control of non-incubated plasmid was also loaded on the gel. The electrophoresis was carried out for 2h30 min at 90 V. After the run, the gel was stained with GelRed (Biotium) and visualized under UV light and digitally recorded using an Alphamager EP system (Alpha Innotech).

7.17. Radiolabelling Procedures

All procedures that involved the manipulation of non-sealed radioactive compounds were performed in laboratories licensed by the National Authority, Direcção Geral de Saúde, following the procedures approved within the radiation protection programme. Activities were measured in dose calibrator (Capintec CRC25R), or in a gamma counter (Berthold, LB2111, Germany) in the case of activities lower than 37 kBq (1 μ Ci).

7.17.1. Radiolabelling with In-111

Radiolabelling was achieved by the addition of 5 to 20 μ L of $^{111}\text{InCl}_3$ (3.6 MBq to 11.7 MBq) to 200 μ L of an acetate buffer solution (0.1M, pH 5.5) of the ligands in a plastic vial. Ligands were radiolabelled at a concentration of 1.0×10^{-5} M except for DTPA-pY which was radiolabelled at a concentration of 5.5×10^{-6} M.

The ^{111}In -labelling reactions were performed at 95°C for 25-30 min except for the pY-derivatives. In this regard, the DTPA-pY was radiolabelled at room temperature for 10 min while DOTAGA-pY was radiolabelled at 90°C for 10 min.

The radiochemical yield (RCY) and purity (RCP) were assessed by HPLC (γ -detection) taking into account that the uncoordinated In-111 was detected in the solvent front of the radiochromatograms (with a retention time of about 3.1 min). ITLC-SG was used to assess the presence of colloidal species. All radioactive complexes were obtained with RCYs higher than 90%. Whenever necessary (if the RCP was lower than 95%), the radiolabelled ligands were purified by HPLC or by solid phase extraction (using a Sep-Pak C18 cartridge) before being evaluated. The chemical identity of the radiolabelled products was assessed by a co-injection with the corresponding inactive In(III) complexes in the same HPLC method.

The characterization of the ^{111}In -complexes by HPLC is summarized on Table 7.1.

Table 7.1. Characterization of ^{111}In -labelled conjugates.

Complex	HPLC	
	Rt (min)	Method
$[^{111}\text{In}]\text{DOTA-cER1}$	23.08	B
$[^{111}\text{In}]\text{DOTA-ER2}$	21.02	B
$[^{111}\text{In}]\text{DOTA-ER3}$	19.78	B
$[^{111}\text{In}]\text{DTPA-pY}$	13.58	B
$[^{111}\text{In}]\text{DOTAGA-AO}$	22.02	I
$[^{111}\text{In}]\text{ER3AO}$	27.92	I
$[^{111}\text{In}]\text{E2NLS}$	19.07	I
$[^{111}\text{In}]\text{E2AO}$	11.96	J

7.17.2. Radiolabelling of ER3 with I-125

Peptide ER3 (20 μg , 43.5 nmol) in water (20 μL) was radioiodinated by sequentially adding 9.25-33.3 MBq of Na^{125}I and a solution of chloramine-T (50 μg , 178 nmol) in phosphate buffer 0.1 M pH=7.4 (10 μL). The reaction was allowed to proceed for 60 s with constant mixing at room temperature before being quenched by addition of a solution of sodium metabisulphite (50 μg , 263 nmol) in phosphate buffer 0.1 M pH=7.4 (50 μL). The radiochemical yield was determined by HPLC (Method F) and by ITLC-SG using 75% of methanol in water as mobile phase (in this system the radioiodinated peptide is detected in the application point while the free ^{125}I is detected at the solvent front).

The radioiodination mixture was purified on a C_{18} Sep-Pak column using 2-4 mL of water to discard free radioiodine. The ^{125}I -labelled peptide was then recovered using 2-4 mL of methanol containing 0.1% of TFA as eluent. The fractions corresponding to the radioiodinated peptide were evaporated under a nitrogen stream to remove the organic solvents and the product was reconstituted in saline solution containing 2% of DMSO and kept at 4°C. Quality control of the purified radioiodinated peptide was performed by HPLC (Method F) and the chemical identity of $[^{125}\text{I}]\text{-ER3}$ was determined by a co-injection with the inactive $[\text{I}]\text{-ER3}$.

[¹²⁵I]ER3

Rt (HPLC, Method F) = 11.23 min

7.18. In Vitro Stability Studies with the Radiolabelled Compounds

The in vitro stability of the radiolabelled probes reported in this thesis was evaluated after incubation in different media by analysing by HPLC aliquots taken at different time points.

Saline/PBS 0.1 M/Cell Culture Medium: radioactive complexes (50 μ L) were incubated in the medium (500 μ L) at 37°C and aliquots were taken at several time points and analysed by HPLC.

Human serum: radioactive complexes (50 μ L) were incubated with human serum (500 μ L) at 37°C. Aliquots (100 μ L) were taken at different time points and treated with cold ethanol (200 μ L) to induce protein precipitation. Samples were centrifuged at 3000 rpm for 10 min. The supernatants were separated from the *pellets* and analysed by HPLC.

Transchelation to apo-transferrin: 50 μ L of the radioactive complexes were added to a solution of apo-transferrin (3 mg/mL in acetate buffer 0.1 M pH=5) and incubated at 37°C. Aliquots of the solution were analysed by HPLC at different time points.

Transchelation to DTPA: 50 μ L of the radioactive complexes were added to a solution of DTPA (0.1 M in acetate buffer pH=5) and incubated at 37°C. Aliquots of the solution were analysed by HPLC at different time points.

7.19. Lipophilicity Determination

The octanol-water partition coefficient ($P_{o/w}$) of the radioactive complexes were determined by the “shakeflask” method [220]. The radiolabelled conjugate (20 μ L) was added to a mixture of saline (1 mL) and 1-octanol (1 mL) previously saturated in each other by vigorous stirring. The mixture was vortexed and centrifuged (3000 rpm, 10 min, RT) to allow phase separation. After phase separation, an aliquot of the aqueous layer was transferred to another tube and further extracted with 1-octanol. Aliquots (100 μ L) of both octanol and saline phases were counted in a gamma counter and the radioactive ratio between the phases ($P_{o/w}$) was calculated and results expressed as $\log P_{o/w}$.

7.20. Cellular Uptake Studies

Two human breast cancer cell lines from *American Type Culture Collection* (ATCC, Spain) were used in these studies, namely MCF-7 cell line that express ER and MDA-MB-231 without ER expression. Cells were grown in DMEM medium (Gibco), supplemented with 10% fetal bovine serum and 1% penicillin/streptomycin under a humidified 5% CO₂ atmosphere. For the studies, cells were plated at a density of approximately 2×10^5 cells per well in 24-well tissue culture plates in DMEM medium without phenol red and supplemented with 10% charcoal-stripped fetal bovine serum and 1% penicillin/streptomycin. After 24 h, the medium was removed and replaced by fresh medium containing approximately 5×10^5 cpm/0.5mL of the ¹¹¹In/¹²⁵I-compound. After 15 min to 4 h incubation in humidified 5% CO₂ atmosphere at 37°C, the cells were washed twice with cold PBS, lysed with 0.1M NaOH and the cellular extracts were counted for radioactivity in a gamma-counter. Each experiment was performed in quadruplicate. Radioactivity associated to the cell extracts at each time point was expressed as the percentage of the total activity added to the cells or normalized per million of cells, and reported as an average plus the standard deviation.

7.21. Cellular Fractionation Studies

MCF-7 breast cancer cells (3.0×10^6) were incubated with [¹¹¹In]DOTA-ER3 (0.8 MBq) for 1 hour at 37°C. Cells were washed with phosphate buffer saline (PBS), detached with trypsin-EDTA and centrifuged at 1000 rpm for 5 minutes at 4°C to obtain a cellular pellet. After two washing steps with 500 µL PBS, the cytosol, membrane/particulate, nuclear and cytoskeletal fractions were separated using a FractionPREP Cell Fractionation kit (Biovision, USA) according to the manufacture's protocol. Cellular fractions were counted for radioactivity in a gamma-counter and results were expressed as % of the total radioactivity associated with the cell.

7.22. Nuclear Uptake

MCF-7 cells were seeded at a density of 1 million per well in 6 well-plates and allowed to attach overnight. The cells were incubated at 37 °C for a period of 15 min, 1 h and 3 h with about approximately 148 kBq (4 µCi) of the ¹¹¹In/¹²⁵I-compound in 1.8 mL of assay medium

(DMEM without phenol red supplemented with charcoal stripped bovine fetal serum). At each giving time, cells in radioactive media were removed from the plates by scrapping and collected into a 2 mL Eppendorf tube. The unbound radioactive compound was removed by centrifugation of the cell suspension at 210 g for 3 min at 4°C, followed by washing the cellular pellet with ice-cold PBS with 0.2% BSA. The activity of cellular pellet was measured, using a gamma counter, to quantify the total cellular uptake of the radiocompound. The pellet was then resuspended in 1.8 mL ice-cold cell lysis buffer (10 mM Tris, 1.5 mM MgCl₂, 140 mM NaCl) containing 0.1% of IGEPAL-ca 630 (Sigma) and incubated on ice for 10 min to disrupt the cell membrane. After the lysis, the suspension was centrifuged at 1300 g for 2 min at 4°C, the supernatant (cytoplasm + membrane) was separated from the pellet (nuclei) and the activity in both fractions measured. The nuclear uptake will be expressed in percentage of total cellular uptake.

7.23. Evaluation of Radiation-induced Damage to Plasmid DNA

DNA cleavage activity was evaluated by monitoring the conversion of supercoiled plasmid DNA isoform (SC) to open circular DNA (OC) or linear DNA (L) isoforms through a gel electrophoresis assay. The plasmid DNA used was ϕ X174 (Promega, USA) and linear DNA was obtained by digestion with the single-cutter restriction enzyme *Xho*I and used as a reference in agarose gel electrophoresis. Plasmid DNA was incubated with different activities of ¹¹¹In-labelled conjugates (1.1 MBq to 2.5 Mq) and ¹¹¹In-DOTA (0.7 to 3.8 MBq) complexes for 135 hours (approximately 2 semi-disintegration periods) at 4°C in phosphate buffer (pH=7.4) in a total volume of 100 μ L. For each activity a replicate containing the radical scavenger DMSO at a final concentration of 0.2 M was also prepared. After the incubation, plasmid DNA in each sample was purified using a QIAquick nucleotide removal Kit (Qiagen, Germany) and resuspended in 30 μ L of ultrapure water. After this purification, 5 μ L of DNA loading buffer (0.25% bromophenol blue, 0.25% xylene cyanol, 30% glycerol in water, AppliChem) was added and the samples were loaded onto a 0.8% agarose (AppliChem) gel precast with GelRed (0.5 mg.mL⁻¹) (Biotium) in TAE buffer (Tri-acetate EDTA, AppliChem). Controls of non-incubated and of linearized plasmid were loaded on each gel electrophoresis. The electrophoresis was carried out for c.a. 2 hours at 100 V. The gels were visualised under UV light and digitally recorded using an Alphamager EP system (Alpha Innotech). Peak areas were measured by densitometry using the AlphaView Software from Alpha Innotech. Peak areas of the SC form were corrected using the factor 1.47 to account

for its lower staining capacity. The sum of the percentages of SC, OC and L isoforms was assumed to be 100%.

7.24. Animal Studies

7.24.1. Ethical Statement

All animal studies were performed in conformity with the national and EU legislation and were previously approved by the National Authorities. The animal experiments were accomplished in laboratory animal facilities under the supervision of researchers accredited by the National Authorities as outlined by the EU Law. All studies were conducted in accordance with the principles of laboratory animal science on animal care, protection and welfare.

The *Three R Concept* was rigorously applied to the animal experimentation to ensure that maximum information was obtained with a minimal number of animals.

7.24.2. Biodistribution and *In Vivo* Stability in Normal Mice

The *in vivo* behavior of the radiolabelled complexes was evaluated in groups of 3 female CD-1 mice (randomly bred, Charles River) weighting approximately 25 g each. Animals were injected intravenously with 100 μ L (0.74 – 1.59 MBq/ 20 – 43 μ Ci) of each preparation via the tail vein.

The animals were housed in a temperature- and humidity-controlled room with a 12 h light/12 h dark schedule and maintained on normal diet *ad libitum*. Mice were sacrificed by cervical dislocation at different time points post-injection. The injected radioactive dose and the radioactivity remaining in the animal after sacrifice were measured in a dose calibrator. The difference between the radioactivity in the injected and sacrificed animal was assumed to be due to total excretion from whole animal body. Blood samples were taken by cardiac puncture at sacrifice. Tissue samples of the main organs were then dissected, weighted and counted in a gamma counter (Berthold). Biodistribution results were expressed as percentage of the injected activity per gram of tissue (%I.A. / g).

Blood samples, collected at sacrifice time, were centrifuged, the serum separated and treated with ethanol to precipitate the proteins and the supernatant was analyzed by HPLC for stability evaluation. The urine samples were centrifuged at 3,000 rpm for 10 min. and the supernatant was also analyzed by HPLC.

7.24.3. Biodistribution in Mice with MCF-7 Xenografts

Biodistribution of the most promising radioactive compounds was also evaluated in 10-12 weeks old Balb/c-Nude mice (obtained from Charles River, Spain) with MCF-7 xenografts, weighing approximately 16–20 g. A 150 μ L bolus containing a suspension of approximately 8×10^6 freshly harvested human MCF-7 cells in Matrigel:PBS buffer 1:1 was subcutaneously injected in the right flank of each female nu/nu mouse. The animals were kept under aseptic conditions with normal diet and free water supplemented with 4 mg/L estradiol. 2-3 weeks later mice developed well-palpable tumors at the inoculation site.

Then, xenograft-bearing animals were intravenously injected in the tail vein with 100 μ L (0.74 – 1.59 MBq/ 20 – 43 μ Ci) of each preparation. Sacrifice and biodistribution procedures were similar to those described above in 7.24.2 section.

References

References

1. Torre, L.A., et al., *Global cancer statistics, 2012*. CA Cancer J Clin, 2015. **65**(2): p. 87-108.
2. Siegel, R.L., K.D. Miller, and A. Jemal, *Cancer statistics, 2016*. CA Cancer J Clin, 2016. **66**(1): p. 7-30.
3. Luengo-Fernandez, R., et al., *Economic burden of cancer across the European Union: a population-based cost analysis*. Lancet Oncol, 2013. **14**(12): p. 1165-1174.
4. Stewart, B.W. and C.P. Wild, *World cancer report 2014*. World Health Organization, 2014.
5. *Breast Cancer Facts & Figures 2015-2016*. American Cancer Society, 2015.
6. Malvezzi, M., et al., *European cancer mortality predictions for the year 2017, with focus on lung cancer*. Ann Oncol, 2017. **28**(5): p. 1117-1123
7. Bosetti, C., et al., *The decline in breast cancer mortality in Europe: an update (to 2009)*. Breast, 2012. **21**(1): p. 77-82.
8. *Cancer Facts & Figures 2017*. American Cancer Society, 2017.
9. Yersal, O. and S. Barutca, *Biological subtypes of breast cancer: Prognostic and therapeutic implications*. World J Clin Oncol, 2014. **5**(3): p. 412-24.
10. Rakha, E.A., et al., *Breast cancer prognostic classification in the molecular era: the role of histological grade*. Breast Cancer Res, 2010. **12**(4): p. 207-207.
11. Dai, X., et al., *Breast cancer intrinsic subtype classification, clinical use and future trends*. Am J Cancer Res, 2015. **5**(10): p. 2929-2943.
12. Sorlie, T., et al., *Gene expression patterns of breast carcinomas distinguish tumor subclasses with clinical implications*. Proc Natl Acad Sci U S A, 2001. **98**(19): p. 10869-74.
13. Eroles, P., et al., *Molecular biology in breast cancer: intrinsic subtypes and signaling pathways*. Cancer Treat Rev, 2012. **38**(6): p. 698-707.
14. Bustreo, S., et al., *Optimal Ki67 cut-off for luminal breast cancer prognostic evaluation: a large case series study with a long-term follow-up*. Breast Cancer Res Treat, 2016. **157**: p. 363-371.
15. Mendes, D., et al., *The benefit of HER2-targeted therapies on overall survival of patients with metastatic HER2-positive breast cancer – a systematic review*. Breast Cancer Res, 2015. **17**(1): p. 140.
16. Alluri, P. and L. Newman, *Basal-like and Triple Negative Breast Cancers: Searching For Positives Among Many Negatives*. Surg Oncol Clin N Am, 2014. **23**(3): p. 567-577.
17. Brewster, A.M., M. Chavez-MacGregor, and P. Brown, *Epidemiology, biology, and treatment of triple-negative breast cancer in women of African ancestry*. Lancet Oncol, 2014. **15**(13): p. 625-34.
18. Ovcaricek, T., et al., *Triple negative breast cancer – prognostic factors and survival*. Radiol Oncol, 2011. **45**(1): p. 46-52.
19. Sabatier, R., A. Goncalves, and F. Bertucci, *Personalized medicine: present and future of breast cancer management*. Crit Rev Oncol Hematol, 2014. **91**(3): p. 223-33.
20. Duffy, M.J., et al., *Clinical use of biomarkers in breast cancer: Updated guidelines from the European Group on Tumor Markers (EGTM)*. Eur J Cancer, 2017. **75**: p. 284-298.
21. Győrffy, B., et al., *Multigene prognostic tests in breast cancer: past, present, future*. Breast Cancer Res, 2015. **17**(1): p. 11.
22. Coates, A.S., et al., *Tailoring therapies—improving the management of early breast cancer: St Gallen International Expert Consensus on the Primary Therapy of Early Breast Cancer 2015*. Ann Oncol, 2015. **26**(8): p. 1533-1546.
23. Sledge, G.W., et al., *Past, Present, and Future Challenges in Breast Cancer Treatment*. J Clin Oncol, 2014. **32**(19): p. 1979-1986.
24. *Early and locally advanced breast cancer: diagnosis and treatment*. National Institute for Health and Care Excellence, 2009.

25. Chew, H.K., *Adjuvant therapy for breast cancer: who should get what?* West J Med, 2001. **174**(4): p. 284-287.
26. Specht, J. and J.R. Gralow, *Neoadjuvant chemotherapy for locally advanced breast cancer*. Semin Radiat Oncol, 2009. **19**(4): p. 222-8.
27. Teshome, M. and K.K. Hunt, *Neoadjuvant therapy in the treatment of breast cancer*. Surg Oncol Clin N Am, 2014. **23**(3): p. 505-523.
28. Sainsbury, R., *The development of endocrine therapy for women with breast cancer*. Cancer Treat Rev, 2013. **39**(5): p. 507-17.
29. Palmieri, C., et al., *Breast cancer: Current and future endocrine therapies*. Mol Cell Endocrinol, 2014. **382**(1): p. 695-723.
30. Zanardi, E., et al., *Better Together: Targeted Combination Therapies in Breast Cancer*. Semin Oncol, 2015. **42**(6): p. 887-895.
31. Chumsri, S., et al., *Aromatase, aromatase inhibitors, and breast cancer*. J Steroid Biochem Mol Biol, 2011. **125**(1-2): p. 13-22.
32. Dixon, J.M., *Endocrine Resistance in Breast Cancer*. New J Sci, 2014. **2014**: p. 27.
33. Coombes, R.C., et al., *A randomized trial of exemestane after two to three years of tamoxifen therapy in postmenopausal women with primary breast cancer*. N Engl J Med, 2004. **350**(11): p. 1081-92.
34. Tinoco, G., et al., *Treating breast cancer in the 21st century: emerging biological therapies*. J Cancer, 2013. **4**(2): p. 117-32.
35. Cervino, A.R., et al., *Molecular pathways and molecular imaging in breast cancer: an update*. Nucl Med Biol, 2013. **40**(5): p. 581-91.
36. Chung, C. and M.S. Lam, *Pertuzumab for the treatment of human epidermal growth factor receptor type 2-positive metastatic breast cancer*. Am J Health Syst Pharm, 2013. **70**(18): p. 1579-87.
37. Russell, C.A., *Personalized medicine for breast cancer: it is a new day!* Am J Surg, 2014. **207**(3): p. 321-5.
38. Pierce, A., et al., *Comparative antiproliferative effects of iniparib and olaparib on a panel of triple-negative and non-triple-negative breast cancer cell lines*. Cancer Biol Ther, 2013. **14**(6): p. 537-45.
39. Engebraaten, O., H.K. Vollan, and A.L. Børresen-Dale, *Triple-negative breast cancer and the need for new therapeutic targets*. Am J Pathol, 2013. **183**(4): p. 1064-74.
40. Hosford, S.R. and T.W. Miller, *Clinical potential of novel therapeutic targets in breast cancer: CDK4/6, Src, JAK/STAT, PARP, HDAC, and PI3K/AKT/mTOR pathways*. Pharmacogenomics Pers Med, 2014. **7**: p. 203-215.
41. Olefsky, J.M., *Nuclear receptor minireview series*. J Biol Chem, 2001. **276**(40): p. 36863-4.
42. Ellmann, S., et al., *Estrogen and progesterone receptors: from molecular structures to clinical targets*. Cell Mol Life Sci, 2009. **66**(15): p. 2405-26.
43. Billas, I. and D. Moras, *Allosteric controls of nuclear receptor function in the regulation of transcription*. J Mol Biol, 2013. **425**(13): p. 2317-29.
44. Bai, Z. and R. Gust, *Breast cancer, estrogen receptor and ligands*. Arch Pharm, 2009. **342**(3): p. 133-49.
45. Leitman, D.C., et al., *Regulation of specific target genes and biological responses by estrogen receptor subtype agonists*. Curr Opin Pharmacol, 2010. **10**(6): p. 629-36.
46. Ruff, M., et al., *Estrogen receptor transcription and transactivation: Structure-function relationship in DNA- and ligand-binding domains of estrogen receptors*. Breast Cancer Res, 2000. **2**(5): p. 353-9.
47. Muramatsu, M. and S. Inoue, *Estrogen receptors: how do they control reproductive and nonreproductive functions?* Biochem Biophys Res Commun, 2000. **270**(1): p. 1-10.
48. Burris, T.P., et al., *Nuclear receptors and their selective pharmacologic modulators*. Pharmacol Rev, 2013. **65**(2): p. 710-78.

49. Leclercq, G., et al., *Estrogen receptor alpha: impact of ligands on intracellular shuttling and turnover rate in breast cancer cells*. *Curr Cancer Drug Targets*, 2006. **6**(1): p. 39-64.
50. Srivastava, D.P. and P.D. Evans, *GPER 1: trials and tribulations of a Membrane Oestrogen Receptor*. *J Neuroendocrinol*, 2013. **25**: p. 1219-1230.
51. Thomas, P., et al., *Identity of an estrogen membrane receptor coupled to a G protein in human breast cancer cells*. *Endocrinology*, 2005. **146**(2): p. 624-32.
52. Castoria, G., et al., *Cell proliferation regulated by estradiol receptor: Therapeutic implications*. *Steroids*, 2010. **75**(8-9): p. 524-7.
53. Klinge, C.M., *Estrogen receptor interaction with estrogen response elements*. *Nucleic Acids Res*, 2001. **29**(14): p. 2905-19.
54. Leclercq, G., et al., *Peptides targeting estrogen receptor alpha-potential applications for breast cancer treatment*. *Curr Pharm Des*, 2011. **17**(25): p. 2632-53.
55. Bramlett, K.S., Y. Wu, and T.P. Burris, *Ligands specify coactivator nuclear receptor (NR) box affinity for estrogen receptor subtypes*. *Mol Endocrinol*, 2001. **15**(6): p. 909-22.
56. Renoir, J.M., *Estradiol receptors in breast cancer cells: associated co-factors as targets for new therapeutic approaches*. *Steroids*, 2012. **77**(12): p. 1249-61.
57. Savkur, R.S. and T.P. Burris, *The coactivator LXXLL nuclear receptor recognition motif*. *J Pept Res*, 2004. **63**(3): p. 207-12.
58. Varlakhanova, N., et al., *Estrogen receptors recruit SMRT and N-CoR corepressors through newly recognized contacts between the corepressor N terminus and the receptor DNA binding domain*. *Mol Cell Biol*, 2010. **30**(6): p. 1434-45.
59. Manolagas, S.C., C.A. O'Brien, and M. Almeida, *The role of estrogen and androgen receptors in bone health and disease*. *Nat Rev Endocrinol*, 2013. **9**(12): p. 699-712.
60. Renoir, J.M., V. Marsaud, and G. Lazennec, *Estrogen receptor signaling as a target for novel breast cancer therapeutics*. *Biochem Pharmacol*, 2013. **85**(4): p. 449-65.
61. Levin, E.R., *Rapid signaling by steroid receptors*. *Am J Physiol Regul Integr Comp Physiol*, 2008. **295**(5): p. R1425-30.
62. Giraldi, T., et al., *Steroid signaling activation and intracellular localization of sex steroid receptors*. *J Cell Commun Signal*, 2010. **4**(4): p. 161-72.
63. Castoria, G., et al., *PI3-kinase in concert with Src promotes the S-phase entry of oestradiol-stimulated MCF-7 cells*. *EMBO J*, 2001. **20**(21): p. 6050-9.
64. Migliaccio, A., G. Castoria, and F. Auricchio, *Src-dependent signalling pathway regulation by sex-steroid hormones: therapeutic implications*. *Int J Biochem Cell Biol*, 2007. **39**(7-8): p. 1343-8.
65. Lombardi, M., et al., *Hormone-dependent nuclear export of estradiol receptor and DNA synthesis in breast cancer cells*. *J Cell Biol*, 2008. **182**(2): p. 327-40.
66. Auricchio, F., A. Migliaccio, and G. Castoria, *Sex-steroid hormones and EGF signalling in breast and prostate cancer cells: targeting the association of Src with steroid receptors*. *Steroids*, 2008. **73**(9-10): p. 880-4.
67. Revankar, C.M., et al., *A transmembrane intracellular estrogen receptor mediates rapid cell signaling*. *Science*, 2005. **307**(5715): p. 1625-30.
68. Mizukami, Y., *In vivo functions of GPR30/GPER-1, a membrane receptor for estrogen: from discovery to functions in vivo*. *Endocr J*, 2010. **57**(2): p. 101-7.
69. Evans, N.J., et al., *Characterisation of Signalling by the Endogenous GPER1 (GPR30) Receptor in an Embryonic Mouse Hippocampal Cell Line (mHippoE-18)*. *PLoS ONE*, 2016. **11**(3): p. e0152138.
70. Zheng, F.F., et al., *Rapid estrogen-induced phosphorylation of the SRC-3 coactivator occurs in an extranuclear complex containing estrogen receptor*. *Mol Cell Biol*, 2005. **25**(18): p. 8273-84.
71. Osborne, C.K., et al., *Crosstalk between estrogen receptor and growth factor receptor pathways as a cause for endocrine therapy resistance in breast cancer*. *Clin Cancer Res*, 2005. **11**(2): p. 865-70.

72. Migliaccio, A., et al., *Steroid receptor regulation of epidermal growth factor signaling through Src in breast and prostate cancer cells: steroid antagonist action*. *Cancer Res*, 2005. **65**(22): p. 10585-93.
73. Lee, A.V., X. Cui, and S. Oesterreich, *Cross-talk among estrogen receptor, epidermal growth factor, and insulin-like growth factor signaling in breast cancer*. *Clin Cancer Res*, 2001. **7**(12 Suppl): p. 4429-4435.
74. Shou, J., et al., *Mechanisms of tamoxifen resistance: increased estrogen receptor-HER2/neu cross-talk in ER/HER2-positive breast cancer*. *J Natl Cancer Inst*, 2004. **96**(12): p. 926-35.
75. Alcantara, D., et al., *Molecular imaging of breast cancer: present and future directions*. *Front Chem*, 2014. **2**: p. 112.
76. Fowler, A.M., et al., *Imaging Diagnostic and Therapeutic Targets: Steroid Receptors in Breast Cancer*. *J Nucl Med*, 2016. **57 Suppl 1**: p. 75s-80s.
77. Jung, K.-H. and K.-H. Lee, *Molecular Imaging in the Era of Personalized Medicine*. *J Pathol Transl*, 2015. **49**(1): p. 5-12.
78. McDermott, S. and A. Kilcoyne, *Molecular imaging—its current role in cancer*. *QJM Int J Med*, 2016. **109**(5): p. 295-299.
79. Correia, J.D., et al., *Radiometallated peptides for molecular imaging and targeted therapy*. *Dalton Trans*, 2011. **40**(23): p. 6144-67.
80. Saha, G.B., *Radiopharmaceuticals and Methods of Radiolabeling*, in *Fundamentals of Nuclear Pharmacy*, 1992. Springer, New York. p. 80-108.
81. Hicks, R.J. and M.S. Hofman, *Is there still a role for SPECT-CT in oncology in the PET-CT era?*, in *Nat Rev Clin Oncol*. 2012: England. p. 712-20.
82. Jurisson, S., et al., *Coordination compounds in nuclear medicine*. *Chem Rev*, 1993. **93**(3): p. 1137-1156.
83. Saha, G.B., *Fundamentals of Nuclear Pharmacy*, 2003, Springer, New York.
84. Blower, P., *Towards molecular imaging and treatment of disease with radionuclides: the role of inorganic chemistry*. *Dalton Trans*, 2006. **14**: p. 1705-11.
85. Bhattacharyya, S. and M. Dixit, *Metallic radionuclides in the development of diagnostic and therapeutic radiopharmaceuticals*. *Dalton Trans*, 2011. **40**(23): p. 6112-28.
86. Fani, M. and H.R. Maecke, *Radiopharmaceutical development of radiolabelled peptides*. *Eur J Nucl Med Mol Imaging*, 2012. **39 Suppl 1**: p. S11-30.
87. Dalm, S.U., J.F. Verzijlbergen, and M. De Jong, *Review: Receptor Targeted Nuclear Imaging of Breast Cancer*. *Int J of Mol Sci*, 2017. **18**(2): p. 260.
88. Vultos, F., et al., *New estradiol based ¹¹¹In complex towards the estrogen receptor*. *Radiochim Acta.*, 2015. **103**(11): p. 765-776.
89. Imstepf, S., et al., *Towards (99m)Tc-based imaging agents with effective doxorubicin mimetics: a molecular and cellular study*. *Dalton Trans*, 2016. **45**(33): p. 13025-33.
90. Dash, A., et al., *Peptide receptor radionuclide therapy: an overview*. *Cancer Biother Radiopharm*, 2015. **30**(2): p. 47-71.
91. Milenic, D.E., E.D. Brady, and M.W. Brechbiel, *Antibody-targeted radiation cancer therapy*. *Nat Rev Drug Discov*, 2004. **3**(6): p. 488-499.
92. Chaturvedi, S. and A.K. Mishra, *Small Molecule Radiopharmaceuticals – A Review of Current Approaches*. *Front in Med*, 2016. **3**: p. 5.
93. Linden, H.M. and F. Dehdashti, *Novel methods and tracers for breast cancer imaging*. *Semin Nucl Med*, 2013. **43**(4): p. 324-9.
94. Bennink, R.J., et al., *Estrogen receptor status in primary breast cancer: iodine 123-labeled cis-11beta-methoxy-17alpha-iodovinyl estradiol scintigraphy*. *Radiology*, 2001. **220**(3): p. 774-9.
95. van Kruchten, M., et al., *PET imaging of estrogen receptors as a diagnostic tool for breast cancer patients presenting with a clinical dilemma*. *J Nucl Med*, 2012. **53**(2): p. 182-90.

96. Dixit, M., et al., *Synthesis of Clinical-Grade [(18)F]-Fluoroestradiol as a Surrogate PET Biomarker for the Evaluation of Estrogen Receptor-Targeting Therapeutic Drug*. Int J Mol Imaging, 2013. **2013**: 278607.
97. Linden, H.M., et al., *Fluoroestradiol positron emission tomography reveals differences in pharmacodynamics of aromatase inhibitors, tamoxifen, and fulvestrant in patients with metastatic breast cancer*. Clin Cancer Res, 2011. **17**(14): p. 4799-805.
98. Koleva-Kolarova, R.G., et al., *The value of PET/CT with FES or FDG tracers in metastatic breast cancer: a computer simulation study in ER-positive patients*. Br J Cancer, 2015. **112**(10): p. 1617-1625.
99. VanBrocklin, H.F., et al., *Preparation and evaluation of 17-ethynyl-substituted 16 alpha-[18F]fluoroestradiols: selective receptor-based PET imaging agents*. Int J Rad Appl Instrum B, 1992. **19**(3): p. 363-74.
100. VanBrocklin, H.F., et al., *The synthesis of 7 α -methyl-substituted estrogens labeled with fluorine-18: potential breast tumor imaging agents*. Steroids, 1994. **59**(1): p. 34-45.
101. Benard, F., et al., *[18F]Fluorinated estradiol derivatives for oestrogen receptor imaging: impact of substituents, formulation and specific activity on the biodistribution in breast tumour-bearing mice*. Eur J Nucl Med Mol Imaging, 2008. **35**(8): p. 1473-9.
102. Bennink, R.J., et al., *In vivo prediction of response to antiestrogen treatment in estrogen receptor-positive breast cancer*. J Nucl Med, 2004. **45**(1): p. 1-7.
103. Oliveira, M.C., et al., *Estrogen receptor ligands for targeting breast tumours: a brief outlook on radioiodination strategies*. Curr Radiopharm, 2012. **5**(2): p. 124-41.
104. Nayak, T.K., et al., *Pre-clinical development of a neutral, estrogen receptor-targeted, tridentate (99m)Tc(I) estradiol pyridin-2-yl hydrazine derivative for imaging of breast and endometrial cancers*. J Nucl Med, 2008. **49**(6): p. 978-986.
105. Xia, X., et al., *^{99m}Tc-labeled estradiol as an estrogen receptor probe: Preparation and preclinical evaluation*. Nucl Med Biol, 2016. **43**(1): p. 89-96.
106. Chauhan, K., et al., *Bivalent Approach for Homodimeric Estradiol Based Ligand: Synthesis and Evaluation for Targeted Theranosis of ER(+) Breast Carcinomas*. Bioconjug Chem, 2016. **27**(4): p. 961-972.
107. Holland, J.P., P. Cumming, and N. Vasdev, *PET of signal transduction pathways in cancer*. J Nucl Med, 2012. **53**(9): p. 1333-6.
108. McDonald, E.S., D.A. Mankoff, and R.H. Mach, *Novel Strategies for Breast Cancer Imaging: New Imaging Agents to Guide Treatment*. J Nucl Med, 2016. **57** Suppl 1: p. 69-74.
109. Xu, C., et al., *CXCR4 in breast cancer: oncogenic role and therapeutic targeting*. Drug Des Devel Ther, 2015. **28**(9): p. 4953-4964.
110. Kelkar, S.S. and T.M. Reineke, *Theranostics: combining imaging and therapy*. Bioconjug Chem, 2011. **22**(10): p. 1879-903.
111. Penet, M.F., et al., *Theranostic imaging of cancer*. Eur J Radiol, 2012. **81** Suppl 1: p. 124-6.
112. Mahajan, A., et al., *Molecular functional imaging in personalized clinical oncology: The road less traveled*. Indian J Med Paediatr Oncol, 2016. **37**(1): p. 1-3.
113. Ngo Ndjock Mbong, G., et al., *Trastuzumab Labeled to High Specific Activity with (111)In by Site-Specific Conjugation to a Metal-Chelating Polymer Exhibits Amplified Auger Electron-Mediated Cytotoxicity on HER2-Positive Breast Cancer Cells*. Mol Pharm, 2015. **12**(6): p. 1951-60.
114. D'Huyvetter, M., et al., *Development of ¹⁷⁷Lu-nanobodies for radioimmunotherapy of HER2-positive breast cancer: evaluation of different bifunctional chelators*. Contrast Media Mol Imaging, 2012. **7**(2): p. 254-64.
115. Pruszynski, M., et al., *Improved tumor targeting of anti-HER2 nanobody through N-succinimidyl 4-guanidinomethyl-3-iodobenzoate radiolabeling*. J Nucl Med, 2014. **55**(4): p. 650-6.

116. D'Huyvetter, M., et al., *Radiolabelled nanobodies as theranostic tools in targeted radionuclide therapy of cancer*. *Expert Opin Drug Deliv*, 2014. **11**(12): p. 1939-1954.
117. Dalm, S.U., et al., *⁶⁸Ga/¹⁷⁷Lu-NeoBOMB1, a Novel Radiolabelled GRPR Antagonist for Theranostic Use in Oncology*. *J Nucl Med*, 2017. **58**(2): p. 293-299.
118. Zolata, H., F. Abbasi Davani, and H. Afarideh, *Synthesis, characterization and theranostic evaluation of Indium-111 labeled multifunctional superparamagnetic iron oxide nanoparticles*. *Nucl Med Biol*, 2015. **42**(2): p. 164-70.
119. Howell, R.W., *Radiation spectra for Auger-electron emitting radionuclides: report No. 2 of AAPM Nuclear Medicine Task Group No. 6*. *Med Phys*, 1992. **19**(6): p. 1371-83.
120. Kassis, A.I., *The amazing world of auger electrons*. *Int J Radiat Biol*, 2004. **80**(11-12): p. 789-803.
121. Sanche, L., *Cancer treatment: Low-energy electron therapy*. *Nat Mater*, 2015. **14**(9): p. 861-863.
122. Humm, J.L., R.W. Howell, and D.V. Rao, *Dosimetry of Auger-electron-emitting radionuclides: report no. 3 of AAPM Nuclear Medicine Task Group No. 6*. *Med Phys*, 1994. **21**(12): p. 1901-15.
123. O'Donoghue, J.A. and T.E. Wheldon, *Targeted radiotherapy using Auger electron emitters*. *Phys Med Biol*, 1996. **41**(10): p. 1973-92.
124. Kassis, A.I., *Molecular and cellular radiobiological effects of Auger emitting radionuclides*. *Radiat Prot Dosimetry*, 2011. **143**(2-4): p. 241-7.
125. Pereira, E., et al., *Evaluation of Acridine Orange Derivatives as DNA-Targeted Radiopharmaceuticals for Auger Therapy: Influence of the Radionuclide and Distance to DNA*. *Sci Rep*, 2017. **13**(7): p. 42544.
126. Reissig, F., et al., *Direct and Auger Electron-Induced, Single- and Double-Strand Breaks on Plasmid DNA Caused by ^{99m}Tc-Labeled Pyrene Derivatives and the Effect of Bonding Distance*. *PLoS One*, 2016. **11**(9): p. e0161973.
127. Pouget, J.P., et al., *Clinical radioimmunotherapy--the role of radiobiology*. *Nat Rev Clin Oncol*, 2011. **8**(12): p. 720-34.
128. Gao, C., et al., *Auger electron-emitting (¹¹¹In)-DTPA-NLS-CSL360 radioimmunoconjugates are cytotoxic to human acute myeloid leukemia (AML) cells displaying the CD123(+)/CD131(-) phenotype of leukemia stem cells*. *Appl Radiat Isot*, 2016. **110**: p. 1-7.
129. Cai, Z., et al., *¹¹¹In-labeled trastuzumab-modified gold nanoparticles are cytotoxic in vitro to HER2-positive breast cancer cells and arrest tumor growth in vivo in athymic mice after intratumoral injection*. *Nucl Med Biol*, 2016. **43**(12): p. 818-826.
130. Wicki, A., et al., *[Lys40(Ahx-DTPA-¹¹¹In)NH₂]-Exendin-4 is a highly efficient radiotherapeutic for glucagon-like peptide-1 receptor-targeted therapy for insulinoma*. *Clin Cancer Res*, 2007. **13**(12): p. 3696-705.
131. Weiner, R.E. and M.L. Thakur, *Chemistry of Gallium and Indium Radiopharmaceuticals*, in *Handbook of Radiopharmaceuticals*. 2002, John Wiley & Sons, Ltd. p. 363-399.
132. Krenning, E.P., et al., *Somatostatin receptor scintigraphy with indium-111-DTPA-D-Phe-1-octreotide in man: metabolism, dosimetry and comparison with iodine-123-Tyr-3-octreotide*. *J Nucl Med*, 1992. **33**(5): p. 652-8.
133. Capello, A., et al., *Peptide receptor radionuclide therapy in vitro using [¹¹¹In-DTPA]octreotide*. *J Nucl Med*, 2003. **44**(1): p. 98-104.
134. Liu, S., *The role of coordination chemistry in the development of target-specific radiopharmaceuticals*. *Chem Soc Rev*, 2004. **33**(7): p. 445-61.
135. Kulprathipanja, S., et al., *Formation constants of Gallium- and Indium-Transferrin*. *Int J Nucl Med Biol*, 1979. **6**(2): p. 138-141.
136. Wadas, T.J., et al., *Coordinating Radiometals of Copper, Gallium, Indium, Yttrium and Zirconium for PET and SPECT Imaging of Disease*. *Chem Rev*, 2010. **110**(5): p. 2858-2902.

137. Brechbiel, M.W., *Bifunctional chelates for metal nuclides*. Q J Nucl Med Mol Imaging, 2008. **52**(2): p. 166-73.
138. Ginja, M., et al., *Trifunctional somatostatin-based derivatives designed for targeted radiotherapy using auger electron emitters*. J Nucl Med, 2005. **46**(12): p. 2097-103.
139. Price, E.W. and C. Orvig, *Matching chelators to radiometals for radiopharmaceuticals*. Chem Soc Rev, 2014. **43**(1): p. 260-90.
140. Ramogida, C.F. and C. Orvig, *Tumour targeting with radiometals for diagnosis and therapy*. Chem Commun, 2013. **49**(42): p. 4720-39.
141. Liu, S., *Bifunctional coupling agents for radiolabeling of biomolecules and target-specific delivery of metallic radionuclides*. Adv Drug Deliv Rev, 2008. **60**(12): p. 1347-70.
142. Liu, S. and D.S. Edwards, *Synthesis and Characterization of Two ¹¹¹In-Labeled DTPA–Peptide Conjugates*. Bioconjug Chem, 2001. **12**(4): p. 630-634.
143. Lattuada, L., et al., *The synthesis and application of polyamino polycarboxylic bifunctional chelating agents*. Chem Soc Rev, 2011. **40**(5): p. 3019-49.
144. Arano, Y., et al., *Reassessment of diethylenetriaminepentaacetic acid (DTPA) as a chelating agent for indium-111 labeling of polypeptides using a newly synthesized monoreactive DTPA derivative*. J Med Chem, 1996. **39**(18): p. 3451-60.
145. Costantini, D.L., et al., *(¹¹¹In)-labeled trastuzumab (Herceptin) modified with nuclear localization sequences (NLS): an Auger electron-emitting radiotherapeutic agent for HER2/neu-amplified breast cancer*. J Nucl Med, 2007. **48**(8): p. 1357-68.
146. Brechbiel, M.W. and O.A. Gansow, *Backbone-substituted DTPA ligands for yttrium-90 radioimmunotherapy*. Bioconjug Chem, 1991. **2**(3): p. 187-194.
147. Anelli, P.L., et al., *L-Glutamic acid and L-lysine as useful building blocks for the preparation of bifunctional DTPA-like ligands*. Bioconjug Chem, 1999. **10**(1): p. 137-40.
148. Choi, K., et al., *Preparation of an amino acid based DTPA as a BFCA for radioimmunotherapy*. Bull Korean Chem Soc, 2006. **27**(8): p. 1194-1198.
149. Williams, M.A. and H. Rapoport, *Synthesis of enantiomerically pure diethylenetriaminepentaacetic acid analogs. L-Phenylalanine as the educt for substitution at the central acetic acid*. J Org Chem, 1993. **58**(5): p. 1151-1158.
150. Liu, S., et al., *Synthesis, Characterization, and X-ray Crystal Structure of In(DOTA-AA) (AA = p-Aminoanilide): A Model for ¹¹¹In-Labeled DOTA-Biomolecule Conjugates*. Inorg Chem, 2003. **42**(26): p. 8831-8837.
151. Sihver, W., et al., *Radiolabelled Cetuximab Conjugates for EGFR Targeted Cancer Diagnostics and Therapy*. Pharmaceuticals, 2014. **7**(3): p. 311-338.
152. De León-Rodríguez, L.M. and Z. Kovacs, *The synthesis and chelation chemistry of DOTA-peptide conjugates*. Bioconjug Chem, 2008. **19**(2): p. 391-402.
153. Lewis, M.R. and J.E. Shively, *Maleimidocysteineamido-DOTA derivatives: new reagents for radiometal chelate conjugation to antibody sulfhydryl groups undergo pH-dependent cleavage reactions*. Bioconjug Chem, 1998. **9**(1): p. 72-86.
154. Schlesinger, J., et al., *Radiosynthesis of new [⁹⁰Y]-DOTA-based maleimide reagents suitable for the prelabeling of thiol-bearing L-oligonucleotides and peptides*. Bioconjug Chem, 2009. **20**(7): p. 1340-8.
155. Wangler, B., et al., *Application of tris-allyl-DOTA in the preparation of DOTA-peptide conjugates*. Tetrahedron Lett, 2006. **47**(33): p. 5985-5988.
156. Wangler, C., et al., *DOTA derivatives for site-specific biomolecule-modification via click chemistry: synthesis and comparison of reaction characteristics*. Bioorg Med Chem, 2011. **19**(12): p. 3864-74.
157. Martin, M.E., et al., *A DOTA–peptide conjugate by copper-free click chemistry*. Bioorg Med Chem Lett, 2010. **20**(16): p. 4805-4807.
158. Martin, M.E., et al., *"Click"-cyclized (⁶⁸Ga)-labeled peptides for molecular imaging and therapy: synthesis and preliminary in vitro and in vivo evaluation in a melanoma model system*. Recent Results Cancer Res, 2013. **194**: p. 149-75.

159. Eisenwiener, K.P., et al., *NODAGATOC, a new chelator-coupled somatostatin analogue labeled with [67/68Ga] and [111In] for SPECT, PET, and targeted therapeutic applications of somatostatin receptor (hsst2) expressing tumors*. *Bioconjug Chem*, 2002. **13**(3): p. 530-41.
160. Dissoki, S., et al., *Labeling approaches for the GE11 peptide, an epidermal growth factor receptor biomarker*. *J Labelled Comp Radiopharm*, 2011. **54**(11): p. 693-701.
161. Sun, X., et al., *Peptide-based imaging agents for cancer detection*. *Adv Drug Deliv Rev*, 2017. **110-111**: p. 38-51
162. Jamous, M., U. Haberkorn, and W. Mier, *Synthesis of peptide radiopharmaceuticals for the therapy and diagnosis of tumor diseases*. *Molecules*, 2013. **18**(3): p. 3379-409.
163. Signore, A., et al., *Peptide radiopharmaceuticals for diagnosis and therapy*. *Eur J Nucl Med*, 2001. **28**(10): p. 1555-1565.
164. Deutscher, S.L., *Phage display in molecular imaging and diagnosis of cancer*. *Chem Rev*, 2010. **110**(5): p. 3196-211.
165. Koopmans, K.P. and A.W. Glaudemans, *Rationale for the use of radiolabelled peptides in diagnosis and therapy*. *Eur J Nucl Med Mol Imaging*, 2012. **39 Suppl 1**: p. S4-10.
166. Fani, M., H.R. Maecke, and S.M. Okarvi, *Radiolabelled peptides: valuable tools for the detection and treatment of cancer*. *Theranostics*, 2012. **2**(5): p. 481-501.
167. Soudy, R., et al., *Proteolytically stable cancer targeting peptides with high affinity for breast cancer cells*. *J Med Chem*, 2011. **54**(21): p. 7523-34.
168. Varricchio, L., et al., *Inhibition of estradiol receptor/Src association and cell growth by an estradiol receptor alpha tyrosine-phosphorylated peptide*. *Mol Cancer Res*, 2007. **5**(11): p. 1213-21.
169. Jackson, I.M., P.J.H. Scott, and S. Thompson, *Clinical Applications of Radiolabelled Peptides for PET*. *Semin Nucl Med*, 2017. **47**(5): p. 493-523.
170. Krenning, E.P., et al., *Somatostatin receptor scintigraphy with [111In-DTPA-D-Phe1]- and [123I-Tyr3]-octreotide: the Rotterdam experience with more than 1000 patients*. *Eur J Nucl Med*, 1993. **20**(8): p. 716-31.
171. Laznickova, A., et al., *Biodistribution of two octreotate analogs radiolabelled with indium and yttrium in rats*. *Anticancer Res*, 2010. **30**(6): p. 2177-84.
172. de Jong, M., et al., *Comparison of (111)In-labeled somatostatin analogues for tumor scintigraphy and radionuclide therapy*. *Cancer Res*, 1998. **58**(3): p. 437-41.
173. Bison, S.M., et al., *Peptide receptor radionuclide therapy using radiolabelled somatostatin analogs: focus on future developments*. *Clin Transl Imaging*, 2014. **2**(1): p. 55-66.
174. Bihl, H. and G. Antoch. *PET-CT and SPECT-CT of Other Gastrointestinal Tumors: Somatostatin Receptor-Positive and Gastrointestinal Stromal Tumors*. *Radiology Key* (radiologykey.com) [cited 2017 02/08].
175. Opalinska, M., A. Hubalewska-Dydejczyk, and A. Sowa-Staszczak, *Radiolabelled peptides: current and new perspectives*. *Q J Nucl Med Mol Imaging*, 2017. **61**(2): p. 153-167.
176. Decristoforo, C., et al., *68Ga- and 111In-labelled DOTA-RGD peptides for imaging of alphavbeta3 integrin expression*. *Eur J Nucl Med Mol Imaging*, 2008. **35**(8): p. 1507-15.
177. Wild, D., et al., *Exendin-4-based radiopharmaceuticals for glucagonlike peptide-1 receptor PET/CT and SPECT/CT*. *J Nucl Med*, 2010. **51**(7): p. 1059-67.
178. Breeman, W.A., et al., *Preclinical comparison of (111)In-labeled DTPA- or DOTA-bombesin analogs for receptor-targeted scintigraphy and radionuclide therapy*. *J Nucl Med*, 2002. **43**(12): p. 1650-6.
179. Oxboel, J., et al., *Comparison of two new angiogenesis PET tracers 68Ga-NODAGA-E[c(RGDyK)]2 and (64)Cu-NODAGA-E[c(RGDyK)]2; in vivo imaging studies in human xenograft tumors*. *Nucl Med Biol*, 2014. **41**(3): p. 259-67.

180. Coin, I., M. Beyermann, and M. Bienert, *Solid-phase peptide synthesis: from standard procedures to the synthesis of difficult sequences*. Nat Protoc, 2007. **2**(12): p. 3247-56.
181. Behrendt, R., P. White, and J. Offer, *Advances in Fmoc solid-phase peptide synthesis*. J Pept Sci, 2016. **22**(1): p. 4-27.
182. Stawikowski, M. and G.B. Fields, *Introduction to Peptide Synthesis* in *Current protocols in protein science*, 2012. **69**:18.1
183. Carpino, L.A. and G.Y. Han, *9-Fluorenylmethoxycarbonyl function, a new base-sensitive amino-protecting group*. J Am Chem Soc, 1970. **92**(19): p. 5748-5749.
184. Pedersen, S.L., et al., *Microwave heating in solid-phase peptide synthesis*. Chem Soc Rev, 2012. **41**(5): p. 1826-44.
185. Bacsa, B., et al., *Solid-phase synthesis of difficult peptide sequences at elevated temperatures: a critical comparison of microwave and conventional heating technologies*. J Org Chem, 2008. **73**(19): p. 7532-42.
186. Masuda, K., et al., *Microwave-assisted solid-phase peptide synthesis of neurosecretory protein GL composed of 80 amino acid residues*. J Pept Sci, 2015. **21**(6): p. 454-60.
187. Chang, C., et al., *Dissection of the LXXLL nuclear receptor-coactivator interaction motif using combinatorial peptide libraries: discovery of peptide antagonists of estrogen receptors alpha and beta*. Mol Cell Biol, 1999. **19**(12): p. 8226-39.
188. McInerney, E.M., et al., *Determinants of coactivator LXXLL motif specificity in nuclear receptor transcriptional activation*. Genes Dev, 1998. **12**(21): p. 3357-68.
189. Bain, D.L., et al., *Nuclear receptor structure: implications for function*. Annu Rev Physiol, 2007. **69**: p. 201-20.
190. Galande, A.K., et al., *Potent inhibitors of LXXLL-based protein-protein interactions*. ChemBioChem, 2005. **6**(11): p. 1991-8.
191. Galande, A.K., et al., *Thioether side chain cyclization for helical peptide formation: inhibitors of estrogen receptor-coactivator interactions*. J Pept Res, 2004. **63**(3): p. 297-302.
192. Nguyen, H.D., et al., *Estrogen receptor α/β -cofactor motif interactions; interplay of tyrosine 537/488 phosphorylation and LXXLL motifs*. Mol Biosyst, 2012. **8**(12): p. 3134-41.
193. Leduc, A.M., et al., *Helix-stabilized cyclic peptides as selective inhibitors of steroid receptor-coactivator interactions*. Proc Natl Acad Sci U S A, 2003. **100**(20): p. 11273-8.
194. Ko, L., et al., *Ser-884 adjacent to the LXXLL motif of coactivator TRBP defines selectivity for ERs and TRs*. Mol Endocrinol, 2002. **16**(1): p. 128-40.
195. Carraz, M., et al., *Perturbation of estrogen receptor alpha localization with synthetic nona-arginine LXXLL-peptide coactivator binding inhibitors*. Chem Biol, 2009. **16**(7): p. 702-11.
196. Tints, K., et al., *LXXLL peptide converts transportan 10 to a potent inducer of apoptosis in breast cancer cells*. Int J Mol Sci, 2014. **15**(4): p. 5680-98.
197. Pellegrini, M., et al., *Conformational consequences of $i, i + 3$ cystine linkages: nucleation for alpha-helicity?* J Pept Res, 1997. **49**(5): p. 404-14.
198. Lee, M.K., et al., *Structure-activity relationships of anti-HIV-1 peptides with disulfide linkage between D- and L-cysteine at positions i and $i+3$, respectively, derived from HIV-1 gp41 C-peptide*. Exp Mol Med, 2006. **38**(1): p. 18-26.
199. Arabanian, A., M. Mohammadnejad, and S. Balalaie, *A Novel and Efficient Approach for the Amidation of C-Terminal Peptides*. J Iran Chem Soc, 2010. **7**(4): p. 840-845.
200. Valeur, E. and M. Bradley, *Amide bond formation: beyond the myth of coupling reagents*. Chem Soc Rev, 2009. **38**(2): p. 606-31.
201. Collins, J.M., S. Singh, and G.S. Vanier, *Microwave technology for solid phase peptide synthesis: It's not just for difficult peptides*. Chimica oggi, 2012. **30**(2): p. 3.
202. Stathopoulos, P., et al., *Side reactions in the SPPS of Cys-containing peptides*. Amino Acids, 2013. **44**(5): p. 1357-63.

203. Galande, A.K., R. Weissleder, and C.H. Tung, *An effective method of on-resin disulfide bond formation in peptides*. J Comb Chem, 2005. **7**(2): p. 174-7.
204. Poole, L.B., *The basics of thiols and cysteines in redox biology and chemistry*. Free Radic Biol Med, 2015. **80**: p. 148-57.
205. Tam, J.P., et al., *Disulfide bond formation in peptides by dimethyl sulfoxide. Scope and applications*. J Am Chem Soc, 1991. **113**(17): p. 6657-6662.
206. Heppeler, A., et al., *Radiometal-labelled macrocyclic chelator-derivatised somatostatin analogue with superb tumour-targeting properties and potential for receptor-mediated internal radiotherapy*. Chem Eur J, 1999. **5**(7): p. 1974 - 1981.
207. Srivastava, S., et al., *Synthesis and opioid receptor binding of indium (III) and [111In]-labeled macrocyclic conjugates of diprenorphine: novel ligands designed for imaging studies of peripheral opioid receptors*. Tetrahedron, 2016. **72**(40): p. 6127-6135.
208. Jurisson, S., C. Cutler, and S.V. Smith, *Radiometal complexes: characterization and relevant in vitro studies*. Q J Nucl Med Mol Imaging, 2008. **52**(3): p. 222-34.
209. Sosabowski, J.K. and S.J. Mather, *Conjugation of DOTA-like chelating agents to peptides and radiolabeling with trivalent metallic isotopes*. Nat Protoc, 2006. **1**(2): p. 972-6.
210. Lea, W.A. and A. Simeonov, *Fluorescence polarization assays in small molecule screening*. Expert Opin Drug Discov, 2011. **6**(1): p. 17-32.
211. Rossi, A.M. and C.W. Taylor, *Analysis of protein-ligand interactions by fluorescence polarization*. Nat Protoc, 2011. **6**(3): p. 365-87.
212. Teichert, A., et al., *Quantification of the vitamin D receptor-coregulator interaction*. Biochemistry, 2009. **48**(7): p. 1454-61.
213. Ozers, M.S., et al., *Analysis of ligand-dependent recruitment of coactivator peptides to estrogen receptor using fluorescence polarization*. Mol Endocrinol, 2005. **19**(1): p. 25-34.
214. Goksel, H., et al., *An on-bead assay for the identification of non-natural peptides targeting the androgen receptor-cofactor interaction*. Bioorg Med Chem, 2011. **19**(1): p. 306-11.
215. Rodriguez, A.L., et al., *Design, synthesis, and in vitro biological evaluation of small molecule inhibitors of estrogen receptor alpha coactivator binding*. J Med Chem, 2004. **47**(3): p. 600-11.
216. Bapat, A.R. and D.E. Frail, *Full-length estrogen receptor alpha and its ligand-binding domain adopt different conformations upon binding ligand*. J Steroid Biochem Mol Biol, 2003. **86**(2): p. 143-9.
217. Reubi, J.C., et al., *Affinity profiles for human somatostatin receptor subtypes SST1-SST5 of somatostatin radiotracers selected for scintigraphic and radiotherapeutic use*. Eur J Nucl Med, 2000. **27**(3): p. 273-82.
218. Brom, M., et al., *Improved labelling of DTPA- and DOTA-conjugated peptides and antibodies with 111In in HEPES and MES buffer*. EJNMMI Res, 2012. **2**: p. 4.
219. Krohn, K.A. and A.-L. Jansholt, *Radiochemical quality control of short-lived radiopharmaceuticals*. Int J Appl Radiat, 1977. **28**(1): p. 213-227.
220. Wilson, A.A., et al., *An admonition when measuring the lipophilicity of radiotracers using counting techniques*. Appl Radiat Isot, 2001. **54**(2): p. 203-8.
221. Moshtaghi, A.A. and M.A. Ghaffari, *Study of the Binding of Iron and Indium to Human Serum Apo-Transferrin*. Iran Biomed J, 2003. **7**(2): p. 73-77.
222. Good, S., et al., *Macrocyclic chelator-coupled gastrin-based radiopharmaceuticals for targeting of gastrin receptor-expressing tumours*. Eur J Nucl Med Mol Imaging, 2008. **35**(10): p. 1868-77.
223. Mier, W., et al., *Influence of chelate conjugation on a newly identified tumor-targeting peptide*. J Nucl Med, 2007. **48**(9): p. 1545-52.
224. Muttenthaler, M., et al., *Modulating oxytocin activity and plasma stability by disulfide bond engineering*. J Med Chem, 2010. **53**(24): p. 8585-96.

225. Nguyen, L.T., et al., *Serum stabilities of short tryptophan- and arginine-rich antimicrobial peptide analogs*. PLoS One, 2010. **5**(9).
226. Werle, M. and A. Bernkop-Schnürch, *Strategies to improve plasma half life time of peptide and protein drugs*. Amino Acids, 2006. **30**(4): p. 351-67.
227. Huang, Y., et al., *Alpha-helical cationic anticancer peptides: a promising candidate for novel anticancer drugs*. Mini Rev Med Chem, 2015. **15**(1): p. 73-81.
228. Zaro, J.L. and W.-C. Shen, *Cationic and amphipathic cell-penetrating peptides (CPPs): Their structures and in vivo studies in drug delivery*. Front Chem Sci Eng, 2015. **9**(4): p. 407-427.
229. Kocanova, S., et al., *Ligands specify estrogen receptor alpha nuclear localization and degradation*. BMC Cell Biol, 2010. **11**: p. 98.
230. Laverman, P., et al., *Comparative biodistribution of 12 ¹¹¹In-labelled gastrin/CCK2 receptor-targeting peptides*. Eur J Nucl Med Mol Imaging, 2011. **38**(8): p. 1410-6.
231. Vallabhajosula, S., R.P. Killeen, and J.R. Osborne, *Altered biodistribution of radiopharmaceuticals: role of radiochemical/pharmaceutical purity, physiological, and pharmacologic factors*. Semin Nucl Med, 2010. **40**(4): p. 220-41.
232. Akizawa, H., et al., *Renal metabolism of ¹¹¹In-DTPA-D-Phe1-octreotide in vivo*. Bioconjug Chem, 1998. **9**(6): p. 662-70.
233. Alirezapour, B., et al., *Preclinical evaluation of ¹¹¹In-DOTA-trastuzumab for clinical trials*. J Cancer Res Ther, 2014. **10**(1): p. 112-120.
234. Akizawa, H., et al., *Effect of molecular charges on renal uptake of ¹¹¹In-DTPA-conjugated peptides*. Nucl Med Biol, 2001. **28**(7): p. 761-8.
235. Ali, H., et al., *2- and 4-fluorinated 16 alpha(-)[¹²⁵I]iodoestradiol derivatives: synthesis and effect on estrogen receptor binding and receptor-mediated target tissue uptake*. J Med Chem, 1993. **36**(26): p. 4255-63.
236. Enginar, H., et al., *Synthesis of ¹³¹I labeled estrone derivatives and biodistribution studies on rats*. J Radioanal Nucl Chem, 2005. **264**(3): p. 535-539.
237. Melo e Silva, M.C., et al., *Synthesis and biological evaluation of two new radiolabelled estrogens: [¹²⁵I](E)-3-methoxy-17 α -iodovinylestra-1,3,5(10),6-tetraen-17 β -ol and [¹²⁵I](Z)-3-methoxy-17 α -iodovinylestra-1,3,5(10),6-tetraen-17 β -ol*. Appl Radiat Isot, 2001. **54**(2): p. 227-239.
238. Biscardi, J.S., et al., *Tyrosine kinase signalling in breast cancer: epidermal growth factor receptor and c-Src interactions in breast cancer*. Breast Cancer Res, 2000. **2**(3): p. 203-10.
239. Guest, S.K., et al., *Src Is a Potential Therapeutic Target in Endocrine-Resistant Breast Cancer Exhibiting Low Estrogen Receptor-Mediated Transactivation*. PLoS One, 2016. **11**(6): p. e0157397.
240. Chiu, J.H., et al., *Role of estrogen receptors and Src signaling in mechanisms of bone metastasis by estrogen receptor positive breast cancers*. J Transl Med, 2017. **15**(1): p. 97.
241. McMurray, J.S., et al., *The synthesis of phosphopeptides*. Biopolymers, 2001. **60**(1): p. 3-31.
242. Ottinger, E.A., et al., *Synthesis of phosphotyrosine-containing peptides and their use as substrates for protein tyrosine phosphatases*. Biochemistry, 1993. **32**(16): p. 4354-4361.
243. Ottinger, E.A., Q. Xu, and G. Barany, *Intramolecular pyrophosphate formation during N alpha-9-fluorenylmethyloxycarbonyl (Fmoc) solid-phase synthesis of peptides containing adjacent phosphotyrosine residues*. Pept Res, 1996. **9**(5): p. 223-8.
244. Yang, Y., *Chapter 12 - Side Reactions in Peptide Phosphorylation*, in *Side Reactions in Peptide Synthesis*. 2016, Academic Press: Oxford. p. 293-298.
245. Pennington, M.W., et al., *Engineering a Stable and Selective Peptide Blocker of the Kv1.3 Channel in T Lymphocytes*. Mol Pharmacol, 2009. **75**(4): p. 762-773.

246. Arano, Y., et al., *Conventional and high-yield synthesis of DTPA-conjugated peptides: application of a monoreactive DTPA to DTPA-D-Phe1-octreotide synthesis*. *Bioconjug Chem*, 1997. **8**(3): p. 442-6.
247. Kunys, A.R., W. Lian, and D. Pei, *Specificity Profiling of Protein-Binding Domains Using One-Bead-One-Compound Peptide Libraries*. *Curr Protoc Chem Biol*, 2012. **4**(4): p. 331-355.
248. Varasteh, Z., et al., *The effect of macrocyclic chelators on the targeting properties of the ⁶⁸Ga-labeled gastrin releasing peptide receptor antagonist PEG2-RM26*. *Nucl Med Biol*, 2015. **42**(5): p. 446-454.
249. Eisenwiener, K.P., P. Powell, and H.R. Mäcke, *A convenient synthesis of novel bifunctional prochelators for coupling to bioactive peptides for radiometal labelling*. *Bioorg Med Chem Lett*, 2000. **10**(18): p. 2133-5.
250. Tryfonopoulos, D., et al., *Src: a potential target for the treatment of triple-negative breast cancer*. *Ann Oncol*, 2011. **22**(10): p. 2234-40.
251. Bhojani, M.S., et al., *Synthesis and Investigation of a Radioiodinated F3 Peptide Analog as a SPECT Tumor Imaging Radioligand*. *PLOS ONE*, 2011. **6**(7): p. e22418.
252. Ogawa, K., et al., *Evaluation of radioiodinated vesamicol analogs for sigma receptor imaging in tumor and radionuclide receptor therapy*. *Cancer Sci*, 2009. **100**(11): p. 2188-92.
253. Wang, R. and H. Sun, *Radioiodinated HSP90 α -mAb as Novel Tumor Target Imaging Agent in Prostate Cancer Xenograft*. *J Nucl Med*, 2015. **56**(S3): p. 1151-1151.
254. Kiess, A.P., et al., *Auger Radiopharmaceutical Therapy Targeting Prostate-Specific Membrane Antigen*. *J Nucl Med*, 2015. **56**(9): p. 1401-7.
255. Karonen, S.-L., *Developments in techniques for radioiodination of peptide hormones and other proteins*. *Scand J Clin Lab Invest*, 1990. **50**(S201): p. 135-138.
256. Behr, T.M., et al., *Radioiodination of monoclonal antibodies, proteins and peptides for diagnosis and therapy A review of standardized, reliable and safe procedures for clinical grade levels kBq to GBq in the Goettingen/Marburg experience*. *Nuklearmedizin*, 2002. **41**(2): p. 71-79.
257. Cavina, L., et al., *Design of Radioiodinated Pharmaceuticals: Structural Features Affecting Metabolic Stability towards in Vivo Deiodination*. *European J Org Chem*, 2017. **2017**(24): p. 3387-3414.
258. Carvalho, D.P. and A.C. Ferreira, *The importance of sodium/iodide symporter (NIS) for thyroid cancer management*. *Arq Bras Endocrinol Metabol*, 2007. **51**(5): p. 672-82.
259. Silberstein, E.B., *Radioiodine: the classic theranostic agent*. *Semin Nucl Med*, 2012. **42**(3): p. 164-70.
260. Yeong, C.-H., M.-h. Cheng, and K.-H. Ng, *Therapeutic radionuclides in nuclear medicine: current and future prospects*. *Journal of Zhejiang University. Science. B*, 2014. **15**(10): p. 845-863.
261. Phan, T.T., et al., *Diagnostic I-131 scintigraphy in patients with differentiated thyroid cancer: no additional value of higher scan dose*. *Ann Nucl Med*, 2004. **18**(8): p. 641-6.
262. Michel, R.B., M.W. Brechbiel, and M.J. Mattes, *A comparison of 4 radionuclides conjugated to antibodies for single-cell kill*. *J Nucl Med*, 2003. **44**(4): p. 632-40.
263. Kim, E.J., et al., *Enhanced tumor retention of radioiodinated anti-epidermal growth factor receptor antibody using novel bifunctional iodination linker for radioimmunotherapy*. *Oncol Rep*, 2016. **35**(6): p. 3159-68.
264. Läppchen, T., et al., *Radioiodinated Exendin-4 Is Superior to the Radiometal-Labelled Glucagon-Like Peptide-1 Receptor Probes Overcoming Their High Kidney Uptake*. *PLoS ONE*, 2017. **12**(1): p. e0170435.
265. Bertrand, R., et al., *Mild and Selective Mono-Iodination of Unprotected Peptides as Initial Step for the Synthesis of Bioimaging Probes*. *Bioconjug Chem*, 2016. **27**(10): p. 2281-2286.

266. Lane, D. and D.R. Richardson, *William Hunter and radioiodination: revolutions in the labelling of proteins with radionuclides of iodine*. *Biochem J*, 2011: p. 4.
267. Greenwood, F.C., W.M. Hunter, and J.S. Glover, *The preparation of (131)I-labelled human growth hormone of high specific radioactivity*. *Biochem J*, 1963. **89**(1): p. 114-123.
268. Bayse, G.S., A.W. Michaels, and M. Morrison, *Lactoperoxidase-catalyzed iodination of tyrosine peptides*. *Biochim Biophys Acta*, 1972. **284**(1): p. 30-3.
269. Vergote, V., et al., *LC-UV/MS characterization and DOE optimization of the iodinated peptide obestatin*. *J Pharm Biomed Anal*, 2008. **46**(1): p. 127-36.
270. Okarvi, S.M. and I. Al Jammaz, *Synthesis and evaluation of a technetium-99m labeled cytotoxic bombesin peptide conjugate for targeting bombesin receptor-expressing tumors*. *Nucl Med Biol*, 2010. **37**(3): p. 277-88.
271. Sugiura, G., et al., *Radiolabeling strategies for tumor-targeting proteinaceous drugs*. *Molecules*, 2014. **19**(2): p. 2135-65.
272. Liu, Z. and R.R. Julian, *Deciphering the peptide iodination code: influence on subsequent gas-phase radical generation with photodissociation ESI-MS*. *J Am Soc Mass Spectrom*, 2009. **20**(6): p. 965-71.
273. Wolff, J. and I. Covelli, *Factors in the iodination of histidine in proteins*. *Eur J Biochem*, 1969. **9**(3): p. 371-7.
274. Fernandes, C., et al., *Radioiodination of new EGFR inhibitors as potential SPECT agents for molecular imaging of breast cancer*. *Bioorganic Med Chem*, 2007. **15**(12): p. 3974-3980.
275. Mandel, S.J. and L. Mandel, *Radioactive iodine and the salivary glands*. *Thyroid*, 2003. **13**(3): p. 265-71.
276. Zitzmann, S., et al., *Identification of a new prostate-specific cyclic peptide with the bacterial FliTrx system*. *J Nucl Med*, 2005. **46**(5): p. 782-5.
277. Geissler, F., et al., *Intracellular catabolism of radiolabelled anti-mu antibodies by malignant B-cells*. *Cancer Res*, 1992. **52**(10): p. 2907-15.
278. Niedel, J., S. Wilkinson, and P. Cuatrecasas, *Receptor-mediated uptake and degradation of 125I-chemotactic peptide by human neutrophils*. *J Biol Chem*, 1979. **254**(21): p. 10700-6.
279. Boswell, C.A. and M.W. Brechbiel, *Auger electrons: lethal, low energy, and coming soon to a tumor cell nucleus near you*. *J Nucl Med*, 2005. **46**(12): p. 1946-7.
280. Shrivastava, A., et al., *Heterobivalent dual-target probe for targeting GRP and Y1 receptors on tumor cells*. *Bioorg Med Chem Lett*, 2013. **23**(3): p. 687-92.
281. Liu, Z., et al., *(18)F, (64)Cu, and (68)Ga labeled RGD-bombesin heterodimeric peptides for PET imaging of breast cancer*. *Bioconjug Chem*, 2009. **20**(5): p. 1016-1025.
282. Morais, M., et al., *Radiolabelled mannosylated dextran derivatives bearing an NIR-fluorophore for sentinel lymph node imaging*. *Bioconjug Chem*, 2014. **25**(11): p. 1963-70.
283. Fischer, C.A., S. Vomstein, and T.L. Mindt, *A bombesin-shepherdin radioconjugate designed for combined extra- and intracellular targeting*. *Pharmaceuticals (Basel)*, 2014. **7**(6): p. 662-75.
284. Kluba, C.A., et al., *Dual-targeting conjugates designed to improve the efficacy of radiolabelled peptides*. *Org Biomol Chem*, 2012. **10**(37): p. 7594-602.
285. Esteves, T., et al., *Nuclear targeting with cell-specific multifunctional tricarbonyl M(II) (M is Re, (99m)Tc) complexes: synthesis, characterization, and cell studies*. *J Biol Inorg Chem*, 2011. **16**(8): p. 1141-53.
286. Imstepf, S., et al., *Nuclear Targeting with an Auger Electron Emitter Potentiates the Action of a Widely Used Antineoplastic Drug*. *Bioconjug Chem*, 2015. **26**(12): p. 2397-407.

287. Ginj, M. and H.R. Maecke, *Synthesis of trifunctional somatostatin based derivatives for improved cellular and subcellular uptake*. Tetrahedron Lett, 2005. **46**(16): p. 2821-2824.
288. Yan, Y. and X. Chen, *Peptide heterodimers for molecular imaging*. Amino acids, 2011. **41**(5): p. 1081-1092.
289. Esteves, T., et al., *Nuclear targeting with cell-specific multifunctional tricarbonyl M(I) (M is Re, ^{99m}Tc) complexes: synthesis, characterization, and cell studies*. J Biol Inorg Chem, 2011. **16**(8): p. 1141-1153.
290. Wuts, P.G.M. and T.W. Greene, *Protection for the Carboxyl Group*, in *Greene's Protective Groups in Organic Synthesis*. 2006, John Wiley & Sons, Inc. p. 533-646.
291. Cakić, N., et al., *Synthetic strategies for preparation of cyclen-based MRI contrast agents*. Tetrahedron Lett, 2015. **56**(6): p. 759-765.
292. Li, C. and W.-T. Wong, *A convenient method for the preparation of mono N-alkylated cyclams and cyclens in high yields*. Tetrahedron Lett, 2002. **43**(17): p. 3217-3220.
293. Cornelissen, B. and K.A. Vallis, *Targeting the nucleus: an overview of Auger-electron radionuclide therapy*. Curr Drug Discov Technol, 2010. **7**(4): p. 263-79.
294. Zelenka, K., L. Borsig, and R. Alberto, *Trifunctional ^{99m}Tc based radiopharmaceuticals: metal-mediated conjugation of a peptide with a nucleus targeting intercalator*. Org Biomol Chem, 2011. **9**(4): p. 1071-8.
295. Ihmels, H. and D. Otto, *Intercalation of Organic Dye Molecules into Double-Stranded DNA -- General Principles and Recent Developments*, in *Supramolecular Dye Chemistry*. 2005, Springer Berlin Heidelberg, p. 161-204.
296. Ji, H., et al., *Monitoring the Intercalation of Acridine Orange (AO) Molecules into 6-Methyl isoxanthopterin (6-MI)-Labeled DNA by Circular Dichroism and Single-Molecule FRET*. Biophys J, 2017. **112**(3, Supplement 1): p. 288a.
297. Omelon, S., J. Georgiou, and W. Habraken, *A cautionary (spectral) tail: red-shifted fluorescence by DAPI-DAPI interactions*. Biochem Soc Trans, 2016. **44**(1): p. 46-9.
298. Belmont, P., et al., *Acridine and acridone derivatives, anticancer properties and synthetic methods: where are we now?* Anticancer Agents Med Chem, 2007. **7**(2): p. 139-69.
299. Wang, A.H., G.J. Quigley, and A. Rich, *Atomic resolution analysis of a 2:1 complex of CpG and acridine orange*. Nucleic Acids Res, 1979. **6**(12): p. 3879-90.
300. Esteves, T., et al., *Tricarbonyl M(I) (M = Re, (^{99m}Tc) complexes bearing acridine fluorophores: synthesis, characterization, DNA interaction studies and nuclear targeting*. Org Biomol Chem, 2010. **8**(18): p. 4104-16.
301. Kusuzaki, K., et al., *Review. Acridine orange could be an innovative anticancer agent under photon energy*. In Vivo, 2007. **21**(2): p. 205-14.
302. de Andrade, C.T., et al., *Acridine orange as radiosensitizer to improve cell damage caused by radiotherapy in breast cancer cells line*. Photodiagnosis Photodyn Ther, 2015. **12**(3): p. 343-344.
303. Nakamura, T., et al., *Determination of the LD50 of acridine orange via intravenous administration in mice in preparation for clinical application to cancer therapy*. In Vivo, 2014. **28**(4): p. 523-7.
304. Gama, S., et al., *Synthesis and biological studies of pyrazolyl-diamine Pt(II) complexes containing polyaromatic DNA-binding groups*. Chembiochem, 2012. **13**(16): p. 2352-62.
305. Esteves, T., et al., *Tricarbonyl M(I) (M = Re, ^{99m}Tc) complexes bearing acridine fluorophores: synthesis, characterization, DNA interaction studies and nuclear targeting*. Org Biomol Chem, 2010. **8**(18): p. 4104-4116.
306. *Protection for the Amino Group*, in *Greene's Protective Groups in Organic Synthesis*. 2014, John Wiley & Sons, Inc. p. 895-1193.
307. Carpino, L.A., et al., *Comparison of the Effects of 5- and 6-HOAt on Model Peptide Coupling Reactions Relative to the Cases for the 4- and 7-Isomers*. Org Lett, 2000. **2**(15): p. 2253-2256.

308. Mishra, A., et al., *A new class of Gd-based DO3A-ethylamine-derived targeted contrast agents for MR and optical imaging*. *Bioconjug Chem*, 2006. **17**(3): p. 773-80.
309. Kohl Stephan, W., et al., *New Synthetic Routes for 1-Benzyl-1,4,7,10-tetraazacyclododecane and 1,4,7,10-Tetraazacyclododecane-1-acetic Acid Ethyl Ester, Important Starting Materials for Metal-coded DOTA-Based Affinity Tags*. *Zeitschrift für Naturforschung B.*, 2007. **62**(3): p. 397.
310. Silva, P.P., et al., *Platinum(II) compounds of tetracyclines as potential anticancer agents: cytotoxicity, uptake and interactions with DNA*. *J Braz Chem Soc*, 2010. **21**: p. 1237-1246.
311. Kleinwächter, V. and J. Koudelka, *Ultraviolet spectra of the complexes of acridine orange with deoxyribonucleic acid and polyphosphates*. *Biophysik*, 1968. **5**(2): p. 119-125.
312. Kumar, C.V., E.H.A. Punzalan, and W.B. Tan, *Adenine-Thymine Base Pair Recognition by an Anthryl Probe from the DNA Minor Groove*. *Tetrahedron*, 2000. **56**(36): p. 7027-7040.
313. Lyles, M.B. and I.L. Cameron, *Interactions of the DNA intercalator acridine orange, with itself, with caffeine, and with double stranded DNA*. *Biophys Chem*, 2002. **96**(1): p. 53-76.
314. Tomita, G., *Fluorescence-excitation spectra of acridine orange-DNA and -RNA systems*. *Biophysik*, 1967. **4**(1): p. 23-9.
315. Balagurumoorthy, P., et al., *Auger electron-induced double-strand breaks depend on DNA topology*. *Radiat Res*, 2008. **170**(1): p. 70-82.
316. He, Y., et al., *Sequence-specific DNA strand cleavage by ¹¹¹In-labeled peptide nucleic acids*. *Eur J Nucl Med Mol Imaging*, 2004. **31**(6): p. 837-45.
317. Adelstein, S.J. and A.I. Kassis, *Strand breaks in plasmid DNA following positional changes of Auger-electron-emitting radionuclides*. *Acta Oncol*, 1996. **35**(7): p. 797-801.
318. Sahu, S.K., et al., *The effects of indium-111 decay on pBR322 DNA*. *Radiat Res*, 1995. **141**(2): p. 193-8.
319. Yoneda, Y., et al., *A long synthetic peptide containing a nuclear localization signal and its flanking sequences of SV40 T-antigen directs the transport of IgM into the nucleus efficiently*. *Exp Cell Res*, 1992. **201**(2): p. 313-20.
320. Kalderon, D., et al., *A short amino acid sequence able to specify nuclear location*. *Cell*, 1984. **39**(3 Pt 2): p. 499-509.
321. Han, Y., et al., *Preparation and Applications of Xanthenylamide (XAL) Handles for Solid-Phase Synthesis of C-Terminal Peptide Amides under Particularly Mild Conditions(1-3)*. *J Org Chem*, 1996. **61**(18): p. 6326-6339.
322. Aletras, A., et al., *Preparation of the very acid-sensitive Fmoc-Lys(Mtt)-OH. Application in the synthesis of side-chain to side-chain cyclic peptides and oligolysine cores suitable for the solid-phase assembly of MAPs and TASPs*. *Int J Pept Protein Res*, 1995. **45**(5): p. 488-96.
323. Anstead, G.M., K.E. Carlson, and J.A. Katzenellenbogen, *The estradiol pharmacophore: ligand structure-estrogen receptor binding affinity relationships and a model for the receptor binding site*. *Steroids*, 1997. **62**(3): p. 268-303.
324. Saha, P., et al., *Design, synthesis, cytotoxic activity and estrogen receptor alpha affinity of doxorubicin conjugates at 16alpha-position of estrogen for site-specific treatment of estrogen receptor positive breast cancer*. *Steroids*, 2012. **77**(11): p. 1113-22.
325. Descoteaux, C., et al., *Improved synthesis of unique estradiol-linked platinum(II) complexes showing potent cytotoxic activity and affinity for the estrogen receptor alpha and beta*. *Steroids*, 2008. **73**(11): p. 1077-89.
326. Fevig, T.L. and J.A. Katzenellenbogen, *A short, stereoselective route to 16.alpha.-(substituted-alkyl)estradiol derivatives*. *J Org Chem*, 1987. **52**(2): p. 247-251.
327. Goto, G., et al., *A Stereoselective Synthesis and Nuclear Magnetic Resonance Spectral Study of Four Epimeric 17-Hydroxy-16-ethylestranes*. *Chem Pharm Bull*, 1977. **25**(6): p. 1295-1301.

328. Isenman, L.D. and J.F. Dice, *Secretion of intact proteins and peptide fragments by lysosomal pathways of protein degradation*. J Biol Chem, 1989. **264**(36): p. 21591-6.
329. Pomper, M.G., et al., *11 beta-methoxy-, 11 beta-ethyl- and 17 alpha-ethynyl-substituted 16 alpha-fluoroestradiols: receptor-based imaging agents with enhanced uptake efficiency and selectivity*. J Med Chem, 1990. **33**(12): p. 3143-55.
330. Cunha, S., *Avaliação do potencial Clínico de Novos Ligandos para o Receptor Estrogénico em Diagnóstico e Terapia de Tumores da Mama*. 2015, Faculdade de Ciências, Universidade de Lisboa.
331. Pazos, E., et al., *DNA recognition by synthetic constructs*. Chembiochem, 2011. **12**(13): p. 1958-73.
332. Vázquez, M.E., A.M. Caamaño, and J.L. Mascareñas, *From transcription factors to designed sequence-specific DNA-binding peptides*. Chem Soc Rev, 2003. **32**(6): p. 338-49.
333. Stewart, A.L. and M.L. Waters, *Structural effects on ss- and dsDNA recognition by a beta-hairpin peptide*. Chembiochem, 2009. **10**(3): p. 539-44.
334. Sánchez, M.I., et al., *Sequence-selective DNA recognition with peptide-bisbenzamidine conjugates*. Chemistry, 2013. **19**(30): p. 9923-9.
335. Moretti, R. and A.Z. Ansari, *Expanding the specificity of DNA targeting by harnessing cooperative assembly*. Biochimie, 2008. **90**(7): p. 1015-1025.
336. Segal, D.J. and C.F. Barbas, *Design of novel sequence-specific DNA-binding proteins*. Curr Opin Chem Biol, 2000. **4**(1): p. 34-39.
337. Mosquera, J., et al., *Stimuli-responsive selection of target DNA sequences by synthetic bZIP peptides*. Nat Commun, 2013. **4**: p. 1874.
338. Talanian, R.V., C.J. McKnight, and P.S. Kim, *Sequence-specific DNA binding by a short peptide dimer*. Science, 1990. **249**(4970): p. 769-71.
339. Ueno, M., et al., *Arranging quaternary structure of peptides by cyclodextrin-guest inclusion complex: sequence-specific DNA binding by a peptide dimer with artificial dimerization module*. J Am Chem Soc, 1993. **115**(26): p. 12575-12576.
340. Caamano, A.M., et al., *A Light-Modulated Sequence-Specific DNA-Binding Peptide*. Angew Chem Int Ed Engl, 2000. **39**(17): p. 3104-3107.
341. Talanian, R.V., et al., *Minimum length of a sequence-specific DNA binding peptide*. Biochemistry, 1992. **31**(30): p. 6871-5.
342. Rodriguez, J., et al., *A designed DNA binding motif that recognizes extended sites and spans two adjacent major grooves*. Chem Sci, 2016. **7**(5): p. 3298-3303.
343. Mosquera, J., et al., *Sequence-selective DNA binding with cell-permeable oligoguanidinium-peptide conjugates*. Chem Commun (Camb), 2015. **51**(23): p. 4811-4.
344. Joshi, R., et al., *Facile synthesis of peptide nucleic acids and peptide nucleic acid-peptide conjugates on an automated peptide synthesizer*. J Pept Sci, 2011. **17**(1): p. 8-13.
345. Athanassiou, Z., et al., *Structural mimicry of retroviral tat proteins by constrained beta-hairpin peptidomimetics: ligands with high affinity and selectivity for viral TAR RNA regulatory elements*. J Am Chem Soc, 2004. **126**(22): p. 6906-13.
346. Moehle, K., et al., *Design of β -Hairpin Peptidomimetics That Inhibit Binding of α -Helical HIV-1 Rev Protein to the Rev Response Element RNA*. Angew Chem Int Ed, 2007. **46**(47): p. 9101-9104.
347. Zhao, B., et al., *A Thioether-Stabilized d-Proline-l-Proline-Induced beta-Hairpin Peptide of Defensin Segment Increases Its Anti-Candida albicans Ability*. Chembiochem, 2016. **17**(15): p. 1416-20.
348. Lloyd-Williams, P., F. Albericio, and E. Giralt, *Convergent solid-phase peptide synthesis*. Tetrahedron, 1993. **49**(48): p. 11065-11133.
349. Rinnová, M., M. Souček, and M. Lebl, *Solid-phase peptide synthesis by fragment condensation: Coupling in swelling volume*. Lett Pept Sci, 1999. **6**(1): p. 15-22.

350. Benz, H., *The Role of Solid-Phase Fragment Condensation (SPFC) in Peptide Synthesis*. Synthesis, 1994. **1994**(04): p. 337-358.
351. Gatos, D. and C. Tzavara, *Comparison of the solid-phase fragment condensation and phase-change approaches in the synthesis of salmon I calcitonin*. J Pept Res, 2001. **57**(2): p. 168-174.
352. Heinlein, C., et al., *Fragment Condensation of C-Terminal Pseudoproline Peptides without Racemization on the Solid Phase*. Angew Chem Int Ed, 2011. **50**(28): p. 6406-6410.
353. Paradis-Bas, M., J. Tulla-Puche, and F. Albericio, *The road to the synthesis of "difficult peptides"*. Chem Soc Rev, 2016. **45**(3): p. 631-654.
354. Yue, C., J. Thierry, and P. Potier, *2-phenyl isopropyl esters as carboxyl terminus protecting groups in the fast synthesis of peptide fragments*. Tetrahedron Lett, 1993. **34**(2): p. 323-326.
355. Guo, H., F. Gallazzi, and Y. Miao, *Design and Evaluation of New Tc-99m-Labeled Lactam Bridge-Cyclized Alpha-MSH Peptides for Melanoma Imaging*. Mol Pharm, 2013. **10**(4): p. 1400-1408.
356. Diaz-Mochon, J.J., L. Bialy, and M. Bradley, *Full orthogonality between Dde and Fmoc: the direct synthesis of PNA-peptide conjugates*. Org Lett, 2004. **6**(7): p. 1127-9.
357. Vaidyanathan, G., et al., *Evaluation of an anti-p185(HER2) (scFv-C(H)2-C(H)3)(2) fragment following radioiodination using two different residualizing labels: SGMIB and IB-Mal-D-GEEEK*. Nucl Med Biol, 2009. **36**(6): p. 671-680.
358. Boswell, C.A., et al., *Enhanced tumor retention of a radiohalogen label for site-specific modification of antibodies*. J Med Chem, 2013. **56**(23): p. 9418-26.
359. Choi, J., et al., *N-Succinimidyl guanidinomethyl iodobenzoate protein radiohalogenation agents: Influence of isomeric substitution on radiolabeling and target cell residualization*. Nucl Med Biol, 2014. **41**(10): p. 802-812.
360. Wrobel, J. and A. Dietrich, *Preparation of L-(Phosphonodifluoromethyl)phenylalanine derivatives as non-hydrolyzable mimetics of O-phosphotyrosine*. Tetrahedron Lett, 1993. **34**(22): p. 3543-3546.
361. Johnson, E.C. and S.B. Kent, *Insights into the mechanism and catalysis of the native chemical ligation reaction*. J Am Chem Soc, 2006. **128**(20): p. 6640-6.
362. Perrin, D.D. and W.L.F. Armarego, *Purification of Laboratory Chemicals*. 3th Edition ed. 1988, Oxford: Pergamon Press.